Universidad de Valladolid

Escuela de Doctorado Universidad de Valladolid

PHD PROGRAMME IN INDUSTRIAL ENGINEERING

DOCTORAL THESIS:

DEVELOPMENT OF MODELING AND CONTROL STRATEGIES IN MICROALGAE-BACTERIA PHOTOBIOREACTORS FOR WASTEWATER TREATMENT

Submitted by Irina Bausa Ortiz in fulfillment of the requirements for the PhD degree by the Universidad de Valladolid

Supervised by:
Dr. César de Prada Moraga
Dr. Raúl Muñoz Torre
Dra. Smaranda Podar Cristea

Agradecimientos

A mis directores de tesis César de Prada, Raúl Muñoz y Smaranda Podar, por su inestimable guía y enseñanzas durante todo el proceso. Infinitamente agradecida a César por su dedicación y apoyo constantes. Muchas gracias a Raúl por su compromiso y guía en cada detalle para obtener mejores resultados experimentales.

A todos los miembros del Departamento de Ingeniería de Sistemas y Automática, especialmente a los del grupo de investigación "Control y Supervisión de Procesos", muchas gracias por su cálida acogida y continuo respaldo durante todo el camino. Muchas gracias a todos los profesores del grupo y a los colaboradores externos, por su orientación y sus valiosas contribuciones. Gracias especialmente a Gloria y César, por guiarnos a todos durante este camino. Muchas gracias a todos los técnicos, especialmente a Teresa Álvarez, por su inmediata disposición a ayudar en todo momento. A Erika Oliveira, muchas gracias por todo el apoyo prestado y las ideas aportadas. A Carlos, José Luis, Cristian y Suní, muchas gracias por la acogida.

A los profesores, técnicos e investigadores del Departamento de Ingeniería Química y Ambiental, gracias por estar siempre disponibles para aclarar dudas y aportar soluciones. Quisiera agradecer a todos los investigadores del Instituto de Procesos Sostenibles, especialmente a los del grupo de microalgas, por su inestimable ayuda y ánimos en todo momento. Muchas gracias a Bárbara Muñoz y Lara Méndez, por su paciencia y dedicación en el entrenamiento para el trabajo de laboratorio. Muchísimas gracias al profesor Daniel Navia, de la Universidad Técnica Federico Santa María y a Bárbara Muñoz, por la colaboración en el montaje de la instalación experimental. A Sara Rodríguez, Nerea Rodríguez, Thalita, Frida, Patty, Marianela, Diego, Xochitl y Gulsum, por su colaboración durante los experimentos en el laboratorio. Muchas gracias a Andrés Felipe, por su ayuda y valiosas contribuciones para la redacción del primer artículo.

A mi familia, especialmente a mi madre, muchas gracias por el apoyo, comprensión y fuerzas. A mi tía, tíos, primas y primos, por seguir de cerca con cariño todo el proceso.

A la familia que hemos construido durante el doctorado: Erika, Tomás, Dani, Alejandra, Rogelio, Yury, Felipe y Sergio, muchas gracias por todos los buenos momentos compartidos.

A todos mis amigos, por su cariño y ánimos en todo el camino: a los “jefes” Ania y Reinel, Elaine, Rodolfo, Daily, Javier, Ernesto, César Ernesto, Pedro Fernández, José A, Dalmay, Ramón, Lily, Jorge y Marita; muchas gracias por tantos años de amistad. Muchas gracias a Alina y Fanny, por los consejos y compañía.

A las mejores embajadoras de Brasil en Valladolid: Rafaella, Erika, Aline y Fabiana. Gracias por su amistad y por ayudarme a hacer de esta ciudad mi casa.

Summary

English

Population growth and industrialization have resulted into a substantial increase in wastewater production, thereby establishing water purification as a primary concern on a global scale. In this context, microalgae-bacteria based wastewater treatment has emerged as a solution for wastewater treatment and nutrient recovery at a low-energy demand. The increasing number of microalgae-based applications demands the development of model-based information and decision support systems that can deal with their complex behavior.

From an engineering perspective, production processes in the field of biotechnology cannot be modeled and controlled in the same manner as other types of industrial processes. Significant adaptation is necessary to leverage the knowledge, modeling, and control techniques commonly utilized in process control. Microalgae-based wastewater treatment exhibits nonlinear and complex dynamics, hallmarks of biotechnological processes, and also encompasses persistent non-stationary regime behavior and influence of fluctuating perturbations. In order to confront the manifold challenges associated with the design, operation, and control of wastewater treatment systems based on microalgae-bacteria consortia, new mathematical models must be developed. Correspondingly, control strategies, state- estimation techniques, and process optimization techniques must be revisited and adapted to the context of multiple perturbations and evolving environmental conditions that affect these processes.

Objectives

The present thesis focuses on the proposal of models and estimation methods in novel facilities for wastewater treatment using microalgae and bacteria, as well as the proposal of state estimation and model-based control strategies for these facilities. To this end, the modeling of anoxic-aerobic photobioreactor configurations is proposed, as well as a library of components that allows the reuse of models across diverse applications. The objective of the present study is to estimate states, parameters, and uncertainties in a

microalgae-bacteria wastewater treatment plant, thereby facilitating the design and implementation of an online economic model predictive controller.

Methodology

In order to address the objectives of the thesis, the methodology employed has entailed the study of a variety of models that take into account the interactions between microalgae and bacteria in wastewater treatment. This study facilitates the selection of models for adequate representation of a microalgae-bacteria based wastewater treatment plant, as well as for the subsequent utilization of the model in the design of model-based control strategies. The modeling of a two-stage (anoxic-aerobic) wastewater treatment plant with biomass recycling was conducted and validated with real data from two lab-scale facilities under different operational conditions. Sensitivity analysis was conducted in both cases to ascertain the most influential parameters. Subsequently, parameter estimation was conducted via dynamic optimization, leveraging a robust objective function to address the uncertainties stemming from unreliable measurements. The model library of components was designed using the EcosimPro|PROOSIS® software and contains a variety of components for wastewater treatment. This library facilitates reuse of models and the connectivity of components. A novel approach for parameter estimation is presented and tested in a microalgae-bacteria photobioreactor.

The challenges associated with the monitoring and control of industrial-scale wastewater treatment plants were examined. This study enables the identification of the primary limitations associated with the processes of monitoring and control. Among these limitations is the necessity of accessing online information regarding the status of the system, a requirement that poses a significant challenge in the context of biological processes. This challenge arises from the need for more reliable measuring devices or the high cost of on-line sensors. Subsequently, the Moving Horizon Estimation (MHE) technique was employed to estimate the states, parameters, and uncertainties in a simulation of a real-scale wastewater treatment plant. The online estimation of the system state facilitates the implementation of an economic Model Predictive Controller (eMPC), considering the microalgae biomass as a valuable product.

Results and Conclusions

Existing models in the literature were adapted to represent novel configurations of anoxic–aerobic algal–bacterial photobioreactors for wastewater treatment. Simulation results revealed the model's versatility in photobioreactors with one or two stages, including sedimentation and biomass recirculation. At the same time, the simulation results for two different plants confirmed the model's capability to reproduce the experimental data, even in the treatment of high-strength wastewaters. Parameter estimation allowed the determination of the values of the most influential parameters of the microalgae–bacteria process. In the same line, parameter estimation in the settler allows the estimation of the main parameters related to settleability properties, which are not well-established in microalgae–bacteria processes. The simulation results closely match the experimental data, further validating the accuracy of the model and its potential for further application in the system operation, control, and monitoring.

The methodology for parameter estimation, when multiple outputs and parameters are involved in the optimization problem, was tested in a photobioreactor for wastewater treatment. This approach prevents convergence issues and facilitates a more optimal alignment between the experimental and simulated data.

The library of model components for a microalgae-bacteria wastewater treatment plant was developed. The components developed can be reutilized for multiple simulations and allow the easy interconnection between plant components.

The MHE technique was applied to a microalgae-based wastewater treatment process. The focus was on estimating multiple states and parameters concurrently in order to evaluate effluent water quality. This study employed an estimation model incorporating multiple states and parameters with a significant structural mismatch between the estimation model and the actual plant. Multi-rate measurements obtained from online measurements and analytical procedures enhanced the estimator's performance. Simulation results confirmed MHE's efficacy in the online estimation of pertinent microalgae-based wastewater treatment process variables.

The MHE provided an estimation of the system’s states, parameters, and uncertainties, which were then used in the model of an economic predictive controller for an industrial wastewater treatment plant. The controller is designed to maximize biomass production despite process uncertainties.

Español

El crecimiento demográfico y la industrialización han provocado un aumento sustancial de la producción de aguas residuales, lo que ha convertido la purificación del agua en una preocupación fundamental a escala mundial. En este contexto, el tratamiento de aguas residuales basado en microalgas y bacterias se ha convertido en una solución para el tratamiento de aguas residuales y la recuperación de nutrientes con un bajo consumo energético. El creciente número de aplicaciones basadas en microalgas exige el desarrollo de sistemas de información y apoyo a la toma de decisiones basados en modelos que puedan hacer frente a su complejo comportamiento.

Desde el punto de vista de la ingeniería, los procesos de producción en el campo de la biotecnología no pueden modelarse y controlarse de la misma manera que otros tipos de procesos industriales. Es necesaria una adaptación significativa para aprovechar los conocimientos, la modelización y las técnicas de control que se utilizan habitualmente en el control de procesos. El tratamiento de aguas residuales basado en microalgas presenta una dinámica no lineal y compleja, comportamiento persistente en régimen no estacionario y la influencia de perturbaciones fluctuantes. Para hacer frente a los múltiples retos asociados al diseño, funcionamiento y control de los sistemas de tratamiento de aguas residuales basados en consorcios de microalgas y bacterias, es necesario desarrollar nuevos modelos matemáticos. En consecuencia, las estrategias de control, las técnicas de estimación de estados y las técnicas de optimización de procesos deben revisarse y adaptarse al contexto de múltiples perturbaciones y condiciones ambientales cambiantes que afectan a estos procesos.

Objetivos

La presente tesis se centra en la propuesta de modelos y métodos de estimación en instalaciones novedosas para el tratamiento de aguas residuales mediante microalgas y bacterias, así como en la propuesta de estrategias de estimación de estados y control basado en modelo para dichas instalaciones. Con este fin, se propone el modelado de configuraciones de fotobiorreactores anóxicos-aeróbicos, así como una biblioteca de componentes que permite la reutilización de modelos en diversas aplicaciones. El objetivo del presente estudio es estimar los estados, los parámetros y las incertidumbres

en una planta de tratamiento de aguas residuales con microalgas y bacterias, facilitando así el diseño y la implementación de un controlador predictivo económico en línea.

Metodología

Para abordar los objetivos de la tesis, la metodología empleada ha consistido en el estudio de diversos modelos que tienen en cuenta las interacciones entre microalgas y bacterias en el tratamiento de aguas residuales. Este estudio facilita la selección de modelos para la representación adecuada de una planta de tratamiento de aguas residuales basada en microalgas y bacterias, así como para la posterior utilización del modelo en el diseño de estrategias de control basadas en modelos. Se llevó a cabo el modelado de una planta de tratamiento de aguas residuales de dos etapas (anóxica-aeróbica) con reciclaje de biomasa y se validó con datos reales de dos instalaciones a escala de laboratorio en diferentes condiciones de operación. Se realizó un análisis de sensibilidad en ambos casos para determinar los parámetros más influyentes. Posteriormente, se llevó a cabo la estimación de parámetros mediante optimización dinámica utilizando una función objetivo robusta para abordar las incertidumbres derivadas de mediciones poco fiables. Se diseñó una biblioteca de modelos de componentes utilizando el software EcosimPro|PROOSIS® , esta biblioteca contiene una variedad de componentes utilizados en las plantas de tratamiento de aguas residuales con microalgas y bacterias. Esta biblioteca facilita la reutilización del modelo y la conectividad de los componentes. Además, se presentó y se probó un enfoque novedoso para la estimación de parámetros en un fotobiorreactor de microalgas y bacterias.

Se examinaron los retos y limitaciones asociados con la supervisión y el control de plantas de tratamiento de aguas residuales a escala industrial. Entre las principales limitaciones encontradas, se encuentra la necesidad de acceder a información en línea sobre el estado del proceso, un requisito que plantea un reto importante en el contexto de los procesos biológicos. Este reto surge de la necesidad de disponer de dispositivos de medición más fiables o del elevado coste de los sensores en línea. Para superar esta limitación, se empleó la técnica de estimación de horizonte móvil para estimar los estados, los parámetros y las incertidumbres en una simulación de una planta de tratamiento de aguas residuales a escala industrial. La estimación en línea de los estados del proceso permitió la implementación de un controlador predictivo económico, considerando la biomasa de microalgas como un producto valioso.

Resultados y conclusiones

Los modelos existentes en la bibliografía se adaptaron para representar nuevas configuraciones de fotobiorreactores anóxicos-aeróbicos de algas y bacterias para el tratamiento de aguas residuales. Los resultados de las simulaciones realizadas revelaron la versatilidad del modelo en fotobiorreactores de una o dos etapas, incluyendo sedimentación y recirculación de biomasa. Al mismo tiempo, los resultados de simulación para dos plantas diferentes confirmaron la capacidad del modelo para reproducir los datos experimentales, incluso en el tratamiento de aguas residuales de alta concentración. Se realizó la estimación de parámetros del modelo, la cual permitió determinar los valores de los parámetros más influyentes del proceso de microalgas-bacterias. De igual manera, la estimación de parámetros en el sedimentador permitió estimar los principales parámetros relacionados con las propiedades de sedimentación, que no están bien establecidos en los procesos de microalgas-bacterias. Los resultados de simulación del modelo coinciden con los datos experimentales, lo que valida la precisión del modelo y su potencial para su futura aplicación en la operación, control y supervisión del sistema.

Se desarrolló una metodología para la estimación de parámetros cuando hay múltiples salidas y parámetros involucrados en el problema de optimización, la misma se probó en un fotobiorreactor para el tratamiento de aguas residuales. Este enfoque evita problemas de convergencia y facilita una alineación más óptima entre los datos experimentales y los simulados.

Se desarrolló una biblioteca de componentes del modelo para una planta de tratamiento de aguas residuales con microalgas y bacterias. Los componentes desarrollados pueden reutilizarse para múltiples simulaciones y permiten una fácil interconexión entre los componentes de la planta.

Se aplicó la técnica MHE a un proceso de tratamiento de aguas residuales basado en microalgas. La aplicación de esta técnica permitió la estimación simultánea de múltiples estados y parámetros con el fin de evaluar la calidad del agua efluente. En este estudio se empleó un modelo de estimación que incorporaba múltiples estados y parámetros con un desajuste estructural significativo entre el modelo usado para la estimación y la planta real. Se utilizaron medidas con diferente período de muestreo, obtenidas a partir de mediciones en línea y procedimientos analíticos, las cuales mejoraron el rendimiento del estimador. Los resultados de la simulación confirmaron la eficacia de MHE en la

estimación en línea de variables pertinentes del proceso de tratamiento de aguas residuales basado en microalgas.

El MHE proporcionó los valores estimados de los estados, parámetros e incertidumbres del sistema, que luego se utilizaron en el modelo del controlador predictivo económico para una planta de tratamiento de aguas residuales industriales. El controlador se diseñó con el objetivo de maximizar la producción de biomasa a pesar de las incertidumbres del proceso.

This work was supported by the Regional Government of Castilla y León and the EU-FEDER program (CL-EI-2021-07, UIC 233, UIC 379). It has also been supported by a pre-doctoral contract from the *Consejería de Educación de la Junta de Castilla y León* and the European Social Fund (Order EDU/601/2020), and by the Project a-CIDiT (PID2021-123654OB-C31).

The author thanks the European Social Fund and the *Consejería de Educación de la Junta de Castilla y León*.

Nomenclature:

ABACO: microAlgae-BActeria COnsortia model

ASMs: Activated Sludge Models

BOD: Biological Oxygen Demand

BSOM: Biodegradable soluble organic matter

C: Carbon

CO_2: Carbon dioxide

COD: Chemical Oxygen Demand

CVP: Control Vector Parameterization

CWM1: Constructed Wetland Model No. 1

DAEs: Differential and Algebraic Equations

DO: Dissolved Oxygen concentration

EKF: Extended Kalman Filter

ELO: Extended Luenberger Observer

eMPC: economic Model Predictive Control

FHGO: Filtered High Gain Observer

FSP: Filtered Smith Predictor

GPC: Generalized Predictive Controllers

HRAPs: High-Rate Algal Ponds

HRT: Hydraulic Retention Time

IC: Inorganic carbon

IDAS: Implicit Differential-Algebraic solver with Sensitivity capabilities

IWA: International Water Association

KF: Kalman Filter

LBMPC: Learning-Based Model Predictive Control

LS: Least squares

M-estimators: Maximum Likelihood Estimators

MHE: Moving Horizon Estimation

MPC: Model Predictive Control

N: Nitrogen

$N\text{-}NH_4^+$: Nitrogen in the form of ammonium

$N–NO_3^-$: Nitrogen in the form of nitrate

$N–NO_2^-$: Nitrogen in the form of nitrite

NARMAX: Nonlinear AutoRegressive Moving Average model with eXogenous inputs

NLP: Nonlinear programming

NMPC: Nonlinear Model Predictive Control

O_2: Oxygen

ODEs: Ordinary Differential Equations

OOP: Object-oriented programming

OCP: Optimal control problem

P: Phosphorus

PAR: Photosynthetically Active Radiation

PDEs: Partial Differential Equations

PI controllers: Proportional Integral controllers

PID controllers: Proportional - Integral - Derivative controllers

PPFD: Photosynthetic Photon Flux Density

$P–PO_4^{2-}$: Phosphorus in the form of phosphate

PWM: Plant-Wide Model

RTO: Real-Time Optimization

RWQM1: River Water Quality Model 1

SFWD: Synthetic Food Waste Digestate

SHGO: Standard High Gain Observer

SMC: Sliding Mode Control

SNOPT: Sparse Nonlinear OPTimizer

SQP: Sequential Quadratic Programming

SRT: Sludge Retention Time

STOs: Super Twisting Observers

SWW: Synthetic wastewater

TOC: Total Organic Carbon

TN: Total Nitrogen

TSS: Total Suspended Solids

UKF: Unscented Kalman Filter

VSS: Volatile Suspended Solids

WLS: Weighted least squares

WW: Wastewater

WWTPs: Wastewater Treatment Plants

Contents

Figure Index

Table Index

1. Introduction to microalgae-bacteria based wastewater treatment processes

One of the greatest challenges facing humanity today is the availability of water resources suitable for direct human consumption. At the same time, population growth and industrialization have led to a significant increase in wastewater production. As a result, water purification is currently a primary concern on a global scale.

Wastewater contains a wealth of organic and inorganic nutrients that, if discharged untreated, can cause ecosystem imbalances due to excessive biological and chemical oxygen demands (BOD and COD, respectively). In addition, the presence of high concentrations of nutrients such as dissolved nitrogen and phosphorus can lead to eutrophication of water bodies, resulting in environmental problems such as oxygen depletion and unpleasant malodorous emissions to the air. Eutrophication also promotes the growth of unwanted microbes that threaten other aquatic life and degrade the quality of drinking water.

The traditional three-stage treatment process for wastewater treatment at wastewater treatment plants (WWTPs) includes primary solids removal, secondary biodegradable organic matter removal, and tertiary nutrient removal (Fig. 1.1). In primary treatment, wastewater enters large sedimentation tanks where suspended solids settle to the bottom. This process helps removing about 60% of the suspended solid waste present in the wastewater. During secondary treatment, the remaining organic matter is broken down by microorganisms in an oxygen-rich environment, eliminating up to 90% of pollutants through this biological treatment. Tertiary treatment is designed to remove any remaining contaminants, pathogens, and nutrients from wastewater. Several advanced techniques are used in tertiary treatment, which are WWTPs specific.

In WWTPs, secondary and tertiary treatment face significant challenges associated with high costs, energy-intensive treatment, and difficulties in the simultaneous removal of nitrogen and phosphorus. In fact, the mechanical aeration required for organic matter degradation in activated sludge systems can account for 45-60% of the total operating costs in conventional WWTPs (Chae and Kang, 2013). In addition to these challenges, today's wastewater treatment systems must deal with increasing demands for higher water quality and the presence of new chemical products and emerging contaminants in wastewater.

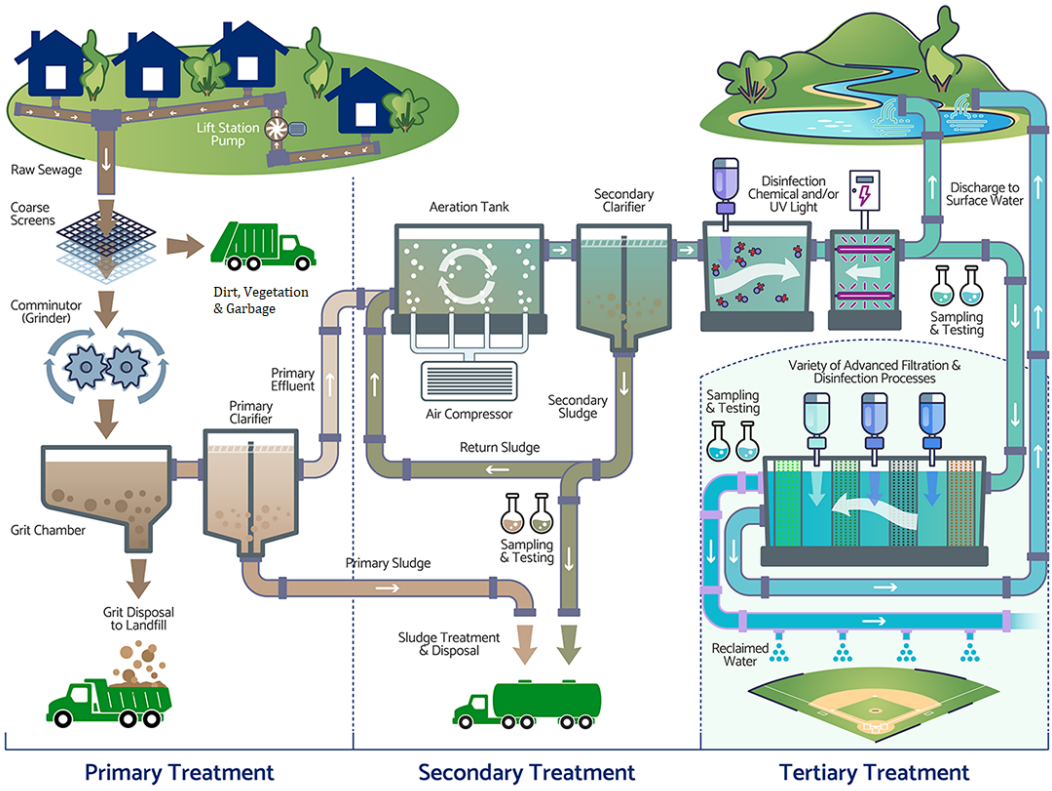

Fig. 1.1. Simplified schematic of the wastewater treatment process (Water Service Corporation, 2024)

Microalgae and bacteria-based wastewater treatment systems in high-rate algal ponds (HRAPs) were proposed in the late 1950s as an alternative for secondary or tertiary wastewater treatment (Oswald and Gotaas, 1957). In these treatment systems, microalgae grow using inorganic carbon as a carbon source and light as an energy source. During this process, microalgae provide the oxygen (O_2) required by heterotrophic bacteria to oxidize the organic matter present in the influent wastewater. Concurrently, heterotrophic bacteria provide carbon dioxide (CO_2) for photosynthetic activity, thereby completing the cycle. Furthermore, the oxygen produced by microalgae can be utilized by nitrifying bacteria to oxidize ammonium to nitrate (nitrification process), once again consuming CO_2 as a carbon source. This in situ photosynthetic oxygen supply has the potential to reduce carbon dioxide emissions from organic matter oxidation and to significantly decrease the costs associated with mechanical aeration in activated sludge systems. Furthermore, photosynthetic aeration limits the risks for pollutant volatilization and pathogen release under mechanical aeration.

Domestic and industrial wastewaters, as well as anaerobic digestion effluents, which are characterized by high carbon (C), nitrogen (N), and phosphorus (P) concentrations, require treatment before discharge into natural water bodies. Consequently, the capacity of microalgae to simultaneously remove carbon, nitrogen, and phosphorus via assimilation confers another notable advantage over conventional aerobic activated sludge or anaerobic digestion techniques in terms of enhanced nutrient recovery. Moreover, microalgae can enhance the removal of heavy metals and the aerobic degradation of hazardous contaminants (Muñoz and Guieysse, 2006).

Notwithstanding the fact that microalgae cultivated with wastewaters is not suitable for feed and food applications, the harvested microalgae biomass possesses potential for further utilization in the production of biofertilizers, biofuels, and other bioproducts. This renders the technology an attractive alternative for cost-effective wastewater treatment and nutrient management (Muñoz and Guieysse, 2006; Alcántara, García-Encina and Muñoz, 2013; Stiles *et al.*, 2018). Furthermore, the utilization of microalgae biotechnology for the capture of carbon dioxide from industrial plants is anticipated to emerge as a globally significant and economically viable environmental technology.

Despite the previously mentioned benefits, several challenges must be addressed to capitalize on the primary benefits of incorporating microalgae in wastewater treatment. The dynamic interactions between microalgae and bacteria are subject to temporal fluctuations due to the daily variations in environmental variables, such as solar radiation and temperature, as well as operational variables, including hydraulic retention time (HRT), nutrient concentrations, and the organic load present in the influent wastewater. The ability to maintain an effective algal activity at low temperatures and low light levels during winter months also poses a significant challenge.

Although these systems have been studied for many years, only recently, these technologies are being improved to align with industry demands. These developments encompass a reduction in hydraulic retention time and accomplishing the effluent water quality regulation, among other notable improvements. In the context of large-scale microalgae-bacteria systems, novel techniques from biotechnology and control engineering must be employed to ensure the robustness, durability, and optimization of these processes.

From an engineering perspective, production processes in the field of biotechnology cannot be modeled and controlled in the same manner as other types of industrial

processes. Significant adaptation is necessary to leverage the knowledge, modeling, and control techniques commonly utilized in process control. Microalgae-based wastewater treatment exhibits nonlinear and complex dynamics, hallmarks of biotechnological processes, and also encompasses persistent non-stationary regime behavior, the influence of fluctuating perturbations, and substantial feedback from the population level to the cellular level through light attenuation.

In order to confront the manifold challenges associated with the design, operation, and control of wastewater treatment systems based on microalgae-bacteria consortia, new mathematical models must be developed. Correspondingly, control strategies, state-estimation techniques, and process optimization techniques must be revisited and adapted to the context of multiple perturbations and evolving environmental conditions that affect these processes.

This Chapter revises the state of the art in modeling, parameter and state estimation, control, and optimization techniques in microalgae-based wastewater treatment processes. By identifying the aspects that need improvement in the automatic control of microalgae-based wastewater treatment processes, this review has set the stage for the thesis. This review provides a comprehensive overview of the field and is the cornerstone for establishing the research's motivation and goals.

1.1. State of the art in modeling, control, and optimization of microalgae-bacteria based wastewater treatment

This section presents a review of the current state of the art regarding the modeling, parameter and state estimation, control, and optimization of microalgae-bacteria processes and microalgae cultivation processes. Concerning modeling, this section presents a comprehensive review of research works conducted in the field, encompassing detailed mechanistic models described using nonlinear differential equations and more simplified linear and nonlinear models. In the same vein, the problem of parameter estimation was also revisited. This review also discusses a variety of works dealing with the problem of state estimation in microalgae-based processes, where plenty of research has been conducted, on the contrary of state estimation in wastewater treatment processes based on microalgae-bacteria consortia, with few case studies reported in the literature. Furthermore, a review of diverse control and optimization approaches in the microalgae cultivation field is presented, with a particular focus on advanced control strategies.

1.1.1. Modeling of microalgae-bacteria interactions in wastewater treatment processes

The use of mechanistic bacterial mathematical models to describe conventional wastewater treatment systems is a widely accepted practice. Some of these models, such as the Activated Sludge Models (ASMs) (Henze *et al.*, 2000), have been successfully developed, validated, and applied. On the other hand, mathematical models for microalgae growth have evolved from early steady-state formulations considering a single factor (e.g., nitrogen, carbon, phosphorus, light intensity) (Novak and Brune, 1985; Eilers and Peeters, 1988; Martinez *et al.*, 1997; Aslan and Kapdan, 2006) to more complicated dynamic models that consider multiple substrates or physical factors limitations following a structure according to Droop's or Monod kinetics (Solimeno *et al.*, 2015; Solimeno, Acien and García, 2017). However, mechanistic models that describe the internal complexity of the interactions between microalgae and bacteria in wastewater treatment systems (microalgae-bacteria models) are still being developed and tested (Solimeno and García, 2017).

In the last decades, the use of microalgae for wastewater treatment has promoted the development of mathematical models as a valuable tool to predict, control and optimize wastewater treatment systems based on microalgae-bacteria consortia. The integration of microalgae and bacteria processes in a model is not trivial: these models should be able to integrate the physical, chemical and biological phenomena occurring in these systems. These phenomena occur on different time scales and are strongly interdependent (García *et al.*, 2006). The reactions of microalgae and bacteria change with time due to the daily variation of environmental variables. Furthermore, microalgae can promote or inhibit bacterial growth in these systems and vice versa (Marsollier *et al.*, 2004; Awuah, 2007; Ruiz-Marin, Mendoza-Espinosa and Stephenson, 2010).

The River Water Quality Model 1 (RWQM1) (Reichert *et al.*, 2001), developed by the International Water Association (IWA) Task Group on River Water Quality Modeling, was a milestone in the modeling of microalgae and bacteria interactions. This mechanistic model included the growth of microalgae and bacteria (heterotrophs and nitrifiers) on nitrogen (ammonium and nitrate) and phosphorus (orthophosphate). The model also assumes the presence of consumers (feeding on algae, heterotrophic and autotrophic organisms, and biodegradable organic matter). This model is compatible with the existing activated sludge models (ASM1, ASM2, and ASM3) (Henze *et al.*, 2000). The model

contained equations for the formulation of biochemical transformation processes for a river water model that attempts to include the essential processes for C, O, N and P cycling in a river under aerobic or anoxic conditions. The model is based on the main elementary composition of organisms (C, H, N, O, and P) and the stoichiometry of biochemical conversion processes instead of only using chemical oxygen demand, as it is a common practice in wastewater treatment. The model includes all variables of ASM series models, considering 26 processes and 24 components (9 particulate and 15 soluble components). The kinetic expressions of RWQM1 are based on switching functions of nutrient availability, light, and temperature (Monod function, Lambert and Beer's Law, and Arrhenius equations, respectively). This model has been implemented in different simulation platforms to simulate practical cases studies. Most model components and equations of the RWQM1 have been used or adapted in subsequent models for microalgae-bacteria processes.

The RWQM1 has significantly influenced subsequent research in the field of microalgae-bacteria interactions. For instance, a modification of the RWQM1 was proposed by (Broekhuizen *et al.*, 2012) to simulate water quality characteristics in two pilot-scale HRAPs. The model introduced important structural changes such as the introduction of explicit dissolved inorganic carbon limitation, the representation of the form in which nitrate concentration influences algal growth, and the adoption of a differential/algebraic equation formulation for the acid/base reactions.

Sah et al. (Sah *et al.*, 2011) developed a mechanistic model to simulate wastewater treatment in a secondary facultative pond using a 3D hydrodynamic model coupled to an ASM-type biochemical model. The mathematical equations representing different aerobic and anoxic biochemical transformations by bacteria in the pond were based on the Activated Sludge Model 2 (Gujer *et al.*, 1995). Anaerobic process equations were selected from the Constructed Wetland Model No. 1 (CWM1) (Langergraber *et al.*, 2009), and the equation for algal growth was derived from RWQM1 (Reichert *et al.*, 2001). Monod-type rate equations described the nutrient and light limitation on growth. Light attenuation and temperature dependency are based on Lambert Beer’s Law and the Arrhenius-type equation, respectively. This model uses the same notation and structure of the ASM series and considers 19 processes and 18 components (nine particulate and nine soluble). One distinguishing characteristic of this model is that it considers five

functional groups of bacteria (heterotrophic, nitrifying, fermenting, sulfate-reducing, and sulfide-oxidizing bacteria).

Most previously referred models do not combine the overall biochemical processes involved in microalgae-bacteria systems and the simultaneous effects of light intensity, temperature, pH, or the effect of high dissolved oxygen concentration on biomass growth (Solimeno and García, 2017). To address these limitations, the dynamic model BIO_ALGAE (Solimeno *et al.*, 2017a) was developed, integrating crucial biokinetic, chemical, and physical processes of microalgae and bacteria in wastewater treatment systems. Microalgae processes are described using the previous model developed by the authors (Solimeno *et al.*, 2015), inspired by the RWQM1 (Reichert *et al.*, 2001). The modeling of bacteria processes is inspired in the modified ASM3 model (Iacopozzi *et al.*, 2007). The most relevant feature of the model was the inclusion of carbon limitation on the growth of microalgae and the growth of autotrophic bacteria. Light attenuation, photorespiration, temperature and pH dependence, and the transfer of gases to the atmosphere are also included in the model. This model uses the standard nomenclature of the IWA models and considers 19 components (6 particulate and 13 dissolved). The model was calibrated and validated in two identical pilot HRAPs treating real wastewater (Solimeno *et al.*, 2017a) and in a pilot HRAP during two different seasons (summer and winter) and operating at different HRT (Solimeno and García, 2019).

A second version of this model, the model BIO_ALGAE 2 (Solimeno, Gómez-Serrano and Acién, 2019a) was proposed to overcome some limitations of the BIO_ALGAE model (Solimeno *et al.*, 2017a), including new sub-models that consider the variation of microalgae and bacteria performance as a function of culture conditions prevailing in microalgae cultures (pH, temperature, dissolved oxygen). The model BIO_ALGAE 2 uses a cardinal temperature sub-model to describe microalgae growth dependence instead of the normal distribution of the thermic photosynthetic factor used in the model BIO_ALGAE (Solimeno *et al.*, 2015). The cardinal temperature sub-model is also used to replace the Arrhenius equation of the thermal factor, which describes the temperature dependence of nitrifying bacteria in previous model formulations (Reichert *et al.*, 2001; Langergraber *et al.*, 2009; Sah *et al.*, 2011; Solimeno, Acien and García, 2017). A cardinal pH sub-model was included to represent the inhibitory effects on the growth response of microalgae and bacteria at high pH. The cardinal pH sub-model is based on the cardinal temperature model presented in (Bernard and Rémond, 2012). Both temperature and pH

cardinal sub-models use the maximum, optimum, and minimum values to represent the influence of temperature and pH on microalgae and bacteria growth. The model was calibrated using data from a laboratory reactor fed with real wastewater, and the effect of CO_2 injection and the influence of wastewater composition on treatment performance was investigated through practical case studies (Solimeno, Gómez-Serrano and Acién, 2019a).

The microalgae-bacteria consortia (ABACO) model (Sánchez-Zurano *et al.*, 2021) for wastewater treatment includes the most relevant features of microalgae, such as light dependence, endogenous respiration, and growth and nutrient consumption as a function of nutrient availability (mainly inorganic carbon). The model also includes the most relevant factors influencing the activity of heterotrophic and nitrifying bacteria. The model equations are inspired in the BIO_ALGAE model (Solimeno *et al.*, 2017a). Contrary to the BIO_ALGAE model, the ABACO model considers the influence of nutrient concentration (CO_2, N-NH_4^+, N–NO_3^-, P–PO_4^{2-} and biodegradable soluble organic matter) in both microalgal and bacterial growth, and in the coefficient yields. The model was calibrated and validated with experimental data from duplicate laboratory-scale photobioreactors using pig slurry as a nutrient source.

The ALBA model (Casagli *et al.*, 2021) shares some common choices with the above-cited algae-bacteria models, particularly with the ones simulating outdoor environments (Broekhuizen *et al.*, 2012) and the BIO_ALGAE 2 model (Solimeno, Gómez-Serrano and Acién, 2019a). The model is based on mass balances of COD, C, N, P, H, and O. It describes growth and interactions among algae, heterotrophic and nitrifying bacteria, and other relevant chemical/physical processes. One of the most innovative characteristics of this model is the philosophy of biological kinetics based on Liebig's minimum law (De Baar, 1994), which assumes that the most limiting nutrient drives the growth kinetics. In addition, the pH sub-model includes a detailed chemical speciation described by an algebraic system. The model also includes the evaporation process and its effect on dissolved and suspended compounds. The model was calibrated and successfully validated using an original data set recorded from an outdoor demonstrative raceway pond treating synthetic wastewater for fifteen months (Casagli *et al.*, 2021).

Most of the models mentioned above describing raceway photobioreactors consider complete mixing in the entire reactor, thus evaluating the cultures' performance as a function of the average value of culture parameters such as light availability, pH, and nutrient concentration. However, raceway reactors are plug-flow reactors exposed to

changing solar light, thus culture conditions change on time and space inside the reactor. Consequently, dynamic models that account for the temporal-spatial distribution of culture parameters are essential for detailed simulation of this type of reactor. In this sense, a dynamic model of microalgae production in raceway reactors was developed (Fernández, Acién, *et al.*, 2016) based on a previously reported model for tubular reactors (Fernández *et al.*, 2012; Fernández, Acién, Berenguel and Guzmán, 2014). The model includes mass balances, transport phenomena, thermodynamic relationships, and biological phenomena taking place in the reactor, thus based on fundamental principles instead of empirical equations. Mass balances are applied to each reactor section to model the raceway reactor. Thus, partial differential equations (PDEs) are used to cope with plug-flow behavior in some parts of the reactor, while ordinary differential equations (ODEs) are used to describe the stirred tank sections of the reactor as sump and paddle to reduce the computational effort in simulating the model. In this model, the biological model for microalgae previously reported by (Costache *et al.*, 2013) and the engineering characterization of the raceway reactor used in previous works (Mendoza, Granados, de Godos, Acién, Molina, Banks, *et al.*, 2013; Mendoza, Granados, de Godos, Acién, Molina, Heaven, *et al.*, 2013; de Godos, Mendoza, *et al.*, 2014) were used to describe this bioprocess's biological and engineering aspects, respectively. The model was calibrated and validated with experimental data from a 100 m^2 pilot-scale raceway reactor (Fernández, Acién, *et al.*, 2016).

Mechanistic models, such as those previously referred to, provide a thorough understanding of the different phenomena that occur in photobioreactors, leading to the creation of simulators that can be used for process simulation, prediction purposes, or as a tool for optimizing and designing photobioreactors. These models are also a powerful tool for applying advanced control strategies, where an appropriate optimization of the whole system is performed in an upper layer. On the other hand, dynamic nonlinear first principles-based models are challenging to obtain due to the necessity of previous knowledge about the system and the large number of experimental tests needed to calibrate their parameters.

In addition to mechanistic models, reduced models for control purposes have been developed and applied in many photobioreactor configurations. These models assume certain system dynamics simplifications to reduce the computational complexity

associated with designing and applying control algorithms in nonlinear systems (Guzmán, Acién and Berenguel, 2021).

With the aim to obtain a trade-off between model complexity and performance, Fernández *et al.* (Fernández, Acién, Berenguel, Guzmán, *et al.*, 2014) developed a simplified model that would include the main non-linear dynamics of tubular photobioreactors. This model represented a simplified version of the model presented in (Fernández, Acién, Berenguel and Guzmán, 2014) and can be used for advanced control purposes and as a tool for the design and operation optimization of photobioreactors. The model consisted of fluid-dynamic and mass transfer processes and biological phenomena, all of which are based on chemical, physical, and biological principles. In addition, the model considered the physical characteristics of the photobioreactor. The model was calibrated and validated using a large number of experimental results from a pilot-scale tubular photobioreactor under different solar and culture conditions. This model was used to develop hierarchical control algorithms (Fernández, Berenguel, *et al.*, 2016), reporting a significant reduction in the computation time.

As previously mentioned, microalgae-bacteria processes are complex systems, often described using numerous variables, parameters, and equations. From a control perspective, simplified models are preferred for designing control strategies for low-level feedback control loops. To this end, intermediate and low-complexity models have been developed to capture the dynamics of certain variables in microalgae photobioreactors, such as pH models. Based on the fact the pH of the culture media strongly influences the photosynthesis rate and, consequently, the microalgae biomass production, many studies have focused on developing pH models for control purposes (Fernández *et al.*, 2010; Pawlowski *et al.*, 2019).

In this sense, the pH NARMAX (Nonlinear AutoRegressive Moving Average model with eXogenous inputs) model of 18^{th} order presented in (Fernández, Acién, Berenguel, Guzmán, *et al.*, 2014) was able to describe the main non-linearities of this variable. This model considered the effects of radiation and CO_2 injection over pH dynamics and was validated with real data and compared with first principles-based models. The main drawback of this model was the complexity due to the high order of the parameters obtained. On this context, Pawlowski et al. (Pawlowski *et al.*, 2019) presented another model for pH dynamics, looking for a trade-off between model accuracy and complexity. The Wiener model presented in this work combined linear and nonlinear dynamics. A

first-order linear term was used to represent the main dynamics of pH, while a third-order nonlinear polynomial term was used to represent the nonlinear component. In this work, the model was used in a model-based control approach that allows decoupling the linear and nonlinear terms, making designing control algorithms easy.

Despite the nonlinear nature of variables involved in microalgae processes, linear models have also been used to represent particular dynamics in photobioreactors around specific operation points. For instance, Berenguel et al. (Berenguel *et al.*, 2004) used a linear model to describe the pH dynamics related to the CO_2 injection input and solar radiation through two transfer functions in the Laplace domain. This linear model was used in an on-off model predictive control (MPC) to control pH and minimize CO_2 losses in a microalgal tubular photobioreactor. This simplified model was successfully validated in both open and closed photobioreactors (Fernández *et al.*, 2010; Fernández, Acién, Berenguel, Guzmán, *et al.*, 2014; Pawlowski *et al.*, 2015).

Table 1.1 and Table 1.2 provide a concise overview of the main characteristics and applications of the aforementioned models. As illustrated in Table 1.1, mechanistic microalgae-bacteria models have been predominantly utilized to simulate the dynamics of diverse components under varying operational conditions. These models function as a predictive tool, allowing for the estimation of the relative proportions of microalgae and bacteria within the system. Conversely, in the domain of microalgae cultivation for high-value product production, significant advancements have been made in the development of specific models for control purposes, as illustrated in Table 1.2. The current state of the art in microalgae-bacteria processes modeling encompasses a range of models with successful applications under various photobioreactor configurations and operational conditions. However, the selection of an appropriate model structure for a given application or intended use (prediction, estimation, control, and optimization) remains a challenging task, as does the calibration of models due to the number of implicated parameters, the prevalence of nonlinear dynamics, and potential identifiability issues between model parameters.

Table 1.1. List of mechanistic microalgae-bacteria models and main applications.

Model and Intended use	Model type/ Distinctive characteristics	Model applications	Process/ Reactor type/ Culture media
• **RWQM1** (Reichert *et al.*, 2001)			
River water quality and wastewater treatment modeling. Simulation.	Mechanistic/ Complex model with several parameters.	Assessment of the impact of wastewater effluents and combined sewer overflows (Borchardt and Reichert, 2001).	River Lahn (Germany)
		Simplifications of RWQM1 to study oxygen and nitrogen conversion processes (Reichert, 2001).	River Glatt (Switzerland)
• **Modification of the RWQM1** by (Broekhuizen *et al.*, 2012)			
Modeling and simulation of HRAPs (overcoming the limitations of RWQM1 in modeling HRAPs).	Mechanistic/ Complex model with several parameters.	Simulate microalgae-bacteria interactions in HRAPs. Long term validation.	Wastewater treatment/ Pilot-scale HRAPs/ Domestic wastewater
• **Sah et al.** (Sah *et al.*, 2011)			
Wastewater treatment modeling and simulation in secondary facultative ponds.	Mechanistic/ Combines a 3D hydrodynamic with a mechanistic water quality model.	Evaluate the effect of wind and the addition of baffles on water flow patterns, pond temperature profiles and treatment efficiency. No validation with real data.	Wastewater treatment/ Secondary facultative pond/ Domestic wastewater

• **BIO_ALGAE** (Solimeno *et al.*, 2017a) and **BIO_ALGAE 2** (Solimeno, Gómez-Serrano and Acién, 2019a)			
Modeling and simulation of microalgae-bacteria systems.	Mechanistic/ Includes carbon-limited microalgae and autotrophic bacteria growth, light attenuation, photorespiration, temperature and pH dependency.	Simulate microalgae-bacteria interactions. Predict the microalgae and bacteria proportions in the system. Model calibration and validation (Solimeno *et al.*, 2017a). Long-term validation (Solimeno and García, 2019).	Wastewater treatment/ Pilot-scale HRAPs/ Municipal wastewater
		Predict the microalgae and bacteria proportions in the reactor, estimate daily biomass production. Predict the removal efficiency (Solimeno, Gómez-Serrano and Acién, 2019a).	Wastewater treatment/ Cylindrical-type stirred tank reactors (lab-scale)/ Municipal wastewater. Centrate and manure wastewater.
• **ABACO** (Sánchez-Zurano *et al.*, 2021)			
Wastewater treatment modeling and simulation.	Mechanistic/ Includes the most relevant features of microalgae and bacteria growth. Model calibration using genetic algorithms.	Simulate the dynamics of different components in the system. Predict the relative proportion of microalgae and bacteria in the system. Model calibration and validation.	Wastewater treatment/ Laboratory-scale photobioreactors/ Pig slurry
• **ALBA** (Casagli *et al.*, 2021)			
Wastewater treatment modeling and simulation.	Mechanistic/ Includes the most relevant features of microalgae and bacteria growth. Biological kinetics based on Liebig's minimum law.	Simulate the dynamics of different components in the system under different scenarios. Long-term validation.	Wastewater treatment/ Outdoor pilot-scale HRAP/ Synthetic municipal wastewater

Table 1.2. List of microalgae models intended for control and optimization.

Model and Intended use	Model type/ Distinctive characteristics	Model applications	Process/ Reactor type/ Culture media
• **Dynamic model of microalgae production in tubular** (Fernández *et al.*, 2012; Fernández, Acién, Berenguel and Guzmán, 2014) **and raceway photobioreactors** (Fernández, Acién, *et al.*, 2016)			
Simulation of the effects of different designs and/or operational conditions into the performance of the system. Optimization of design and operation of photobioreactors. Analysis and design of advanced control strategies.	Mechanistic/ The model integrates biological and engineering aspects: in addition to biological phenomena, it also considers fluid dynamics and mass transfer.	Predicting the evolution of the main variables of the system. Determine the values of characteristic parameters. Model calibration and validation	Microalgae production/ Pilot-scale tubular photobioreactor (Fernández *et al.*, 2012)/ Outdoor industrial tubular photobioreactor (Fernández, Acién, Berenguel and Guzmán, 2014)/ Mann and Myers medium using agricultural fertilizers.
		Predicting the evolution of the main variables of the system. Determine the influence of design parameters in the performance of the system. Model calibration and validation (Fernández, Acién, *et al.*, 2016).	Microalgae production/ Pilot-scale HRAP/ Arnon medium using fertilizers
• **Dynamic lumped parameter model for microalgal production in tubular photobioreactors** (Fernández, Acién, Berenguel, Guzmán, *et al.*, 2014)			
Advanced control purposes and as a tool for the design and operation optimization of photobioreactors.	Simplified model/ Based on fundamental principles, maintaining the main physical characteristics and non-linear dynamics.	Development of hierarchical control algorithms (Fernández, Berenguel, *et al.*, 2016), reporting a significant reduction in the computation time.	Microalgae production/ Pilot-scale tubular photobioreactor/ Mann and Myers medium using agricultural fertilizers.

• **Reduced models for pH control**			
pH control minimizing CO_2 losses	Linear model/ Model of the pH evolution based on changes in CO_2 injection and in solar radiation (Berenguel *et al.*, 2004).	Development of a branch-and-bound on–off model-based predictive control strategy. Application in a real photobioreactor (Berenguel *et al.*, 2004)	Microalgae production/ Tubular photobioreactor/ N.S*
		Designing of a PI control and a feedforward compensator to achieve desired regulation properties. Comparison of these control strategies with ON/OFF regulation (Fernández *et al.*, 2010).	Microalgae production/ Tubular photobioreactor/ Filtered sterilized culture medium
pH control in raceway photobioreactors	Wiener model/ Model intended to trade-off between model accuracy and complexity. It combines linear and nonlinear dynamics.	Development of a model-based control approach that allows to decouple the linear and nonlinear terms. Control scheme based on a PID controller and a robust filter (Pawlowski *et al.*, 2019).	Microalgae production/ Raceway photobioreactor/ N.S*

*N.S. (Not specified)

1.1.2. Parameter estimation in microalgae-bacteria processes

The development of a model is an iterative procedure, which can be roughly divided into multiple steps: preliminary analysis, model fitting, and model validation. During the preliminary analysis stage, initial experiments are executed to determine the relation between the process inputs and measurement data. These relations are typically described by dynamic, deterministic models expressed as differential and algebraic equations (DAEs) with a set of parameters that characterize the kinetics of the key processes and chemical reactions. In addition to finding the correct equations to describe process phenomena, new experiments are required to generate measurement data. Utilizing the experimental data, a set of model parameters is found which minimizes the difference between the measured data and the predicted model response. The validation of the model is based on the accuracy of its predictions and the precision of its parameters.

The accuracy of parameter estimation (and, consequently, of the mechanistic model) is significantly influenced by the availability of experimental data. However, it is challenging to obtain a sufficient amount of data, particularly for bioprocesses. This is primarily because cultivation experiments are generally costly and time-consuming, and the measures of the key states of the cultivation are predominantly from analytic procedures, which are significantly scarcer than those measures provided from online sensors.

In order to effectively model microalgae-bacteria interactions and enhance the precision of identified parameters, a meticulous experimental design is imperative to provide data of substantial informative content for the model calibration stage. In many cases, a single experiment is insufficient to estimate the model parameters adequately, and thus the procedure of experiment design, experiment execution, and parameter estimation must be repeated. The experiment design must take into account the limitations on process facilities and the rate of information acquisition, which may be limited by the experimental budget. When monitoring a microalgae-bacteria process, a number of system outputs (typically flow rates, temperature, pH, and dissolved oxygen) are measured continuously, while other responses (typically concentration measurements) can only be acquired by discrete sampling at a significantly reduced sampling frequency. These experimental data are essential both to assess the formal validity of the model and to estimate the model parameters that allow the model to match the process response over the selected range of operating conditions.

In the context of microalgae-bacteria processes, particularly in outdoor facilities, the final experimentation time is of paramount importance. This is because it is essential to record sufficient experimental data to support parameter estimation and model validation. These data must capture both rapid dynamics, occurring within hours, and slow dynamics, occurring over days or even months, within the culture.

The extant literature provides numerous examples of parameter estimation in microalgae and microalgae-bacteria processes, employing a variety of approaches. Irrespective of the parameter estimation approach used (manual trial and error adjustment of parameters, optimization), another important aspect is related to the proper selection of the parameters to be estimated within the entire set of model parameters. This is especially salient in the context of mechanistic models, which are frequently employed to describe microalgae-bacteria interactions and are characterized by an elevated number of parameters. In this sense, different approaches have also been used to determine those parameters with the greatest impact on model outputs that should be estimated.

Parameter estimation via optimization was used to estimate the parameter values of the simplified model developed by Fernández *et al.* (Fernández, Acién, Berenguel, Guzmán, *et al.*, 2014) for tubular microalgae photobioreactors. The estimation of parameters was achieved using a computer program developed in the MATLAB® environment, employing experimental data of the dissolved oxygen and pH of the culture registered for a period of three months. In the validation stage, a distinct dataset, not employed for identification purposes, was utilized to account for both bias and variance errors in the identification procedure. The experimental data for parameter estimation and model validation were recorded under different solar and culture stage conditions.

In the research conducted by Solimeno *et al.* (Solimeno *et al.*, 2015), the Morris's uncertainty method was applied to the screening of parameters with a greater influence on the simulation response. The model for microalgae growth was calibrated using a manual trial-and-error procedure to adjust the values of the maximum specific growth rate of microalgae and the mass transfer coefficients. The calibration was conducted by comparing simulated and experimental data from a microalgae culture. Details of the application of the Morris method of elementary effects to perform a global sensitivity analysis were illustrated in (Solimeno, Samsó and García, 2016) using the same initial conditions, parameter values, and geometry as in the previous work of the authors (Solimeno *et al.*, 2015). Furthermore, uncertainty parameters derived from a prior

sensitivity analysis (Solimeno, Samsó and García, 2016) were calibrated for two different tubular photobioreactors (Solimeno, Acien and García, 2017), thereby substantiating the impact of these parameters on model outputs across diverse photobioreactor configurations and operational conditions.

In the same way, a Morris sensitivity analysis was conducted to evaluate the parameters that predominantly influenced the simulation response of the BIO_ALGAE model in duplicated microalgae-bacteria pilot raceway ponds (Solimeno *et al.*, 2017a). The microalgae and heterotrophic bacteria parameters, as well as the mass transfer coefficients, were calibrated in order to fit the model outputs with the experimental data. Given the pivotal role of mass transfer coefficients over model response, these parameters were also calibrated in a pilot microalgae-bacteria photobioreactor (Solimeno, Gómez-Serrano and Acién, 2019a).

The sensitivity analysis was also employed in the research conducted by Casagli *et al.* (Casagli *et al.*, 2021) to ascertain the most sensitive parameters of the ALBA model. The sensitivity analysis was carried out using the AQUASIM toolboxes (Reichert, 1994) and accounting for the environmental conditions that define each season pattern. Consequently, the parameters to be calibrated are the most sensitive ones in every season investigated. Parameter values were obtained via optimization using a cost function which minimizes the sum of square errors between simulated and experimental data weighted by standard deviations. The model was calibrated and successfully validated using an original data set recorded from an outdoor demonstrative raceway pond treating synthetic wastewater for fifteen months. Model calibration was performed using a data set from autumn and winter (29 days), while model validity was assessed using the data from the monitoring campaign which were not used during calibration (414 days). The model exhibited a remarkable capacity to accurately replicate the experimental data trend across all seasons, employing a unique set of parameters. This finding serves to substantiate the robustness of the model and the precision of the parameter estimation procedure utilized.

Parameter estimation using genetic algorithms was carried out in laboratory-scale microalgae-bacteria photobioreactors fed with pig slurry (Sánchez-Zurano *et al.*, 2021). The use of genetic algorithms for calibration proved to be a valuable and reliable approach for the estimation of uncertain parameters. In this study, genetic algorithms were employed to minimize a cost function, which quantifies the discrepancy between the model output and the actual output of the system by modifying the parameter values

within predefined limits. This calibration procedure facilitated the estimation of the values of 17 model parameters of the ABACO model. In addition to parameter estimation, the genetic algorithm method was also employed to determine the initial percentage of each species in the photobioreactor. The calibration process using genetic algorithms was implemented in MATLAB® software using the Genetic Algorithm Optimization Toolbox. This calibration procedure offers a straightforward and efficient approach to adjusting the model parameters, facilitating recalibration with different scenarios, such as different strains and culture media, with minimal effort.

Table 1.3 provides a synopsis of different approaches used for model calibration. Furthermore, Table 1.3 provides a comprehensive overview of the key parameters estimated in microalgae and microalgae-bacteria models. Despite the extensive research conducted on the growth rates of various microorganisms, the growth of microalgae and bacteria in wastewater is characterized by significant variability in model parameters. This variability is influenced by the composition of the wastewater. Moreover, microalgae-bacteria-based wastewater treatment systems comprise a consortium of diverse microalgae and bacteria strains, with fluctuating proportions of microorganisms over time. Furthermore, HRAPs are vulnerable to contamination, which can result in alterations in microbial population dynamics. Additionally, the identification of each microorganism strain present in the culture to ascertain its specific biokinetic parameters is a resource-intensive and often unfeasible task. This underscores the predominant approach in extant literature, which involves the estimation of biokinetic parameters for each microorganism group, as opposed to distinguishing between the parameter estimation for each individual strain. This underscores the necessity of model parameter estimation for each specific situation. Model calibration through a trial-and-error approach can yield satisfactory results when a limited number of parameters and model outputs is considered. Conversely, when the objective is to estimate multiple parameters and adjust a comprehensive set of outputs, optimization-based methods should be used.

Table 1.3. Parameter estimation approaches in microalgae and microalgae-bacteria processes

Model (Reference)	Parameter estimation approach/ Details	Main calibrated or estimated parameters
Dynamic lumped parameter model for microalgal production (Fernández, Acién, Berenguel, Guzmán, *et al.*, 2014).	Using optimization. The optimization problem was solved using a sequential quadratic programming (SQP) method.	Light availability in each part of the photobioreactor and the extinction coefficient. Maximum photosynthesis rate, form parameters, respiration rate. Volumetric gas-liquid coefficients for the bubble column and the external loop.
Mechanistic model to simulate microalgae growth (Solimeno *et al.*, 2015; Solimeno, Samsó and García, 2016).	Using manual trial-and-error procedure for calibration. The Morris's uncertainty method was applied to determine the parameters with a greater influence on the simulation response (Solimeno *et al.*, 2015, 2017a; Solimeno, Samsó and García, 2016).	The maximum specific growth rate of microalgae. Mass transfer coefficients for oxygen, carbon dioxide, and ammonia.
Mechanistic model to simulate microalgae growth (Solimeno, Acien and García, 2017).		The maximum specific growth rate of microalgae. Mass transfer coefficients for oxygen and carbon dioxide
BIO_ALGAE (Solimeno *et al.*, 2017a)		The maximum specific growth rate of microalgae. The maximum growth and decay rate of heterotrophic bacteria. Mass transfer coefficients for oxygen, carbon dioxide, and ammonia.
BIO_ALGAE 2 (Solimeno, Gómez-Serrano and Acién, 2019a)		Mass transfer coefficients for oxygen, carbon dioxide, and ammonia.

ALBA (Casagli *et al.*, 2021)	Using optimization. Sensitivity analysis was employed to ascertain the most sensitive parameters of the model.	The maximum specific growth rate of microalgae, ammonium oxidizing bacteria, and nitrite oxidizing bacteria. Light optimal value for growth and light extinction coefficient. Mass transfer coefficient. Coefficients for temperature correction for hydrolysis and ammonification. Cardinal temperature values for microalgae, heterotrophic bacteria, and nitrifying bacteria. Cardinal pH values for microalgae, heterotrophic bacteria, and nitrifying bacteria.
ABACO (Sánchez-Zurano *et al.*, 2021)	Using optimization. Parameter estimation was carried out using genetic algorithms.	The maximum specific growth rate of microalgae, heterotrophic bacteria, and nitrifying bacteria. Maximum and minimum microalgae endogenous respiration rate. Microalgae consumption rate of ammonium, nitrate, and phosphate. Heterotrophic bacteria consumption rate of ammonium and phosphate. Nitrifying bacteria consumption rate of ammonium and phosphate. Biodegradable soluble organic matter (BSOM) generation rate from microalgae, heterotrophic bacteria, and nitrifying bacteria. BSOM consumption rate from heterotrophic bacteria. Nitrate generation rate from nitrifying bacteria

1.1.3. State estimation in microalgae processes

Advanced control strategies have emerged as promising instruments to enhance the performance of microalgae production systems, particularly within the context of large-scale cultivation plants (Tebbani, Lopes and Becerra Celis, 2015). The implementation of state feedback control laws and model-based control techniques, such as MPC, necessitates complete online information of the system. However, in practical scenarios, only a subset of the states or key variables of microalgae-bacteria processes can be measured online due to the necessity for more reliable measuring devices or the high cost of on-line sensors (Mohd Ali *et al.*, 2015).

The basic hardware instrumentation in microalgae-bacteria-based wastewater treatment plants typically provides online measurements of temperature, pH, dissolved oxygen, and flow rate. However, this is not the case for other component concentrations (biomass, substrates, and metabolites), which are crucial for understanding the system state. Despite of the significant progress in the field, many current hardware sensors for concentration measurement still exhibit significant drawbacks, including expensive probes, discrete-time measurements, and offline solutions, among others. Consequently, state estimators (often termed software sensors) emerge as a promising alternative to determine the non-measurable states and concurrently reduce the utilization of costly sensors.

State estimators typically use a dynamical model of the process, knowledge about the applied inputs, and the availability of hardware sensors to measure some state components to estimate unmeasured state variables. Their application is crucial, as they help preventing process disruptions, shutdowns, and the severe consequences of process failures (Mohd Ali *et al.*, 2015). The diversity of state estimation techniques arising from intrinsic differences in chemical process systems underscores the importance of selecting the proper technique for design and implementation in specific applications.

The seminal contributions of Luenberger (Luenberger, 1964, 1966, 1967, 1971) and Kalman (Kalman, 1960; Kalman and Bucy, 1961) in the 1960s laid the foundation for the development of state observers and Kalman Filter (KF)-based estimators. However, over the years, research in the design of state estimators has become increasingly popular yet challenging due to the requirements of high accuracy, low cost, and good prediction performances.

In the case of linear systems, the standard solutions are the Kalman filter and the Luenberger observer. Today, many estimators are simply modifications and extended

versions of the classical Luenberger observer and Kalman filter. However, in the context of bioprocesses, the estimator design problem is particularly challenging. In addition to the scarcity of online measurements, additional challenges are presented by considerable nonlinearities in the cultivation and the consequent modeling complexity. In recent years, multiple observers and estimators applied to estimate state variables in biochemical processes have emerged (Haverbeke *et al.*, 2008; Bogaerts and Coutinho, 2014; Araujo Pimentel *et al.*, 2015; Dewasme *et al.*, 2015; Moreno and Alvarez, 2015; Yoo *et al.*, 2015; Yin, Decardi-Nelson and Liu, 2018; Tuveri *et al.*, 2023).

In the context of microalgae processes, a range of observers and state estimators have been employed. Therefore, distinguishing between these approaches is imperative to facilitate a comprehensive understanding. Fundamentally, the observer design (as the case of Luenberger-based observers) is predicated on perfect knowledge of system parameters.

Considering a bioprocess described by the continuous-time nonlinear system in state-space form in equations (1.1) - (1.2):

$$\dot{\mathbf{x}} = F(\mathbf{x}, \mathbf{u}) \coloneqq f(\mathbf{x}) + g(\mathbf{x})\mathbf{u} \tag{1.1}$$

$$\mathbf{y} = h(\mathbf{x}) \tag{1.2}$$

where the state vector is $\mathbf{x} = [x_1 \quad , \cdots, \quad x_n]^T \in \mathbb{R}^n$, the output vector is $\mathbf{y} = [y_1 \quad , \cdots, \quad y_q]^T \in \mathbb{R}^q$, and the input vector is $\mathbf{u} = [u_1 \quad , \cdots, \quad u_m]^T \in \mathbb{R}^m$. $F(\mathbf{x}, \mathbf{u})$ is a nonlinear function with respect to x and u. The function $f(\cdot), g(\cdot)$ and $h(\cdot)$ are matrices of dimension $n \times 1$, $n \times m$, and $q \times 1$, respectively.

The Extended Luenberger observer (ELO) has been proposed for nonlinear processes as natural extension of Luenberger observer. The goal of the state observer is to provide an estimation of the unmeasured internal states of a given system by utilizing measured states from the process along with the implemented inputs. The extended Luenberger observer for the nonlinear system of equation (1.1) is:

$$\hat{\mathbf{x}} = F(\hat{\mathbf{x}}, \mathbf{u}) + \mathbf{K}(\mathbf{y} - h(\hat{\mathbf{x}})) \tag{1.3}$$

where $\hat{\mathbf{x}}$ represents the estimated state vector, and the observer gain is denoted by $\mathbf{K}$. It is observed from equation (1.3) that the first term is the process model, and the second term $\mathbf{K}(\mathbf{y} - h(\hat{\mathbf{x}}))$ is known as the output prediction error, which is considered as a correction term.

The goal of the ELO is to minimize the estimation error ($\mathbf{e} = \mathbf{x} - \hat{\mathbf{x}}$), in which the dynamic of the error is determined by equation (1.4):

$$\dot{\mathbf{e}} = F(\hat{\mathbf{x}} + \boldsymbol{e}, \mathbf{u}) - F(\hat{\mathbf{x}}, \mathbf{u}) - \mathbf{K}(h(\hat{\mathbf{x}} + \boldsymbol{e}) - h(\hat{\mathbf{x}})) \tag{1.4}$$

As shown in equation (1.4), the problem is to determine in which conditions $\boldsymbol{e}$ can decay to zero. Therefore, it is important to design **K** to achieve this goal.

As mentioned above, the observer formulation assumes perfect knowledge of the system parameters, a condition that is far from being met in microalgae-based processes, where uncertainties in model parameters and noise are common. In such cases, the use of an estimator design based on probability distributions and mathematical inference of the system is preferable.

The Extended Kalman Filter (EKF) is a simple and widely used estimator for nonlinear systems because the estimation of unknown variables is not limited to state estimation, but also includes the estimation of unknown parameters and noise in the formulation. The model of equations (1.1) - (1.2) has been restructured to the form of equations (1.5) - (1.6) to be represented in discrete time (where k represents the actual time instant) in order to formulate the EKF algorithm:

$$x_k = f\left(x_{k-1}, u_{s_k}\right) + w_{k-1} \tag{1.5}$$

$$y_k = h\left(x_k, u_{m_k}\right) + v_k \tag{1.6}$$

where **x** is the state vector of the model, f is the nonlinear state transition function, and h is a function that relates the state vector with the measurable outputs of the model. Functions f and h have input arguments denoted as u_s and u_m, respectively. These arguments can be the process inputs for function f, for example. Process noise (w) and measurement noise (v) are assumed to be zero-mean white noises, with no correlation and with covariance matrices Q and R, respectively:

$$w_k \sim (0, Q) \tag{1.7}$$

$$v_k \sim (0, Q) \tag{1.8}$$

The recursive Kalman filter algorithm consists of two steps: correction (a *priori* estimation) and prediction (a *posteriori* estimation). In the correction step, the predicted state vector is updated with the available information from the measurable variables of the process. In the prediction step, estimation for the states is generated based on the previous values of the state vector.

The designed state estimator initially performs (in each cycle) the correction step because measurable variables are always available from the beginning. In the initialization step given by equations (1.9) and (1.10), the state estimator is initialized based on a first value for the state vector ($\mathbf{x_0}$). The predicted state vector and state estimation covariance are denoted as $\hat{\mathbf{x}}$ and **P**, respectively.

$$\hat{\mathbf{x}}_{0|-1} = E(x_0) \tag{1.9}$$

$$\mathbf{P}_{0|-1} = E\left[\left(x_0 - \hat{x}_{0|-1}\right)\left(x_0 - \hat{x}_{0|-1}\right)^T\right] \tag{1.10}$$

In the correction step, given by equations (1.11) - (1.13), the predicted state vector is corrected using real output measurement data (**y**), the Kalman gain (**K**) is computed, and state estimation covariance is updated.

$$\hat{\mathbf{x}}_{k|k} = \hat{\mathbf{x}}_{k|k-1} + \mathbf{K}_k\left(\mathbf{y}_k - h\left(\hat{\mathbf{x}}_{k|k-1}, u_{m_k}\right)\right) \tag{1.11}$$

$$\mathbf{K}_k = \mathbf{P}_{k|k-1}\mathbf{C}_k^T\left(\mathbf{C}_k\mathbf{P}_{k|k-1}\mathbf{C}_k^T + \mathbf{S}_k\mathbf{R}_{k|k-1}\mathbf{S}_k^T\right)^{-1} \tag{1.12}$$

$$\mathbf{P}_{k|k} = \mathbf{P}_{k|k-1} - \mathbf{K}_k\mathbf{C}_k\mathbf{P}_{k|k-1} \tag{1.13}$$

where the Jacobians **C** and **S** are defined in equations (1.14) - (1.15):

$$\boldsymbol{C}_k = \left.\frac{\partial h}{\partial x}\right|_{\hat{x}_{k|k-1}} \tag{1.14}$$

$$\mathbf{S}_k = \left.\frac{\partial h}{\partial v}\right|_{\hat{x}_{k|k-1}} \tag{1.15}$$

In the prediction step, the future state vector and the state estimation covariance are predicted according to equations (1.16) and (1.17):

$$\hat{x}_{k+1|k} = f\left(\hat{x}_{k|k}, u_{s_k}\right) \tag{1.16}$$

$$P_{k+1|k} = A_k P_{k|k} A_k^T + G_k Q G_k^T \tag{1.17}$$

where the Jacobians for the state transition function are defined in equations (1.18) and (1.19):

$$A_k = \left.\frac{\partial f}{\partial x}\right|_{\hat{x}_{k|k}} \tag{1.18}$$

$$G_k = \left.\frac{\partial f}{\partial w}\right|_{\hat{x}_{k|k}} \tag{1.19}$$

Kalman filter-based estimators are the most applied estimators in microalgae cultivation (Su, Li and Xu, 2003; Tebbani, Lopes and Becerra Celis, 2015; García-Mañas *et al.*, 2019), mainly in processes using real data. The current state of the art regarding KF-based estimators in microalgae processes includes various reports of estimators applied together with control and optimization techniques due to the necessity of the entire state vector for system monitoring and control (Tebbani, Lopes and Becerra Celis, 2015; Yoo *et al.*, 2016; García-Mañas *et al.*, 2019). These applications have mainly focused on estimating biomass concentration because the online monitoring of biomass concentration is a crucial aspect of photobioreactor operation to optimize its performance (García-Mañas *et al.*, 2019), while using online measurements remains challenging today.

Of the nonlinear filtering methods, the EKF method has received most attention due to its relative simplicity and demonstrated effectiveness in handling some nonlinear systems. An Extended Kalman Filter was used in a lab-scale photobioreactor (Li, Xu and Su, 2003) to estimate a photobioreactor's biomass density, dissolved oxygen concentration, and average light intensity based on incident light information and online dissolved oxygen measurement.

The EKF was also employed to estimate the biomass concentration in a bubble column photobioreactor with a total culture volume of 9.6 L (Tebbani, Lopes and Becerra Celis, 2015). On-line measurements of dissolved carbon dioxide, pH, and incident light intensity were used for the estimation. The estimation was conducted to propose a control strategy to regulate biomass concentration in a photobioreactor. The efficacy of this approach was validated with experimental data.

To account for discrete-time measurements with different sampling rates, a continuous-discrete EKF was proposed (Jerono, Schaum and Meurer, 2018) and tested with experimental data for the growth of *Haematococcus pluvialis* in a lab-scale photobioreactor. This study addressed the problem of state estimation with biased optical measurements. The EKF developed estimated the biomass and nitrate concentrations based on offline nitrate and optical density measurements, and biased online optical density measurements.

In the research conducted by Tebbani *et al*, an Unscented Kalman filter (UKF) methodology was proposed to estimate the biomass, carbon dioxide, and oxygen

concentrations in the liquid phase of a torus photobioreactor (Tebbani, Titica, *et al.*, 2013). Online measurements of CO_2 and O_2 molar fractions in the output gas, pH, temperature, and input and output flow rates were used for the estimation.

Unlike previous research conducted in lab-scale photobioreactors, García Mañas and co-workers developed a state estimator using the EKF algorithm to estimate the biomass concentration in an outdoor industrial raceway photobioreactor (García-Mañas *et al.*, 2019). The state estimator was based on a dynamic model for microalgae production for this type of photobioreactor (Fernández, Acién, *et al.*, 2016). In this work, the EKF accurately estimated the biomass concentration using the available experimental measurements of dissolved oxygen, pH, gas injections, and solar radiation. The low estimation times obtained confirmed the potentialities of the state estimation techniques in automatic process control.

In addition to the prevalent utilization of KF-based estimators, alternative design methodologies have been employed in the context of microalgae cultivation, predominantly within the scope of simulations. The Filtered High Gain Observer (FHGO) was used to estimate the biomass and carbon dioxide concentrations, assuming measures of the average light intensity (Farza *et al.*, 2019). The FHGO was first designed by assuming continuous measurements of the system outputs, and then redesigned to account for the sampling period of these outputs. The comparison of the obtained estimates with estimates provided by a Standard High Gain Observer (SHGO) demonstrated the filtering capabilities of the proposed FHGO (Farza *et al.*, 2019).

The nonlinear integral high-gain observer (NL-PI) was also used to estimate the substrate concentration in a wastewater treatment photobioreactor (Rodríguez-Mata *et al.*, 2011). This estimator proved to be able to cancel the dynamical disturbances due to parameter changes.

Besides the previously works mainly focused on estimating biomass concentration in microalgae cultures, state estimation techniques have also been applied to estimating specific components of the microalgal biomass. Microalgal biomass is a valuable source of lipids, proteins, carbohydrates, pigments, and vitamins. These components are intracellular and can be separated and upgraded into various products in the biofuel, food, fodder, cosmetic, and pharmaceutical industries. Efficient medium- and large-scale microalgal cultivations require online monitoring methods to control these processes. The online monitoring of these components in these processes is complicated due to their

intracellular nature. For this reason, online sensors measuring these biological components are yet in an early developmental stage. The reviews presented by Havlik *et al.* (Havlik *et al.*, 2022) and Porras *et al.* (Porras Reyes, Havlik and Beutel, 2024) discussed the current state of the art and future outlook in the design and use of software sensors in the monitoring of biological parameters, primarily concentrations of intracellular components.

Kalman filter-based estimators have been extensively applied to bioprocesses, often yielding satisfactory results, provided that linear approximation remains valid, the signal has low noise, and constraints are negligible. Another approach for nonlinear systems that has gained popularity over the past two decades among researchers and industrial practitioners of MPC is the Moving Horizon Estimation (MHE) approach (Rawlings and Bakshi, 2006; Rawlings, 2014; Alessandri and Battistelli, 2020). This approach formulates the state estimation problem as an optimization problem over a moving time window, akin to the MPC formulation. The strategy of MHE has been demonstrated to exhibit numerous advantages over other nonlinear state estimation techniques. It has the capacity to incorporate a priori process knowledge by including constraints on the estimated states and disturbances. Furthermore, its performance is frequently superior because nonlinear model equations can be used directly without the necessity of linearization. A salient benefit of this approach is its capacity to generate both filtered and smoothed estimates of states within the same window. A notable benefit of the MHE formulation is its ability to estimate states and parameters in a concurrent manner, as well as modeling inaccuracies.

The aforementioned confirms MHE as a more powerful (but complicated) estimation method, with certain applications in bioprocesses (Raïssi, Ramdani and Candau, 2005; Tebbani, Le Brusquet, *et al.*, 2013; Elsheikh *et al.*, 2021), including the state estimation in conventional wastewater treatment plants (Arnold and Dietze, 2001; Busch *et al.*, 2013; Yin, Decardi-Nelson and Liu, 2018).

As illustrated in Table 1.4, a compendium of state estimators and observers has been applied in the context of microalgae processes. A thorough examination of this review discloses a prevailing emphasis on Kalman Filter-based estimators. Conversely, the application of MHE is restricted to a limited number of research works (Abdollahi and Dubljevic, 2012). The inherent nonlinear characteristics of microalgae-based wastewater treatment processes, coupled with the operational constraints associated with these

processes, underscore the viability of MHE as a solution to the state estimation problem in this context. This assertion is further supported by previous experience in applying MHE to other biological and conventional wastewater treatment processes. However, a review of the literature reveals that MHE has not yet been applied for state estimation in microalgae-based wastewater treatment processes.

Table 1.4. State estimators and observers applied in microalgae processes

Observer/ estimator	Available measurements	States/parameters estimated	Application Process/ Reactor type (Reference)
EKF	Local irradiance (using a quantum sensor).	Biomass concentration and microalgae specific growth rate. Phosphate and dissolved oxygen concentrations.	*Dunaliella salina* culture in a 3 L stirred tank microalgal photobioreactor (Su, Li and Xu, 2003).
EKF	Incident light information and online dissolved oxygen measurement.	Biomass density, microalgae specific growth rate, photosynthetic efficiency, and average light intensity in the photobioreactor	*Dunaliella salina* culture in a 3 L stirred tank microalgal photobioreactor (Li, Xu and Su, 2003).
NL-PI	Biomass.	Substrate concentration.	Simulation study considering a batch culture of *Spirulina maxima* for the pollutant removal in a wastewater treatment photobioreactor (Rodríguez-Mata *et al.*, 2011)
MHE	Biomass, glucose, and lipid content.	Nitrogen concentration	Simulation study considering the heterotrophic growth and lipid production of *Auxenochlorella protothecoides* in a fed-batch bioreactor (Abdollahi and Dubljevic, 2012).
UKF	Online measurements of CO_2 and O_2 molar fractions in the output gas (provided by a mass spectrometer).	Biomass concentration, carbon dioxide and oxygen concentrations in the liquid phase.	*Chlamydomonas reinhardtii c*ulture in a 1.5 L torus photobioreactor (Tebbani, Titica, *et al.*, 2013).
Interval observer	pH and dissolved CO_2 concentration.	Biomass concentration.	*Chlorella vulgaris* culture in a laboratory-scale bubble column photobioreactor (9.6 L) (Tebbani *et al.*, 2014).
EKF	Online measurements of pH, incident light intensity and dissolved carbon dioxide concentration.	Biomass concentration.	*Porphyridium purpureum* culture in a 9.6 L bubble column photobioreactor (Tebbani, Lopes and Becerra Celis, 2015).

UKF	Biomass and glucose data.	Lipid concentration.	*Chlorella protothecoides* culture in a 3 L photobioreactor (Yoo *et al.*, 2016).
EKF	Online and offline optical density measurements, offline nitrate measurements.	Biomass and nitrate concentration.	*Haematococcus pluvialis* culture in a 2 L photobioreactor (Jerono, Schaum and Meurer, 2018).
FHGO	Average light intensity irradiated over the photobioreactor.	Biomass concentration and dissolved carbon dioxide concentration.	Simulation study (Farza *et al.*, 2019).
EKF	Online measurements of pH and dissolved oxygen concentration.	Biomass concentration	*Scenedesmus almeriensis* culture in an outdoor industrial raceway photobioreactor (García-Mañas *et al.*, 2019).

1.1.4. Control and optimization of microalgae-bacteria processes

The literature is rich with a diverse array of control strategies for operating photobioreactors, whether they are closed photobioreactors designed to produce high-added-value products or raceway reactors used for wastewater treatment.

Regardless of the photobioreactor configuration and the process goal, the pH of the culture media must be controlled through the injection of carbon dioxide. This is because pH significantly influences the photosynthesis rate and the speciation of CO_2 and NH_3, directly affecting biomass productivity. Several research works have proposed a variety of strategies for pH control, ranging from ON/OFF control and conventional Proportional Integral (PI) controllers to advanced control strategies (Guzmán, Acién and Berenguel, 2021).

Classic PI controllers with feedforward scheme were developed based on simplified linear models for pH control in tubular (Fernández *et al.*, 2010) and vertical flat panel (Buehner *et al.*, 2009) photobioreactors. A Filtered Smith Predictor (FSP) strategy (which includes a PI controller), was proposed to tackle the problem of pH control in processes with significant time delay due to pH sensor location (Romero-García *et al.*, 2012). The PI controller was also employed for the pH control in both raceway and thin-layer photobioreactors for wastewater treatment (Rodríguez-Torres *et al.*, 2021), thereby demonstrating the enhancement of system performance in comparison to the ON/OFF control strategy regarding to CO_2 consumption.

The supply of carbon dioxide represents a significant cost in microalgae production processes, particularly pronounced in cultures in tubular photobioreactors. Here, pH control is achieved by injecting pure carbon dioxide, a process that can account for up to 30% of the overall microalgae production cost (Acién *et al.*, 2012). Several control strategies have been developed to regulate pH and minimize CO_2 losses in different photobioreactor configurations to address this. MPC strategies have been applied to accomplish this goal, ranging from MPC using linear models (Berenguel *et al.*, 2004; Hoyo *et al.*, 2019) to event-based Generalized Predictive Controllers (GPC) (Pawlowski, Fernández, *et al.*, 2014; Pawlowski, Mendoza, *et al.*, 2014). A learning-based model predictive control strategy (LBMPC) for pH control in raceway photobioreactors was also developed to deal with model uncertainties (Pataro *et al.*, 2023). The validity of the strategy was confirmed through experimental validation using freshwater and wastewater culture media. A comparison was made between the strategy and the conventional

nominal MPC approach. The results demonstrated the superior performance of LBMPC in comparison to the conventional MPC strategy.

Literature also encompasses the utilization of alternative strategies for pH regulation in different photobioreactor configurations, including the sliding mode control (SMC) (de Andrade et al., 2016), the event-based PI control (Rodríguez-Miranda *et al.*, 2019, 2020), the robust control (Hoyo *et al.*, 2022), and the linear active disturbance rejection control (Carreño-Zagarra *et al.*, 2019). The application of parameter adaptation techniques has also been employed in the context of pH control in raceway reactors (Caparroz *et al.*, 2023). In this final work, the utilization of regression tree models for the purpose of predicting pH enables the adjustment of the PI controller parameters according to the model selected in the regression tree.

The dissolved oxygen concentration is another variable that significantly influences the microalgae photosynthesis rate. High concentrations of dissolved oxygen in the cultures pose a severe inhibition of microalgae growth, necessitating the use of aeration or stirring mechanisms as a solution. However, the application of the aeration mechanism can lead to a deterioration in CO_2 assimilation (for pH control), thereby complicating the control task. To overcome this issue, a selective event-based control approach was proposed for simultaneous control of the pH of the culture media and the dissolved oxygen concentration (Pawlowski *et al.*, 2015, 2017). The application of a selective event-based scheme allowed for improved biomass productivity since the controlled variables were kept within limits for an optimal photosynthesis rate. Moreover, this control scheme allowed for effective CO_2 utilization and energy minimization for the aeration system. The event-based control system configurations were evaluated in both tubular and raceway photobioreactors by Pawlowski and coworkers (Pawlowski *et al.*, 2017). Furthermore, the impact of different pH and dissolved oxygen control strategies on the efficacy of pilot-scale microalgae production were appraised for two distinct culture media: one comprising clean water plus fertilizers and the other comprising wastewater (Nordio *et al.*, 2023). This investigation yielded invaluable insights into the substantial phenomena that ensue when a consortium of multiple biological groups is present.

A novel control scheme approach for the dissolved oxygen concentration was proposed using a PI controller and a variable mass transfer coefficient (Barceló-Villalobos *et al.*, 2022). The proposed control algorithm permits the implementation of variable air-gas injections, thereby enhancing biomass productivity while reducing injection costs.

The monitoring and control of biomass concentration in photobioreactors is of paramount importance for two reasons. Firstly, the biomass yield should be optimized in order to maximize economic profit. Secondly, high biomass concentrations within the reactor affect the penetration of solar radiation into the culture, which in turn affects the growth of microalgae. In order to achieve this objective, a number of control strategies have been proposed in the literature at both simulation and laboratory scales (Mailleret, Gouzé and Bernard, 2005; Ifrim *et al.*, 2013; Tebbani, Lopes and Becerra Celis, 2015). Moreover, some of the proposed strategies simultaneously consider pH control of the culture media (Ifrim *et al.*, 2013; Tebbani, Lopes and Becerra Celis, 2015). Therefore, the most suitable approach involves the use of advanced control strategies, which will facilitate achieving optimal biomass production while maintaining the desired operational conditions and minimizing resource utilization.

The research conducted by Tebbani *et al.* (Tebbani *et al.*, 2014) proposed the application of a nonlinear model predictive control (NMPC) strategy for maximizing the carbon dioxide fixation rate of the green microalga *Chlorella vulgaris* (by maximizing the biomass productivity). The optimization problem was solved using control vector parameterization (CVP) techniques and an interval observer was developed to estimate the biomass concentration based on online dissolved CO_2 measurements. The approach presented in this study was validated experimentally, confirming the advantages of advanced control strategies in microalgae cultivation control and optimization.

Additionally, optimal and near-optimal strategies were developed with the objective of maximizing biomass production in outdoor tubular photobioreactors (Gustavo. A. de Andrade *et al.*, 2016). The optimization system calculates the culture medium flow rate with the objective of optimizing biomass production over the course of one day. Given the outdoor conditions, the approach considered the influence of sunlight, day/night phases, and the auto-shading effect, all of which influence the biological activity within the reactor. The results of the proposed strategies were validated in simulation and with experimental data.

To maximize the biomass productivity of the microalgae *Scenedesmus* AMDD, a model-based approach was proposed in a continuously operated photobioreactor (McGinn *et al.*, 2017). In the proposed approach, a simple mathematical model was utilized to solve the real-time optimization (RTO) problem, and then the optimal solution was implemented via flow control based on real-time cell density estimations. The proposed approach

demonstrated an improvement of 70% compared to the same photobioreactor operated as a turbidostat.

The problem of biomass growth control was also addressed from a hierarchical perspective, employing a receding horizon strategy (Fernández, Berenguel, *et al.*, 2016). The hierarchical control strategy for microalgal production in a tubular photobioreactor was composed of two layers. The lower layer is responsible for tracking the pH set-point through the use of a PI controller in conjunction with a feed-forward compensator. The upper layer of the control scheme calculates optimal pH set-points based on an economic model predictive control (eMPC) approach. The objective of the proposed control scheme was to maximize profits, which were computed as the difference between the incomes obtained from the final production sale and the associated production costs (including the environmental impact of the exhausted CO_2 losses). This hierarchical control architecture demonstrated improvements with respect to a static reference tracking used in this kind of system in terms of cost savings.

Table 1.5 and Table 1.6 provide a synopsis of the control and optimization strategies, respectively, that have been implemented in the context of microalgae production and microalgae-based wastewater treatment. A thorough examination of the data presented in these tables suggests a more widespread implementation of control strategies in microalgae production systems. The principal objective of the control strategies implemented within microalgae-bacteria photobioreactors was directed toward regulating specific variables, such as pH or biomass concentration, to maintain the desired operational conditions, while disregarding the monitoring of other process variables. Nevertheless, the mounting global concern over ensuring effluent quality and the numerous perturbations that affect wastewater treatment processes require the development of control and optimization approaches capable of maintaining operational conditions while achieving the stipulated discharge limits set by legislation.

Moreover, a considerable proportion of the control and optimization strategies documented in the extant literature for such processes assume a perfect model, an assumption that is not realistic in the context of microalgae-bacteria processes. Additionally, the paucity of online measures of many pertinent variables entails a high degree of complexity in the design and implementation of control and optimization strategies. In this regard, the development of strategies that consider model uncertainties is imperative to propose adequate formulations for microalgae-bacteria processes.

Table 1.5. Control strategies applied in microalgae and microalgae-bacteria processes

	Control strategies	Controlled variables	Application Process/ Reactor type (Reference)
PID and PID-based strategies	PI+feed-forward controller	pH	*Nannochloropsis oculata* culture in a vertical flat panel photobioreactor (644 L) (Buehner *et al.*, 2009). *Scenedemus almeriensis* culture in a tubular photobioreactor (2600 L) (Fernández *et al.*, 2010).
	FSP strategy	pH	*Scenedemus almeriensis* culture in an industrial tubular photobioreactor (3 m^3) (Romero-García *et al.*, 2012).
	Robust PI control with linear active disturbance rejection	pH	Microalgae culture in a raceway reactor (20 m^3) (Carreño-Zagarra *et al.*, 2019).
	Event-based PI control	pH	Simulation study of the *Scenedesmus almeriensis* culture in a raceway reactor (20 m^3) (Rodríguez-Miranda *et al.*, 2019). *Golenkinia* culture in a raceway reactor (10 m^3) (Rodríguez-Miranda *et al.*, 2020).
	PI	pH	Raceway (1m^3) and thin-layer (0.45m^3) reactors for wastewater treatment (Rodríguez-Torres *et al.*, 2021).
	Robust PID control	pH	*Scenedesmus almeriensis* culture in a raceway reactor (Hoyo *et al.*, 2022).
	PI	Dissolved oxygen concentration	*Scenedesmus almeriensis* culture in an industrial raceway photobioreactor (80 m^2) (Barceló-Villalobos *et al.*, 2022).
	PI control with parameter adaptation	pH	Simulation study of a raceway reactor treating freshwater (Caparroz *et al.*, 2023).
MPC	Event-based GPC	pH	Microalgae culture in a raceway reactor (20 m^3) (Pawlowski, Mendoza, *et al.*, 2014). *Scenedesmus almeriensis* culture in a tubular photobioreactor (2600 L) (Pawlowski, Fernández, *et al.*, 2014).
	MPC using linear models	pH	Microalgae culture in a raceway reactor (20 m^3) (Hoyo *et al.*, 2019).
	LBMPC	pH	Two raceway reactors (20 m^3): one operated with freshwater plus fertilizers and the other one with wastewater as the nutrient source (Pataro *et al.*, 2023).

Other strategies	SMC	pH	*Scenedesmus almeriensis* culture in a tubular photobioreactor (2600 L) (de Andrade et al., 2016).
	Selective event-based control approach.	pH and dissolved oxygen concentration	Microalgae culture in a raceway reactor (20 m^3) (Pawlowski *et al.*, 2015).
	Selective event-based control approach. Simultaneous control strategy using ON/OFF control.	pH and dissolved oxygen concentration	Two pilot-scale raceway reactors (80 m^2): one operated with freshwater plus fertilizers and the other with wastewater as the nutrient source (Nordio *et al.,* 2023).
	Nonlinear output feedback controller.	Biomass concentration	Simulation study for *Dunaliella tertiolecta* growth in a chemostat (Mailleret, Gouzé and Bernard, 2005).
	Nonlinear multivariable control, based on the exact feedback linearization technique.	pH and biomass concentration	*Chlamydomonas reinhardtii* culture on a laboratory torus photobioreactor (1.5 L) (Ifrim *et al.*, 2013).
	Nonlinear control strategy (based on state feedback linearizing control law + PI controller).	pH and biomass concentration	*Porphyridium purpureum* culture in a laboratory-scale bubble column photobioreactor (9.6 L) (Tebbani, Lopes and Becerra Celis, 2015)

Table 1.6. Optimization strategies applied in microalgae and microalgae-bacteria processes

Strategies	**Optimization objective**	**Application** **Process/ Reactor type (Reference)**
NMPC	Maximize CO_2 bio-fixation.	*Chlorella vulgaris* culture in a laboratory-scale bubble column photobioreactor (9.6 L) (Tebbani *et al.*, 2014).
Optimal and near-optimal strategy	Maximize biomass production	Simulation and experimental study of the *Scenedesmus almeriensis* culture in a tubular photobioreactor (2600 L) (Gustavo. A. de Andrade *et al.*, 2016)
RTO	Maximize biomass production	*Scenedesmus AMDD* culture in a continuous flow photobioreactor (300 L) (McGinn *et al.*, 2017).
Hierarchical control strategy: PI+feedforward and eMPC	Maximize profits.	*Scenedemus almeriensis* culture in a tubular photobioreactor (2600 L) (Fernández, Berenguel, *et al.*, 2016).

1.2. Motivation and Objectives

The development of accurate models and control strategies has been identified as a promising approach to enhance the control and optimization of industrial microalgae production processes. However, this task is inherently challenging, particularly in the context of wastewater treatment plants, where the intricate interactions between microalgae and bacteria, in addition to the variable weather conditions and dynamics of the inlet flow/composition of the wastewater, adds complexity to the process operation. While numerous models have been developed and validated for conventional microalgae-based wastewater treatment plants (even over the long term) and for different microalgae photobioreactor configurations producing high-value products, the modeling of other novel microalgae-bacteria photobioreactor configurations has not been conducted to date. Furthermore, parameter estimation applied to innovative wastewater treatment processes with microalgae remains an open research topic, with many challenges to address.

In a different line of research, the extant literature on developing state estimators for microalgae-bacteria processes is scarce, with most research being limited to simulations or laboratory settings. In addition, the development of state estimators in these processes is primarily based on linearized approximations, simple models, and low noise values, providing estimations of a limited number of states. However, these assumptions are not realistic in the context of these complex bioprocesses. This underscores the imperative need for state estimators that employ a more realistic depiction of the process, while concurrently accounting for the inherent process constraints in the pivotal parameters and state variables.

Similarly, in the context of control and optimization strategies, many applications continue to refer to the control of a limited number of variables (predominantly in small-scale facilities or closed photobioreactors for the production of high-value biomass), without considering the behavior of certain relevant process variables, which are key to evaluate the effluent water quality. Concurrently, the development of control and optimization strategies that encompass the numerous perturbations impacting these processes and the inherent model uncertainties remains an active research domain.

Within this framework, the motivation of this thesis relies on modeling innovative configurations for microalgae-bacteria-based wastewater treatment plants, as well as contributing to the state estimation and control of industrial microalgae-based wastewater treatment plants considering model uncertainties.

The general objective of this thesis is to contribute to the modeling, control, and optimization of algal-bacterial based wastewater treatment plants.

To accomplish this aim, the following specific goals will be considered:

- Developing and validating dynamics models of microalgae-bacteria based wastewater treatment plants, with special emphasis in anoxic-aerobic photobioreactor configurations, in which modeling has yet to be conducted to date.
- Adapting parametrization methods that facilitate the fitting of the model to wastewater treatment processes.
- Developing model libraries of components using the software PROOSIS® to facilitate the reuse of models across diverse applications.
- Designing a state estimator using the Moving Horizon Estimation approach to estimate non-measure variables in microalga-bacteria processes with model uncertainties and perturbations. Nonlinear model and process constraints are considered in the estimator design.
- Developing an economic MPC controller for process control and optimization considering process variability and model uncertainties.
- Validating the proposed approaches in a lab-scale plant.

1.3. Structure of the thesis

Following this Chapter one that revised the state-of-the-art in the topic, the thesis is organized into seven chapters as follows:

Chapter 2 delineates the methodological framework employed in this thesis for the modeling, state estimation, and control strategy design.

Chapter 3 presents the modeling of microalgae bacteria processes with biomass recycling. This chapter includes a model of anoxic-aerobic algal-bacterial photobioreactor configurations treating domestic wastewater and digestates. Additionally, a library of diverse model components for a wastewater treatment plant is also presented.

Chapter 4 presents the parameter estimation applied to two case studies of anoxic-aerobic algal-bacterial photobioreactors. The chapter presents a methodology for parameter estimation in biological processes involving multiple outputs and parameters in the optimization problem.

Chapter 5 is devoted to the problem of estimating non-measured variables in microalgae-bacteria processes. The Moving Horizon Estimator approach is presented to estimate the non-measurable variables in an industrial wastewater treatment plant involving different sampling times for the output variables.

Chapter 6 is devoted to developing an economic MPC controller for an industrial wastewater treatment plant. The controller is designed to maintain the limits of nutrient concentration in the plant's effluent while maximizing biomass production in spite of the uncertainties that are present in the process.

Chapter 7 compiles the thesis conclusions and outlook perspectives.

1.4. Contributions

Journal contributions:

- Bausa-Ortiz, I., Muñoz, R., Torres-Franco, A. F., Cristea, S. P., and Prada, C. Parameter estimation in anoxic aerobic algal-bacterial photobioreactor devoted to carbon and nutrient removal. Algal Research, Vol. 86, March 2025, Ref. 103917, ISSN 2211-9264. DOI: 10.1016/j.algal.2025.103917, https://doi.org/10.1016/j.algal.2025.103917
- Bausa-Ortiz, I., Oliveira-Silva, E., Muñoz, R., Cristea, S. P., and de Prada, C. Moving horizon estimation in microalgae-bacteria based wastewater treatment using online and analytical multi-rate measurements. Algal Research, Vol. 91, October 2025, Ref. 104338, ISSN 2211-9264. DOI: 10.1016/j.algal.2025.104338, https://doi.org/10.1016/j.algal.2025.104338.

Book chapters:

- Bausa, I., Muñoz, R., Podar, S., and de Prada, C. “Modeling and simulation of anoxic-aerobic algal-bacterial photobioreactor for nutrients removal,” in: COMPUTER-AIDED CHEMICAL ENGINEERING, 51 - PROCEEDINGS OF THE 32nd European Symposium on Computer Aided Process Engineering (ESCAPE32), vol. 2, L. Montastruc and S. Negny, Eds. © 2022 Elsevier B.V. All rights reserved 2022, pp. 151–156. DOI: http://dx.doi.org/10.1016/B978-0-323-95879-0.50026-6.

- Bausa-Ortiz, I., Muñoz, R., Cristea, S. P., and Prada, C. “Parameter estimation approach applied to microalgae-bacteria photobioreactor”, in: COMPUTER-AIDED CHEMICAL ENGINEERING, 52 - PROCEEDINGS OF THE 33rd European Symposium on Computer Aided Process Engineering (ESCAPE33), vol. 1, A. Kokossis, M. C. Georgiadis, E. N. Pistikopoulos Eds. © 2023 Elsevier B.V. All rights reserved 2023, pp. 721–726. DOI: https://doi.org/10.1016/B978-0-443-15274-0.50115-3. ISBN (Volume 1): 978-0-443-23553-5, ISBN (Set): 978-0-443-15274-0, ISSN: 1570-7946.

Congress contributions:

- Bausa, I., Muñoz, R., Podar, S., and de Prada, C. “Modelo para la estimación de la concentración de biomasa en una instalación reactor anóxico-fotobiorreactor aerobio de algas y bacterias para el tratamiento de aguas residuales domésticas”. *XLII Jornadas de Automática: libro de actas*. Castellón, 1-3 de septiembre de 2021. DOI: https://doi.org/10.17979/spudc.9788497498043.
- Bausa, I., Muñoz, R., Podar, S., and de Prada, C. “Modelado de un Fotobiorreactor en una configuración Reactor Anóxico-Fotobiorreactor”. *Actas del Simposio Conjunto de los Grupos Temáticos de CEA Modelado, Simulación, Optimización e Ingeniería de Control*. Universidad de Burgos, 27-29 abril 2022, Burgos, España, pp. 1–6. ISBN: 978-84-09-41387-4. http://hdl.handle.net/10259/6683.
- Bausa, I., Muñoz, R., Podar, S., and de Prada, C. “Modeling and simulation of anoxic-aerobic algal-bacterial photobioreactor for nutrients removal”. *32nd European Symposium on Computer Aided Process Engineering (ESCAPE32)*, June 12-15, 2022, Toulouse, France. DOI: http://dx.doi.org/10.1016/B978-0-323-95879-0.50026-6.
- Bausa, I., Podar, S., Muñoz, R., de Prada, C., and Oliveira-Silva, E. “Librería para sistemas de tratamiento de aguas residuales con microalgas y bacterias”. *XLIII Jornadas de Automática: libro de actas*. 7-9 de septiembre de 2022, Logroño, La Rioja, España, pp. 493-499. A Coruña: Universidade da Coruña, Servizo de Publicacións, 2022. XXI, 1075 p. ISBN: 978-84-9749-841-8. DOI: https://doi.org/10.17979/spudc.9788497498418.

- Bausa, I., Muñoz, R., Podar, S., and de Prada, C. “Modeling and simulation of a photobioreactor for wastewater treatment”. *PSE @RESEARCH DAY UK*. September 9, 2022, Imperial College London, London, UK.
- Bausa, I., Muñoz, R., Podar, S., and de Prada, C. “Modeling and parameter estimation of a Photobioreactor for wastewater treatment”. *Book of Extended Abstracts of the ProGres 3rd Workshop: From biomass characterization to process synthesis*. November 3-4, 2022, Salamanca, Spain.
- Bausa-Ortiz, I., Muñoz, R., Cristea, S. P., and de Prada, C. “Alternativa para la estimación de parámetros en sistemas biológicos”. *Actas del II Simposio Conjunto de los Grupos Temáticos de CEA Modelado, Simulación, Optimización e Ingeniería de Control*. Universidad Nacional de Educación a Distancia (UNED), 19-21 abril 2023, Madrid, España, pp. 5–6. ISBN: 978-84-09-51177-8. https://blogs.uned.es/simposioceamsoic/2023/05/18/actas.
- Bausa-Ortiz, I., Muñoz, R. Cristea, S. P., and Prada, C. “Parameter estimation approach applied to microalgae-bacteria photobioreactor”. *33rd European Symposium on Computer Aided Process Engineering (ESCAPE33)*, June 18-21, 2023, Athens, Greece. DOI: https://doi.org/10.1016/B978-0-443-15274-0.50115-3.
- Bausa-Ortiz, I., Muñoz, R., Cristea, S. P., and Prada, C. “An alternative for parameter estimation in biological processes”. *Book of Abstracts: Workshop on Simulation and Optimization for Sustainable Engineering*. September 28-29, 2023, Santander, Cantabria, Spain. © Editorial de la Universidad de Cantabria, 2023. ISNI: https://isni.org/isni/0000000506860180. ISBN: 978-84-19024-59-6 (pdf). DOI: https://doi.org/10.22429/Euc2023.026.
- Bausa-Ortiz, I., Muñoz, R., de Prada, C., and Cristea, S. P. “Modeling and parameter estimation in microalgae-bacteria photobioreactor for wastewater treatment”. *PSE Forum 2024: Process System Engineering Forum*, April 3-5, 2024, Universidad de Valladolid, Valladolid, Spain.
- Bausa-Ortiz, I., de Prada, C., Cristea, S. P., Muñoz, R., and Gutiérrez, G. “Estimación de estados en el tratamiento de aguas residuales”, en: *Actas del III Simposio Conjunto de los Grupos Temáticos de CEA: Modelado, Simulación, Optimización e Ingeniería de Control*. Vigo, Galicia, España, 10-12 de abril de 2024. ISBN: 978-84-09-61199-7.

- Bausa-Ortiz, I., Oliveira-Silva, E., Podar, S., Muñoz, R., de Prada, C., and Gutiérrez, G. “Optimización económica en el tratamiento de aguas residuales con algas y bacterias”, en: *Libro de Abstracts del I Simposio Conjunto de los Grupos Temáticos de CEA de Ingeniería de Control, de Modelado, Simulación y Optimización, y de Educación en Automática*. Sevilla, España, 22-24 de enero de 2025.
- Bausa-Ortiz, I., Oliveira-da Silva, E., Muñoz, R., P. Cristea, S., de Prada, C. “Development of a software sensor in microalgae-bacteria wastewater treatment plant”. *YAS - Young Algaeneers Symposium 2025*, June 3-6, Almería, Spain.

2. Integrated methodology: experimental research, modeling, and validation for advanced control strategies synthesis

The development and application of dynamic models constitutes the methodological framework employed in this doctoral thesis. Mathematical models can facilitate a more profound comprehension of process behavior and function as a decision-support instrument. In a similar vein, model-based controllers have been demonstrated to be a suitable instrument for the operation of complex processes. The core challenge addressed is the precise characterization of system dynamics, a prerequisite for the subsequent formal controller synthesis and comprehensive performance evaluation. This chapter delineates the process, which commences with the analytical derivation or system identification of a high-fidelity dynamic model. This establishes the foundational element upon which all subsequent experimental validation, calibration, and large-scale simulation studies are built.

2.1. Analytical system modeling and simulation

The foundational approach to system representation in this research involved the critical analysis of extant dynamic models from the specialized literature (as was detailed in the comprehensive revision of Section 1.1.1). The present study focused on the examination of models that effectively capture the intricate biological and chemical interactions between microalgae and bacteria within wastewater treatment processes. The objective of this study was twofold: first, to select a model that provides an adequate representation of the microalgae-bacteria wastewater treatment plant dynamics for system understanding and prediction; and second, to establish a robust platform for the subsequent design and evaluation of model-based control strategies.

The selection process prioritized mechanistic models of intermediate complexity. This choice is fundamentally justified by two core considerations in control engineering:

- Physical relevance: These models are explicitly formulated based on physical and chemical laws, including mass balances, kinetic rates, and energy transfers. Consequently, any change in the model's parameters possesses a direct physical or biological interpretation, which is crucial for system analysis, calibration, and ensuring the robustness of the control synthesis.
- Computational efficiency: In contrast to highly complex, high-order models that frequently demand exorbitant computational resources, models of intermediate complexity offer a better trade-off. These models maintain essential non-linear dynamics necessary for realistic control design while maintaining sufficient computational speed for real-time simulation and eventual implementation in control hardware.

Conversely, simplified, low-order representations, such as classical transfer functions or local linear state-space models, were deemed unsuitable for the present study. This exclusion is fundamentally methodological, as these reduced models possess inherent limitations. Specifically, they fail to adequately capture the pronounced non-linearities, the multivariable dynamics, and the operational constraints that fundamentally characterize biological wastewater treatment systems. Indeed, models lacking this complexity are insufficient for the synthesis of advanced control strategies (such as MPC), which require high-fidelity dynamic predictions and accurate modeling of the entire operating envelope to ensure stability and optimal performance.

This study adapted mechanistic models previously documented in the specialized literature to accurately represent the microalgae-bacteria interactions specific to the case studies evaluated in this research. The model that was selected was confirmed to adequately capture the dynamics of a microalgae-bacteria-based wastewater treatment plant. This choice ensures the model's suitability as a high-fidelity platform for the subsequent design and evaluation of advanced model-based control strategies.

As a fundamental element of the modeling strategy employed in this thesis, a reusable object-oriented model library of components was developed. This library has been developed to facilitate the easy reuse of validated models and the flexible connectivity of different process components. The library contains a variety of validated components relevant to wastewater treatment. It enables the rapid simulation of various WWTP configurations under a wide range of operational conditions.

The library was constructed on the principles of object-oriented programming (OOP), and its implementation involved the utilization of the specialized simulation software EcosimPro|PROOSIS®. The OOP structure ensures that components can be easily interconnected and managed, promoting modularity and potentially lowering the entry barrier for users without deep knowledge on modeling and simulation fundamentals. This structured approach significantly enhances the reproducibility and scalability of the modeling efforts presented herein. A thorough exposition of the library development and components is furnished in Chapter 3, Section 3.2.

2.2. Methods for model calibration and validation

The rigorous calibration and subsequent validation of mathematical models constitute an essential step in the modeling of complex biological processes. The inherent complexity and dynamic nature of biological systems, such as the microalgae and bacteria-based wastewater treatment systems studied here, necessitate empirical investigation involving intensive, high-time-consuming experimentation to reliably establish operational fundamentals across a comprehensive range of conditions. The development of a high-fidelity model thus provides a critical analytical advantage.

Leveraging a validated model enables the efficient simulation of novel configurations, such as the anoxic-aerobic system studied in this thesis, to assess the influence of varying operational conditions and inlet nutrient concentrations. This methodology effectively

minimizes the time and cost dedicated to physical experimentation, enabling the rapid and systematic evaluation of the global performance and nutrient removal efficiency of the system under scenarios that would be impractical or prohibitively expensive to test in a physical laboratory environment.

In this research, a systemic analysis and validation were conducted across two fundamentally distinct operational scales, which required the implementation of differentiated methodological approaches:

- Pilot-plant scale (empirical validation): This scale served as the primary source of empirical data. The model was rigorously calibrated and validated against real experimental data obtained from the physical pilot facility. The primary objective of this step was to ensure the predictive fidelity of the model parameters and structure under controlled conditions. This approach validates the model's capacity to accurately replicate the system dynamics prior to scaling. The application of this approach is delineated in Chapter 4.
- Industrial scale (simulated validation and scalability assessment): In light of the paucity of data from an industrial-scale facility, the industrial scenario was assessed entirely through the use of high-fidelity simulation. In this context, the model—already validated at the pilot scale—was used to conduct scalability assessment and evaluate the performance of the designed control strategies under the complex, real-world constraints and operational demands of a large-scale plant.

2.2.1. Methods using experimental data

To address the modeling objective related to the anoxic-aerobic configurations, previously generated data from experimental campaigns developed at the Institute of Sustainable Processes at the University of Valladolid were utilized. These datasets correspond to two distinct anoxic-aerobic algal-bacterial photobioreactor configurations operating under a variety of operational conditions while treating domestic synthetic wastewater and synthetic food waste digestate.

To ensure the predictive accuracy of the selected model, a rigorous, multi-step calibration and validation process was conducted using the PROOSIS® simulation software:

a) Sensitivity Analysis. Due to the high dimensionality and large number of parameters that mechanistic microalgae-bacteria models frequently exhibit, an initial sensitivity analysis was conducted. This step was essential to determine the minimum set of parameters with the greatest influence on system outputs, focusing subsequent efforts on those parameters with the highest identifiability.
b) Parameter estimation of model biokinetic parameters and mass transfer coefficients. The optimal values for the selected biokinetic parameters and mass transfer coefficients within the reactors were determined through dynamic optimization. This estimation was performed using a robust objective function designed to minimize the impact of uncertainties from unreliable or noisy experimental measurements.
c) Parameter estimation of settling velocity parameters. The values of parameters characterizing the settling process were determined using a robust objective function. Additionally, modeling the settling velocity equation required fitting parameters using a sigmoid function to accurately represent the non-linear sedimentation behavior.
d) Cross-validation and goodness-of-fit. The final stage of this phase involved the cross-validation of the fully calibrated model. The simulated dynamics were directly compared with independent experimental data sets from anoxic-aerobic facilities. The results were graphically presented to demonstrate the model's effective range of validity and goodness-of-fit.
e) Metrics of model performance: To objectively quantify the model's quality of adjustment to the experimental data, two performance indices were used: the Mean Absolute Error (MAE) and the Mean Absolute Relative Error (MARE). These metrics provided quantitative proof of the model's predictive accuracy across the observed variables.

The application of the aforementioned process for model calibration and validation in an anoxic-aerobic algal-bacteria photobioreactor configuration treating different dilutions of digestate is detailed in Chapter 4, Section 4.1.

In light of the challenges associated with parameter estimation in complex biological processes, this thesis proposes a novel methodological approach for parameter estimation. This approach is designed to address the challenges posed by the presence of multiple variables and parameters in optimization problems. This novel methodology was

successfully applied and tested using real experimental data from the microalgae-bacteria photobioreactor of an anoxic-aerobic configuration treating domestic synthetic wastewater in Chapter 4, Section 4.2.

2.2.2. Methods using model simulation

The predictive capacity of the calibrated model (established via experimental data, Chapters 3 and 4) enables its use for comprehensive system analysis and control design. In accordance with the methodological objective of optimizing research resources by minimizing the reliance on costly and time-consuming physical experimentation, model simulations were employed to achieve objectives that are impractical or unachievable through pilot-plant testing. These simulations were specifically designed to assess scalability and to exhaustively evaluate control strategies under diverse operational scenarios.

This methodological step is crucial for two main reasons:

- Exploration of the operating envelope: Simulations allow for the systematic study of the system's operation across a substantially broader spectrum of operational conditions and under extreme perturbation events that are not economically or safely viable to replicate in the physical pilot plant.
- Control strategy design and validation: The validated dynamic model provides the necessary analytical platform for the synthesis, tuning, and closed-loop testing of the advanced control strategies proposed in this thesis (Chapter 6), prior to any potential physical implementation.

The decision to evaluate state estimation techniques and control strategies through high-fidelity simulation of an industrial-scale plant (Chapters 5 and 6), as opposed to depending exclusively on the physical pilot facility, is a fundamental methodological necessity driven by the inherent differences between the scales and the objectives of advanced control design. The industrial plant model, state estimation technique, and model-based control strategy were developed within the MATLAB® software environment.

The simulation of the industrial environment enables the rigorous exploration of critical factors that are either absent or significantly mitigated at the pilot scale, providing a stringent testbed for both the controller and the state estimator:

- Pronounced non-linearities: Industrial systems often exhibit more pronounced non-linear dynamics (e.g., in settling, reaction kinetics) due to their larger operational volumes and flow rates. These complex effects, which are typically less evident at laboratory scale, are crucial for challenging the convergence and stability of non-linear state estimation algorithms or for testing the performance of the subsequent non-linear control algorithms.
- Wider operational and perturbation ranges: Simulation enables the testing of wider ranges of system input loads and the introduction of larger, more realistic magnitude of disturbances that characterize real-world municipal wastewater treatment plants. It is imperative to assess the robustness of the estimator under these conditions, particularly with regard to its resilience against high measurement uncertainty and noise propagation.
- Influence of external and coupling conditions: The industrial-scale model allows for the assessment of the pronounced influence of external conditions (e.g., realistic, large-scale diurnal and seasonal temperature/radiation fluctuations) and the inter-component coupling effects (e.g., recycling streams and settler dynamics) that dominate the overall system behavior at full scale.
- Economic and safety constraints: Critically, testing advanced control strategies under extreme conditions, large disturbances, or complex failure scenarios on a physical industrial plant is often prohibitively expensive, time-consuming, and potentially unsafe. A simulation environment provides a risk-free platform for thorough robustness analysis and optimization.

Thus, industrial-scale simulation is a vital bridge for transferring the technology of the proposed state estimation and control strategies, ensuring their robustness, stability, and viability before costly physical implementation.

Simulation conditions

To ensure the representativeness and robustness of the industrial-scale evaluations of both control and state estimation strategies, the simulation environment was configured using calibrated parameters and real input data. Key system inputs were driven by real time-series data to accurately capture the stochastic and dynamic nature of operational wastewater treatment plants:

- Urban wastewater influent load: Industrial-scale plant simulations were based on real-time series data of urban wastewater influent quality. This data was sourced from representative municipal wastewater, allowing for evaluation under the typical diurnal fluctuations inherent to real-world operation.
- Environmental conditions: The dynamic effects on microalgae growth and reactor temperature were modeled using real meteorological data. Specifically, typical data on solar radiation and ambient temperature from a suitable geographical location were used to accurately reflect the influence of external conditions on biological dynamics.
- Model parameters and scaling: The dynamic models for the reactors and settlers were scaled up to typical industrial dimensions. Typical biokinetic and mass transfer parameters for HRAPs were used to ensure that the fundamental kinetic and biological behavior of the simulated system corresponded directly with prior experimental evidence.

Scenarios for robustness analysis and state estimation evaluation

- **Model-plant mismatch setup**

A fundamental aspect of this simulation methodology was the introduction of a deliberate model-plant mismatch to accurately emulate the real conditions encountered in industrial control applications. This setup involved utilizing two distinct dynamic models within the closed-loop simulation:

- Plant model: The full, high-fidelity, validated mechanistic model (developed in Chapter 3) was employed to represent the true dynamic behavior of the industrial plant.
- Controller/Estimator model: A simplified version of the full model was embedded within the state estimator and the controller. This model utilized a distinct set of fixed parameters and a reduced number of states to represent the unavoidable modeling errors, simplifications, and uncertainties characteristic of real-time operational models. The details and simplifications performed in the reduced model can be found in Chapter 5, Section 5.4.

This rigorous approach ensures that the performance and stability of the designed control and estimation techniques are tested against realistic structural and parametric uncertainties, verifying their true robustness.

- **Simulation of measurement noise and uncertainty evaluation**

To further enhance the realism of the evaluation, the industrial simulation environment incorporated stochastic noise into the measurements, accurately mimicking the uncertainty and measurement quality issues found in real instrumentation and analytical measurement procedures.

- Measurement noise: Additive noise was introduced to both the simulated analytical and online measurements. This noise component effectively models the combined effects of high-frequency uncertainty, calibration errors, signal drift, and process-related fluctuations present in real-world sensors and analytical procedures.
- Uncertainty evaluation: Testing the state estimator under this noisy environment is critical, as the performance and convergence of non-linear observers are highly sensitive to measurement noise propagation and the effects of model simplifications. This rigorous evaluation confirms the estimator's capability to provide reliable state estimations in realistic operational context.

2.3. State estimator design and tuning methodology

The methodology for the state estimator design was structured around two principal aspects: the selection of the most pertinent state estimation technique for the system's non-linear dynamics, and the rigorous tuning of its parameters to ensure operational robustness.

- **Selection of the estimation technique**

To effectively address the non-linear nature of the biological system and, critically, the necessity of incorporating state and measurement constraints, the Moving Horizon Estimator was selected. The MHE was selected due to its methodological advantages over linear or extended Kalman filters in this particular context:

- Explicit constraint handling: The MHE explicitly incorporates operational constraints directly into its optimization formulation, a crucial aspect for ensuring the safety and physical significance of state estimation.
- Global optimization: By utilizing an objective function that minimizes the estimation error over a receding time horizon, the MHE provides a more robust and consistent state estimation, particularly in systems characterized by slow, non-linear dynamics such as WWTPs.
- Embedded model: The MHE utilizes a simplified version of the complete dynamic plant model. This approach offers a realistic simulation of the model-plant mismatch condition, verifying the estimator's ability to converge despite structural and parametric uncertainties.

- **MHE tuning and configuration**

The performance of the MHE is critically dependent on the adjustment of its weighting parameters and the correct inclusion of constraints:

- Covariance matrices:
    - Process noise covariance matrix: This matrix weights the noise affecting the model dynamics. The weights were tuned to reflect the level of uncertainty inherent in the reduced model and the unmeasured disturbances of the WWTP.
    - Measurement noise covariance matrix: The weights were directly adjusted based on the variance of the stochastic noise introduced into the simulations. Proper tuning of this matrix is essential for balancing the estimator's confidence in the measurements versus its confidence in the model predictions.
- Estimation constraints: Constraints were included in the MHE's optimization problem to ensure that the estimated state variables remain within their known physical and operational bounds.
- Horizon: The estimation horizon was chosen as a compromise between estimation accuracy and computational feasibility.

This design and tuning process ensures that the MHE is not only theoretically suitable for the system but has also been configured to operate robustly under industrial conditions of

uncertainty and constraint. The specific tuning parameters are delineated in Chapter 5, section 5.5.1.

2.4. Economic model predictive control design and tuning methodology

The eMPC was designed to optimize the economic performance of the wastewater treatment plant, using biomass productivity as the primary economic driver.

- **Optimization problem formulation and tuning**

The eMPC is formulated as an online optimization problem that is solved at every sampling instant. Its distinctive feature is the definition of an economic objective function. The tuning of the eMPC was an iterative process focused on achieving a robust balance between economic maximization and the maintenance of stringent quality constraints.

- Economic term: This dominant term is defined to maximize biomass productivity.
- Control effort term: This penalizes excessive changes in the manipulated variables.
- Prediction and control horizons: These horizons were selected based on the slow dynamics of the biological system.
- Embedded model: The eMPC utilizes the reduced dynamic model of the plant (the same version used in the MHE, Section 5.4) to predict the future behavior of the system over the prediction horizon. The employment of this reduced model is critical to ensure real-time computational feasibility.
- Operational and quality constraints: The optimization must be subjected to equality and inequality constraints, which are vital for real-world application:
    - Biomass constraints: Strict biomass constraints within the reactor, in the effluent flow and in the wastage flow.
    - Actuator constraints: Physical limits were imposed on the manipulated control variables.

This methodology ensures that the eMPC operates as a robust hierarchical control system, striving for economic optimization within a framework of strict safety and regulatory adherence.

2.5. Laboratory-scale plant for wastewater treatment

In this thesis, a laboratory-scale plant for wastewater treatment was designed to allow the validation of modeling, estimation, and control strategies. This plant is located at the University of Valladolid's Institute of Sustainable Processes in Spain.

2.5.1. Pilot plant description

The laboratory-scale wastewater treatment plant developed in this thesis comprised two independently operated microalgae-bacteria photobioreactors. The photobioreactors are identical 3.85 L cylindrical PVC (polyvinylchloride) plastic tanks with a total working volume of 3.2 L. The photobioreactors are illuminated by an array of LED strip lights (Philips 150 W-0.7 A, Spain) placed 0.44 m above the surface of the photobioreactors. The photobioreactors are subjected to constant agitation through the use of magnetic stirring plates (LBX instruments S20, Spain). To ensure a suitable temperature range for microalgae cultivation, a cooling system is employed, utilizing hoses surrounding the photobioreactors to circulate water from a thermal bath (Fisher Scientific, Spain). Both reactors are fed with synthetic wastewater, which is supplied to the reactors using HYGIAFLEX HF-SK-HandyPump peristaltic flow pumps. Fig. 2.1 presents a schematic representation of the laboratory-scale plant.

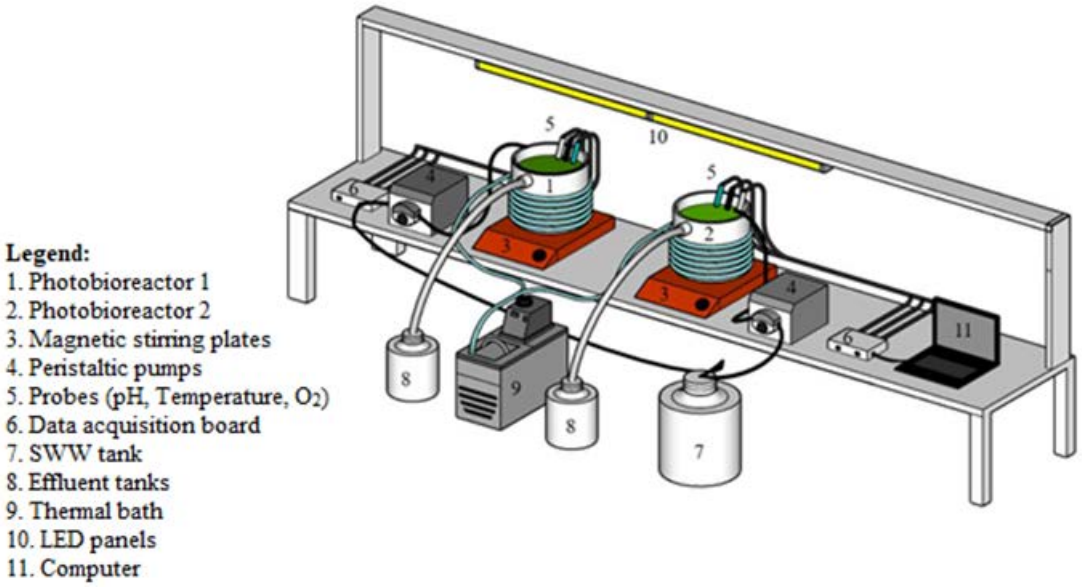

Fig. 2.1. Schematic representation of the laboratory-scale plant (Ruíz Guirola, 2023)

- **Operational conditions**

The reactors were inoculated with a consortium of microalgae and bacteria from the photosynthetic wastewater treatment plants of Almeria, Spain. The microalgae strains present in the inoculum were *Dictyosphaerium sp.*, *Scenedesmus sp.*, *Nitzschia sp.* and *Pseudanabaena sp.*, with *Dictyosphaerium sp.* predominating.

Both reactors are fed with synthetic wastewater, which is maintained at a constant temperature of 4 °C before feeding to prevent degradation. To ensure controlled operating conditions, synthetic wastewater was employed to simulate the physicochemical characteristics and composition of medium-load urban wastewater. The composition of the wastewater utilized is delineated in Table 2.1. The utilization of synthetic wastewater in this laboratory-scale facility offers several advantages, including the ability to regulate the characteristics and composition of the water, facilitate the comparison and evaluation of treatment technologies, eliminate the risk of hazardous contaminants, and reduce the cost of treating and managing real water. Furthermore, it enables the modeling of various scenarios, thereby reducing the impact of perturbations resulting from heterogeneous wastewater composition.

Table 2.1. Synthetic wastewater composition

Component	**Concentration [units]**
Glucose anhydrous	625 mg/L
Meat Extract	137.5 mg/L
Peptone from casein	200 mg/L
$NaHCO_3$	1375 mg/L
NaCl	8.75 mg/L
$CaCl_2 \cdot H_2O$	5 mg/L
$MgSO_4 \cdot 7H_2O$	2.5 mg/L
$K_2 \cdot HPO_4$	140 mg/L
CH_4N_2O (urea)	37.5 mg/L
$CuCl_2 \cdot 2H_2O$	0.625 mg/L

The temperature and pH of the culture medium varying between 24-27 ºC and 8-9.8, respectively, throughout the experimental process. In order to guarantee a narrow range of temperatures, the cooling systems circulates water at 24 ºC from a thermal bath. The photobioreactors are illuminated with LED panels, and the radiation provided by these panels at each time of the day emulates the sunlight cycle. The Arduino Leonardo controller transmits the appropriate voltage levels to the LED panels, corresponding to the radiation values for the various hours of the day. The sunlight cycle programmed in the Arduino for this experimentation corresponds to the summer radiation conditions in Castilla y León, with a maximum intensity of 1495 $\mu mol/m^2 s$ over the surface of the photobioreactors. The LED panels ensure sufficient illumination, thereby promoting optimal growth and development of the microalgae.

- **Online data acquisition and automatic operation system**

The experimental system is designed for the collection of online data concerning the pH level, the temperature, and the dissolved oxygen concentration. To this end, tree probes (Vernier®) were positioned within each reactor to obtain precise measurements of the internal conditions. Each probe is connected to a data acquisition (DAQ) board (LabQuest Mini, Model 2, Vernier®), which is connected to the computer via USB ports. This interface enables the real-time transfer of data from the probes to the computer. A Supervisory Control and Data Acquisition (SCADA) system was developed to address the necessity for efficient data visualization, storage and processing, as well as the autonomous operation of the system. This system utilizes LabVIEW 2021 software (National Instruments, NI).

The SCADA system has been developed for the purpose of facilitating the acquisition of measurement values at user-defined intervals. Throughout the experiment, the daily data are stored in an Excel file.

The implementation of the SCADA system facilitates the regulation of synthetic wastewater flow to both photobioreactors, with each pump functioning independently. This configuration is guaranteed to provide the necessary synthetic wastewater to each reactor, thereby ensuring the achievement of the desired hydraulic retention time value. The control of the pumps for the SCADA system is performed using the Input/Output device USB-1408FS-Plus (Measurement Computing Corporation). Fig. 2.2 represents the

instrumentation used to facilitate the exchange of information between the plant and the SCADA system.

The SCADA is composed of four windows. The first is the main window, which displays the fundamental operational conditions of the system. The second and third windows provide detailed information regarding each reactor operation. The fourth window is the settings window, which allows the user to configure the flow particularities for each reactor. Details of the SCADA operation are provided in Appendix 4.

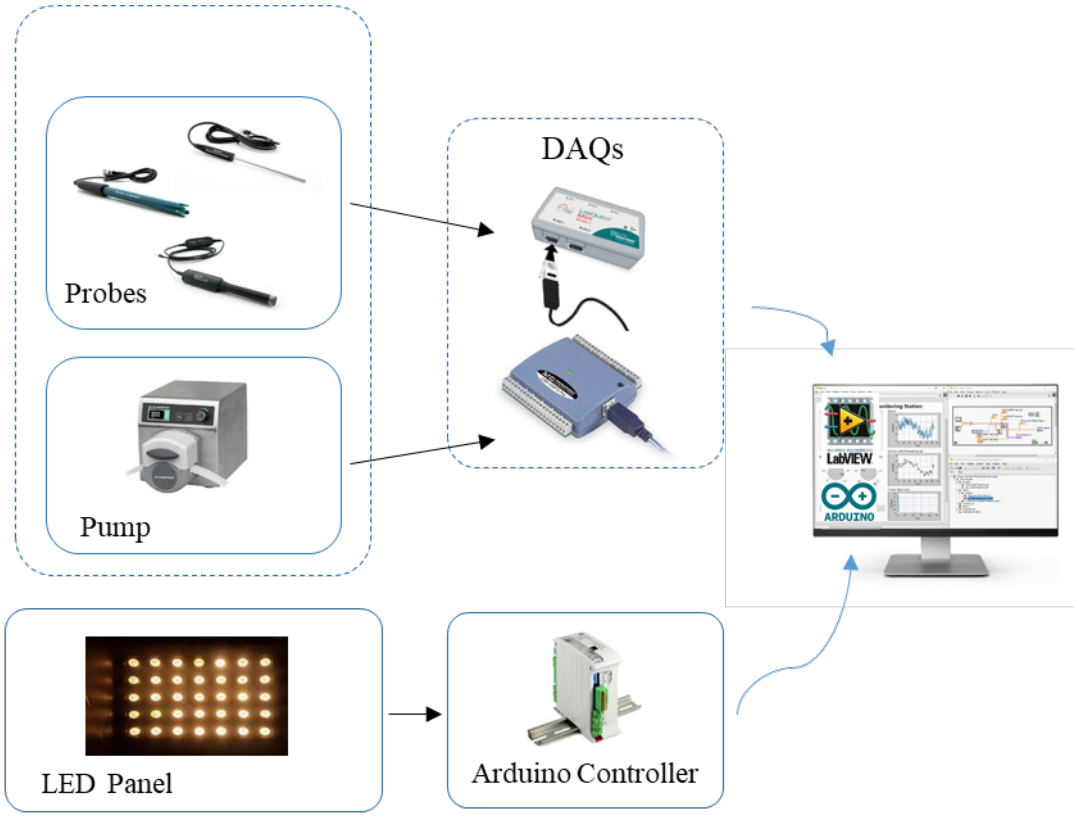

Fig. 2.2. Instrumentation of the laboratory-scale wastewater treatment plant

2.6. Conclusions

The methodological framework established herein ensures the viability, robustness, and industrial applicability of the contributions presented in this thesis. The strategy, grounded in a model-centric and hybrid approach, commenced with the establishment of a high-fidelity predictive platform through the calibration of the dynamic model against pilot-plant experimental data. The aforementioned model, which has been proven to be

valid, serves as a foundation for the estimation and evaluation of control strategies. The simulation environment was configured to prioritize realism, incorporating both real-world time-series data and a deliberate model-plant mismatch to assess the performance of algorithms in the face of inevitable uncertainties. The methodology culminates in the design and tuning of advanced control components: the Moving Horizon Estimator, selected for its constraint-handling and robustness to non-linearities, and the Economic Model Predictive Controller, formulated to optimize high-level objectives while strictly adhering to operational and regulatory constraints. This comprehensive approach provides the validated and rigorous foundation necessary for the successful synthesis and technology transfer of the proposed control and estimation strategies.

3. Modeling of anoxic-aerobic algal-bacterial processes

This chapter is devoted to the modeling of an anoxic-aerobic algal-bacterial photobioreactor configuration. The utilization of anoxic-aerobic algal-bacterial systems has emerged as a highly efficient alternative for the removal of nutrients from wastewater with low carbon to nutrient ratio (de Godos, Vargas, *et al.*, 2014; Alcántara *et al.*, 2015; García *et al.*, 2017; Dhaouefi *et al.*, 2018). However, these systems are still in an embryonic stage, and further research must be conducted before being implemented in a larger scale. As part of the experimental stage, anoxic-aerobic microalgae-bacteria systems require a series of experiments to evaluate their performance and nutrient removal efficiencies under various operational conditions and treating different types of wastewater. In this regard, mathematical modeling applied to this novel photobioreactor configuration is a useful tool for predicting and understanding the processes occurring in each plant element, allowing the simulation of a broad range of experimental and operational conditions in a relatively short period of time.

3.1. Description of the anoxic-aerobic microalgae-bacteria photobioreactor configuration

The lab-scale plant was configured as a two-stage anoxic-aerobic system, engineered with biomass settling and recirculation, as illustrated in Fig. 3.1. The facility was designed with the objective of promoting nitrogen removal via denitrification and the development of a rapidly settling algal-bacterial population. The design was based on the hypothesis that algal-bacterial photobioreactors for wastewater treatment can support the oxidation of NH_4^+ into NO_2^-/NO_3^-, which can then be easily removed through denitrification (using the organic matter present in wastewater) under pre-anoxic conditions via internal recycling of the photobioreactor broth (de Godos, Vargas, *et al.*, 2014).

The aerobic tank (open photobioreactor) was illuminated by LED lamps, whereas the anoxic reactor consisted of a gas-tight tank maintained in the dark. Synthetic wastewater (SWW) was fed to the anoxic tank and continuously overflowed by gravity into the aerobic photobioreactor. The algal-bacterial broth was recycled from the photobioreactor to the anoxic tank in order to provide the NO_2^- and NO_3^- (generated in the photobioreactor via biological nitrification) required for denitrification. An Imhoff cone, interconnected to the outlet of the photobioreactor, functioned as a settler, wherein the algal-bacterial biomass settled and was recycled from the bottom of the settler into the anoxic tank. Biomass was daily wasted from the bottom of the secondary settler to maintain the value of the sludge retention time (SRT).

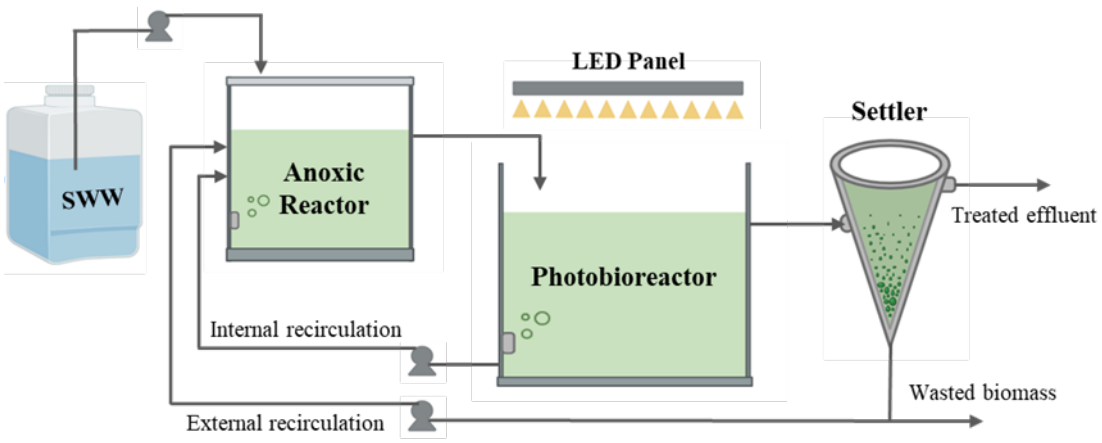

Fig. 3.1. Schematic of the anoxic-aerobic algal-bacterial photobioreactor configuration

3.1.1. Photobioreactor and anoxic unit modeling

The BIO_ALGAE2 model (Solimeno, Gómez-Serrano and Acién, 2019a) (with some minor modifications) was used to represent the biochemical reactions and processes in both anoxic and aerobic reactors. The BIO_ALGAE2 model uses the standard nomenclature of the IWA models and considers 19 components - 6 particulate and 13 dissolved - as variables involved in the physical, chemical, and biokinetic processes. These components are listed in Table 3.1 and described in detail in (Solimeno *et al.*, 2017a), along with their main roles in the processes and their interactions with other components.

The process rates of the model and the factors equations representing the processes occurring in the anoxic and aerobic reactors are described in Table 3.2 and Table 3.3, respectively. Appendix 1 contains the matrix of stoichiometric parameters (Table A1.1), the values of the parameters (Table A1.2), the fractions of carbon, hydrogen, oxygen, and nitrogen in microalgae and bacterial biomass (Table A1.3), and a summary of the mathematical expressions of the stoichiometric coefficients (Table A1.4).

Model modifications considered in the present work (Table 3.2) were related to the radiation factor (used in equations describing the microalgae growth (ρ_1 and ρ_2)) and the addition of one factor in the equation representing the aerobic growth of heterotrophic bacteria on dissolved nitrate (ρ_6) to indicate that when ammonium (or ammonia) and nitrate are both present, ammonium is generally preferred. Differences in a few stoichiometric parameters were also considered (Table A1.1).

Table 3.1. Dissolved and particulate components in the BIO_ALGAE2 model

	Component [units]	**Description**
Particulate components	X_{ALG} [mgCOD/L]	Microalgae biomass
	X_H [mgCOD/L]	Heterotrophic bacteria
	X_{AOB} [mgCOD/L]	Ammonium oxidizing bacteria
	X_{NOB} [mgCOD/L]	Nitrite oxidizing bacteria
	X_S [mgCOD/L]	Slowly biodegradable particulate organic matter
	X_I [mgCOD/L]	Inert particulate organic matter
Dissolved components	S_{NH4} [mgN-NH_4/L]	Ammonium nitrogen
	S_{NH3} [mgN-NH_3/L]	Ammonia nitrogen
	S_{NO3} [mgN-NO_3/L]	Nitrate nitrogen
	S_{NO2} [mgN-NO_2/L]	Nitrite nitrogen
	S_{PO4} [mgP-PO_4/L]	Phosphate phosphorus
	S_{O2} [mgO_2/L]	Dissolved oxygen
	S_{CO2} [mgC-CO_2/L]	Dissolved carbon dioxide
	S_{HCO3} [mgC-HCO_3/L]	Bicarbonate
	S_{CO3} [mgC-CO_3/L]	Carbonate
	S_H [mgH/L]	Hydrogen ions
	S_{OH} [mgH-OH/L]	Hydroxide ions
	S_S [mgCOD/L]	Readily biodegradable soluble organic matter
	S_I [mgCOD/L]	Inert soluble organic matter

Table 3.2. Process rates of the model

Processes	**Process rate [M L^{-3} T^{-1}]**
Microalgae (X_{ALG}) processes	
Growth on S_{NH}	$\rho_1 = \mu_{ALG} \cdot f_I \cdot f_{DO} \cdot f_{T_{ALG}} \cdot f_{pH_{ALG}} \cdot \frac{S_{CO2} + S_{HCO3}}{K_{C,ALG} + S_{CO2} + S_{HCO3} + \frac{{S_{CO2}}^2}{I_{CO2,ALG}}} \cdot \frac{S_{NH3} + S_{NH4}}{K_{N,ALG} + S_{NH3} + S_{NH4}} \cdot \frac{S_{PO4}}{K_{P,ALG} + S_{PO4}} \cdot X_{ALG}$
Growth on S_{NO3}	$\rho_2 = \mu_{ALG} \cdot f_I \cdot f_{DO} \cdot f_{T_{ALG}} \cdot f_{pH_{ALG}} \cdot \frac{S_{CO2} + S_{HCO3}}{K_{C,ALG} + S_{CO2} + S_{HCO3} + \frac{{S_{CO2}}^2}{I_{CO2,ALG}}} \cdot \frac{S_{NO3}}{K_{N,ALG} + S_{NO3}} \cdot \frac{K_{N,ALG}}{K_{N,ALG} + S_{NH3} + S_{NH4}} \cdot \frac{S_{PO_4}}{K_{P,ALG} + S_{PO4}} \cdot X_{ALG}$
Endogenous respiration	$\rho_3 = k_{resp,ALG} \cdot f_{T_{ALG}} \cdot f_{pH_{ALG}} \cdot \frac{S_{O2}}{K_{O2,ALG} + S_{O2}} \cdot X_{ALG}$
Decay	$\rho_4 = k_{death,ALG} \cdot f_{T_{ALG}} \cdot f_{pH_{ALG}} \cdot X_{ALG}$
Heterotrophic bacteria (X_H) (aerobic and denitrifying activity)	
Aerobic growth on S_{NH}	$\rho_5 = \mu_H \cdot f_{T_H} \cdot f_{pH_H} \cdot \frac{S_S}{K_{S,H} + S_S} \cdot \frac{S_{O2}}{K_{O2,H} + S_{O2}} \cdot \frac{S_{NH3} + S_{NH4}}{K_{N,H} + S_{NH3} + S_{NH4}} \cdot \frac{S_{PO4}}{K_{P,H} + S_{PO4}} \cdot X_H$
Aerobic growth on S_{NO3}	$\rho_6 = \mu_H \cdot f_{T_H} \cdot f_{pH_H} \cdot \frac{S_S}{K_{S,H} + S_S} \cdot \frac{S_{O2}}{K_{O2,H} + S_{O2}} \cdot \frac{S_{NO3}}{K_{N,H} + S_{NO3}} \cdot \frac{K_{N,H}}{K_{N,H} + S_{NH3} + S_{NH4}} \cdot \frac{S_{PO4}}{K_{P,H} + S_{PO4}} \cdot X_H$
Anoxic growth on S_{NO2} (denitrification on S_{NO2})	$\rho_7 = \mu_H \cdot \eta_H \cdot f_{T_H} \cdot f_{pH_H} \cdot \frac{S_S}{K_{S,H} + S_S} \cdot \frac{K_{O2,H}}{K_{O2,H} + S_{O2}} \cdot \frac{S_{NO2}}{K_{NO2,H,anox} + S_{NO2}} \cdot \frac{S_{PO4}}{K_{P,H} + S_{PO4}} \cdot X_H$
Anoxic growth on S_{NO3} (denitrification on S_{NO3})	$\rho_8 = \mu_H \cdot \eta_H \cdot f_{T_H} \cdot f_{pH_H} \cdot \frac{S_S}{K_{S,H} + S_S} \cdot \frac{K_{O2,H}}{K_{O2,H} + S_{O2}} \cdot \frac{S_{NO3}}{K_{NO3,H,anox} + S_{NO3}} \cdot \frac{S_{PO4}}{K_{P,H} + S_{PO4}} \cdot X_H$

Aerobic endogenous respiration	$\rho_9 = k_{resp,H} \cdot f_{T_H} \cdot f_{pH_H} \cdot \frac{S_{O2}}{K_{O2,H} + S_{O2}} \cdot X_H$
Anoxic endogenous respiration	$\rho_{10} = k_{resp,H} \cdot \eta_H \cdot f_{T_H} \cdot f_{pH_H} \cdot \frac{K_{O2,H}}{K_{O2,H} + S_{O2}} \cdot \frac{S_{NO3} + S_{NO2}}{K_{NO3,H,anox} + S_{NO2} + S_{NO3}} \cdot X_H$
Decay	$\rho_{11} = k_{death,H} \cdot f_{T_H} \cdot f_{pH_H} \cdot X_H$
Autotrophic bacteria (X_{AOB}, X_{NOB}) (nitrifying activity)	
Growth of X_{AOB}	$\rho_{12} = \mu_{AOB} \cdot f_{T_N} \cdot f_{pH_N} \cdot \frac{S_{O2}}{K_{O2,AOB} + S_{O2}} \cdot \frac{S_{NH3} + S_{NH4}}{K_{NH4,AOB} + S_{NH3} + S_{NH4}} \cdot \frac{S_{CO2} + S_{HCO3}}{K_{C,AOB} + S_{CO2} + S_{HCO3}} \cdot \frac{S_{PO4}}{K_{P,AOB} + S_{PO4}} \cdot X_{AOB}$
Growth of X_{NOB}	$\rho_{13} = \mu_{NOB} \cdot f_{T_N} \cdot f_{pH_N} \cdot \frac{S_{O2}}{K_{O2,NOB} + S_{O2}} \cdot \frac{K_{I,NH4}}{K_{I,NH4} + S_{NH3} + S_{NH4}} \cdot \frac{S_{NO2}}{K_{NO2,NOB} + S_{NO2}} \cdot \frac{S_{CO2} + S_{HCO3}}{K_{C,NOB} + S_{CO2} + S_{HCO3}} \cdot \frac{S_{PO4}}{K_{P,NOB} + S_{PO4}} \cdot X_{NOB}$
Endogenous respiration of X_{AOB}	$\rho_{14} = k_{resp,AOB} \cdot f_{T_N} \cdot f_{pH_N} \cdot \frac{S_{O2}}{K_{O2,AOB} + S_{O2}} \cdot X_{AOB}$
Endogenous respiration of X_{NOB}	$\rho_{15} = k_{resp,NOB} \cdot f_{T_N} \cdot f_{pH_N} \cdot \frac{S_{O2}}{K_{O2,NOB} + S_{O2}} \cdot X_{NOB}$
Decay of X_{AOB}	$\rho_{16} = k_{death,AOB} \cdot f_{T_N} \cdot f_{pH_N} \cdot X_{AOB}$
Decay of X_{NOB}	$\rho_{17} = k_{death,NOB} \cdot f_{T_N} \cdot f_{pH_N} \cdot X_{NOB}$
Hydrolysis, Chemical equilibrium and Transfer of gases	
Aerobic hydrolysis	$\rho_{18} = k_{HYD} \cdot \frac{X_S/X_H}{K_{HYD} + (X_S/X_H)} \cdot X_H$
Chemical equilibrium $CO_2 \leftrightarrow HCO_3^-$	$\rho_{19} = k_{eq,1} \cdot (S_{CO2} - S_H S_{HCO3}/K_{eq,1})$
Chemical equilibrium $HCO_3^- \leftrightarrow CO_3^{2-}$	$\rho_{20} = k_{eq,2} \cdot (S_{HCO3} - S_H S_{CO3}/K_{eq,2})$

Chemical equilibrium $NH_4^+ \leftrightarrow NH_3$	$\rho_{21} = k_{eq,3} \cdot \left(S_{NH4} - S_H S_{NH3}/K_{eq,3}\right)$
Chemical equilibrium $H^+ \leftrightarrow OH^-$	$\rho_{22} = k_{eq,w} \cdot \left(1 - S_H S_{OH}/K_{eq,w}\right)$
S_{O2} transfer to the atmosphere	$\rho_{23} = K_{la,O2} \cdot \left(S_{O2}^{WAT} - S_{O2}\right)$
S_{CO2} transfer to the atmosphere	$\rho_{24} = K_{la,CO2} \cdot \left(S_{CO2}^{WAT} - S_{CO2}\right)$
S_{NH3} transfer to the atmosphere	$\rho_{25} = K_{la,NH3} \cdot \left(-S_{NH3}\right)$

Table 3.3. Factors and submodels

Model factor	Submodel	
Photosynthetic factories model (Eileers and Peeters) (Eilers and Peeters, 1988)		
$f_I = x_2$	$\frac{dx_1}{dt} = -\alpha \cdot I \cdot x_1 + \gamma \cdot x_2 + \delta \cdot x_3$ $\frac{dx_2}{dt} = \alpha \cdot I \cdot x_1 - \gamma \cdot x_2 - \beta \cdot I \cdot x_2$ $\frac{dx_3}{dt} = \beta \cdot I \cdot x_2 - \delta \cdot x_3$ $x_1 + x_2 + x_3 = 1$ where: $I = I_{av}$ The average light intensity ($I_{av)}$ was described using Lambert-Beer's Law: $I_{av} = \frac{I_0(1-exp(-K_i \cdot TSS \cdot d))}{K_i \cdot TSS \cdot d}$ where: $TSS = X_{ALG} + X_H + X_I + X_S + X_{AOB} + X_{NOB}$	x_1: Microalgae in open state (ready to capture a photon). x_2: Microalgae in activated state (microalgae can go back to open state or can capture another photon). x_3: Microalgae in inhibited state (ready to turn back to the open state. α: Rate of activation $[(\mu E\ m^{-2})^{-1}]$ γ: Rate constant of production $[s^{-1}]$ β: Rate constant of inhibition $[(\mu E\ m^{-2})^{-1}]$ δ: Rate of recovery $[s^{-1}]$ I_{av}: Average light intensity $[\mu mol\ m^{-2} s^{-1}]$ I_0: Incident light intensity $[\mu mol\ m^{-2} s^{-1}]$ K_i: Extinction coefficient for particulate biomass $[m^2 g^{-1}]$ TSS: Particulate components $[gTSS\ m^{-3}]$ d: Photobioreactor depth $[m]$

Photorespiration model		
f_{DO}	$f_{DO} = \begin{cases} 1 - tanh\left(\dfrac{K_{PR} \cdot \dfrac{S_{O2}}{\tau \cdot S_{O2}^{SAT}}}{1 - \dfrac{S_{O2}}{\tau \cdot S_{O2}^{SAT}}}\right), & S_{O2} \leq \tau \cdot S_{O2}^{SAT} \\ 0, \quad S_{O2} > \tau \cdot S_{O2}^{SAT} \end{cases}$	S_{O2}^{SAT}: Saturation concentration of oxygen in the air $[gO_2\ m^{-3}]$ K_{PR}: Photorespiration inhibition constant τ: Coefficient of excess dissolved oxygen

pH model		
f_{pH_i}	$f_{pH_i} = \dfrac{(pH - pH_{i,max})(pH - pH_{i,min})^2}{(pH_{i,opt} - pH_{i,min})[(pH_{i,opt} - pH_{i,min})(pH - pH_{i,opt}) - (pH_{i,opt} - pH_{i,max})(pH_{i,opt} + pH_{i,min} - 2pH)]}$	i: Refers to the i-th species of microorganism considered in the model (microalgae, heterotrophic bacteria, and nitrifying bacteria)
Temperature model		
f_{T_i}	$f_{T_i} = \dfrac{(T - T_{i,max})(T - T_{i,min})^2}{(T_{i,opt} - T_{i,min})[(T_{i,opt} - T_{i,min})(T - T_{i,opt}) - (T_{i,opt} - T_{i,max})(T_{i,opt} + T_{i,min} - 2T)]}$	i: Refers to microalgae and nitrifying bacteria)
f_{T_H}	$f_{T_H} = \theta^{T - T_{H,opt}}$	$T_{H,opt}$: Optimal temperature for heterotrophic bacteria [°C] θ: Temperature coefficient

Table 3.4 summarizes the main reactions related to the activity of the microorganisms in each reactor. Since the anoxic tank is maintained under dark conditions, the growth of microalgae is not considered in this reactor. Similarly, due to the occurrence of anoxic conditions, the growth of autotrophic bacteria and the aerobic growth of heterotrophic bacteria are not considered in the anoxic reactor. Reactions related to chemical equilibrium were assumed to occur in the photobioreactor and the anoxic reactor, while the transfer of gases was considered to occur only in the photobioreactor since the anoxic reactor was a closed unit. Evaporation was also considered in the mass balance expressions in the photobioreactor.

Table 3.4. Processes considered in each compartment of the anoxic-aerobic algal-bacterial photobioreactor

	Process	**Anoxic Reactor**	**Aerobic Reactor**
Microalgae processes	Growth on S_{NH4}	Not Considered	Considered
	Growth on S_{NO3}	Not Considered	Considered
	Endogenous respiration	Considered	Considered
	Decay	Considered	Considered
Heterotrophic bacteria processes	Aerobic growth on S_{NH4}	Not Considered	Considered
	Aerobic growth on S_{NO3}	Not Considered	Considered
	Anoxic growth on S_{NO2} (denitrification on S_{NO2})	Considered	Considered
	Anoxic growth on S_{NO3} (denitrification on S_{NO3})	Considered	Considered
	Aerobic endogenous respiration	Not Considered	Considered
	Anoxic endogenous respiration	Considered	Considered
	Decay	Considered	Considered
Autotrophic bacteria processes	Growth of X_{AOB}	Not Considered	Considered
	Growth of X_{NOB}	Not Considered	Considered
	Endogenous respiration of X_{AOB}	Considered	Considered
	Endogenous respiration of X_{NOB}	Considered	Considered
	Decay of X_{AOB}	Considered	Considered
	Decay of X_{NOB}	Considered	Considered
Hydrolysis	Hydrolysis	Considered	Considered
Chemical equilibrium	Chemical equilibrium $CO_2 \leftrightarrow HCO_3^-$	Considered	Considered
	Chemical equilibrium $HCO_3^- \leftrightarrow CO_3^{2-}$	Considered	Considered
	Chemical equilibrium $NH_4^+ \leftrightarrow NH_3$	Considered	Considered
	Chemical equilibrium $H^+ \leftrightarrow OH^-$	Considered	Considered
Transfer of gases	S_{O2} transfer to the atmosphere	Not Considered	Considered
	S_{CO2} transfer to the atmosphere	Not Considered	Considered
	S_{NH3} transfer to the atmosphere	Not Considered	Considered

3.1.2. Settler modeling

The settler was described using the mass balance expressions of the model of Takács *et al*. (Takács, Patryioand and Nolasco, 1991). The model is a multilayer dynamic model of clarification and thickening processes based on the concept of solids flux and mass balance around each layer of a one-dimensional settler. This model can simulate the solids profile throughout the settling column, including the underflow and effluent suspended solids concentrations under steady-state and dynamic conditions.

The model of Tákacs *et al*. (Takács, Patryioand and Nolasco, 1991) assumes that no biological reactions take place in the settler. The model considers the settler as a set of layers, so that the gravitational flow of solids depends on the concentration of sludge in the settler. Two important assumptions are also made in this model:

(1) incoming particles are instantaneously and uniformly distributed over the entire cross-sectional area of the settler layer,

(2) the model equations only consider flow in the vertical direction.

The basic principle of this model is based on the mass balance of the suspended solids in each layer. The flux of solids in each layer (J) depends on the concentration of solids (X) in the layer and the velocity of the solids (v) as given in equation (3.1). The solids flux due to the bulk motion of the liquid can be upward or downward depending on the position of the layer with respect to the feed point.

$$J = v(X)X \tag{3.1}$$

Five different groups of layers are described with the Tákacs model, depending on their position relative to the feed point: the top layer, the layers above the feed point, the feed layer, the layers below the feed point, and the bottom layer.

Considering the settler divided into *n* layers, layer 1 is the top layer and *m* is the feed layer. The state equations describing the concentrations in each layer are represented by the expressions (3.2)-(3.6):

$$\frac{dx_1}{dt} = \frac{1}{h}\left(J_{up,2} - J_{up,1} - J_{s,1}\right) \tag{3.2}$$

$$\frac{dx_i}{dt} = \frac{1}{h}\left(J_{up,i+1} - J_{up,i} + J_{s,i-1} - J_{s,1}\right) \qquad 2 \leq i < m \tag{3.3}$$

$$\frac{dx_m}{dt} = \frac{1}{h}\left(\frac{Q_{in}X_{in}}{A} - J_{up,m} - J_{dn,m} + J_{s,m-1} - J_{s,m}\right) \tag{3.4}$$

$$\frac{dx_j}{dt} = \frac{1}{h}\left(J_{dn,j-1} - J_{dn,j} + J_{s,j-1} - J_{s,j}\right) \qquad m < j < n \tag{3.5}$$

$$\frac{dx_n}{dt} = \frac{1}{h}\left(J_{dn,n-1} - J_{dn,n} + J_{s,n-1}\right) \tag{3.6}$$

where A represents the surface area of the settler, Q_{in} and X_{in} represent the influent flow rate, and the influent suspended solids concentration to the settler, respectively. Expressions (3.7) and (3.8) describe the upward (J_{up}) and downward (J_{dn}) solids flux due to the bulk motion of the liquid, respectively. Q_{ef} is the treated effluent flow rate and Q_{out} is the sum of the recycle and wastage flow rates.

$$J_{up,i} = \frac{Q_{ef}X_i}{A} \qquad 2 \le i \le m \tag{3.7}$$

$$J_{dn,j} = \frac{Q_{out}X_j}{A} \qquad m \le j \le n \tag{3.8}$$

In each layer the solids flux due to gravity settling is determined using (3.9):

$$J_{s,k} = \min\left(V_{s,k}X_k, V_{s,k+1}X_{k+1}\right) \qquad 1 \le k \le n-1 \tag{3.9}$$

The generalized settling velocity (3.10) is described using the double-exponential model proposed by Takács and co-workers (Takács, Patryioand and Nolasco, 1991). This model is valid for both: thickening and clarified zone.

$$V_{s,k} = V_0 e^{-r_h(X_k - X_{min})} - V_0 e^{-r_p(X_k - X_{min})} \quad 1 \le k \le n \quad 0 \le V_s \le V_0' \tag{3.10}$$

where:

$V_{s,k}$: Settling velocity of the solids particles in the layer k [dm/d]

X_{min}: Minimum attainable suspended solids concentration in the effluent [mg/L]

V_0: Maximum theoretical settling velocity [dm/d]

V_0': Maximum practical settling velocity [dm/d]

r_h: Settling parameter associated with the hindered settling component of settling velocity equation [L/mg]

r_p: Settling parameter associated with the low concentration and slowly settling component of the suspension [L/mg]

This work considers a 10-layer settler of equal volume and assumes that no biological reactions occur in the settler. The model considers only biomass dynamics to predict the biomass concentration in each layer of the settler. Thus, to estimate the concentration of components in the settler (and in the external recirculation and effluent streams), this assumption implies:

- the concentration of the dissolved components in the settler is assumed to be the same as in the photobioreactor, and
- the percentage of each component of the biomass in the settler is assumed to be exactly the same as in the photobioreactor.

3.2. Library for microalgae-bacteria wastewater treatment modeling

This section presents the development of a library of components for the simulation of wastewater treatment plants based on microalgae-bacteria consortia using the dynamic programming environment EcosimPro|PROOSIS® (EA Internacional, 2024).

As mentioned in the previous chapter, several models have been proposed in the last two decades to represent microalgae-bacteria interactions (Reichert *et al.*, 2001; Solimeno *et al.*, 2017a; Solimeno, Gómez-Serrano and Acién, 2019a; Casagli *et al.*, 2021; Sánchez-Zurano *et al.*, 2021). For the simulation of these models, different programming tools have been used, such as MATLAB®, COMSOL Multiphysics®, AQUASIM, among others.

Using these models requires a broad understanding of the variables and equations that describe the dynamics of the process, as well as mathematical and programming skills that make them difficult to use for students and staff unfamiliar with all the elements of the models. In most cases, this makes adding new process units or modifying existing ones too complex for anyone outside the programming team.

The main tools that make models accessible to non-experts users are graphical environments and model libraries, especially those based on object-oriented programming, also known as structured programming. On the one hand, the former allows the user to handle models intuitively (for example, by using icons to represent a particular process). On the other hand, OOP facilitates software updates, teamwork, or the creation of graphical environments through features such as model reuse, inheritance, encapsulation, or abstraction. OOP allows the user to utilize a component without the

understanding of the implementation details of the model. The user's knowledge is limited to the component's intended purpose, inputs, and outputs. Object-oriented modeling facilitates the reuse of previously developed models and also encourages the creation of parameterizable component libraries with broad applicability across a variety of simulation projects.

The use of object-oriented programming and library development to simulate industrial processes is a common practice, as evidenced by numerous studies (Vilas *et al.*, 2008; Mazaeda *et al.*, 2011; Palacin *et al.*, 2011). In the context of wastewater treatment systems based on microalgae-bacteria consortia, a comparable methodology has only been proposed through the plant-wide model (PWM) for the description of microalgal processes in wastewater treatment plant simulations (Tejido-Núñez, 2020).

3.2.1. Library development using EcosimPro|PROOSIS®

EcosimPro|PROOSIS ® is a modeling and simulation tool for multidisciplinary systems. Based on algebraic differential equations and discrete events, it allows the modeling of a wide range of systems, including control, thermal, hydraulic, and mechanical systems. PROOSIS® allows the creation of physical system models based on object-oriented concepts similar to those used in programming languages such as C++ and Java. Using PROOSIS's proprietary modeling language (EL), the data and dynamic behavior of the system can be encapsulated in reusable components that provide a well-defined public interface while hiding the intricacies of their internal implementation. PROOSIS® allows the construction of more complex components by integrating basic components. It also allows the definition of a component as an extension or specialization of another basic component through inheritance mechanisms. The object-oriented modeling technology of PROOSIS® facilitates the creation of sophisticated dynamic models through the interconnection of components, thereby promoting a highly productive methodology of reusing parameterizable components that have already been tested. Furthermore, the open source code of the libraries allows for the integration of additional components not included in the existing functionality. The following are basic concepts that are involved in a simulation using PROOSIS®:

- Component: Represents a model of a physical object that incorporates variables, differential algebraic equations, topology, and discrete behavior. (Examples of components included in the software: pump, valve, and pipe).
- Ports: These define the connection points of a component with other components, allowing for the exchange of materials, energy, or information. Different ports are required for each discipline, for example, electrical, hydraulic, and chemical systems.
- Experiment: This refers to the process of defining how the model is going to be used in the simulation.
- Library: This includes all the library's components, ports, and global variables.

The library developed was called ALG_BACT_WWTP. This library includes the essential components that allow the modeling of a simple wastewater treatment plant: ports, sources and sinks, reactors, and settler. These components are shown in Fig. 3.2.

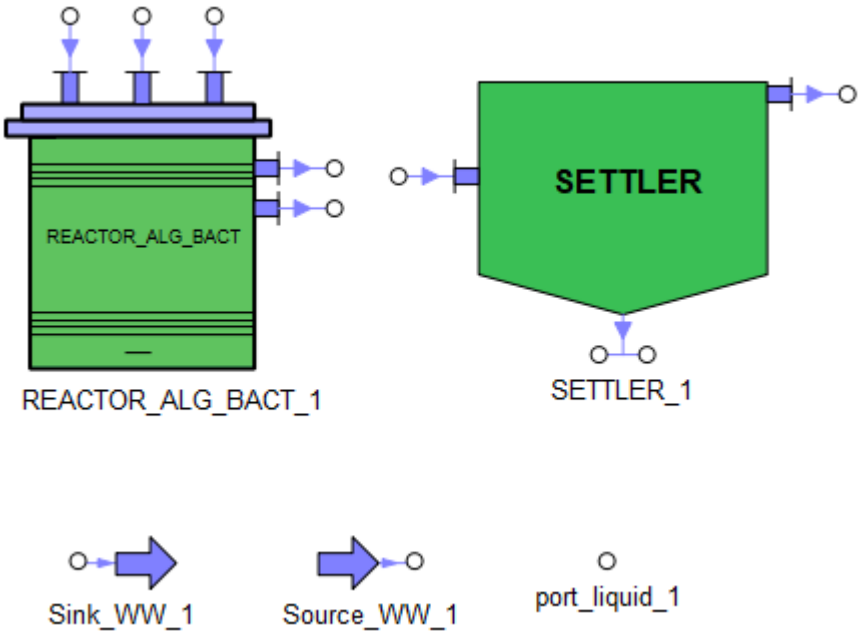

Fig. 3.2. Components of the library ALG_BACT_WWTP.

The definition of a special data type that will be used for all library components is essential to library design. The PROOSIS® software offers a variety of language

resources that facilitate a more concise definition. These resources are based on arrays and a specialized data type (ENUM), which is particularly useful for defining elements of a specific type, such as chemical species or microorganisms present in wastewater (WW). In the ALG_BACT_WWTP library, a data type (*WW_components*), is defined to include the potential elements present in wastewater. The enumeration of these elements was previously established in Table 3.1.

The components developed in the library ALG_BACT_WWTP are described below:

- *Port_liquid:* This port is used to connect the different elements of the WWTP.
- *Source_WW:* Wastewater source. Wastewater inlet to the facility. In this component, only the dissolved elements of Table 3.1 are considered. The user should assign a value to each dissolved component (depending on the wastewater concentration used in the simulation).
- *Sink_WW:* Wastewater sink. Wastewater or biomass outlet. The facility's output streams may contain both dissolved and particulate components.
- *REACTOR_ALG_BACT:* Algal-bacterial photobioreactor. This component encapsulates the differential equations described in Table 3.2. It can be used to describe different photobioreactor configurations. The user should define the photobioreactor type, size, and the incident radiation surface. By defect, *REACTOR_ALG_BACT* has three inputs and two outputs that can be used to connect different components in configurations with two or more stages. The user can modify the initial concentration of components and model parameters in a simple way.
- *SETTLER:* This component encapsulates the equations of the model of Takács et al. (Takács, Patryioand and Nolasco, 1991) (Section 3.1.2). The number of layers considered in the model and the physical dimensions of the settler can be modified. The component has one input and two outputs (for the clarified effluent and settled biomass).

Using the advantages of the OOP, more components could be included in the library ALG_BACT_WWTP, thereby enhancing its functionality. In a similar manner, components from other PROOSIS® libraries (e.g., tanks, valves, pumps, pipes, or controllers) could be added to simulate a WWTP. Components of the PROOSIS®

standard libraries, including HYDRAULIC, CONTROL, and PORTS, can be utilized by adding these libraries to the workspace and subsequently interconnecting the graphical symbols of the components according to the user's preference. The construction of a model of a microalgae-bacteria wastewater treatment plant can be achieved through the integration of its distinct components, akin to the physical world, and the subsequent allocation of values to the various parameters and boundary conditions that govern the plant's operation.

As illustrated in Fig. 3.3, a model for simulating a microalgae-bacteria wastewater treatment plant is presented, utilizing the components of the ALG_BACT_WWTP library. The anoxic-aerobic configuration described in Section 3.1 is represented by the components of the developed library. To specify the characteristics of the plant and operating conditions, the user can easily modify the component parameters and names by clicking on each component. This process is illustrated in the edition window of the photobioreactor represented in Fig. 3.4. This library empowers users to execute a diverse array of simulations, manipulating biological or operational parameters, without necessitating a comprehensive understanding of biological modeling principles.

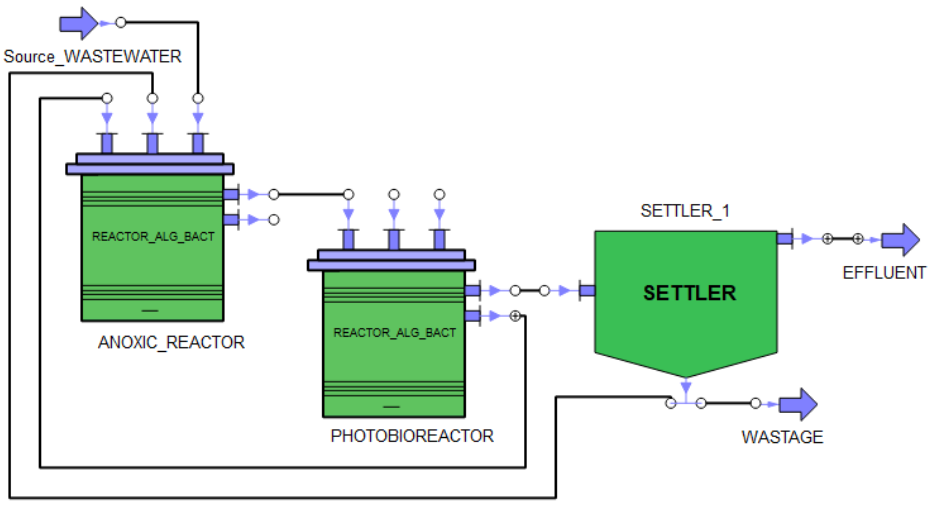

Fig. 3.3. Wastewater treatment plant with biomass recirculation using components of the library ALG_BACT_WWTP.

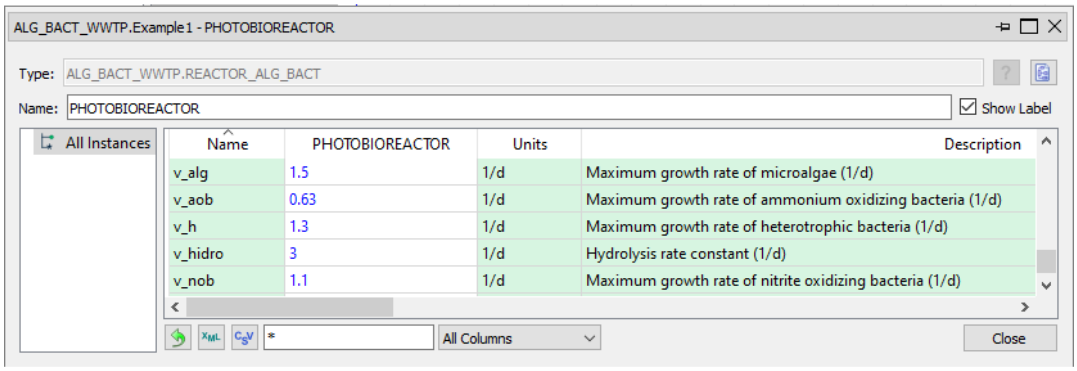

Fig. 3.4. Edition window of the component *REACTOR_ALG_BACT.*

3.3. Conclusions

In this chapter, the established models from the extant literature were adapted to represent novel configurations of anoxic-aerobic algal-bacterial photobioreactors for wastewater treatment. The proposed models allow for the simulation of anoxic-aerobic configurations with biomass recirculation under a range of operational conditions. A library of model components for microalgae and bacteria-based wastewater treatment plants was developed. The components developed can be reused for multiple simulations and allow for easy interconnection between plant components.

4. Parameter estimation in microalgae-bacteria processes

This chapter presents the parameter estimation for the anoxic-aerobic configuration described in Chapter 3. Parameter estimation, defined as the process of aligning a specified mathematical model with observed data, poses significant challenges in the context of bioprocesses. This complexity arises from the intricate nature of the model parameters, which are often characterized by high dimensionality. Consequently, a sensitivity analysis is conducted in the present study to ascertain the subset of parameters that exert the most significant influence on the system outputs. Subsequently, parameter estimation through optimization is performed to determine the optimal values of the model parameters. Finally, model validation is performed using the previously obtained model parameters. Fig. 4.1 provides a synopsis of the modeling and parameter estimation process employed in this thesis. The modeling, sensitivity analysis, parameter estimation, and model validation were conducted using the software PROOSIS®.

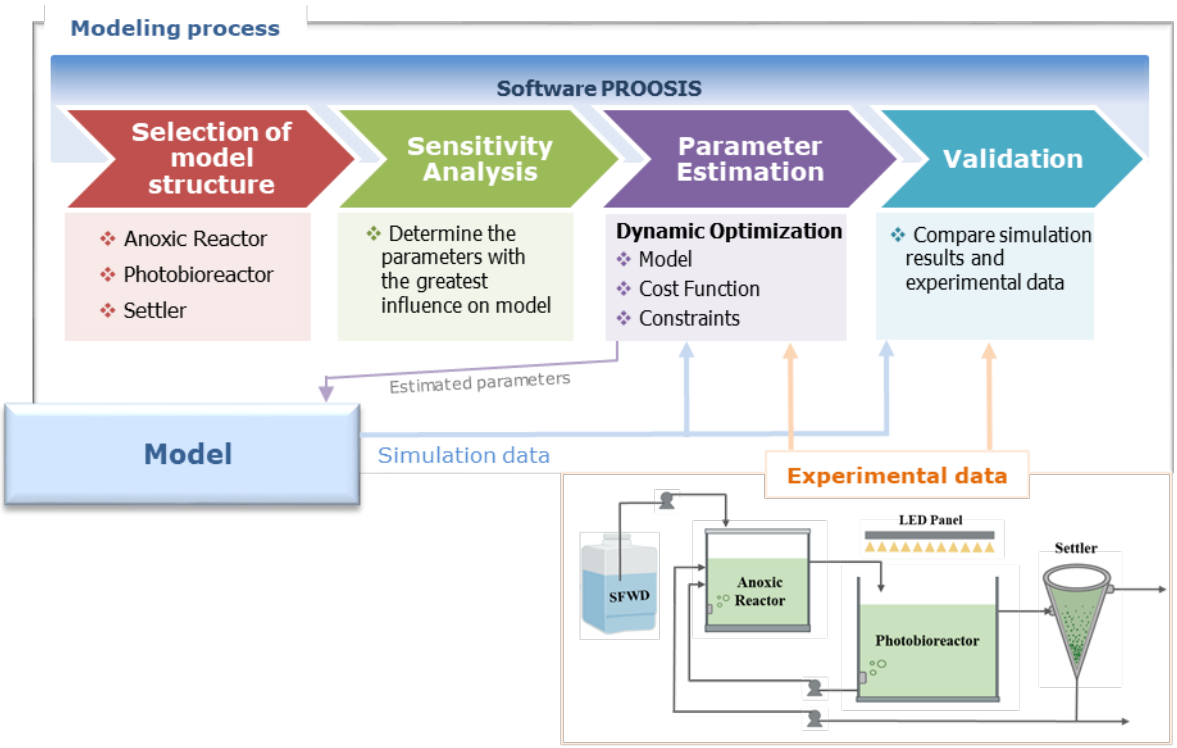

Fig. 4.1. Schematic of the modeling and parameter estimation process.

In the estimation of parameters, two approaches have been employed: the first involves the simultaneous determination of all parameters pertinent to the optimization problem (Section 4.1), while the second involves the division of the optimization problem into subproblems of increasing complexity (Section 4.2). This second approach enables the presentation of a methodology for parameter estimation that could be used in a variety of biological processes when multiple model outputs and parameters are involved in the optimization problem.

The initial approach to parameter estimation was evaluated in an anoxic-aerobic algal-bacterial photobioreactor configuration that treated synthetic food waste digestate (SFWD). The methodology of the subsequent approach was implemented in a comparable facility that treated synthetic domestic wastewater.

4.1. Parameter estimation in anoxic-aerobic algal bacterial system

The data utilized in this section to adjust the model of the anoxic-aerobic reactor configuration were collected by researchers from the Institute of Sustainable Processes at the University of Valladolid (Spain) from July to December of 2019. The experimental setup was operated with the objective of evaluating the performance of this photobioreactor configuration in the treatment of wastewater with high carbon and nitrogen loads.

The laboratory-scale plant utilized in the present study (Fig. 3.1) comprised an open photobioreactor with a working volume of 9.15 L. The photobioreactor was illuminated for 12 hours daily by LED lamps (1314±12 μE/m^2s). The anoxic reactor consisted of a gas-tight tank with a total working volume of 2.85 L maintained in the dark. The SFWD was fed to the anoxic tank at 1.2 L/d, continuously overflowing by gravity into the aerobic photobioreactor. The algal-bacterial broth was recycled at a rate of 2.4 L/d from the photobioreactor to the anoxic tank. The Imhoff cone, with a volume of 1 L, was utilized as a settler. The algal-bacterial biomass that accumulated at the bottom of the settler was subsequently transferred into the anoxic tank at a rate of 0.6 L/d. The system was operated continuously at a hydraulic retention time of 10 days and a temperature of 27 ± 2 ºC. Biomass was wasted from the bottom of the secondary settler to maintain the solids retention time at 18 d.

The experimental configuration was operated for 138 days under step changes in SFWD load. During the initial stage (Stage I), the anoxic-aerobic system was supplied with 25% diluted SFWD. Subsequently, SFWD load was augmented to 50% (Stage II), and finally, to 100% during the final stage of operation (Stage III). The details of SFWD composition, experimental setup, operational conditions, and the ensuing results can be found in the study by (Torres-Franco *et al.*, 2021).

The data utilized for model calibration and validation were the results obtained for the composition of the influent SFWD, anoxic tank, photobioreactor, settled biomass, and effluent (Torres-Franco *et al.*, 2021). The recorded variables included the pH, the concentration of dissolved oxygen (DO), dissolved total organic carbon (TOC), inorganic carbon (IC), dissolved N species (total nitrogen (TN), N-NH_4^+, N-NO_2^-, N-NO_3^-), dissolved phosphate (P-PO_4^{3-}), and biomass concentration, expressed as the total suspended solids (TSS) concentration. The measurement of DO and pH was conducted

on a daily basis, while the characterization of other variables occurred on a biweekly basis.

Similar to previous research in anoxic-aerobic systems (Alcántara *et al.*, 2015; Torres-Franco *et al.*, 2021), the model was built over the assumption that significant removals of N-NH_4^+, IC, and P-PO_4^{3-}, were mainly attributed to the contribution of the microbiology in the photobioreactor. In accordance with the aforementioned rationale, this study has considered eight key output variables in the reactors: TSS and TOC concentration in the photobioreactor and anoxic reactor; and dissolved oxygen, IC, N-NH_4^+ and P-PO_4^{3-} in the photobioreactor. In the settler, the TSS concentration in the effluent and the biomass wastage stream were considered output variables to adjust in the optimization problem. Table 4.1 summarized the output variables considered in the model.

Model simulation considers the processes occurring in the anoxic and aerobic reactors described in Table 3.4. As previously referred, biomass concentration in both reactors and settler was measured twice a week using standard procedures to determine the concentration of TSS and Volatile Suspended Solids (VSS). In the model used in this study, the concentrations of particulate components are expressed in terms of the Chemical Oxygen Demand. Results from COD tests developed in (Torres-Franco *et al.*, 2021) were used here to obtain the ratio VSS/COD used in the model. In the simulation, the average value of the experimental ratio gTSS/gCOD used was 1.28.

Equations (4.1) and (4.2) related the state model variables described in Table 3.1 and the measured variables (Table 4.1).

$$TSS[mgTSSL^{-1}] = X_{ALG} + X_H + X_{AOB} + X_{NOB} + X_I + X_S \quad (4.1)$$

$$TOC[mgCL^{-1}] = i_{C,SS}S_S + i_{C,SI}S_I \quad (4.2)$$

Where $i_{C,SS}$ and $i_{C,SI}$ are the fraction of carbon in the readily biodegradable soluble organic matter (S_s) and in the inert soluble organic matter (S_I), respectively, which accounted for:

$$i_{C,SS} = 0.318\ gC \cdot gCOD^{-1}$$

$$i_{C,SI} = 0.327 gC \cdot gCOD^{-1}$$

Table 4.1. Output variables considered in the model

Output variable [units]	Description	Sampling frequency
TSS_{anoxic} [mgTSS/L]	Total suspended solids concentration in the anoxic reactor	Twice a week
TOC_{anoxic} [mgC/L]	Total organic carbon concentration in the anoxic reactor	Twice a week
$TSS_{photobioreactor}$ [mgTSS/L]	Total suspended solids concentration in the photobioreactor	Twice a week
$TOC_{photobioreactor}$ [mgC/L]	Total organic carbon concentration in the photobioreactor	Twice a week
$IC_{photobioreactor}$ [mgC/L]	Inorganic carbon concentration in the photobioreactor	Twice a week
$S_{O2\ photobioreactor}$ [mgO_2/L]	Dissolved oxygen concentration in the photobioreactor	Daily
S_{NH4} [mgN-NH_4/L]	Dissolved ammonium concentration in the photobioreactor	Twice a week
S_{PO4} [mgP-PO_4/L]	Dissolved phosphate concentration in the photobioreactor	Twice a week
$TSS_{effluent}$ [mgTSS/L]	Total suspended solids concentration in the effluent flow	Twice a week
$TSS_{wastage}$ [mgTSS/L]	Total suspended solids concentration in the wastage flow	Twice a week

4.1.1. Sensitivity analysis

Parameter estimation in the anoxic-aerobic system poses a significant challenge due to the extensive number of model parameters involved, as evidenced by the data presented in Table A1.2 of Appendix 1. Previous to parameter estimation, a sensitivity analysis is needed to identify the parameters with the most significant impact on the model. Equation (4.3) describes the sensitivity functions $(s_{i,j})$ from the *i*-output of the model concerning the *j*-parameter (p_j):

$$s_{i,j} = \frac{\partial y_i}{\partial p_j} \tag{4.3}$$

In order to compare the values of the sensitivities, scale factors (Eq. (4.4)) should be used to normalize them:

$$\bar{s}_{i,j} = \frac{p_j}{\bar{y}_i}\frac{\partial y_i}{\partial p_j} \tag{4.4}$$

Here, $\bar{s}_{i,j}$ denotes the scaled sensitivity, and $\bar{y}_i$ represents the average value of the experimental output.

Then, the norm of column *j* of the output sensitivity matrix (4.5) provides a measure of the importance of the parameter p_j in the value of the model outputs (y_i). This allows to compare the influence of each parameter in the process response and decide which ones need to be accurately estimated and which ones can be assigned a reasonable value without significantly affecting the output.

$$\begin{bmatrix} s_{11} & s_{12} & \cdots & s_{1d} \\ s_{21} & s_{22} & \cdots & s_{2d} \\ \vdots & \vdots & \cdots & \vdots \\ s_{m1} & s_{m1} & \cdots & s_{md} \end{bmatrix} \tag{4.5}$$

Given the dynamic model described by Equation (4.6),

$$\dot{x}(t) = f(x(t), u(t), p) \qquad \mathrm{y}(t) = g(x(t), u(t), p) \tag{4.6}$$

The sensitivities (4.3) can be computed by differentiating the model represented by Eq. (4.6), then, integrating in parallel the so-called extended model, equations (4.7) and (4.8) are obtained:

$$\frac{d}{dt}\frac{\partial x}{\partial p} = \frac{\partial f}{\partial x}\frac{\partial x}{\partial p} + \frac{\partial f}{\partial p} \tag{4.7}$$

$$\frac{\partial y}{\partial p} = \frac{\partial g}{\partial x}\frac{\partial x}{\partial p} + \frac{\partial g}{\partial p} \tag{4.8}$$

Sensitivity analyses were conducted for reactors and the settler using the software PROOSIS® with IDAS. The name IDAS stands for Implicit Differential-Algebraic solver with Sensitivity capabilities (Hindmarsh *et al.*, 2005). Some model parameters are well-established in the literature, but others are strongly related to the operational conditions and microorganism strains used in the study. Thus, the sensitivity analysis was carried

out considering a subset of all the model parameters to determine those significantly influencing the model outputs for this specific study case, providing crucial insights into the system's behavior.

The sensitivity analysis took into account a subset of 11 parameters: the maximum specific growth rate of microalgae (μ_{ALG}), heterotrophic bacteria (μ_H), and nitrifying bacteria (μ_{AOB} and μ_{NOB}); the decay rate of microalgae ($k_{death,ALG}$), heterotrophic bacteria ($k_{death,H}$), and nitrifying bacteria ($k_{death,AOB}$ and $k_{death,NOB}$); and the mass transfer coefficients for oxygen ($K_{la,O2}$), carbon dioxide ($K_{la,CO2}$), and ammonia ($K_{la,NH3}$). The scaled sensitivity matrix for the study case is represented by Eq. (4.9):

$$
\begin{array}{c}
 \\
\mu_{ALG} \\
k_{inact,ALG} \\
\mu_H \\
k_{inact,H} \\
\mu_{AOB} \\
k_{inact,AOB} \\
\mu_{NOB} \\
k_{inact,NOB} \\
K_{la,O2} \\
K_{la,CO2} \\
K_{la,NH3}
\end{array}
\begin{array}{c}
\begin{array}{cccccccc}
TSS_{phot.} & S_{NH4} & S_{O2} & S_{PO4} & S_{IC} & TOC_{phot.} & TSS_{anoxic} & TOC_{anoxic}
\end{array} \\
\begin{bmatrix}
0.482 & -7.934 & 0.459 & -1.244 & -0.791 & 0.001 & 0.208 & -0.057 \\
-0.065 & 1.561 & -0.119 & 0.188 & 0.108 & 0.004 & -0.033 & 0.027 \\
-0.005 & -0.534 & 0.086 & 0.201 & -0.100 & -0.328 & 0.009 & -3.556 \\
0.255 & -0.220 & -0.086 & 0.194 & -0.008 & 0.207 & 0.141 & 1.963 \\
0.043 & -1.463 & -0.030 & -0.007 & -0.001 & 0.007 & 0.007 & 0.018 \\
-0.006 & 0.628 & 0.014 & 0.011 & 0.011 & -0.002 & -0.002 & -0.005 \\
0.023 & 0.643 & -0.081 & -0.018 & -0.019 & 0.002 & 0.009 & 0.016 \\
-0.004 & -0.014 & 0.022 & 0.006 & 0.006 & -0.000 & -0.002 & -0.003 \\
-0.002 & -0.065 & 0.030 & 0.000 & 0.002 & -0.001 & -0.001 & -0.001 \\
-0.000 & 0.000 & 0.000 & 0.000 & -0.042 & -0.000 & -0.000 & -0.000 \\
0.004 & -0.694 & -0.016 & -0.006 & -0.007 & 0.002 & 0.002 & 0.003
\end{bmatrix}
\end{array}
\tag{4.9}
$$

The results of the sensitivity analysis for both reactors revealed that the model outputs are particularly sensitive to 7 of the 11 parameters assessed. These include the maximum specific growth rates of microalgae and heterotrophic bacteria, the decay rates of microalgae and heterotrophic bacteria, and the mass transfer coefficients for oxygen, carbon dioxide, and ammonia. Graphical representations of the sensitivity analysis for these significant parameters are presented in Fig. 4.2 and Fig. 4.3.

Fig. 4.2A showcases the scaled sensitivity (Eq. (4.4)) for the dissolved ammonium (S_{NH_4}) in the photobioreactor. The graphical results highlight the significant sensitivity of the dissolved ammonium to the microalgae's maximum specific growth rate (blue line) and the mass transfer coefficient for ammonia (purple line). These results show the high inverse effect of the maximum specific growth rate of microalgae over the dissolved ammonium: an increase in μ_{ALG} implies a decrease in S_{NH_4} in the photobioreactor due to the fact that microalgae are the primary consumers of dissolved ammonium. On the

contrary, an increase in the microalgae decay rate (red line) mediates an increase in S_{NH_4}. In this facility, the mass transfer coefficient for ammonia significantly affects S_{NH_4} in the photobioreactor since ammonium is in equilibrium with ammonia. Dissolved ammonium is also affected (to a lower extent) by the parameters relative to the activity of heterotrophic bacteria since they consume ammonium during aerobic growth.

Fig. 4.2B shows the scaled sensitivity for the dissolved phosphate concentration (S_{PO_4}) in the photobioreactor. The results indicate that in this photobioreactor, the dissolved phosphate concentration is mainly affected by microalgae's maximum specific growth rate: an increase in μ_{ALG} (blue line) promotes a significant reduction in the dissolved phosphate concentration. Because heterotrophic bacteria assimilate phosphate during growth, S_{PO_4} is also sensitive to the decay rate of these microorganisms (yellow line). In a lower extent, the dissolved phosphate concentration is affected by the microalgae decay rate (red line) and heterotrophic bacteria growth rate (gray line).

Fig. 4.2C shows the results of the graphical sensitivity analysis over the inorganic carbon in the photobioreactor. These results indicate that inorganic carbon is especially sensitive to the parameters concerning microalgae activity, especially to the maximum specific growth rate. Microalgae growth consumes inorganic carbon (in the form of CO_2 and HCO_3), promoting a decrease in IC concentration, and microalgae death contributes to an increase in the dissolved IC in the photobioreactor. In addition, inorganic carbon is significantly affected by heterotrophic bacteria decay rate: an increase in $k_{death,H}$ promotes a decrease in the CO_2 release to the culture medium as a result of heterotrophic bacteria respiration.

Fig. 4.2D represents the sensitivity results for the concentration of dissolved total organic carbon. The parameters related to heterotrophic bacteria growth and decay rates are the most influential over TOC concentration: an increase in the maximum specific growth rate of heterotrophic bacteria promotes a decrease in the dissolved TOC as result of a significant assimilation of TOC into the heterotrophic biomass. On the contrary, an increase in the decay rate of heterotrophic bacteria implies a decrease in the assimilation of TOC by heterotrophic microorganisms (and, consequently, an increase in dissolved TOC in the photobioreactor).

With microalgae dominating the microbial population (50% of the inoculum corresponded to microalgae biomass (Torres-Franco *et al.*, 2021)), the maximum specific

growth rate of microalgae was the parameter with the most substantial influence over the concentrations of NH_4^+, PO_4^{3-}, and IC in the photobioreactor, as confirmed in Fig. 4.2A, Fig. 4.2B, and Fig. 4.2C, respectively. Similarly, the maximum specific growth rate of heterotrophic bacteria was the most influential parameter over the dissolved TOC, as evidenced in Fig. 4.2D. The differences in the values of graphical sensitivities observed during the period shown in Fig. 4.2 are the result of the stabilization of microbial populations in the photobioreactor.

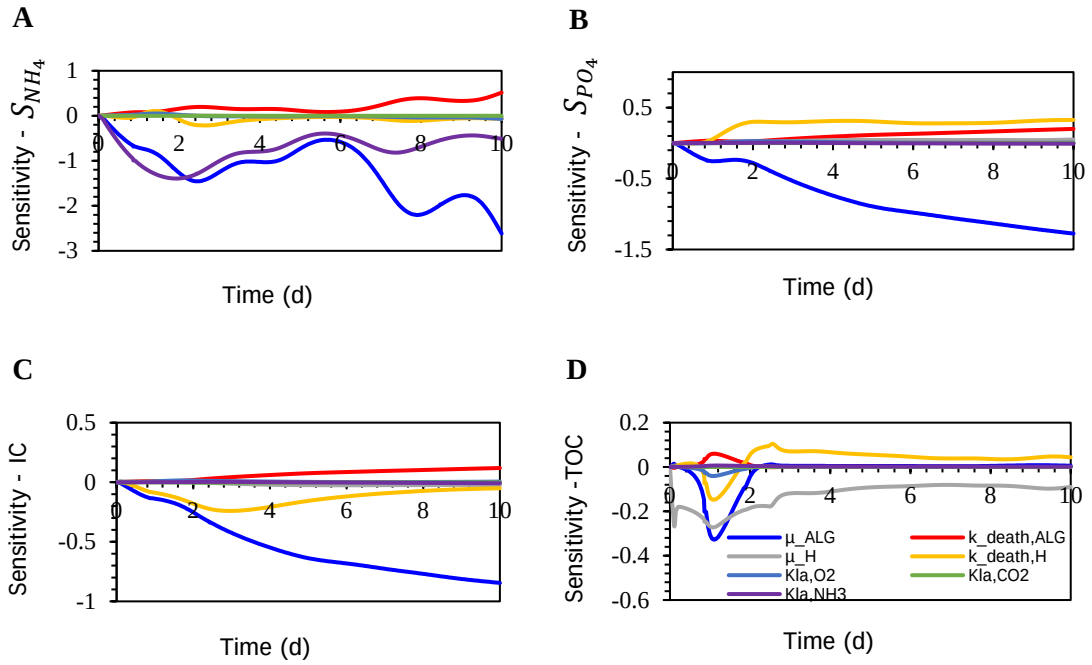

Fig. 4.2. Scaled sensitivities of the dissolved ammonium concentration (A), dissolved phosphate concentration (B), dissolved inorganic carbon concentration (C) and dissolved total organic carbon concentration (D) in the photobioreactor.

The scaled sensitivity over the dissolved oxygen concentration (S_{O_2}) is represented in Fig. 4.3A. It can be noted that the parameter with the most significant impact is the maximum specific growth rate of microalgae (blue line) as a result photosynthetic oxygen production. The decay rate of the microalgae (red line) also influences the dissolved oxygen concentration. Heterotrophic bacteria consume oxygen for organic matter assimilation, which explains that parameters related to heterotrophic bacteria activity also influence S_{O_2}. The mass transfer coefficient for oxygen is another parameter that affects the dissolved oxygen concentration.

Fig. 4.3B represents the scaled sensitivity of the total suspended solids concentration in the photobioreactor. Sensitivities of the parameters (without scaled, Eq. (4.3)) over microalgae concentration (X_{ALG}) and heterotrophic bacteria concentration (X_H) are presented in Fig. 4.3C and Fig. 4.3D, respectively. Biomass concentration was considered equivalent to the sum of all particulate components in the model (microalgae biomass, bacteria biomass, inert particulate organic matter, and slowly biodegradable particulate organic matter). Biomass concentration is affected mainly by the maximum specific growth rate of microalgae (blue line). In addition, the inactivation growth rates of microalgae (red line) and heterotrophic bacteria (yellow line) influence the biomass concentration (due to the decrease in these populations and the formation of particulate organic matter from microalgae and bacteria decay). The effect of parameters represented over microalgae and heterotrophic bacteria biomass represented in Fig. 4.3C and Fig. 4.3D evidences the critical role of normalization in sensitivity analysis for a correct interpretation of the results.

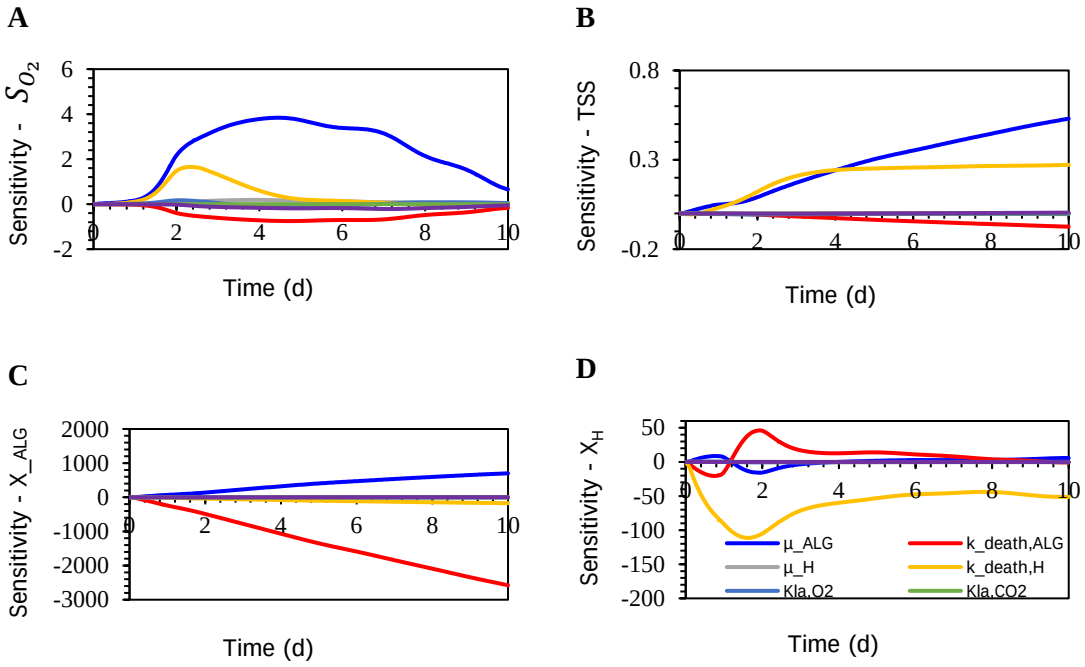

Fig. 4.3. Scaled sensitivity of the dissolved oxygen concentration (A) and for the total suspended solids concentration (B) in the photobioreactor. Unscaled sensitivity of microalgae biomass (C) and heterotrophic bacteria biomass concentration (D) in the photobioreactor.

Regarding the settler, the model parameters of the settling velocity equation (3.10) in the model of Takács *et al*. (Takács, Patryioand and Nolasco, 1991) are typically obtained using nonlinear dynamic optimization. Fig. 4.4 represents the sensitivity analysis for the parameters of the settling velocity equation over the TSS concentration in the effluent and wastage flow of the settler. Fig. 4.4A confirms the influence over the biomass concentration in the effluent flow of the parameter related to the minimum attainable suspended solids concentration in the effluent (X_{min} – blue line), the parameter associated with the low concentration of solids (r_p – gray line), and the maximum theoretical settling velocity (V_0 – yellow line). Fig. 4.4B represents the scaled sensitivity of TSS concentration in the wastage flow. This variable is affected by the maximum theoretical settling velocity and the settling parameters associated with the low solids concentration zone (r_p) and the hindered zone (r_h – red line). Fig. 4.4C and Fig. 4.4D represent the unscaled sensitivity for the biomass concentration in the effluent and wastage flow in the settler, respectively. Considerable scale differences between both analyzed output variables confirm the critical role of graphical and analytical sensitivity analysis (with and without normalization) as a previous stage in the calibration or parameter estimation process. This process ensures the precision and reliability of the results, enhancing the confidence in them.

The sensitivity analysis results in Fig. 4.2 to Fig. 4.4 provide valuable insights into the magnitude in which each selected parameter influences model outputs. These results underscore the importance of sensitivity analysis for each photobioreactor configuration, inoculum characteristics, and operational values.

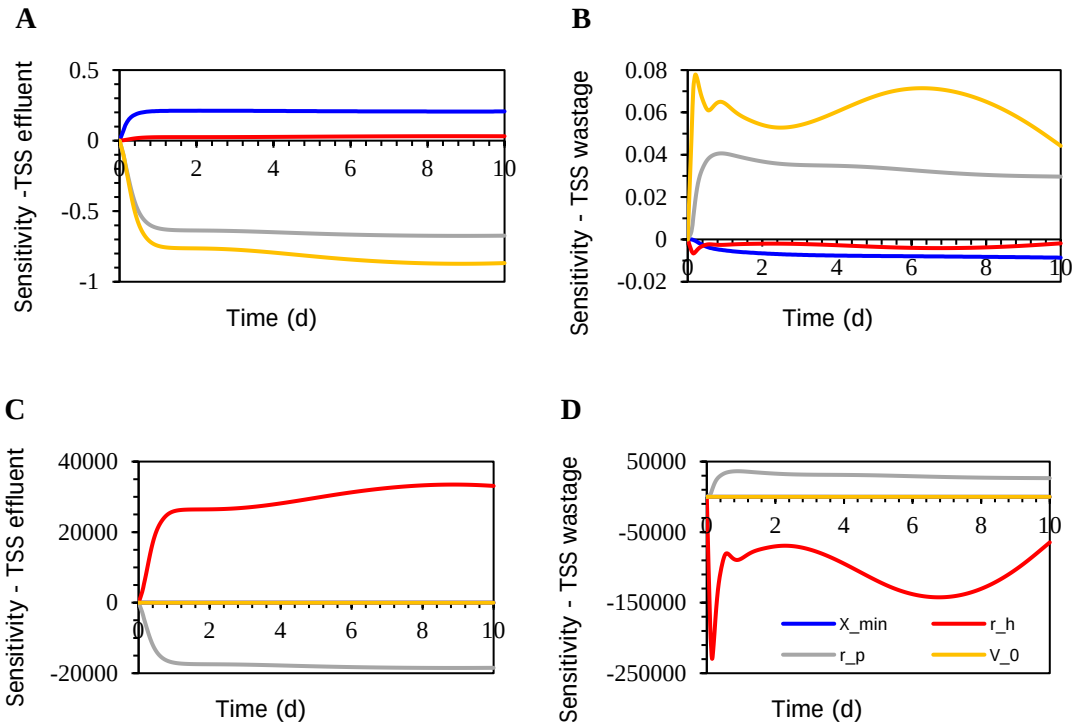

Fig. 4.4. Scaled sensitivity of the TSS concentration in the effluent (A) and in the wastage flow (B) in the settler. Unscaled sensitivity for biomass concentration in the effluent (C) and wastage flow (D).

4.1.2. Parameter estimation

The sequential approach to solving a parameter estimation problem in terms of optimization considers that for each value of the vector of parameters $\boldsymbol{\theta}$ (decision variables), the model predicts the system's response $\hat{y}(t, \boldsymbol{\theta})$ in each experiment over time t. For this purpose, a set of data samples from the inputs $\boldsymbol{u}(t)$ and outputs $\boldsymbol{y}(t)$ of the process are selected. The exact sequence of process inputs $\boldsymbol{u}(t)$ applied to the process is also used in the model, and both outputs $\boldsymbol{y}(t)$ from the process and $\hat{\boldsymbol{y}}(t, \boldsymbol{\theta})$ from the simulation are compared at every sampling time t. At each t, the prediction error $(\hat{\boldsymbol{y}}(t, \boldsymbol{\theta}) - \boldsymbol{y}(t))$ indicates model goodness, and the parameterization procedure looks for the set of model parameters $\boldsymbol{\theta}$ that minimizes a cost function of the prediction errors. The parameter estimation problem can be formulated as a dynamic optimization problem, which can be solved, for instance, through a nonlinear programming (NLP) software using a control vector parameterization technique and a proper procedure for computing the cost function, following the architecture of Fig. 4.5. This work uses the SNOPT algorithm

(Gill, Murray and Saunders, 2005), a well-known sequential quadratic programming code for nonlinear optimization within the PROOSIS® dynamic simulation environment. The selected integration method was IDAS.

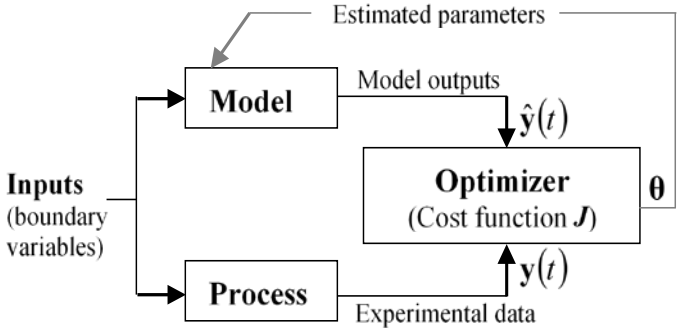

Fig. 4.5. Estimator in sequential optimization.

Although there are several methods for obtaining the statistically coherent value of variables and estimating the parameters of the mathematical model based on available data, the weighted least squares (WLS) method is used most frequently. The estimator WLS described by Eq. (4.10) consists of the squared difference between the measurement y and the model prediction $\hat{y}$. The differences are scaled with their respective standard deviation σ to account for varying dimensions of the model. This method assumes that measurement errors follow the Normal distribution model. The assumption of Normal distribution can be severely violated if one or more gross errors, which are not easy to detect, are present in the measured data set. Even when the majority of the data conforms to a Normal distribution, such anomalies can lead in poor or deviated estimates (de Menezes *et al.*, 2021).

$$J_{LS} = \frac{1}{2}[((\hat{\boldsymbol{y}} - \boldsymbol{y})/\sigma))^2\,] \tag{4.10}$$

In order to avoid this problem, a robust estimator can be used instead. Robust estimation can be understood as “insensitivity to large deviations from idealized hypotheses” for which the estimator is optimized (Huber and Ronchetti, 2009). To define the concept of robust estimation, a set of observations $\{y_1, \cdots, y_n\}$ drawn from some distribution $h(x)$ must be considered. This set will be used to estimate some parameters θ, where $\hat{\theta}_n$ is the estimate. The sampling distribution of this estimate is noted as $\varphi(\hat{\theta}_n, h)$ and depends

upon $h(x)$. However, $h(x)$ is not typically known; instead, an approximated model $f(x)$ is available. Roughly speaking, $\hat{\theta}_n$ is robust if it scarcely depends upon the difference between $h(x)$ and $f(x)$, i.e. we expect $\varphi(\hat{\theta}_n, h)$ and $\varphi(\hat{\theta}_n, f)$ to be close together.

More precisely, $\hat{\theta}_n$ is considered robust with respect to distribution f (and to h) if

$$d(h,f) < \eta \Longrightarrow d\left[\varphi(\hat{\theta}_n, h), \varphi(\hat{\theta}_n, f)\right] < \epsilon \tag{4.11}$$

For small positive ϵ and η, and $d(h,f)$ defines the distance between the distributions h and f, associated with the measures of the plant and the outputs on the simulation model (Rey, 1983).

Robust statistics provides methods that emulate conventional statistical ones but are less affected by spurious values or other deviations from the reference statistical distribution model. Among the robust estimators, M-estimators (the generalization of the Maximum Likelihood Estimator) have been successfully applied to several problems in the chemical process industry. The review presented in (de Menezes *et al.*, 2021), which analyzed 50 estimators (48 robust estimators), shows that the Contaminated Normal (quasi-robust), Welsch, Hampel, Fair, Lorentzian, Correntropy, and Cauchy M-estimators were the most used for regression analysis in chemical engineering problems.

The Fair function is a convex estimator with continuous first and second order derivatives. It is defined by Equation (4.12), where $c \in \mathbb{R}+$ is a user-defined fitting parameter to tune the slope for large residues.

$$J_{FF} = c^2 \left[\frac{\left| \frac{\hat{y} - y}{\sigma} \right|}{c} - ln\left(1 + \frac{\left| \frac{\hat{y} - y}{\sigma} \right|}{c} \right) \right] \tag{4.12}$$

M-estimators are robust because of their intrinsic mathematical structure, which renders the estimation less sensitive to spurious deviations (Rey, 1983; Huber and Ronchetti, 2009; Huber, 2011). These estimators, which use cost functions different from least squares (LS) or WLS, tend to value most of the data around the mean and ignore the influence of spurious values (usually located far from the mean) simultaneously. This performance is represented in Fig. 4.6, which compare the fair estimator (4.12) and the LS estimator (4.10), evidencing the influence of scaled error over the estimator function.

Thus, an accurate regression can be performed using robust estimators even if nothing is known a priori about outliers or the structure of gross errors.

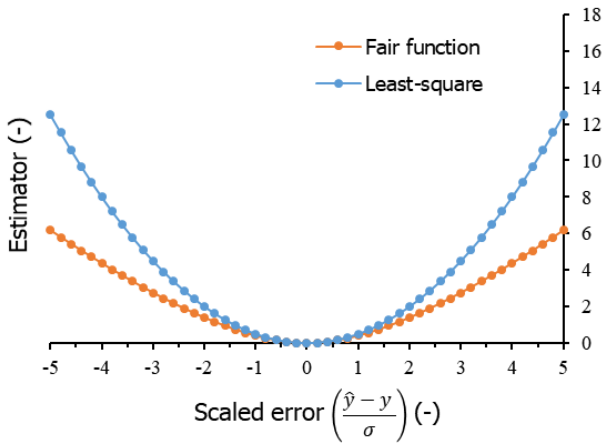

Fig. 4.6. Comparison of Least squares and Fair function (c=3) estimators.

In the present work, the Fair function estimator was used as a robust objective function *J* for parameter estimation. This robust estimator was employed to address the uncertainties stemming from unreliable measurements, which may be attributable to various sources:

- Many analytical procedures used to obtain the data are based on the use of external standards for calibration or data comparison. These solutions are subject to human errors during preparation
- Human errors in sample preparation and analysis can play a significant role in the accuracy of the experimental data obtained through analytical methods. For instance, errors in sample dilution preparation, non-homogeneous mixing, or sample degradation can lead to inaccurate results.
- The incorrect use of calibration curves: methods used to determine the concentration of dissolved NH_4^+, NO_2^-, NO_3^-, and PO_4^{3-} use external calibration curves. The accuracy of the measurement largely depends on the expertise of the person analyzing the sample.
- The methods used to determine biomass concentration (TSS and VSS) can be significantly influenced by human errors in sample collection, such as non-homogeneous mixing of the sample and the presence of flocculated biomass. Additionally, procedure errors like filter obstruction, irregular oven and muffle

temperatures, and violations of recommended drying times can also affect these measurements. Incorrect preservation of the samples (that can result in sample degradation and changes in the properties due to light and high-temperature exposition).

- The use of non-updated calibration curves in equipment.

The resulting dynamic optimization problem is formulated using Eq. (4.13):

$$\min_{\hat{\theta}} J(\hat{\theta}, \theta) = \sum_{j \in M} c^2 \left[\frac{|\varepsilon_j|}{c} - ln\left(1 + \frac{|\varepsilon_j|}{c}\right) \right] \tag{4.13}$$

Subject to constraints imposed by the model in Equation (4.14) and the upper and lower limits on the values of the parameters described by Equations (4.15), states (4.16), and outputs (4.17),

$$\frac{d\mathbf{x}(t)}{dt} = \mathbf{f}(\mathbf{x}(t), \mathbf{u}(t), \boldsymbol{\theta}, t) \qquad \hat{\mathbf{y}}(t) = \mathbf{g}(\mathbf{x}(t), \mathbf{u}(t), \boldsymbol{\theta}, t) \tag{4.14}$$

$$\underline{\boldsymbol{\theta}} \leq \hat{\boldsymbol{\theta}} \leq \overline{\boldsymbol{\theta}} \tag{4.15}$$

$$\underline{\mathbf{x}} \leq \hat{\mathbf{x}} \leq \overline{\mathbf{x}} \tag{4.16}$$

$$\underline{\mathbf{y}} \leq \hat{\mathbf{y}} \leq \overline{\mathbf{y}} \tag{4.17}$$

where $\varepsilon_j = \left(\hat{\boldsymbol{y}}(t_j, \hat{\theta}) - \boldsymbol{y}(t_j)\right)/\sigma_m$ is the error between available process measurements $\boldsymbol{y}(t_j)$ and their estimated values $\hat{\boldsymbol{y}}(t_j, \hat{\theta})$ limited between user-defined minimum and maximum values (Eq. (4.15) - (4.17)). Besides robust properties, the simplicity of tuning (just one tuning parameter) is another remarkable advantage of the Fair estimator. In the present work, all simulations were carried out using a value of c=2.9 in the tuning parameter of the cost function (4.13).

To comprehensively capture the dynamics of the anoxic-aerobic photobioreactor configuration treating different dilutions of digestate within the model, the data from 138 days of operation (Torres-Franco *et al.*, 2021) were divided into two datasets. The first dataset was devoted to parameter estimation in the reactors and the settler, and the second was utilized for model validation. Specifically, data from stage II and 25 days of stage III (50% and 100% digestate, respectively) were used for parameter estimation. Validation

was then conducted using data from the first stage (25% digestate – 40 days of operation) and days 116 to 138 from stage III (undiluted digestate – 22 days of operation).

Several decisions were made to improve the solution of parameter estimation, taking into account the specific experimental conditions:

1- Experimental data were obtained under illumination cycles of 12 h ON/12 h OFF (Torres-Franco *et al.*, 2021) (considered in daily fraction with illumination between 2 am (0.083 d) and 2 pm (0.583 d)). Because of this, the time step used for the simulations was 0.1 d. Using superior time steps could result in an accuracy loss for the simulation of day/night cycles (and their influence over the model state variables).
2- The values of some variables vary significantly between day and night in the photobioreactor. Because samples were always drawn during illuminated periods, output data interpolation may result in non-representative data values of the internal dynamics in the photobioreactor. Therefore, only the recorded data at the exact time were considered in the cost function.
3- Since the values of experimental data broadly differ from stage I to stage III, different limits on state and output variables (Eq. (4.16) and Eq. (4.17)), were considered in the optimization problem for each simulation stage.

The initial concentration of the components in the reactors and the settler used to conduct the model simulation are shown in Table A2.1 and Table A2.2, respectively, in Appendix 2.

Table 4.2 shows the limits for the decision variables (Eq. (4.15)) and the initial values of parameters needed for parameter estimation via optimization in the anoxic and aerobic reactors. These values were established from a comprehensive review of similar studies reported in the literature (Solimeno *et al.*, 2017a; Solimeno, Gómez-Serrano and Acién, 2019a; Casagli *et al.*, 2021; Bausa *et al.*, 2022).

Table 4.3 shows the values of the decision variables for both bioreactors estimated in this study via optimization (4.13). All parameter values obtained are within the ranges reported in the literature for similar systems (Solimeno *et al.*, 2017a; Solimeno, Gómez-Serrano and Acién, 2019a; Casagli *et al.*, 2021; Bausa *et al.*, 2022). Parameter estimation was an essential aspect of this study since it provided the maximum specific growth and

decay rates of the biomass, as well as information about parameters that strongly depended on photobioreactor size, shape, and stirring (like the mass transfer coefficients). The adequate calibration of these parameters provides insights into the system model that will be helpful in using the model for prediction and control purposes.

Table 4.2. Initial values and limits for decision variables in the anoxic and aerobic photobioreactor

Parameter [units]	**Description**	**Initial value**	**Limits for optimization**
μ_{ALG} [d^{-1}]	Maximum specific growth rate of microalgae	1.5	0.4 – 4
$k_{death,ALG}$ [d^{-1}]	Decay rate of microalgae	0.1	0.05-0.21
μ_H [d^{-1}]	Maximum specific growth rate of heterotrophic bacteria	4	1-6
$k_{death,H}$ [d^{-1}]	Decay rate of heterotrophic bacteria	0.6	0.12-0.9
$K_{la,\ O2}$ [d^{-1}]	Mass transfer coefficient for oxygen	1	0.3-30
$K_{la,\ CO2}$ [d^{-1}]	Mass transfer coefficient for carbon dioxide	1	0.3-30
$K_{la,\ NH3}$ [d^{-1}]	Mass transfer coefficient for ammonia	0.8	0.3-30

Table 4.3**.** Values of estimated parameters in anoxic and aerobic reactor

Parameter	**Value [units]**
μ_{ALG}	0.70 d^{-1}
μ_H	2.50 d^{-1}
$k_{death,ALG}$	0.05 d^{-1}
$k_{death,H}$	0.80 d^{-1}
$K_{la,\ O2}$	0.5 d^{-1}
$K_{la,\ CO2}$	2.17 d^{-1}
$K_{la,\ NH3}$	0.5 d^{-1}

The settling properties of microalgae biomass (and consequently, the models to predict them) are nowadays an open-research field. Settling parameters in microalgae processes are widely dependent on the settler size, shape, and the structure of the microbial population. Therefore, those parameters should be determined for each specific configuration.

During the treatment of undiluted digestate, an increase in the TSS concentration in the effluent and a decrease in the average TSS concentration in the wastage stream were reported (Torres-Franco *et al.*, 2021) as a consequence of a reduction of the settling efficiency (promoted by the decline in the biomass entering the settler from the photobioreactor). The research conducted in (Torres-Franco *et al.*, 2021), when analyzing the microalgae populations, reported the dominance of *C. vulgaris, Tetradesmus obliquus*, and *Cryptomonas* sp. during stages I and II, while the dominant algal strains during stage III where *Chlorella vulgaris* and *Pseudoanabaena* sp. Similarly, considerable differences in total microalgae densities per liter and per gram of VSS, as well as in the total microalgae biovolume during stage III, were reported (Torres-Franco *et al.*, 2021). Therefore, the high differences noted for the TSS concentration in the effluent and wastage flow during stage III were attributed to the reduction of the settling efficiency, differences in microalgae densities, and the different populations of microorganisms prevailing in this operational stage (consequently, these substantial changes in biomass characteristics imply different settling velocities and different values in the parameters related to biomass concentration). The previous assumption underscores the importance of estimating parameters in such a way that may be able to describe stages with remarkable differences in biomass composition. For this purpose, a sigmoid function (Fig. 4.7) was used to represent the variation of parameter values during the experiment. According to the sigmoid function, each parameter $\hat{\theta}_i$ $\left(\hat{\theta}_i = V_0, r_{h,} r_p\right)$ varying between two values ($\hat{\theta}_{i_{min}}$ and $K_i + \hat{\theta}_{i_{min}}$). Then, instead of estimating the parameter values of the settling velocity equation (V_0 , r_h, r_p), the optimization problem estimates the values of the parameters of the sigmoid function ($\hat{\theta}_{i_{min}}$, K_i, and t_c) in Eq. (4.18) - (4.20), where t represents the current simulation time, and t_c is the time where a significant change in biomass properties was considered.

For parameter estimation in the settler, the limits in the parameter related to the maximum settling velocity were selected according to values reported in the literature for microalgae

systems or microalgae-bacteria consortia systems (Smith and Davis, 2013; Passos *et al.*, 2017; Parakh *et al.*, 2020). The ranges of the other parameters in the settling velocity equation were selected similar to those reported for activated sludge processes (Takács, Patryioand and Nolasco, 1991). These values are shown in Table 4.4.

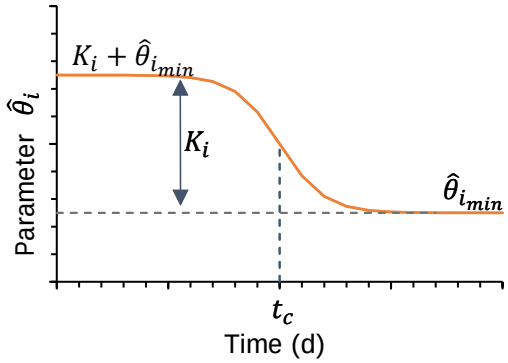

Fig. 4.7. Sigmoid function used to adjust the parameters of the settling velocity equation.

$$V_0 = K_{V_0} \cdot \frac{1}{1 + e^{(t - t_c)}} + V_{0_{min}} \tag{4.18}$$

$$r_h = K_{r_h} \cdot \frac{1}{1 + e^{(t - t_c)}} + r_{h_{min}} \tag{4.19}$$

$$r_p = K_{r_p} \cdot \frac{1}{1 + e^{(t - t_c)}} + r_{p_{min}} \tag{4.20}$$

Parameter estimation in the settler was conducted, considering that a biomass composition change during the treatment of undiluted digestate (stage III). Data from stage II were used to determine the model parameters during the treatment of diluted digestate, while data from stage I were used for model validation using these parameter values. Data from stage III were used for parameter estimation (the first half of the data) and validation (the rest) during undiluted digestate treatment. The results of parameter estimation in the settler obtained via optimization in this study are shown in Table 4.5.

Table 4.4. Initial values and limits for decision variables in the settler

Parameter [units] Description	Parameter of the sigmoid function	Initial value	Limits for optimization
X_{min} [mg/L] - Minimum attainable suspended solids concentration in the effluent.	-	40	30 – 80
V_0 [dm/d] - Maximum theoretical settling velocity (Eq. (4.18)).	K_{V_0}	3	2 – 20
	$V_{0_{min}}$	1	0.1 – 10
r_h [L/mg] - Settling parameter associated with the hindered settling component of settling velocity equation (Eq. (4.19)).	K_{r_h}	$1 \cdot 10^{-06}$	$2 \cdot 10^{-08} – 1 \cdot 10^{-04}$
	$r_{h_{min}}$	$4 \cdot 10^{-09}$	$5 \cdot 10^{-12} – 1 \cdot 10^{-04}$
r_p [L/mg] - Settling parameter associated with the low concentration and slowly settling component of the suspension (Eq. (4.20)).	K_{r_p}	$5 \cdot 10^{-03}$	$1 \cdot 10^{-04} – 2 \cdot 10^{-02}$
	$r_{p_{min}}$	$2.5 \cdot 10^{-04}$	$1 \cdot 10^{-04} – 2 \cdot 10^{-02}$
t_c [d] - The time when a significant change in the dominant populations occurred (Eq. (4.18) - (4.20))	-	85	82 – 95

Table 4.5. Values of estimated parameters in the settler

Parameter	Parameter of the sigmoid function	Value [units]
X_{min}	-	50 mg/L
V_0	K_{V_0}	5.040 dm/d
	$V_{0_{min}}$	2.097 dm/d
r_h	K_{r_h}	$4.33 \cdot 10^{-05}$ L/mg
	$r_{h_{min}}$	$7.89 \cdot 10^{-10}$ L/mg
r_p	K_{r_p}	$2.93 \cdot 10^{-04}$ L/mg
	$r_{p_{min}}$	$8.71 \cdot 10^{-04}$ L/mg
t_c	-	88.9 d

4.1.3. Model validation results

Two performance indexes were used to quantify the quality of the model adjustment to the experimental data: the mean absolute error (Eq. (4.21)) and the mean absolute relative error (Eq. (4.22)). Both criteria quantify the difference between model predictions and experimental data, and the MARE criteria normalize the error according to the magnitude of the measured variable. For both criteria, the closer the value to zero, the better the model performance. These values were computed for the complete experimental period (including the data set used for parameter estimation and model validation). The factor φ ($\varphi = 0.1$) in the denominator of Equation (4.22) is included to avoid division by zero in the case of experimental data $y_i = 0$.

$$MAE = \frac{1}{n} \cdot \sum_{i=1}^{n} |y_i - \hat{y}_i| \tag{4.21}$$

$$MARE = \frac{1}{n} \cdot \sum_{i=1}^{n} \frac{|y_i - \hat{y}_i|}{y_i + \varphi} \tag{4.22}$$

Fig. 4.8A, Fig. 4.8B, and Fig. 4.8C show simulation results and experimental measurements for S_{NH_4}, S_{PO_4}, and dissolved inorganic carbon in the photobioreactor, respectively. In Fig. 4.8, the white area indicates the data set used for parameter estimation, and blue shadow areas contain the data sets used for model validation. Ammonium and phosphate assimilation was mainly attributed to the biological processes occurring in the photobioreactor (Torres-Franco *et al.*, 2021), which mediated high removal efficiencies of both nutrients during the treatment of diluted digestate, as confirmed during model validation. The model also reproduced the trend of increasing ammonium concentration and phosphate concentration observed in the photobioreactor during the treatment of undiluted digestate. The MARE values (Table 4.6) computed for ammonium concentration in the photobioreactor (below 0.72 for stages II and III) confirm the model's prediction capability. The model performance for phosphate, which was also quantified with the previously referred metrics, exhibits low MARE values for stages II and III (below 0.16 for both cases). The high values of MARE during the first stage for ammonium and phosphate were caused by the normalization of this metric due to zero-close values reported experimentally for this stage. This error could be acceptable, taking

into account that low values of MAE were obtained during this stage (and due to possible inaccuracies of the experimental methods for low concentrations of dissolved nutrients).

As reported by (Torres-Franco *et al.*, 2021), high values of IC in the influent enhanced the activity of both microalgae and nitrifying bacteria. An intensive autotrophic activity demanded a high consumption of inorganic carbon in the photobioreactor, mainly during the first two operational stages (treating 25% and 50% diluted digestate, respectively). Thus, the model accurately reproduced the dynamic behavior of IC concentration in the photobioreactor during the experiment. This was confirmed with the low values of MARE (Table 4.6) reported for all experimental period (below 0.23).

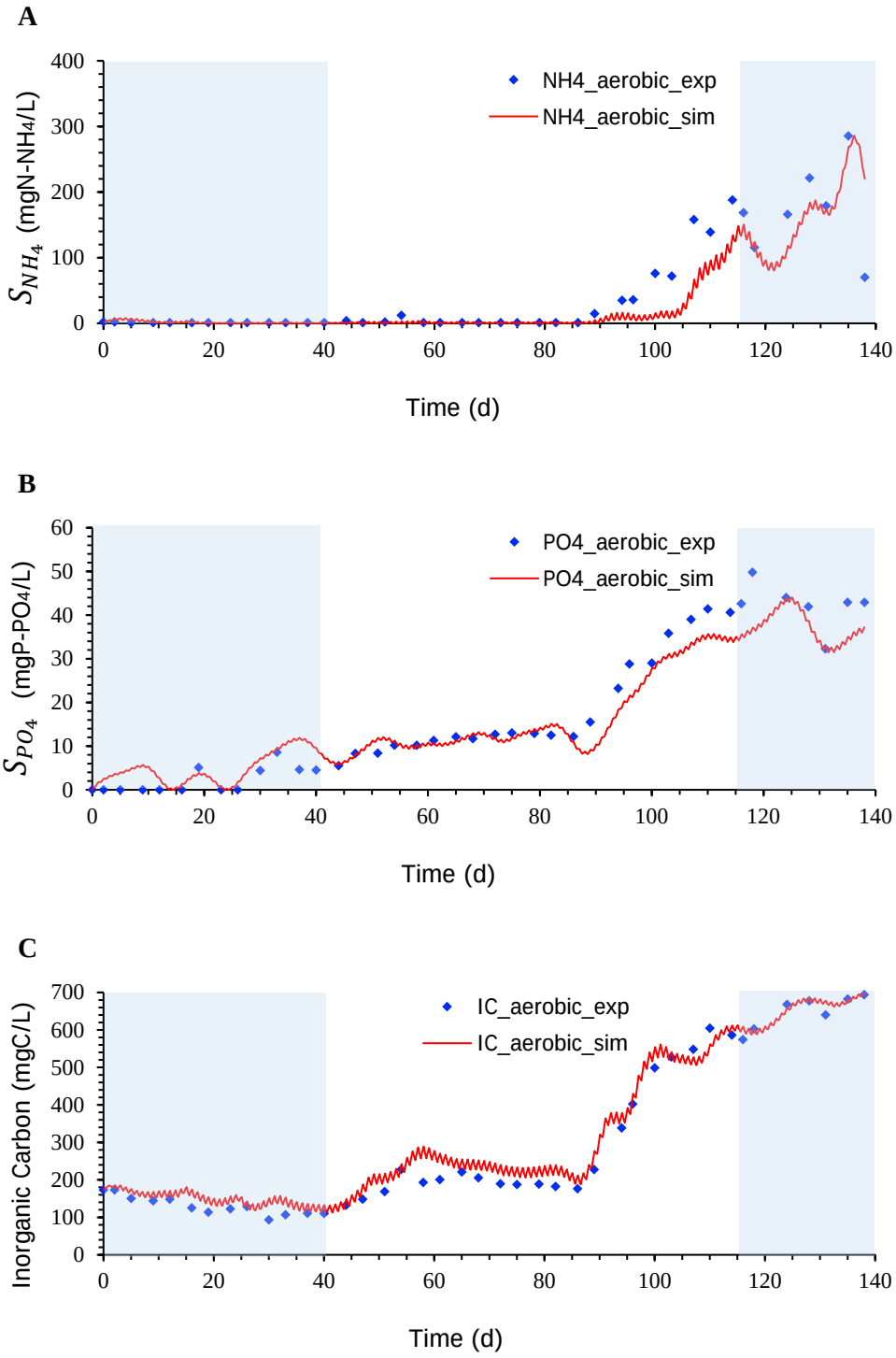

Fig. 4.8. Time course of the concentrations of dissolved ammonium (A), dissolved phosphate (B), and dissolved inorganic carbon (C) in the photobioreactor. The white area indicates the data set used for parameter estimation, and blue shadow areas contain the data sets used for model validation.

Results for parameter estimation and validation for the concentration of TOC in the anoxic reactor and the photobioreactor are presented in Fig. 4.9A and Fig. 4.9B, respectively. The model reproduced the high removal efficiencies of TOC in both reactors, as reported by (Torres-Franco *et al.*, 2021) for diluted digestate. The model also reproduced the decrease in TOC removal efficiency during the treatment of undiluted digestate. The MARE values (Table 4.6) during the three operational stages (values below 0.5 for both reactors) confirmed the model's capability to reproduce the total organic carbon concentration evolution in both reactors.

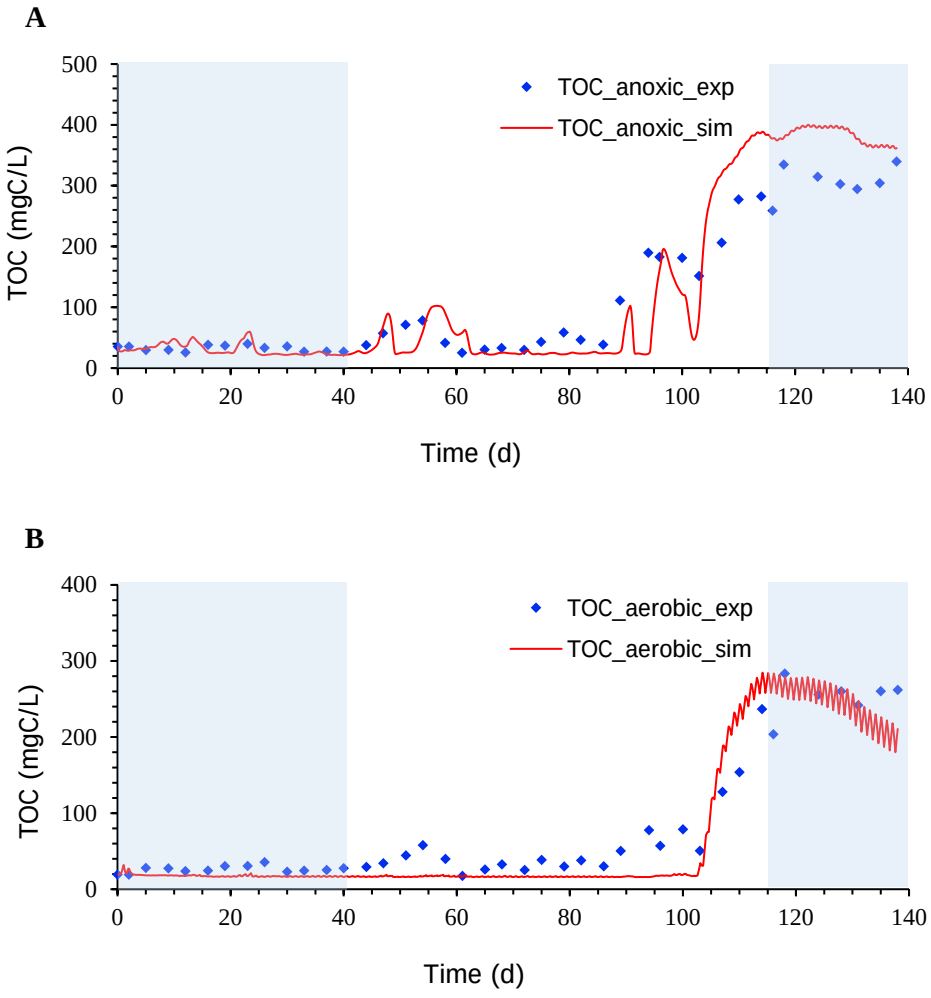

Fig. 4.9. Time course of the total organic carbon concentration in anoxic reactor (A) and in the photobioreactor (B). The white area indicates the data set used for parameter estimation, and blue shadow areas contain the data sets used for model validation.

The results in Fig. 4.8 and Fig. 4.9 showed that the model can effectively predict nitrogen, phosphorus, and carbon removal efficiencies. The validation results, which were performed using data corresponding to digestate dilutions different from those used in parameter estimation, confirm the model's prediction capability under different operational conditions. The validation results suggest that the calibrated model, which boasts broad applicability, may be employed to simulate a wide range of operational conditions with minimal resources and time consumption.

The estimation of dissolved oxygen is of paramount importance in the calibration of any biological model. In the photobioreactor, the dissolved oxygen concentration is the result of the photosynthetic activity of microalgae and bacteria's heterotrophic and nitrifying activity. As illustrated in Fig. 4.10A, the simulation results for the dissolved oxygen concentration in the photobioreactor are presented alongside the recorded experimental data. Although the dissolved oxygen concentration was recorded once a day during the experiment, the model simulation reveals daily variations in the dissolved oxygen concentration due to the effect of incident radiation (Fig. 4.10). This figure contains part of the data set that was used for model validation. As previously mentioned, the intense autotrophic activity observed during the treatment of 25% diluted digestate resulted in elevated dissolved oxygen concentrations during the illuminated periods within the initial 40 days of experimentation. Furthermore, the elevated heterotrophic activity within the photobioreactor throughout the experimental period resulted in a decline in dissolved oxygen levels during the dark phases for the three distinct operational stages. As (Torres-Franco *et al.*, 2021) have demonstrated, significant reductions in the maximum dissolved oxygen values during illuminated periods were reported in stages II and III. These reductions were confirmed through model simulation.

As demonstrated by the trend of simulated variables, the daily fluctuations in dissolved oxygen concentration due to the occurrence of light/dark periods have practical implications for the daily trends of other variables in the photobioreactor. These changes during the diurnal cycle in the assimilation of ammonium, phosphates, inorganic carbon, and total organic carbon (Fig. 4.8A, Fig. 4.8B, Fig. 4.8C, and Fig. 4.9B, respectively) provide valuable insights for the practical model application to operate and monitor the performance and environmental parameters prevailing in the anoxic-aerobic configuration. Concerning the dissolved oxygen results, during the first stage, low values

of MARE were obtained (below 0.5), confirming the model's prediction capability. Instead, high values of MARE were reported for stages II and III, mainly due to high standard deviations reported for the experimental data during stage II and to zero-close experimental values during stage III. Instead, low values of the MAE were reported during the complete period (Table 4.6). The quantitative analysis of this variable may be confusing because both the metrics used were calculated considering the average of all the data for the period. In this case, experimental data may vary significantly depending on the hour of the day, affecting the average value.

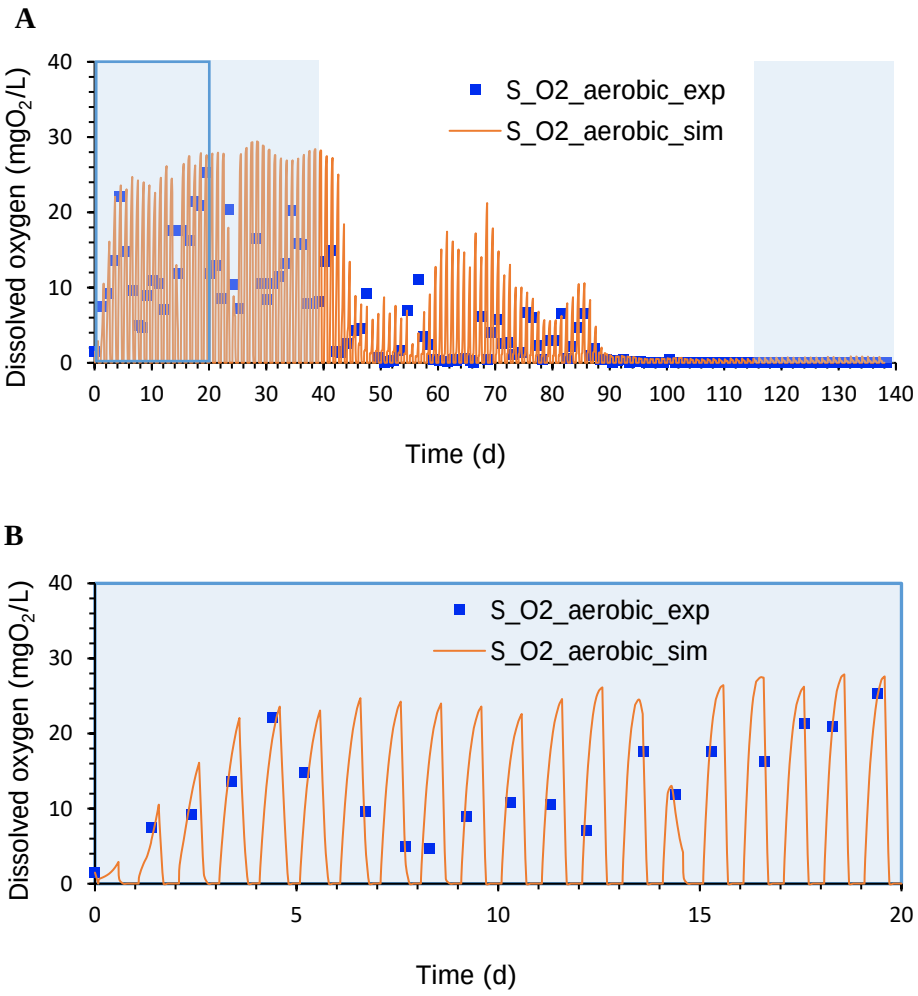

Fig. 4.10. Time course of the dissolved oxygen concentration in the photobioreactor during the experiment (A) (the white area contains the data set used for parameter estimation, and blue shadow areas indicate the data sets used for model validation). The blue rectangle delimited area shows the time course of the dissolved oxygen concentration during 20 days of data used for model validation (B).

Fig. 4.11represents the biomass concentration in both reactors and the settler. Fig. 4.11A and Fig. 4.11B show the simulation results and experimental measurements for the concentration of TSS in the anoxic reactor and in the photobioreactor, respectively. The model replicated the observed decline in TSS concentration during stage III in both reactors (Torres-Franco *et al.*, 2021). In summary, the model demonstrated a satisfactory degree of efficacy in replicating the dynamic behavior of biomass concentration. Small changes in the TSS concentration in the photobioreactor due to daily variations in light irradiation were observed, fundamentally due to microalgae activity as the dominant group of the consortia. Consequently, the increase in microalgae growth during the day led to an increase in the TSS concentration, while microalgae death at night resulted in a decrease in the TSS concentration. The model's capacity to reproduce biomass dynamics is confirmed by the low values of the MARE (below 0.35) reported for both reactors during the experimental time (Table 4.6).

Fig. 4.11C and Fig. 4.11D represent the total suspended solids concentration in the effluent and biomass wastage stream, respectively. An increase in the TSS concentration in the effluent was reported during the treatment of undiluted digestate. This increase was likely due to a decrease in the settling efficiency, different dominant populations of microalgae, and differences in microalgae densities (as referred to by the authors of (Torres-Franco *et al.*, 2021)), which presumably affects the sedimentation capability of the biomass. The model reproduces the trend of increasing TSS concentration in the effluent during stage III. The low MARE values reported for the effluent biomass concentration confirm the match between experimental and simulated data (Table 4.6).

In the wastage flow, low values of the MARE (below 0.22) were reported during the treatment of undiluted digestate (Table 4.6), which confirms the model prediction capability. The high standard deviation reported for the experimental data during stage III in the wastage flow (4742 ± 2529) suggests the presence of flocculated biomass, which could be a source of gross error during the analytical procedure to quantify the biomass concentration. High experimental data dispersion in the TSS concentration in the waste flow makes it difficult for the model to fit during the treatment of undiluted digestate.

The model validation results (Fig. 4.8 - Fig. 4.11) have allowed the evaluation of the model's qualitative responses to input changes and the confirmation of its validity over long periods under changing conditions.

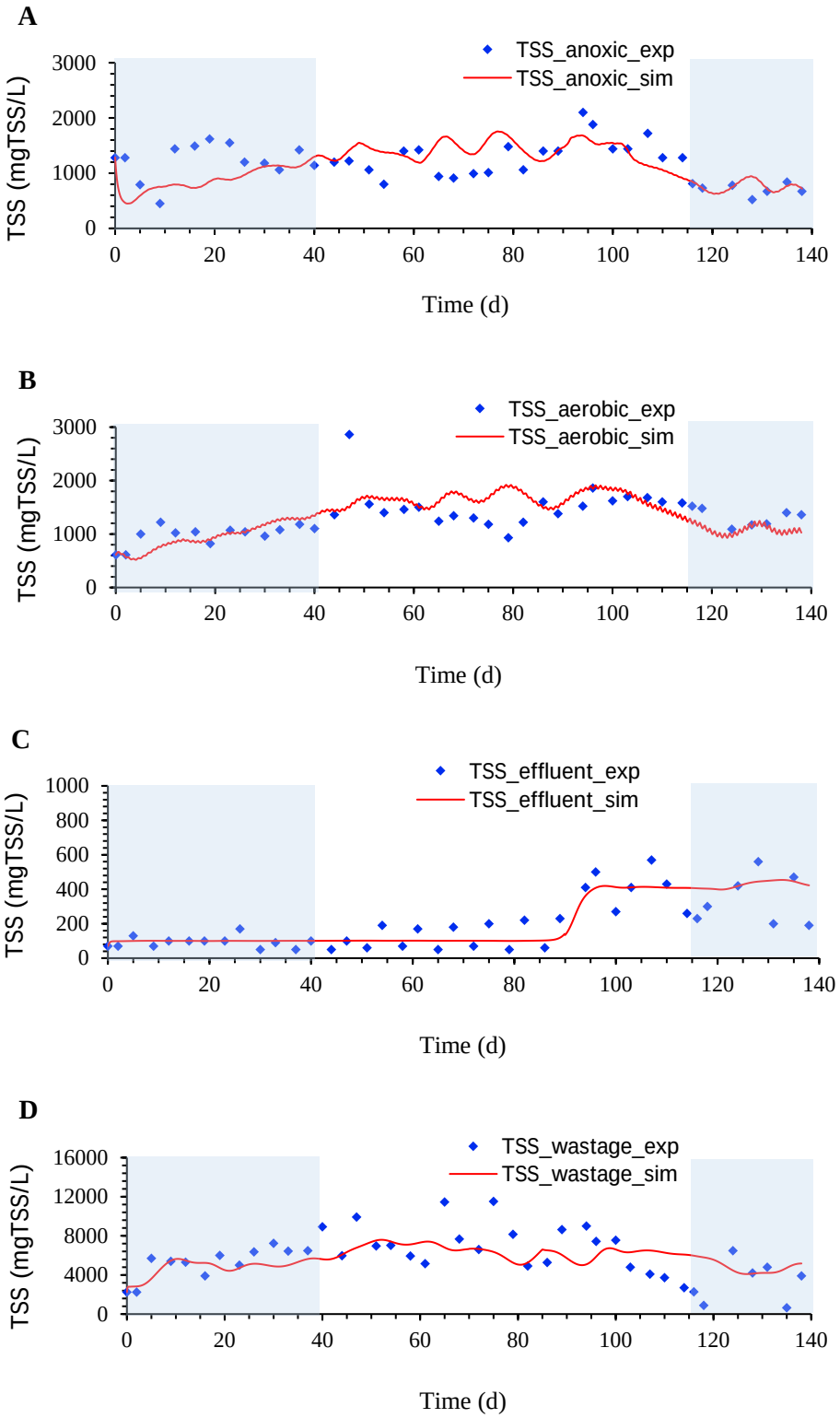

Fig. 4.11. Time course of the total suspended solids concentration in anoxic reactor (A) and in the photobioreactor (B). TSS concentration in the effluent (C) and wastage flow (D) of the settler. White area indicates the data sets used for parameter estimation, and blue shadow areas contain the data sets used for model validation.

Table 4.6 summarizes the computed criteria for the measured variables in each operational stage. Results for the MARE criteria (close to zero in most cases) confirm the model's capability to reproduce the experimental data. The MARE criteria generally constitute a reliable indicator of the model's goodness. However, the MARE value increases for small values of measured variables.

In this research, the model simulation results are of the utmost importance due to the absence of online measurements for fast-dynamic variables, such as dissolved oxygen. The utilization of model simulation facilitates the acquisition of invaluable insights into process behavior, thereby enabling a comprehensive analysis of the dynamic behavior of various variables throughout the day, as opposed to merely at the time of sample collection.

Simulation results revealed the model's versatility in photobioreactors with one or two stages, including sedimentation and biomass recirculation. The model's proficiency in replicating both rapid and slow dynamics further reinforces its potential application to various biological processes, such as biogas upgrading processes with microalgae and the simultaneous treatment of digestates.

Table 4.6. Model evaluation for the three stages of experimentation

Mean absolute error			
	Stage I	**Stage II**	**Stage III**
S_NH_4 - Photobioreactor	1.3877	1.5671	44.3109
S_PO_4 - Photobioreactor	2.7609	1.1039	5.3482
IC - Photobioreactor	26.6770	42.2906	23.1514
TOC - Anoxic Reactor	8.7098	21.6805	76.3308
TOC - Photobioreactor	9.3972	17.6676	39.2998
S_O_2 - Photobioreactor	3.4216	1.1678	0.3025
TSS - Anoxic Reactor	383.2931	348.3835	181.2617
TSS - Photobioreactor	167.9968	393.1145	196.3628
TSS - Effluent	20.9246	58.0595	108.3349
TSS - Wastage	1153.0377	1779.9657	2370.5445
Mean absolute relative error			
S_NH_4 - Photobioreactor	1.2013	0.7172	0.5138
S_PO_4 - Photobioreactor	14.5448	0.1055	0.1560
IC - Photobioreactor	0.2270	0.2274	0.0514
TOC - Anoxic Reactor	0.2641	0.4943	0.3594
TOC - Photobioreactor	0.3459	0.4781	0.3524
S_O_2 - Photobioreactor	0.4867	0.9884	2.1065
TSS - Anoxic Reactor	0.3145	0.3454	0.1598
TSS - Photobioreactor	0.1304	0.2625	0.0847
TSS - Effluent	0.2798	0.5922	0.4039
TSS - Wastage	0.1943	0.2138	1.2124

4.2. Methodology for parameter estimation in microalgae-bacteria based wastewater treatment

This section presents an approach for parameter estimation when dealing with multiple outputs and parameters in the optimization problem (Fig. 4.12).

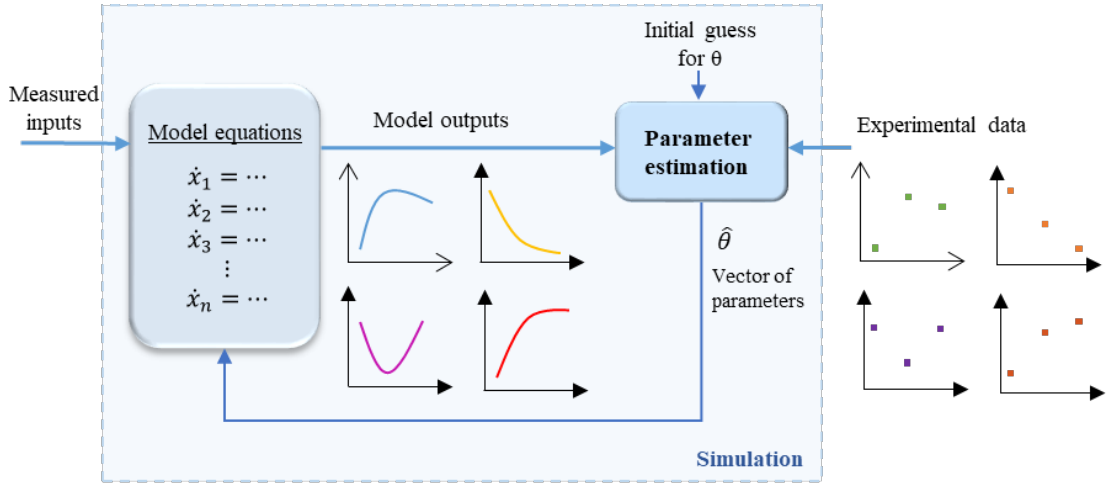

Fig. 4.12. Graphical representation of the parameter estimation process

The proposed approach is designed to solve a series of increasingly complex optimization problems, thereby gradually estimating process parameters and avoiding convergence issues. This approach offers an alternative to handling large optimization problems in parameter estimation, a common challenge in microalgae-bacteria processes. Parameter estimation via dynamic optimization is realized in each optimization step to fit simulated outputs to experimental data. The idea is to formulate one easier parameter estimation problem involving a subset of system outputs and parameters, replace the other output variables with their experimental values, and then use these estimated values as a starting point for the next step of the optimization problem. The selection of subsets is performed based on sensitivity analysis and connectivity.

This approach is illustrated in Fig. 4.13, which shows the division of the total number of output variables to adjust (Fig. 4.12) into subsets. One subset is maintained as output variables to fit, while the other is used as input data (see first step in Fig. 4.13). Due to the common discrete nature of samples in biological processes, the subset used as input data is usually interpolated. This approach reduces the computational complexity by

decreasing the number of outputs variables to adjust, and consequently, the number of state variables in the model (as each output variable frequently involves one or more model states). In general, the total number of parameters to estimate in each step is also reduced, as it is possible that there are parameters only appearing in those equations that were substituted by experimental data. In the first step of this methodological approach, an initial guess of parameter values is derived from a comprehensive review of pertinent literature.

In the subsequent steps, additional outputs to adjust are incorporated (and, consequently, the number of model differential equations increases). Subsequently, the vector of parameters obtained in the preceding step is utilized as the initial estimate. This procedure is repeated until all the system outputs and parameters are included in the optimization problem.

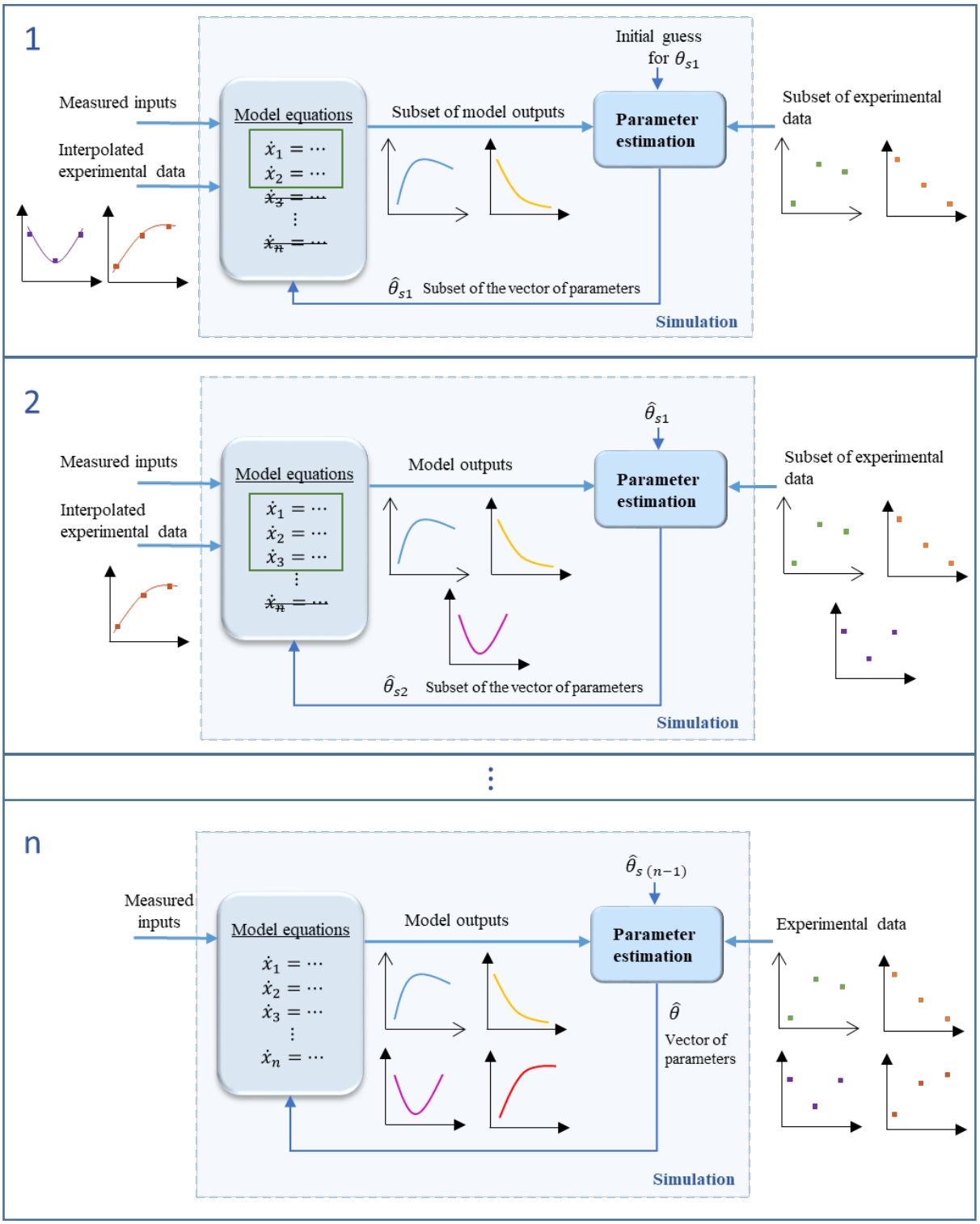

Fig. 4.13. Graphical representation of the methodology for parameter estimation

4.2.1. Case study

The proposed methodology is tested in an anoxic–aerobic algal–bacterial photobioreactor configuration with biomass recycling devoted to wastewater treatment located in the facilities of the Institute of Sustainable Processes at the University of Valladolid. The data utilized in this section were collected from May 2014 to July of 2014. The experimental setup is described in (Alcántara *et al.*, 2015). The laboratory-scale plant corresponds to the scheme of the anoxic-aerobic configuration depicted in Fig. 3.1, with different dimensions and operational values than those referred to in the study case developed in Section 4.1. The facility has been engineered to treat synthetic (domestic) wastewater.

The photobioreactor was composed of an enclosed jacketed 3.5 L glass tank with a total working volume of 2.7 L continuously illuminated by LED lamps. The anoxic reactor consisted of a gas-tight 1 L polyvinyl chloride tank with a total working volume of 0.9 L, which was maintained in the dark. Synthetic wastewater was fed to the anoxic tank and continuously overflowed by gravity into the aerobic photobioreactor. The algal–bacterial broth was continuously recycled from the photobioreactor to the anoxic tank. An Imhoff cone, with a volume of 1 L and interconnected to the outlet of the photobioreactor was used as a settler. The algal–bacterial biomass settled was recycled from the bottom of the settler into the anoxic tank and wasted 3 days a week to control the algal–bacterial sludge retention time. In (Alcántara *et al.*, 2015), a detailed description of the system, microorganisms and culture conditions, experimental design, and analytic procedures is provided.

The design of the experimentation was conducted based on the hypothesis that algal–bacterial photobioreactors for wastewater treatment can support the oxidation of ammonium ($N\text{-}NH_4^+$) into NO_2^-/NO_3^-, which can then be easily removed through denitrification (using the organic matter present in SWW) under anoxic conditions via internal recycling of the photobioreactor broth into the anoxic tank (de Godos, Vargas, *et al.*, 2014). Liquid samples of 100 mL were drawn three times a week from the SWW storage tank, anoxic tank, aerobic tank, wastage, and clarified effluent to monitor the concentration of dissolved TOC, dissolved IC, dissolved N species (total nitrogen, $N\text{-}NH_4^+$, $N\text{-}NO_2^-$, and $N\text{-}NO_3^-$) and biomass concentration, expressed as TSS. The DO, temperature and pH of the cultivation broth in both tanks were in situ recorded every day.

In (Alcántara, et al., 2015), the influence of the HRT, intensity and regime of light supply, and dissolved oxygen concentration in the photobioreactor were analyzed in five-stage experimentation.

4.2.2. Parameter estimation approach applied to the case study

The present study utilized data corresponding to one experimentation stage, with the system operating at an HRT of 4 days (HRT = 1 d in the anoxic reactor, HRT = 3 d in the photobioreactor) and under continuous illumination in the photobioreactor. Table 4.7 summarizes the photobioreactor output variables considered in the objective function.

Table 4.7. Output variables considered in the photobioreactor

Output variable [units]	Description	Sampling frequency
$TSS_{photobioreactor}$ [mgTSS/L]	Total suspended solids concentration in the photobioreactor	Three times a week
$TOC_{photobioreactor}$ [mgC/L]	Total organic carbon concentration in the photobioreactor	Three times a week
$IC_{photobioreactor}$ [mgC/L]	Inorganic carbon concentration in the photobioreactor	Three times a week
$S_{O2\ photobioreactor}$ [mgO_2/L]	Dissolved oxygen concentration in the photobioreactor	Daily
S_{NH4} [mgN-NH_4/L]	Dissolved ammonium concentration in the photobioreactor	Three times a week

The photobioreactor has been described using the model BIO_ALGAE 2 (Solimeno, Gómez-Serrano and Acién, 2019a) with the modifications described in section 3.1.1. The modeling, sensitivity analysis, and simulation were carried out using the dynamic simulation software PROOSIS® (EA International, 2022).

Similarly to the previous case study, model outputs are especially sensitive to the maximum specific growth rate of microalgae (μ_{ALG}) and heterotrophic bacteria (μ_H); the decay rate of microalgae ($k_{death,ALG}$) and heterotrophic bacteria ($k_{death,H}$); and the gas-liquid mass transfer coefficients for ammonia ($K_{la,NH3}$), oxygen ($K_{la,O2}$), and carbon dioxide

($K_{la,CO2}$). The results of sensitivity analysis are also used here as a guide to determine the best selection of subsets of model outputs to consider. In addition, prior knowledge of system dynamics should be considered.

The estimation of parameters has been executed in accordance with the approach delineated in Section 4.2 and Fig. 4.13. In this particular case study, a four-step optimization sequence was employed, as illustrated in Fig. 4.14.

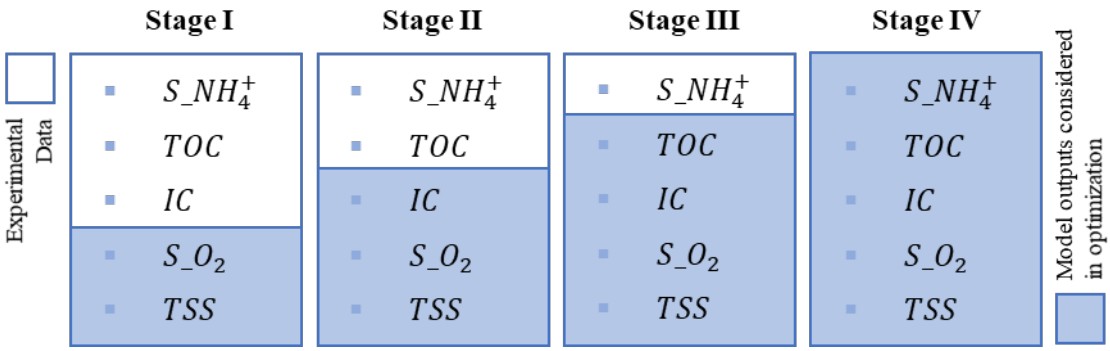

Fig. 4.14. Stages of the optimization problem in the photobioreactor

In the first step of the parameter estimation approach, two model outputs were considered for alignment with the experimental data: TSS concentration and DO concentration. The TSS concentration is associated with numerous model processes, and its value is contingent on the concentration of all particulate components in the photobioreactor. Furthermore, DO concentration plays a pivotal role in numerous processes pertaining to microalgae and bacteria activity. These outputs are contingent upon the maximum specific growth rate of microalgae and the decay rate of microalgae and heterotrophic bacteria. This assertion is substantiated by the graphical sensitivity analysis results presented in Fig. 4.3A and Fig. 4.3B. The selection of this pair of model outputs was based on the effect in the same direction provided by the most influential model parameters. An increase in the microalgae growth rate and in the inactivation growth rate of heterotrophic bacteria has been shown to promote an increase in both the DO concentration in the photobioreactor and in the TSS concentration in the photobioreactor. Conversely, an increase in the inactivation constant of microalgae has been shown to result in a decrease in both the DO and TSS concentrations, as evidenced by the findings presented in Fig. 4.3A and Fig. 4.3B. The analogous effects of the parameters on the

designated outputs preclude convergence issues and prevents that the parameters do not exceed the limits imposed in the formulation of the optimization problem.

Inorganic carbon is incorporated as a model output in the second step of the optimization process. Microalgae employ carbon dioxide as a carbon source for growth. As anticipated, μ_{ALG} has been identified as the parameter exerting the most substantial influence on IC concentration. It is noteworthy that inorganic carbon is also influenced by the decay rate of microalgae and heterotrophic bacteria, as evidenced by the findings presented in Fig. 4.2A. The incorporation of inorganic carbon as a model output in the second stage of the parameter estimation process is predicated on the established correlation between IC and the model outputs that have been previously selected.

In the third step of the methodology, the total organic carbon concentration is also considered as a model output to be fitted. In microalgae-bacteria processes, heterotrophic bacteria oxidize the organic matter present in the wastewater. Consequently, TOC concentration is predominantly influenced by the maximum specific growth rate and the decay rate of heterotrophic bacteria, as illustrated in Fig. 4.2D.

In the final step, the dissolved ammonium concentration is incorporated as model output. As demonstrated in the graphical sensitivity analysis results provided in Fig. 4.2A, the ammonium concentration is mainly affected by μ_{ALG}, $k_{death,ALG}$, and $K_{la,NH3}$.

The initial values for parameter estimation in Step 1 and the ranges of the decision variables for optimization were selected from a comprehensive literature review. These values are reported in Table 4.8. The parameter estimation results are provided in Table 4.9.

Table 4.8. Initial values and limits for decision variables in the photobioreactor

Parameter [units]	Description	Initial value	Limits for optimization
μ_{ALG} [d^{-1}]	Maximum specific growth rate of microalgae	1.5	0.4 – 4
$k_{death,ALG}$ [d^{-1}]	Decay rate of microalgae	0.1	0.05-0.21
μ_H [d^{-1}]	Maximum specific growth rate of heterotrophic bacteria	4	1-6
$k_{death,H}$ [d^{-1}]	Decay rate of heterotrophic bacteria	0.6	0.12-0.9
$K_{la,O2}$ [d^{-1}]	Mass transfer coefficient for oxygen	1	0.3-30
$K_{la,CO2}$ [d^{-1}]	Mass transfer coefficient for carbon dioxide	1	0.3-30
$K_{la,NH3}$ [d^{-1}]	Mass transfer coefficient for ammonia	0.8	0.3-30

Table 4.9. Values of estimated parameters in the photobioreactor

Parameter [units]	Value			
	Step 1	Step 2	Step 3	Step 4
μ_{ALG} [d^{-1}]	1.627	0.990	1.062	1.062
$k_{death,ALG}$ [d^{-1}]	1.656	1.000	1.210	1.211
μ_H [d^{-1}]	0.101	0.050	0.050	0.050
$k_{death,H}$ [d^{-1}]	0.895	0.900	0.900	0.900
$K_{la,O2}$ [d^{-1}]	13.081	4.000	4.000	4.000
$K_{la,CO2}$ [d^{-1}]	-	3.666	3.666	3.666
$K_{la,NH3}$ [d^{-1}]	-	-	-	3.920

4.2.3. Validation results

The data utilized in this study corresponded to 47 days of experimentation. These data were employed for parameter estimation and model validation. In each stage of the parameter estimation methodology, data from the initial 30 days were utilized for parameter estimation. Model validation was performed using data from days 30 to 47.

The simulation results of the Stage 4 of the applied methodology are presented in Fig. 4.15 and Fig. 4.16. As illustrated in Table 4.10, the model fit in the photobioreactor was evaluated using the MAE and MARE criteria (Eq. (4.21) and (4.22), respectively).

The simulation results for the TSS concentration in the photobioreactor are presented in Fig. 4.15A. As previously referenced, the experimental data were recorded under constant HRT and illumination in the photobioreactor. Consequently, variations in the biomass concentration in the photobioreactor (with an experimental standard deviation of 299.78 mgTSS/L) can be attributed primarily to changes in microbial populations and possible errors in the sample drawing. The simulated average values of biomass concentration in the photobioreactor demonstrate a high degree of correlation with the experimental results, as evidenced by the low values of MAE and MARE obtained (Table 4.10).

As illustrated in Fig. 4.15B, the simulation results depict the dissolved oxygen concentration within the photobioreactor. The model effectively reproduces the dynamic behavior of this variable, as confirmed by the low values of MARE reported (lower to 0.3) during the experimental period.

The simulation results of the total organic carbon concentration, inorganic carbon concentration, and ammonium concentration in the photobioreactor are presented in Fig. 4.16A, Fig. 4.16B, and Fig. 4.16C, respectively. The assimilation of TOC by heterotrophic bacteria has been observed to increase since the initial time of experimentation (day 0). This trend has been replicated by the model, as evidenced by Fig. 4.16A and the low values of MARE reported in Table 4.10. In a comparable manner, the assimilation of IC and dissolved ammonium by microalgae has been observed to increase during the experiment. This trend is illustrated in Fig. 4.16B and Fig. 4.16C, which demonstrate the model's capacity to replicate this trend. The low values of MARE reported for these variables confirms the model's effectiveness in reproducing the dynamic behavior of the different measured variables. The proposed optimization approach is designed to avert probable convergence issues and may facilitate a more optimal alignment between the experimental and simulated data.

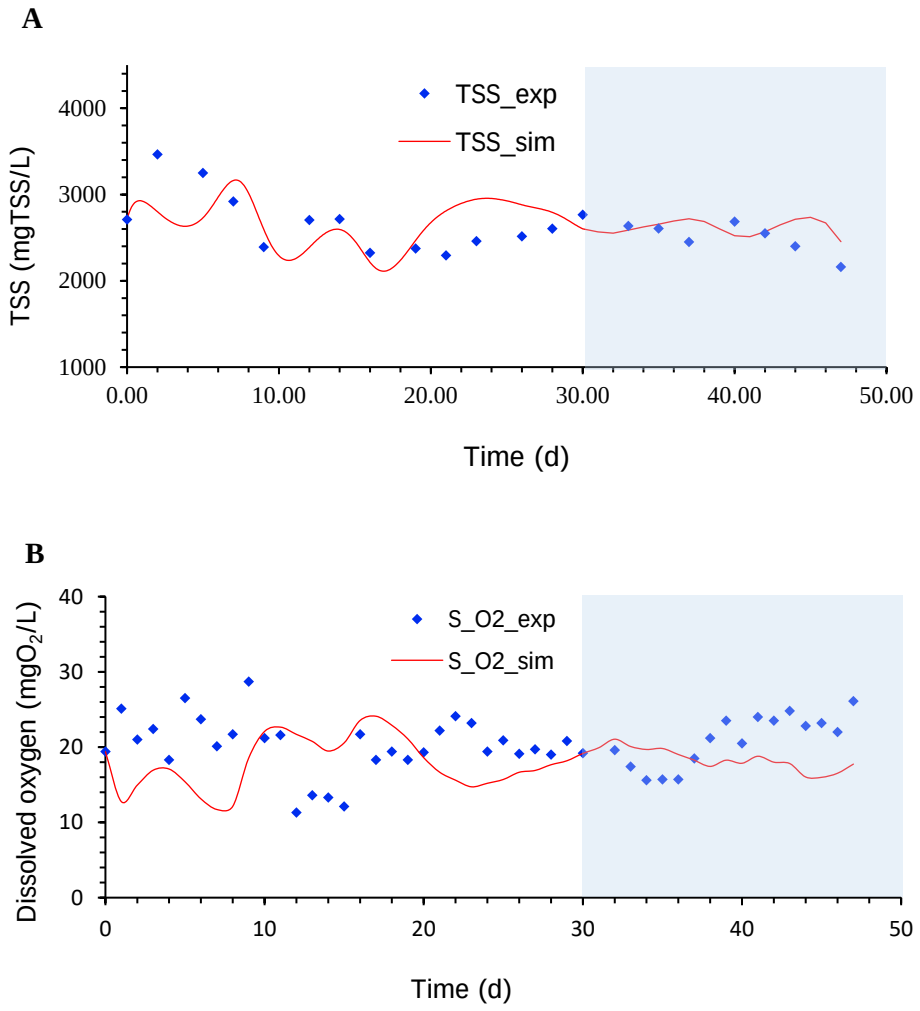

Fig. 4.15. Time course of the total suspended solids concentration (A) and dissolved oxygen concentration in the photobioreactor (B). The white area indicates the data set used for parameter estimation, and blue shadow area contains the data set employed for model validation.

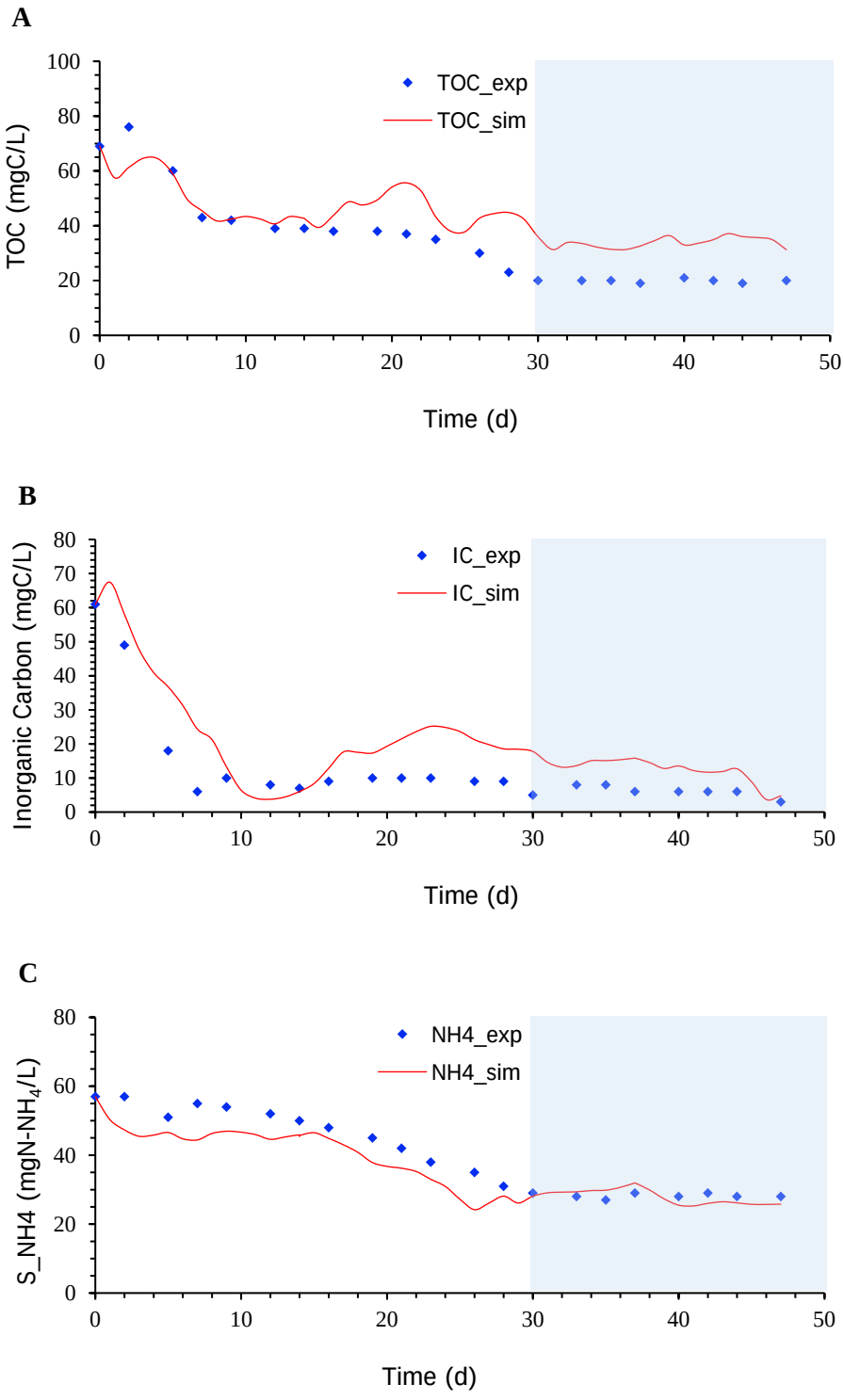

Fig. 4.16. Time course of the dissolved total organic carbon concentration (A), dissolved inorganic carbon concentration (B), and dissolved ammonium concentration in the photobioreactor (C). The white area indicates the data set used for parameter estimation, and blue shadow area contains the data set employed for model validation.

Table 4.10. Model evaluation in the photobioreactor

	Mean absolute error	**Mean absolute relative error**
TSS - Photobioreactor	245.0805	0.0928
S_O_2 - Photobioreactor	5.0598	0.2544
TOC - Photobioreactor	10.1155	0.4058
IC - Photobioreactor	8.1515	1.0105
S_NH_4 - Photobioreactor	4.5492	0.1105

4.3. Conclusions

This chapter presented the dynamic simulation results of anoxic-aerobic algal-bacterial photobioreactor configurations. The simulation results for two distinct plants confirmed the model's capability to replicate the experimental data in photobioreactors comprising one or two stages, including sedimentation and biomass recirculation, while treating domestic or high-strength wastewaters. Parameter estimation was instrumental in ascertaining the most influential parameters of the microalgae–bacteria process. In a similar vein, parameter estimation in the settler facilitated the estimation of the primary parameters associated with settleability properties, which are not well-established in microalgae–bacteria processes.

The methodology for parameter estimation was tested in a photobioreactor for wastewater treatment when multiple outputs and parameters were involved in the optimization problem. This approach has been demonstrated to prevent convergence issues and facilitate a more optimal alignment between the experimental and simulated data.

5. Moving horizon estimation in microalgae-bacteria based wastewater treatment

This chapter expounds on the application of the MHE technique in an industrial microalgae-bacteria based wastewater treatment plant. The inherent nonlinear characteristics of microalgae-based wastewater treatment processes, coupled with the operational constraints associated with these processes, underscore the viability of MHE as a solution to the state estimation problem in this context. The objective of the MHE technique's implementation was to facilitate online estimation of effluent water quality and other pertinent variables associated with plant operation. This research considers the availability of online and analytical measurements, which poses the challenge of multi-rate measurement management. In this chapter, a complex model was employed to represent the hypothetical wastewater treatment plant, while a reduced model with additive noise in the measured outputs and parameter mismatch was utilized for the estimation. The state and parameter estimation was conducted. Furthermore, the MHE technique was employed for the estimation of model uncertainties, output noise, and the inlet wastewater concentration. The results of the estimation are presented via simulation, demonstrating the potentialities of the MHE technique for the online estimation of multiple states and parameters, even in the presence of model uncertainties and parameter mismatch. The implementation of online state estimation would facilitate the subsequent integration of control and optimization strategies within the plant, contingent upon the actual values of the states.

5.1. Moving Horizon estimation

MHE is a powerful tool for state estimation in dynamic systems, transforming the problem into an optimization problem. This approach entails the identification of values for states and parameters that result in a minimization of the discrepancy between measured and model-predicted outputs over a sliding window of past data. Additionally, MHE effectively incorporates unmeasured disturbances and other inaccuracies within this finite sequence of past measurements. Furthermore, the admissible ranges of the different variables involved must be considered.

Unlike filter-based approaches for nonlinear systems such as the Extended Kalman Filter (EKF), MHE offers greater flexibility in handling constraints and system nonlinearities. The ability to incorporate additional constraints on estimated variables allows for enforcing physical limitations, integrating valuable information about the system's characteristics (such as ensuring concentrations remain positive or molar fractions stay within the [0,1] range). These constraints not only improve the physical realism of the estimates but also enhance the efficiency of the optimization solver by reducing the search space. As a result, estimation errors decrease, as more information is utilized in the optimization process.

It is important to acknowledge that nonlinear optimization with constraints increases computational complexity. However, with recent advancements in computing power and improved nonlinear solvers, MHE has become more practical, allowing solutions to be obtained within a reasonable timeframe. In highly nonlinear systems, such as biological processes, MHE typically outperforms EKF, which relies on the assumption that the system behaves linearly during updates, a condition that may not always hold.

Another key advantage of MHE is its versatility in scenarios where plant measurements are available at different frequencies (e.g. measurements from plant transmitters and from the lab). Traditional state estimation methods often assume that all relevant states can be observed from high-frequency measurements, but this is not always the case. Some states may only be inferred from less frequent measurements, making multi-rate measurements essential. By incorporating slower measurements into the estimation process, MHE improves both the quality of state estimates and the overall observability of the system, addressing potential information gaps.

The MHE dynamic optimization problem can be defined as problem (5.1) to (5.7) below and Fig. 5.1. The problem is solved at regular time intervals or sampling times k. At current time k, the estimation considers a past horizon $t \in [t_{k-n_e}, t_k]$, where n_e represents the number of past sampling time included in the estimation. Within this horizon, the inputs $\boldsymbol{u}_{k-i}$ to the process over the intervals $[t_{k-i}, t_{k-i+1}]$, and the process measurements collected at t_{k-i}, denoted as $\boldsymbol{y}_{P,k-i}$, are known for $i = 1, \ldots, n_e$. The past horizon of the MHE is illustrated in Fig. 5.1.

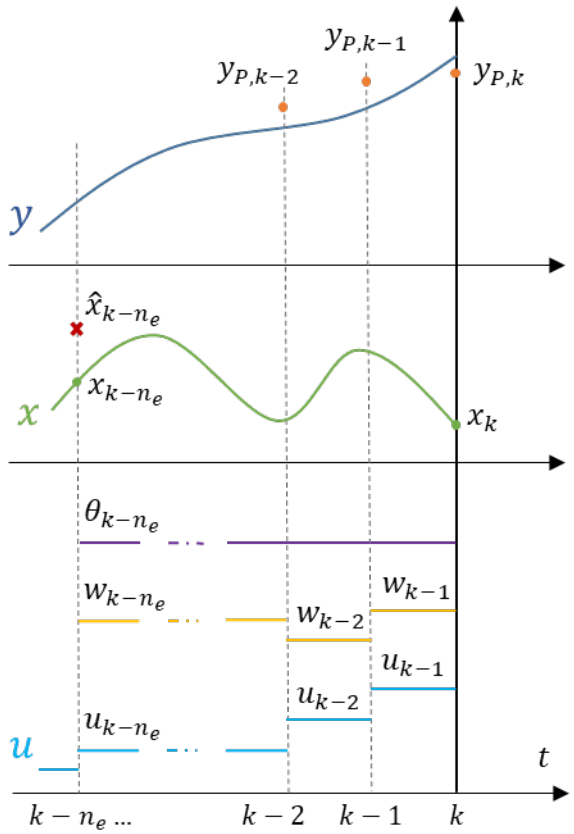

Fig. 5.1. Past values of the MHE estimation

The decision variables in this problem include the state values at the beginning of the sliding window of past data $(\boldsymbol{x}_{k-n_e})$, and the past unmeasured system disturbances, unknown parameters, or system noise accounting for modeling errors (and unknown dynamics) $(\boldsymbol{w}_{k-\mathrm{i}})$. The objective (5.1) is to minimize discrepancies between the model-predicted outputs $(\boldsymbol{y}_k)$ and the measured values $(\boldsymbol{y}_{P,k})$, while also considering the deviation between the newly estimated past initial state $\boldsymbol{x}_{k-n_e}$ and the state estimated

from the previous MHE execution at time $t - n_e$ $(\hat{\boldsymbol{x}}_{k-n_e})$, as well as maintaining consistency or minimizing the past disturbances (or parameters $\boldsymbol{\theta}_{k-i}$) and $\boldsymbol{w}_{k-i}$. Then, the trajectory of the state variables up to time k $[x_{k-n_e}, \dots, x_k]$ is estimated using the process model. The name *moving horizon* estimation is derived from this problem formulation: at each sampling time t_k, a new measurement $\boldsymbol{y}_{P,k}$ enters the horizon, while the oldest measurement $\boldsymbol{y}_{P,k-n_e-1}$ is discarded from the estimation window.

The weighting matrices $\boldsymbol{Q}_y, \boldsymbol{Q}_x$ and $\boldsymbol{Q}_w$ regulate the influence of each term on the cost function. The optimization problem is subjected to the dynamic system model (5.2) and (5.3), as well as the operational and physical constraints defined in (5.4). The problem also incorporates inequality constraints (5.5) to restrict disturbances to the permissible range. The incorporation of additional constraints in the values of the states (5.6) and parameters (5.7) could enhance the estimation performance. This is a dynamic optimization problem that can be solved either with a sequential approach involving a dynamic simulator and a non-linear optimizer or directly with a non-linear solver after full discretization.

$$\min_{\substack{x_{k-ne} w_{k-i} \theta_{k-i} \\ i=1,\dots,n_e}} \sum_{i=0}^{n_e-1} \left\| y_{k-i} - y_{P,k-i} \right\|_{\boldsymbol{Q}_y}^2 + \left\| x_{k-n_e} - \hat{x}_{k-n_e} \right\|_{\boldsymbol{Q}_x}^2 + \sum_{i=1}^{n_e} \| w_{k-i} \|_{\boldsymbol{Q}_w}^2 \qquad (5.1)$$

$$s.t. \qquad f(\dot{\boldsymbol{x}}, \boldsymbol{x}, \boldsymbol{u}, \boldsymbol{w}, \boldsymbol{\theta}) = 0, \forall t \in \left[t_{k-n_e}, t_k\right],\ x\left(t_{k-n_e}\right) = x_{k-n_e} \qquad (5.2)$$

$$h(\boldsymbol{x}, \boldsymbol{u}, \boldsymbol{y}, \boldsymbol{w}, \boldsymbol{\theta}) = 0, \quad \forall t \in \left[t_{k-n_e}, t_k\right] \qquad (5.3)$$

$$g(\boldsymbol{u}, \boldsymbol{y}) \leq 0, \quad \forall t \in \left[t_{k-n_e}, t_k\right] \qquad (5.4)$$

$$\boldsymbol{w^L} \leq w_{k-i} \leq \boldsymbol{w^U}, \qquad i = 1 \dots n_e \qquad (5.5)$$

$$\boldsymbol{x^L} \leq x_{k-i} \leq \boldsymbol{x^U}, \qquad i = 1 \dots n_e \qquad (5.6)$$

$$\boldsymbol{\theta^L} \leq \theta_{k-i} \leq \boldsymbol{\theta^U}, \qquad i = 1 \dots n_e \qquad (5.7)$$

The solution of a problem (5.1) - (5.7) gives $\boldsymbol{x}^*_{k-n_e}$, $\boldsymbol{w}^*_{k-i}$, and $\boldsymbol{\theta}^*_{k-i}, i = 1 \dots n_e$. Then, this solution can be used to estimate the initial value of the model state at time t_k $(\hat{\boldsymbol{x}}_k)$. To obtain $\hat{\boldsymbol{x}}_k$ the model equations must be integrated over $t \in \left[t_{k-n_e}, t_k\right]$ starting from

$\boldsymbol{x}^*_{k-n_e}$, using the estimated disturbances $\boldsymbol{w}^*_{k-i}$ and parameters $\boldsymbol{\theta}^*_{k-i}, i = 1 \dots n_e$, and applying $\boldsymbol{u}_{k-i}$

$$f(\dot{\boldsymbol{x}}, \boldsymbol{x}, \boldsymbol{u}, \boldsymbol{w}^*, \boldsymbol{\theta}^*) = 0, \forall t \in [t_{k-n_e}, t_k], \ \boldsymbol{x}(t_{k-n_e}) = \boldsymbol{x}^*_{k-n_e} \tag{5.8}$$

State estimation employing the MHE technique is also beneficial in scenarios where plant measurements are not available at the same frequency. This situation is illustrated in Fig. 5.2, where the measurements of outputs y_1 and y_2 (represented with circles), are available with a sampling period greater than the sampling period of the measurements of the output y_3. The prevailing state estimation methodologies typically utilize solely the rapid measurements ($y_{3\,P,k}$ in Fig. 5.2), operating under the assumption that all states of interest are observable from them. However, this assumption does not always hold true, and there exist instances where states cannot be observed from the rapid measurements alone. Consequently, the utilization of measurements obtained at varying rates has the potential to enhance the observability properties of the system. Therefore, it is recommended to use methodologies capable of managing multi-rate measurements, with the objective of leveraging the slower measurements to enhance the quality of state estimates or their observability.

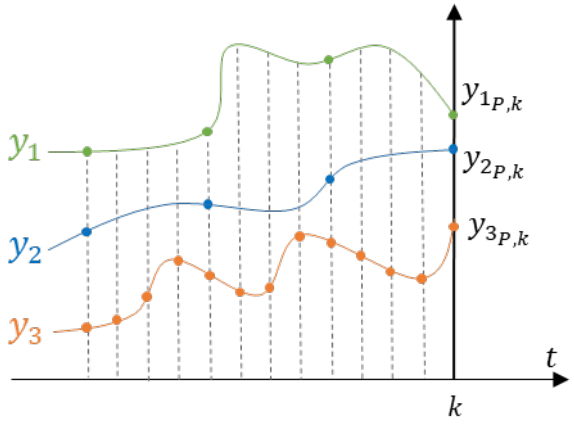

Fig. 5.2. Scenario considering a plant with multi-rate measurements

5.2. Plant description

This study considers a hypothetical wastewater treatment plant for a population of approximately 5,000 inhabitants, treating an average flow rate of 875 m^3/d. The system

consists of two parallel HRAPs, each with an area of 10,208 m^2, designed in the typical form of raceways with two channels and two reversals (452m long and 22.6 m wide). The HRAPs have a depth of 0.3 m and operate at a hydraulic retention time of 7 days. Two settlers, each with a total working volume of 293.75 m^3, are connected to the output of each HRAP. The algal-bacterial biomass settled is recirculated to the HRAP to enhance nutrient assimilation and biomass settling ability. It is hypothesized that the algal-bacterial WWTP is preceded by a pre-treatment stage with primary sedimentation to remove the solid fraction of the wastewater. The schematic representation of the plant is depicted in Fig. 5.3, and the average composition of the inlet domestic wastewater is listed in Table 5.1. The values for wastewater composition were obtained from the typical domestic wastewater concentrations reported in (Henze *et al.*, 2000; Metcalf & Eddy Inc., 2003).

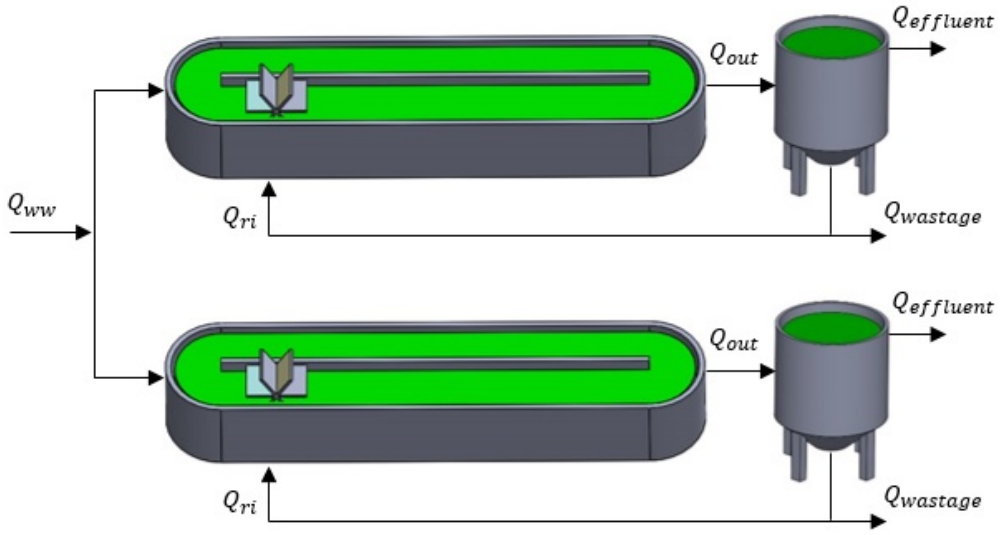

Fig. 5.3. Schematic of the hypothetical WWTP

The algal bacterial broth is composed of a consortium of microalgae and bacteria. The microalgae consortia consist of different strains utilized for wastewater treatment. The bacterial groups encompass heterotrophic bacteria and autotrophic bacteria (ammonium-oxidizing bacteria and nitrite-oxidizing bacteria). It is hypothesized that HRAPs are inoculated with 2.5 gVSS/L of microalgae consortia and 2.5 gVSS/L of activated sludge. The particulate components' relative proportions in the sludge are assumed based on those

proposed in the Activated Sludge Model 2 (ASM2) (Henze *et al.*, 2000). The concentration of particulate components in the inoculum is summarized in Table 5.2.

Table 5.1. Average inlet wastewater composition

Component	**Description**	**Concentration**	**Units**
S_{NH4}	Ammonium nitrogen	45	mgN-NH_4 L^{-1}
S_{NH3}	Ammonia nitrogen	0.15	mgN-NH_3 L^{-1}
S_{NO3}	Nitrate nitrogen	0	mgN-NO_3 L^{-1}
S_{NO2}	Nitrite nitrogen	0	mgN-NO_2 L^{-1}
S_{CO2}	Dissolved carbon dioxide	9.15	mgC-CO_2 L^{-1}
S_{HCO3}	Bicarbonate	290	mgC-HCO_3 L^{-1}
S_{CO3}	Carbonate	0.85	mgC-CO_3 L^{-1}
S_{PO4}	Phosphate phosphorus	8	mgP-PO_4 L^{-1}
S_{O2}	Dissolved oxygen	0	mgO_2 L^{-1}
S_H	Hydrogen ions	0.000010	mgH L^{-1}
S_{OH}	Hydroxide ions	0.017008	mgH-OH L^{-1}
S_S	Readily biodegradable soluble organic matter	100	mgCOD L^{-1}
S_I	Inert soluble organic matter	40	mgCOD L^{-1}

Table 5.2. Inoculum composition

Component	Description	Value	Units
X_{ALG}	Microalgae biomass	3550	mgCOD L^{-1}
X_H	Heterotrophic bacteria	592.85	mgCOD L^{-1}
X_{AOB}	Ammonium oxidizing bacteria	3.55	mgCOD L^{-1}
X_{NOB}	Nitrite oxidizing bacteria	1.775	mgCOD L^{-1}
X_S	Slowly biodegradable particulate organic matter	2463.7	mgCOD L^{-1}
X_I	Inert particulate organic matter	493.45	mgCOD L^{-1}

Fig. 5.4 illustrates the daily variations in inflow and inlet wastewater concentrations for all components, as well as temperature and solar radiation. The inlet wastewater flow rate (Fig. 5.4A) exhibits a trend consistent with the domestic wastewater flow data presented in (Metcalf & Eddy Inc., 2003). The inlet concentration for each wastewater component is represented by the trend described in Fig. 5.4B, in which the average wastewater concentration for each component is described in Table 5.1. The temperature and Photosynthetic Photon Flux Density (PPFD) values were evaluated in the context of summer conditions, as illustrated in Fig. 5.4C and Fig. 5.4D, respectively.

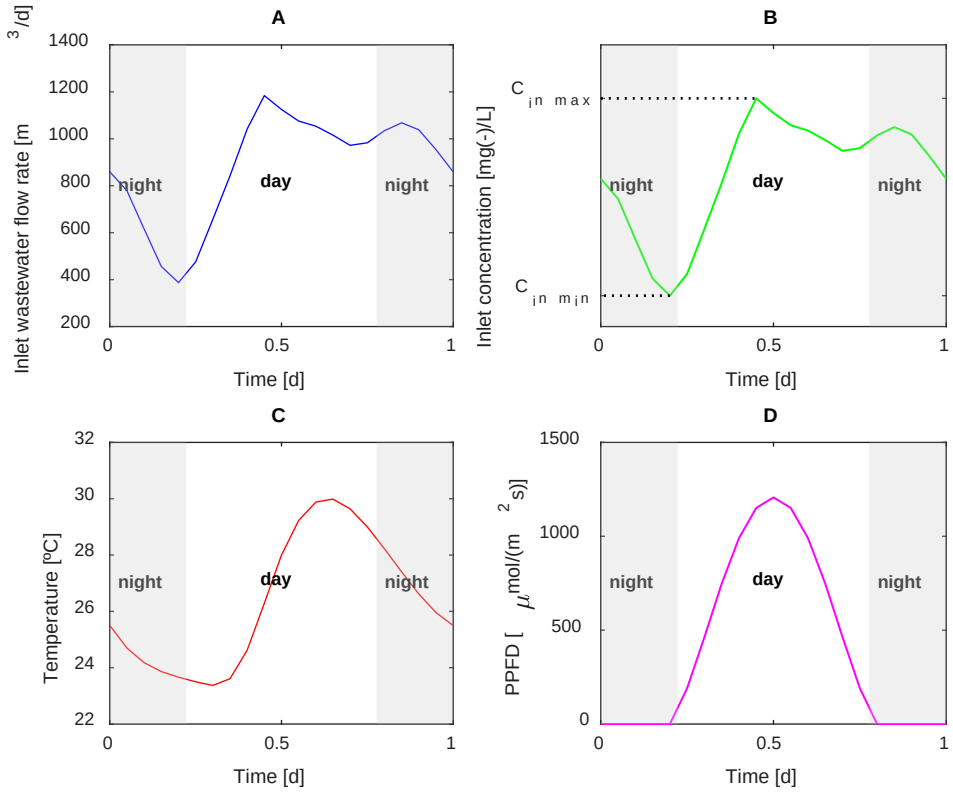

Fig. 5.4. Daily variation profiles of the inlet wastewater flow rate (A), inlet concentration (B), temperature (C), and photosynthetic photon flux density (D).

This study considers the availability of online pH, temperature, and dissolved oxygen measurements, with a sample period of 1.2 hours. It is further assumed that daily measurements of dissolved total organic carbon, dissolved ammonium, dissolved phosphate, and biomass concentration in the effluent are available for quality water monitoring. Additionally, the daily availability of measurements of biomass concentration in the HRAP and in the wastage flow rate is also assumed. The biomass concentration is quantified in terms of the TSS concentration. It is hypothesized that the measurements of dissolved components are drawn from the HRAP, and that the concentration of dissolved components in the effluent is equal to that of the HRAP. The specific measurements and their respective sampling frequencies are summarized in Table 5.3.

Table 5.3. Measured variables in the plant

Measured variable [units]	Description	Type of measurement	Sampling frequency [samples/day]
S_{O2} [mgO_2/L]	Dissolved oxygen	Online	20
pH	pH in the HRAP	Online	20
T [ºC]	Temperature in the HRAP	Online	20
TOC [mgC/L]	Total organic carbon	Analytics	1
S_{NH4} [$mgN\text{-}NH_4/L$]	Dissolved ammonium	Analytics	1
S_{PO4} [$mgP\text{-}PO_4/L$]	Dissolved phosphate	Analytics	1
TSS_{HRAP} [mgTSS/L]	Total suspended solids concentration in the HRAP	Analytics	1
$TSS_{effluent}$ [mgTSS/L]	Total suspended solids concentration in the effluent flow	Analytics	1
$TSS_{wastage}$ [mgTSS/L]	Total suspended solids concentration in the wastage flow	Analytics	1

5.3. Plant model

In this study, a detailed plant model was employed to simulate the dynamics occurring in the HRAP system with biomass recirculation. This sophisticated model was employed "in lieu" of the actual plant, and the measured variables are indeed the outputs of the detailed model.

5.3.1. HRAP model

The present study used the model BIO_ALGAE 2 (Solimeno, Gómez-Serrano and Acién, 2019a) (with minor modifications as outlined in Section 3.1.1) to represent the biochemical reactions and processes occurring within the HRAP. The model has previously undergone validation in HRAPs and other photobioreactor configurations under a range of operational conditions (Solimeno *et al.*, 2017a; Solimeno and García, 2019; Solimeno, Gómez-Serrano and Acién, 2019a; Bausa *et al.*, 2022). Details of the

process rates of the model and factors equations used to represent the processes occurring in the HRAP are summarized in Table 3.2 and Table 3.3, respectively. The matrix of stoichiometric parameters, the values of the parameters, and the fractions of carbon, hydrogen, oxygen, and nitrogen in microalgae and bacteria biomass are described in Appendix 1. This appendix also includes a summary of the mathematical expressions of the stoichiometric coefficients. To simulate the processes occurring in the HRAP, 22 state variables were utilized, including 19 state variables corresponding to model components and 3 state variables corresponding to the photosynthesis model.

In the BIO_ALGAE model, the compositions of the particulate components are expressed in terms of COD. Therefore, it is necessary to perform the transformation from mgCOD/L to mgTSS/L to make a comparison with the considered measured data. The COD/TSS relationships (5.9) and (5.10) were used to perform this adjustment. The relationships between state model variables and measured variables are represented by equations (4.1) and (4.2).

$$1gVSS = 1.42gCOD \tag{5.9}$$

$$1gTSS = 0.85gVSS \tag{5.10}$$

5.3.2. Settler model

The settler was described using the mass-balance expressions of the Takács model (Takács, Patryioand and Nolasco, 1991). The Takács model is a multi-layer dynamic model typically used for the clarification and thickening processes. In this work, a 10-layer settler was considered (this implies that 10 states were used to settler modeling). A comprehensive description of settler model used in this work can be found in Section 3.1.2.

5.4. Reduced model for state estimation

To create a more realistic framework for the application of the MHE technique, the detailed model previously referenced was used to simulate the "real plant," while a reduced model was employed for estimation with MHE. Given that this research was conducted within a simulation framework, the utilization of a reduced model in the

estimation process enables the consideration of potential model uncertainties that invariably arise in practical applications. Furthermore, employing a lower-complexity model for estimation facilitates the reduction of estimation time, a critical factor in addressing nonlinear optimization problems.

The estimation developed in the present research is intended for further use in monitoring and controlling the quality of effluent water in a WWTP with microalgae and bacteria using the MPC strategy. The utilization of the state estimator in the context of effluent water quality monitoring can serve as a valuable instrument for enhancing the operational efficiency of the plant. By offering pertinent real-time information regarding the process's status, the state estimator can reduce the necessity for conducting analytical measurements, thereby facilitating more efficient management of the process. Similarly, the implementation of all real-time control and optimization strategies demands the knowledge of the actual state of the process.

The implementation of a control strategy within the WWTP should ensure compliance with the prevailing legislation (Directive 1/271/CEE for EU states) (Unión Europea, 1991; *Real Decreto 509/1996, de 15 de marzo*, 1996). This directive establishes minimum requirements for the collection, treatment, and discharge of urban wastewater and wastewater from specific industrial sectors within the European Union. According to the directive, the evaluation of the quality of the treated wastewater discharged from urban WWTPs is to be based on the concentration of COD, TSS, total nitrogen, and total phosphorus in the effluent water. Therefore, components not directly associated with these variables are not necessarily subject to estimation by the MHE. Subsequently, the reduced model encompasses the estimation of the following variables:

- Biomass concentration (in the effluent flow, within the HRAP, and in the wastage flow). It is imperative to precisely monitor the TSS concentration in the effluent, as this is a critical factor in ensuring the desired quality of the water. Concurrently, the attainment of optimal biomass values within the HRAP is imperative to ensure sufficient wastewater treatment. The TSS concentration in the wastage flow is also estimated because in a system with recirculation, this value affects the TSS concentration in the HRAP. The biomass concentration is contingent upon the particulate components of the model, as delineated in Equation (4.1). Of the biomass components, the concentration of nitrifying bacteria (X_{AOB} and X_{NOB})

was not incorporated into the reduced model. This was due to the fact that nitrifying bacteria, despite their acknowledged role in wastewater treatment, exhibited considerably lower concentrations compared to the other particulate components present in the HRAP.

- The ammonium concentration. Due to the main role of the ammonium over the microalgae growth and its influence in the total nitrogen concentration that should be guaranteed in the effluent wastewater. In the context of this particular study, the concentrations of nitrites and nitrates are significantly lower in comparison with other nitrogen species, such as ammonium. Consequently, the concentration of these variables was not considered in the reduced model. The legislation establishing limits for components concentrations stipulated values for total nitrogen, rather than for nitrites and nitrates.
- The phosphate concentration. Due to their influence over microalgae and bacteria growth. Additionally, the monitoring of phosphate concentrations is crucial for the overall assessment of total phosphorus in effluent wastewater.
- The dissolved oxygen concentration is a critical factor in achieving a comprehensive understanding of the primary processes within the HRAP. The availability of reliable online S_{O2} measurements, as well as the relation of the dissolved oxygen with the main process variables, allows for the design and implementation of state estimators based on dissolved oxygen measures.
- The TOC concentration, defined by Equation (4.2) is directly related with the COD. Evaluating the COD is imperative to ensure efficient wastewater treatment.

The components of the inorganic carbon (S_{CO2}, S_{HCO3}, and S_{CO3}) are not estimated by the reduced model because the focus of this study is on estimating those components regulated by the legislation that should be analyzed prior to the discharge. Consequently, the concentration of inorganic carbon is not regarded as a limiting factor in the discharge of effluent water.

In order to simplify the reduced model (and consequently improve the estimation time of the MHE), the concentration of S_H and S_{OH} was not calculated. In the reduced model, the pH of the culture medium is regarded as a known measured input.

The reduced model encompasses 10 processes, which are described in Table 5.4. Furthermore, the objective of minimizing the estimation time was pursued by calculating the factors of the photosynthesis model directly using the relations described in Table 5.5, as opposed to the system of differential equations utilized in the model of the plant (Table 3.3).

Summarizing, the reduced model of the HRAP included 10 state variables, as it was not necessary to estimate all components of the system for operation. A comprehensive summary of the state variables considered in both the real plant and MHE model is provided in Table 5.6. The settler model used for estimation, similarly with the one used for plant simulation, encompasses also 10 state variables.

A synopsis of the processes encompassed in the plant and the reduced model is summarized in Table 5.7. The analysis of Table 5.6 and Table 5.7 reveals the substantial structural disparities between the plant and the reduced model for the HRAP, as evidenced by the number of states and equations involved. Additionally, disparities in the values of some parameters were considered in plant and model (Table 5.8). The values of the parameters in the plant were selected based on the values previously reported in the literature for microalgae-bacteria raceway reactors (Solimeno *et al.*, 2017b; Casagli *et al.*, 2021).

Table 5.4. Process rates of the reduced model

Processes	Process rate [M L^{-3} T^{-1}]
Microalgae (X_{ALG}) processes	
Growth on S_{NH}	$\rho_1 = \mu_{ALG} \cdot f_I \cdot f_{DO} \cdot f_{T_{ALG}} \cdot f_{pH_{ALG}} \cdot \frac{S_{CO2} + S_{HCO3}}{K_{C,ALG} + S_{CO2} + S_{HCO3} + \frac{{S_{CO2}}^2}{I_{CO2,ALG}}} \cdot \frac{S_{NH3} + S_{NH4}}{K_{N,ALG} + S_{NH3} + S_{NH4}} \cdot \frac{S_{PO4}}{K_{P,ALG} + S_{PO4}} \cdot X_{ALG}$
Endogenous respiration	$\rho_2 = k_{resp,ALG} \cdot f_{T_{ALG}} \cdot f_{pH_{ALG}} \cdot \frac{S_{O2}}{K_{O2,ALG} + S_{O2}} \cdot X_{ALG}$
Decay	$\rho_3 = k_{death,ALG} \cdot f_{T_{ALG}} \cdot f_{pH_{ALG}} \cdot X_{ALG}$
Heterotrophic bacteria (X_H) (aerobic activity)	
Aerobic growth on S_{NH}	$\rho_4 = \mu_H \cdot f_{T_H} \cdot f_{pH_H} \cdot \frac{S_S}{K_{S,H} + S_S} \cdot \frac{S_{O2}}{K_{O2,H} + S_{O2}} \cdot \frac{S_{NH3} + S_{NH4}}{K_{N,H} + S_{NH3} + S_{NH4}} \cdot \frac{S_{PO4}}{K_{P,H} + S_{PO4}} \cdot X_H$
Aerobic endogenous respiration	$\rho_5 = k_{resp,H} \cdot f_{T_H} \cdot f_{pH_H} \cdot \frac{S_{O2}}{K_{O2,H} + S_{O2}} \cdot X_H$
Decay	$\rho_6 = k_{death,H} \cdot f_{T_H} \cdot f_{pH_H} \cdot X_H$
Hydrolysis, Chemical equilibrium and Transfer of gases	
Aerobic hydrolysis	$\rho_7 = k_{HYD} \cdot \frac{X_S/X_H}{K_{HYD} + (X_S/X_H)} \cdot X_H$
Chemical equilibrium $NH_4^+ \leftrightarrow NH_3$	$\rho_8 = k_{eq,3} \cdot (S_{NH4} - S_H S_{NH3}/K_{eq,3})$
S_{O2} transfer to the atmosphere	$\rho_9 = K_{la,O2} \cdot (S_{O2}^{WAT} - S_{O2})$
S_{NH3} transfer to the atmosphere	$\rho_{10} = K_{la,NH3} \cdot (-S_{NH3})$

Table 5.5. Photosynthesis model used in the reduced model

Photosynthetic factories model (Eileers and Peeters) (Eilers and Peeters, 1988)		
$f_I = x_2$	The photosynthetic factories model is described by the system of differential equations described in Table 3.3. In outdoor conditions, variations in irradiance during the daily solar cycle are very slow with respect to the dynamics of photosynthesis (Eilers and Peeters, 1988; Camacho Rubio *et al.*, 1999; Solimeno *et al.*, 2015). In these conditions x_1 and x_2 are close to equilibrium in less than a second (Solimeno *et al.*, 2015). Assuming this condition, the solution to the system of differential equations is: $x_1 = \frac{\gamma\delta+\beta I\delta}{\alpha\beta I^2+(\alpha+\beta)\delta I+\gamma\delta}$ $x_2 = \frac{\alpha\delta I}{\alpha\beta I^2+(\alpha+\beta)\delta I+\gamma\delta}$ $x_3 = \frac{\alpha\beta I^2}{\alpha\beta I^2+(\alpha+\beta)\delta I+\gamma\delta}$ where: $I = I_{av}$ The average light intensity (I_{av}) was described using Lambert-Beer's Law: $I_{av} = \frac{I_0(1-exp(-K_i \cdot TSS \cdot d))}{K_i \cdot TSS \cdot d}$ where: $TSS = X_{ALG} + X_H + X_I + X_S$	x_1: Microalgae in open state (ready to capture a photon). x_2: Microalgae in activated state (microalgae can go back to open state or can capture another photon). x_3: Microalgae in inhibited state (ready to turn back to the open state. α: Rate of activation $[(\mu E\ m^{-2})^{-1}]$ γ: Rate constant of production $[s^{-1}]$ β: Rate constant of inhibition $[(\mu E\ m^{-2})^{-1}]$ δ: Rate of recovery $[s^{-1}]$ I_{av}: Average light intensity $[\mu mol\ m^{-2}s^{-1}]$ I_0: Incident light intensity $[\mu mol\ m^{-2}s^{-1}]$ K_i: Extinction coefficient for particulate biomass $[m^2 g^{-1}]$ TSS: Particulate components $[gTSS\ m^{-3}]$ d: Photobioreactor depth $[m]$

Table 5.6. State variables considered in the plant and in the reduced model

	State variables		Output or measured variable affected
	Considered in the plant [units]	**Estimated by the reduced model** (Yes/No) / Additional comment	
HRAP model	X_{ALG} [mgCOD/L]	Yes	TSS
	X_H [mgCOD/L]	Yes	
	X_{AOB} [mgCOD/L]	No	
	X_{NOB} [mgCOD/L]	No	
	X_S [mgCOD/L]	Yes	
	X_I [mgCOD/L]	Yes	
	S_{NH4} [mgN-NH_4/L]	Yes	S_{NH4}
	S_{NH3} [mgN-NH_3/L]	Yes	
	S_{NO3} [mgN-NO_3/L]	No	
	S_{NO2} [mgN-NO_2/L]	No	
	S_{PO4} [mgP-PO_4/L]	Yes	S_{PO4}
	S_{O2} [mgO_2/L]	Yes	S_{O2}
	S_{CO2} [mgC-CO_2/L]	No	
	S_{HCO3} [mgC-HCO_3/L]	No	
	S_{CO3} [mgC-CO_3/L]	No	
	S_H [mgH/L]	No/	pH
	S_{OH} [mgH-OH/L]	Used as model input in the reduced model	
	S_S [mgCOD/L]	Yes	TOC
	S_I [mgCOD/L]	Yes	
Photosynthesis model	X_1	No/	
	X_2	Calculated directly, instead as a state variable	
	X_3		
Settler model	$TSS_{effluent}$	Yes	$TSS_{effluent}$
	TSS_2	Yes	
	TSS_3	Yes	
	TSS_4	Yes	
	TSS_5	Yes	
	TSS_6	Yes	
	TSS_7	Yes	
	TSS_8	Yes	
	TSS_9	Yes	
	$TSS_{wastage}$	Yes	$TSS_{wastage}$

Table 5.7. Processes considered in the plant and the model

	Process	Plant	Model
Microalgae processes	Growth on S_{NH4}	Considered	Considered
	Growth on S_{NO3}	Considered	Not Considered
	Endogenous respiration	Considered	Considered
	Decay	Considered	Considered
Heterotrophic bacteria processes	Aerobic growth on S_{NH4}	Considered	Considered
	Aerobic growth on S_{NO3}	Considered	Not Considered
	Anoxic growth on S_{NO2} (denitrification on S_{NO2})	Considered	Not Considered
	Anoxic growth on S_{NO3} (denitrification on S_{NO3})	Considered	Not Considered
	Aerobic endogenous respiration	Considered	Considered
	Anoxic endogenous respiration	Considered	Not Considered
	Decay	Considered	Considered
Autotrophic bacteria processes	Growth of X_{AOB}	Considered	Not Considered
	Growth of X_{NOB}	Considered	Not Considered
	Endogenous respiration of X_{AOB}	Considered	Not Considered
	Endogenous respiration of X_{NOB}	Considered	Not Considered
	Decay of X_{AOB}	Considered	Not Considered
	Decay of X_{NOB}	Considered	Not Considered
Hydrolysis	Hydrolysis	Considered	Considered
Chemical equilibrium	Chemical equilibrium $CO_2 \leftrightarrow HCO_3^-$	Considered	Not Considered
	Chemical equilibrium $HCO_3^- \leftrightarrow CO_3^{2-}$	Considered	Not Considered
	Chemical equilibrium $NH_4^+ \leftrightarrow NH_3$	Considered	Considered
	Chemical equilibrium $H^+ \leftrightarrow OH^-$	Considered	Not Considered
Transfer of gases	S_{O2} transfer to the atmosphere	Considered	Considered
	S_{CO2} transfer to the atmosphere	Considered	Not Considered
	S_{NH3} transfer to the atmosphere	Considered	Considered

Table 5.8. Values of parameters in plant and model

Parameter [units]	Description	Plant	Model
μ_{ALG} [d^{-1}]	Maximum specific growth rate of microalgae	2.5	3.5
μ_{H} [d^{-1}]	Maximum specific growth rate of heterotrophic bacteria	5.8	5.5
$K_{la,\,O2}$ [d^{-1}]	Mass transfer coefficient for oxygen	10	9

The simulated differences between the plant and the reduced model starting from the initial inoculation time of the plant are illustrated in Fig. 5.5 to Fig. 5.9 for a period of 60 days operating under the conditions illustrated in Fig. 5.4. The initial values of the states set in the plant and model simulation are described in Table A3.1 and Table A3.2 of the Appendix 3. The differences in the concentration of particulate components in the HRAP are shown in Fig. 5.5. The biomass concentration into the raceway reactors, in the effluent flow, and in the wastage flow for the plant and the reduced model are illustrated in Fig. 5.6. The effect of daily variations over the biomass due to operational and environmental variables is visible in both the plant and model trend. The concentration of the dissolved components in the HRAP is illustrated in Fig. 5.7, where the ammonium and phosphate assimilation by microalgae (Fig. 5.7A and Fig. 5.7B, respectively) was highly affected by day/night cycles, as well as the TOC assimilation by heterotrophic bacteria (Fig. 5.7C). Concomitantly, substantial variations in the dissolved oxygen concentration within the HRAP, attributable to diurnal fluctuations in irradiation, are evident in both the plant and in the reduced model (Fig. 5.8). States of the photosynthesis model are represented in Fig. 5.9 for the plant and the reduced model. The analysis of Fig. 5.5 to Fig. 5.9 reveals that the reduced model effectively replicates the trend of the primary variables involved in wastewater treatment. This findings validated its use as a prediction model in the MHE approach. Conversely, the discrepancies in the behavior of the reduced model in comparison to the plant depicted in Fig. 5.5 to Fig. 5.9 can be attributed to two primary factors: structural mismatches (summarized in Table 5.6 and Table 5.7) and parameter mismatches (detailed in Table 5.8).

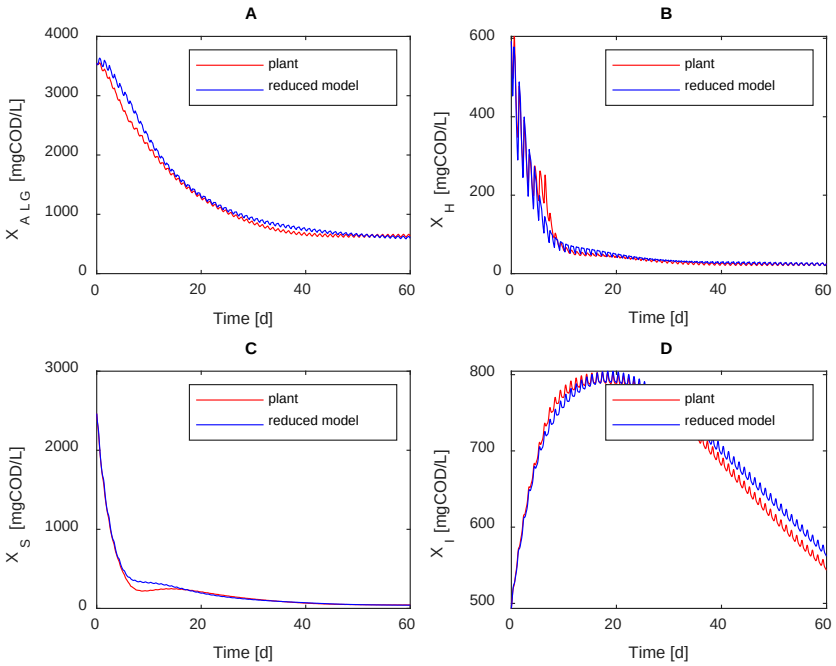

Fig. 5.5. Plant and reduced model differences in the biomass composition in the HRAP: microalgae biomass (A), heterotrophic bacteria (B), slowly biodegradable particulate organic matter (C), and inert particulate organic matter (D).

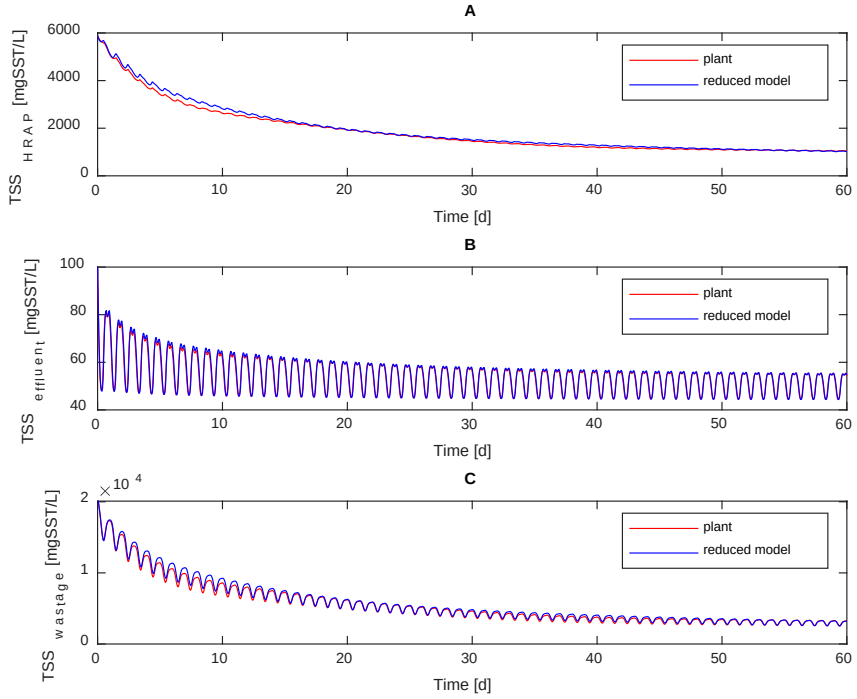

Fig. 5.6. Plant and reduced model differences in biomass concentration: TSS concentration in the HRAP (A), TSS concentration in the effluent flow (B), and TSS concentration in the wastage flow (C).

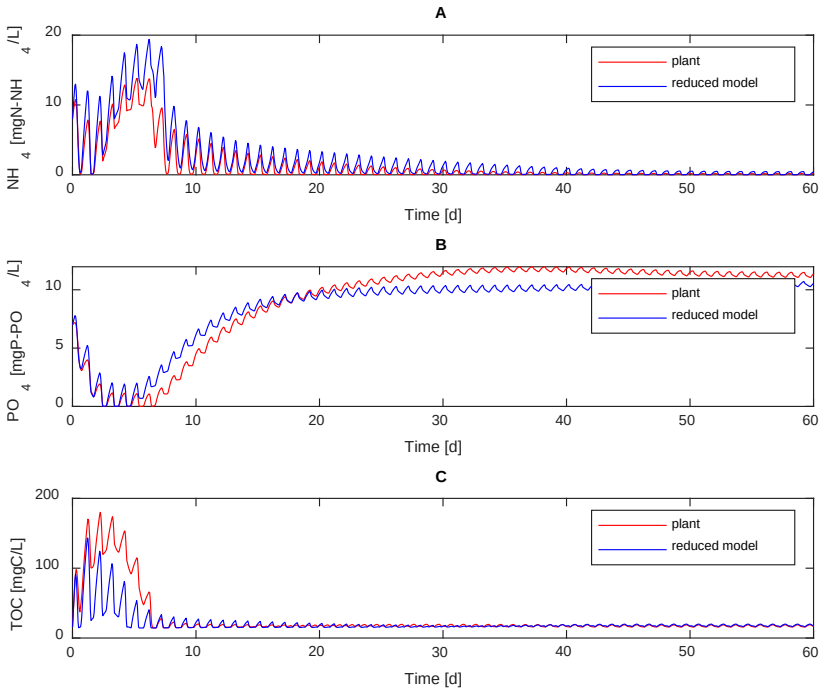

Fig. 5.7. Plant and reduced model differences in the dissolved ammonium concentration (A), the dissolved phosphate concentration (B), and the dissolved total organic carbon concentration (C) in the HRAP.

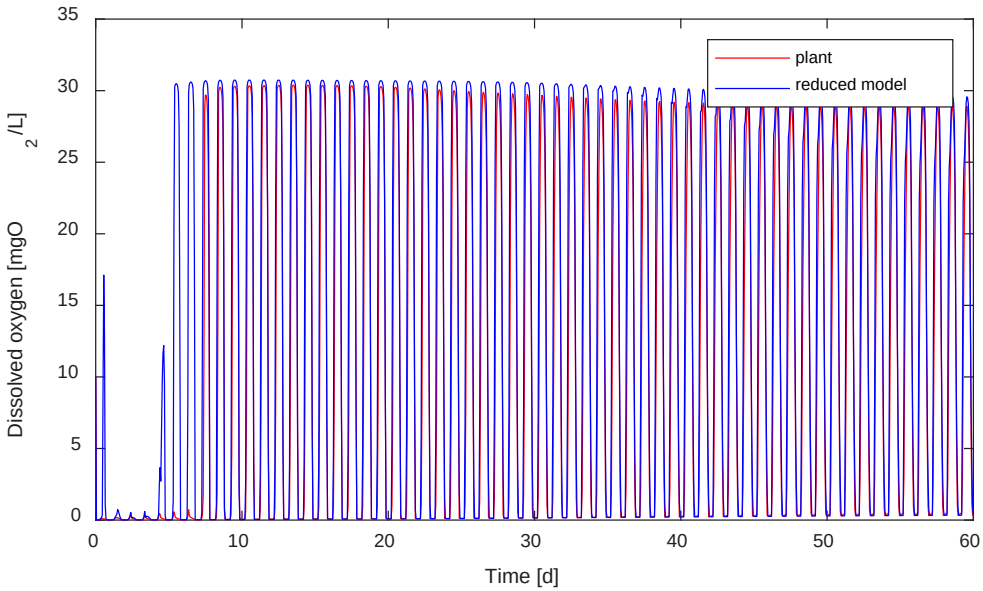

Fig. 5.8. Plant and reduced model differences in the dissolved oxygen concentration in the HRAP.

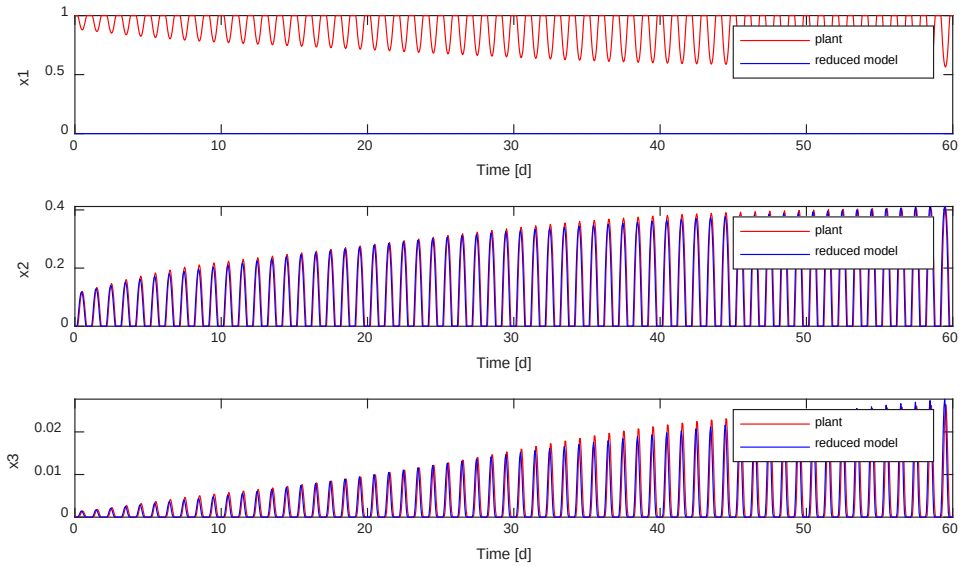

Fig. 5.9. Plant and reduced model differences in photosynthesis model.

5.5. State estimation using MHE in a microalgae-bacteria wastewater treatment plant

MHE was designed to furnish the values of the unmeasured states for prospective implementations of model predictive control algorithms and optimization strategies to enhance system performance. These unmeasured states offer critical information about the system, which is essential for the effective implementation of feedback control strategies. The application of MHE to microalgae-based wastewater treatment systems poses specific challenges, primarily due to i) the scarcity of online measurements, ii) the lack of perfect knowledge of the model structure, iii) uncertainties in the values of parameters and states, iv) the unavailability of direct methods to determine the fractions of particulate components in the biomass, v) the reliability of analytical measurements is highly dependent on human expertise, vi) the elapsed time from the moment the sample is taken to the moment the analytical procedure is completed.

In the hypothetical microalgae-based WWTP studied in this work, multi-rate measurements are presented with the sampling frequency shown in Table 5.3. Online measurements of the high-rate dynamic variables (pH, temperature, and dissolved oxygen) could be available with a higher sampling time. However, the sampling time of 1.2 hours was used considering the slow dynamics of these variables in a large treatment

plant and to avoid excessive computational time in the optimization. The estimator takes into account the availability of Photosynthetically Active Radiation (PAR), pH, temperature, and flow measurements. The schematic of the MHE applied to the case study is depicted in Fig. 5.10.

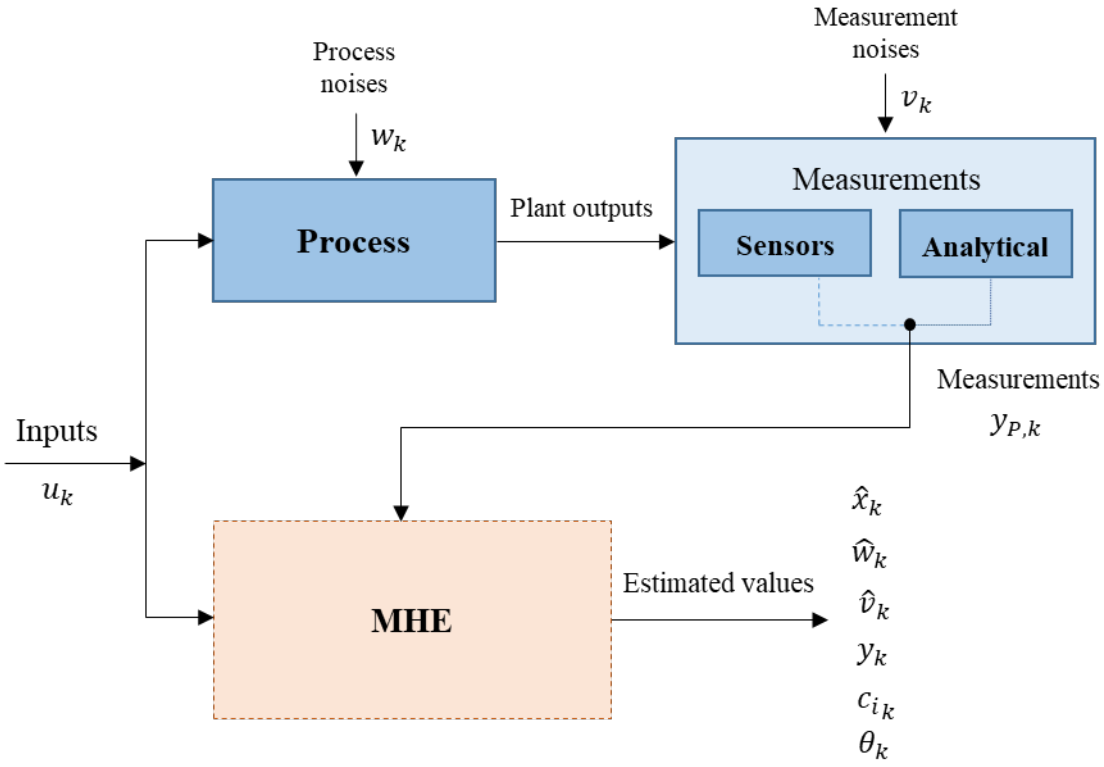

Fig. 5.10. Schematic of MHE for the microalgae-based WWTP

The structure of the state, output, and input vectors employed in the MHE formulation are described by equations (5.11) to (5.13):

$$\mathbf{x} = [X_{ALG} \quad X_H \quad X_S \quad X_I \quad S_S \quad S_I \quad S_{NH4} \quad S_{NH3} \quad S_{PO4} \quad S_{O2} \quad TSS_{effluent} \quad TSS_2 \quad TSS_3 \quad TSS_4 \quad TSS_5 \quad TSS_6 \quad TSS_7 \quad TSS_8 \quad TSS_9 \quad TSS_{wastage}]^T \tag{5.11}$$

$$\mathbf{y_P} = [TSS_{HRAP} \quad TOC_{HRAP} \quad S_{NH4} \quad S_{PO4} \quad S_{O2} \quad TSS_{effluent} \quad TSS_{wastage}]^T \tag{5.12}$$

$$\mathbf{u} = [I \quad pH \quad T \quad Q_{ww} \quad Q_{ri} \quad Q_{wastage}]^T \tag{5.13}$$

The naming of the state variables to estimate (Eq. (5.11)) is detailed in Table 5.1, Table 5.2, and Table A3.2 in Appendix 3. The measurement vector, as developed by Eq. (5.12), encompasses the variables enumerated in Table 5.3. In the MHE formulation, the vector of known inputs, defined by Eq. (5.13), includes the values of PAR (I), pH (pH), and

temperature (T) of the culture media, as well as the values of inlet wastewater flow (Q_{ww}), recirculation flow (Q_{ri}), and wastage flow $(Q_{wastage})$.

The MHE is intended to estimate the state vector values at each sampling time $(\mathbf{x})$, as well as the values of the unknown disturbances $(\mathbf{w})$ and measurement noises $(\mathbf{v})$ that minimize the cost function defined in Eq. (5.1). In order to obtain useful information for system operation and control, the values of the input wastewater concentration $\mathbf{c_i}$ (Eq. (5.14)) and the values of relevant process parameters (vector $\boldsymbol{\theta}$, Eq. (5.15)) are also decision variables in the optimization problem. Estimated parameters are instrumental in characterizing the microbial dynamics in the process. In this sense, the maximum specific growth rates of microalgae (μ_{ALG}) and heterotrophic bacteria were estimated (μ_{H}), as well as the decay rate of microalgae ($k_{death,ALG}$) and heterotrophic bacteria ($k_{death,H}$). Concurrently, the estimation of the mass transfer coefficient of the dissolved oxygen was conducted ($K_{la,O2}$). These parameters were identified as the most relevant parameters to adjust in Section 4.1.1.

$$\mathbf{c_i} = [S_{S_{ww}} \quad S_{I_{ww}} \quad S_{NH4_{ww}} \quad S_{NH3_{ww}} \quad S_{PO4_{ww}}]^T \tag{5.14}$$

$$\boldsymbol{\theta} = [\mu_{\mathrm{ALG}} \quad k_{death,ALG} \quad \mu_{\mathrm{H}} \quad k_{death,H} \quad K_{la,O2}\ ]^T \tag{5.15}$$

Given the availability of multi-rate measurements, the execution time of the MHE is determined by the fastest measurements (dissolved oxygen measurements). It is assumed that analytical measurements are available daily at 0 a.m., implying that a full vector of output measurements is only available on a daily basis. Conversely, at each sampling time (1.2 hours), a new dissolved oxygen measurement is available. An overview of the availability of measurements is given in Table 5.3 . To address the challenge posed by multi-rate measurements in the context of MHE, two decisions were made:

• The consideration of a past horizon, encompassing at least a full vector of output measurements (the estimation past horizon should be a minimum of 1 day).

• The cost function incorporates only the available measurements at each sampling time.

5.5.1. MHE coding and tuning

The MHE was coded using MATLAB® software (MathWorks Inc., 2024), version 24.1, R2024a and the MPCTools (Risbeck and Rawlings, 2016). MPCTools is a control and

estimation tool for linear and nonlinear dynamic models. Its provides an oriented interface to CasADi for Octave and MATLAB. MPCTools provides an interface to CasADi solvers, thereby facilitating the simulation of MPC controllers or MHE on any system of interest. Although CasADi is a more robust software, MPCTools allows code saving in the formulation of MHE or MPC problems (Risbeck and Rawlings, 2016). The estimation problem was addressed by employing the Ipopt (Interior Point Optimizer) solver, which is an open-source software package for large-scale nonlinear optimization. The model used for estimation was discretized using the Runge-Kutta method. The MHE simulations were carried out using the following computer hardware specifications: an 13th Gen Intel® Core™ i9-13900K processor (3.0 GHz), 128 GB of RAM memory, and a 500 GB hard-disk drive.

In order to formulate MHE, it is necessary to provide the values of the weight matrices of the cost function, as defined by (5.1). It is imperative to note that $\mathbf{Q}_{\boldsymbol{x}}$, $\mathbf{Q}_{\boldsymbol{w}}$, and $\mathbf{Q}_{\boldsymbol{y}}$ are positive definite matrices, with weighting and normalization factors. Given the imprecise nature of the initial guesses for the states, the diagonal elements of $\mathbf{Q}_{\boldsymbol{x}}$ are set to a value of 0.5. Table 5.9 and Table 5.10 present the values of the diagonal elements of $\mathbf{Q}_{\boldsymbol{w}}$ and $\mathbf{Q}_{\boldsymbol{y}}$, respectively. The tuning values of $\mathbf{Q}_{\boldsymbol{w}}$ and $\mathbf{Q}_{\boldsymbol{y}}$ were selected based on the standard deviation of the variables in order to normalize the different terms of the cost function. In the WWTP, considerable scale differences in the measured output variables, as well as in the estimated states, necessitated the normalization of these values. This procedure was implemented with the objective of ensuring that each output was accorded equal importance, as well as to guarantee the same importance in the modeling error for each estimated state. The weight values were selected to allocate greater importance to the discrepancies between the model and the measurements, indicating that the reliability of the measurements surpasses that of the model. The constraints on the variables involved in the optimization problem are summarized in Table 5.11 through Table 5.14.

Table 5.9. Diagonal elements of the weight matrix $\mathbf{Q_w}$

States	Weight	Units
X_{ALG}	60	[mgCOD/L]
X_H	5	[mgCOD/L]
X_S	10	[mgCOD/L]
X_I	50	[mgCOD/L]
S_S	2	[mgCOD/L]
S_I	4	[mgCOD/L]
S_{NH4}	0.1	[mgN-NH_4/L]
S_{NH3}	0.1	[mgN-NH_3/L]
S_{PO4}	1	[mgP-PO_4/L]
S_{O2}	2	[mgO_2/L]
$TSS_{effluent}$	5	[mgTSS/L]
TSS_2	10	[mgTSS/L]
TSS_3	10	[mgTSS/L]
TSS_4	10	[mgTSS/L]
TSS_5	10	[mgTSS/L]
TSS_6	20	[mgTSS/L]
TSS_7	50	[mgTSS/L]
TSS_8	50	[mgTSS/L]
TSS_9	50	[mgTSS/L]
$TSS_{wastage}$	300	[mgTSS/L]

Table 5.10. Diagonal elements of the weight matrix $\mathbf{Q_y}$

Output	Weight	Units
TSS_{HRAP}	100	[mgTSS/L]
TOC	2	[mgC/L]
S_{NH4}	0.1	[mgN-NH_4/L]
S_{PO4}	1	[mgP-PO_4/L]
S_{O2}	2	[mgO_2/L]
$TSS_{effluent}$	5	[mgTSS/L]
$TSS_{wastage}$	300	[mgTSS/L]

Table 5.11. Upper and lower bounds on states and process noise

	States		Process noise	
	Upper bound ($\boldsymbol{x^U}$)	**Lower bound** ($\boldsymbol{x^L}$)	**Upper bound** ($\boldsymbol{w^U}$)	**Lower bound** ($\boldsymbol{w^L}$)
X_{ALG}	800	400	500	-500
X_H	60	0	500	-500
X_S	150	40	500	-500
X_I	700	500	100	-100
S_S	25	5	10	-10
S_I	50	38	10	-10
S_{NH4}	1	0	0.05	-0.05
S_{NH3}	2	0	0.01	-0.01
S_{PO4}	13	0	2	-2
S_{O2}	32	0	2	-2
$TSS_{effluent}$	60	0	30	-30
TSS_2	80	0	30	-30
TSS_3	90	0	30	-30
TSS_4	150	0	30	-30
TSS_5	500	0	30	-30
TSS_6	500	0	70	-70
TSS_7	1000	0	100	-100
TSS_8	1000	0	200	-200
TSS_9	1000	300	200	-200
$TSS_{wastage}$	8000	2000	5000	-5000

Table 5.12. Upper and lower bounds on outputs noise

Output	**Upper bound** ($\boldsymbol{v^U}$)	**Lower bound** ($\boldsymbol{v^L}$)
TSS_{HRAP}	100	-100
TOC	5	-5
S_{NH4}	1	-1
S_{PO4}	3	-3
S_{O2}	4	-4
$TSS_{effluent}$	15	-15
$TSS_{wastage}$	400	-400

Table 5.13. Upper and lower bounds on the inlet wastewater concentration

Wastewater component	**Upper bound** $(\mathbf{c_i}^{\mathbf{U}})$	**Lower bound** $(\mathbf{c_i}^{\mathbf{L}})$	**Units**
$S_{S_{ww}}$	135	45	[mgCOD/L]
$S_{I_{ww}}$	55	18	[mgCOD/L]
$S_{NH4_{ww}}$	67	23	[mgN-NH_4/L]
$S_{NH3_{ww}}$	0.20	0.07	[mgN-NH_3/L]
$S_{PO4_{ww}}$	19	6	[mgP-PO_4/L]

Table 5.14. Upper and lower bounds in the estimated parameters

Wastewater component	**Upper bound** $(\boldsymbol{\theta}^{\mathbf{U}})$	**Lower bound** $(\boldsymbol{\theta}^{\mathbf{L}})$	**Units**
μ_{ALG}	1.5	4	[d^{-1}]
$k_{death,\,ALG}$	0.045	0.15	[d^{-1}]
μ_H	3	6.5	[d^{-1}]
$k_{death,\,H}$	0.6	1	[d^{-1}]
$K_{la,\,O2}$	7	13	[d^{-1}]

5.6. MHE simulation results

The results of the MHE execution are presented considering the system operation under a periodic regime. The parameters used for the MHE simulation are enumerated in Table 5.15. The estimation horizon of two days is regarded as sufficient in terms of data availability to support the calculation of an accurate estimation. In the context of the MHE application, it is imperative to align the sampling period with the dynamics of the variables to be estimated. The application under consideration in this research involves the estimation of variables related to water quality. The variables in question exhibit slow dynamics, thereby rendering lower sampling times unnecessary. Despite the fact that commercial sensors for dissolved oxygen measurement provide data with considerably lower sampling times than those employed in the present research, the sampling time used in this paper was selected considering that large estimation times are generally needed for nonlinear estimation with constraints. Moreover, in order to consider the possible

applications of the MPC control strategy in this process, it is essential that the sampling time be adequately long to encompass both the estimation time and the time required for executing the nonlinear constrained MPC controller.

Table 5.15. MHE simulation parameters

Parameter	Description	Value
n_e	Estimation horizon	2 d (40 samples)
Delta	Sampling time	0.05 d

Simulations were executed under the environmental conditions illustrated in Fig. 5.4. Additionally, to simulate possible measurement errors in sensors and analytical procedures, a measurement noise was introduced. This noise was generated using a MATLAB® function which returns a random scalar drawn from the standard normal distribution. For each output, the media of the noise value introduced corresponds to 5 % of the average output value. The simulation results for the MHE application during 10 days (corresponding with 200 samples) are presented in Fig. 5.11 to Fig. 5.16, using initial information of past data corresponding to two previous days. In each sample, the MHE estimation was provided with an average value of 17.97 seconds (the higher estimation time being 37.49 seconds), which means that MHE can be used as the first step of advanced control or process dynamic optimization.

The estimated values (blue line) for the dissolved oxygen concentration in the HRAP are illustrated in Fig. 5.11. The red line in the graph represents the actual values of the dissolved oxygen concentration, which include the noise in the measurements. As this study was conducted within a simulation framework, real-time plant values are available for continuous representation, with the purpose of illustrating the estimator fit. In real-world scenarios, the measured values are only available at discrete time intervals, which are represented by crosses in the data. Error bars (purple bars) are included to illustrate the limits of uncertainty that were assumed in the measurements. The results demonstrate the accuracy of the prediction provided by the MHE, as well as estimator robustness, even considering noisy measurements.

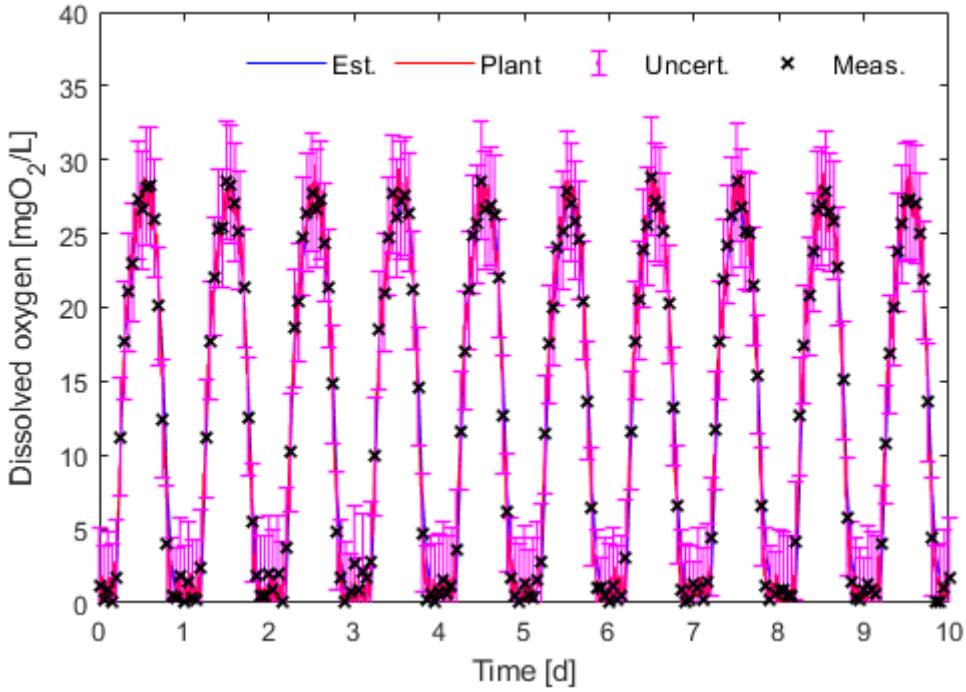

Fig. 5.11. Measured and estimated values of the dissolved oxygen in the HRAP

The estimated values for the biomass concentration in the HRAP, the biomass concentration in the effluent, and the biomass concentration in the wastage stream are illustrated in Fig. 5.12. As demonstrated in Fig. 5.12, the MHE effectively estimates the biomass concentration values for the entire simulation time by leveraging historical output values and dissolved oxygen measurements at each sampling time. The error bars represent the uncertainties in the measured values of the biomass. In such cases, where analytical procedures are employed to ascertain biomass values, low biomass values are deemed to be more susceptible to measurement uncertainties. The online estimation of biomass concentration is imperative for ensuring the optimal operation of photobioreactors taking early actions in response to the values of the estimated variables, without waiting for the lab analysis to arrive. Optimal biomass values in the HRAP are necessary to ensure the adequate wastewater depuration, and high biomass concentrations within the reactor affect the penetration of solar radiation into the culture, which in turn affects the growth of microalgae. In addition, the online monitoring of TSS concentration in the effluent is of a paramount importance in order to guarantee the desired water quality. Conversely, in scenarios where the primary objective is the harvesting of biomass

for the production of diverse bioproducts, it is essential to optimize biomass yield to ensure maximum economic profitability.

The MHE has the capacity to predict the values of the various components of biomass (Fig. 5.13). Conventionally, the assessment of these values does not employ direct or standardized methodologies. Indeed, a salient benefit of the application of state estimators in such processes is that they enable the estimation of the concentrations of different biomass components without the necessity of employing complex analytical methods.

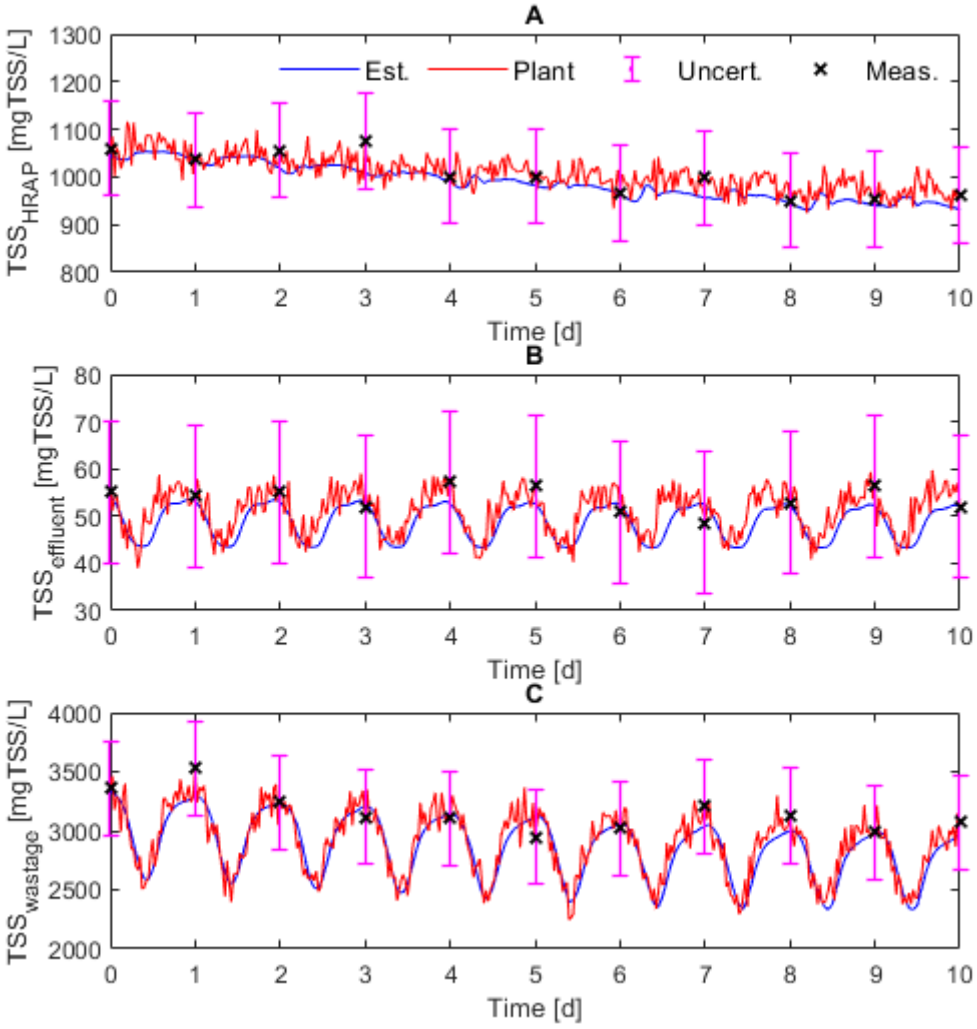

Fig. 5.12. Measured and estimated values of the biomass concentration in the HRAP (A), in the effluent (B), and in the wastage stream (C).

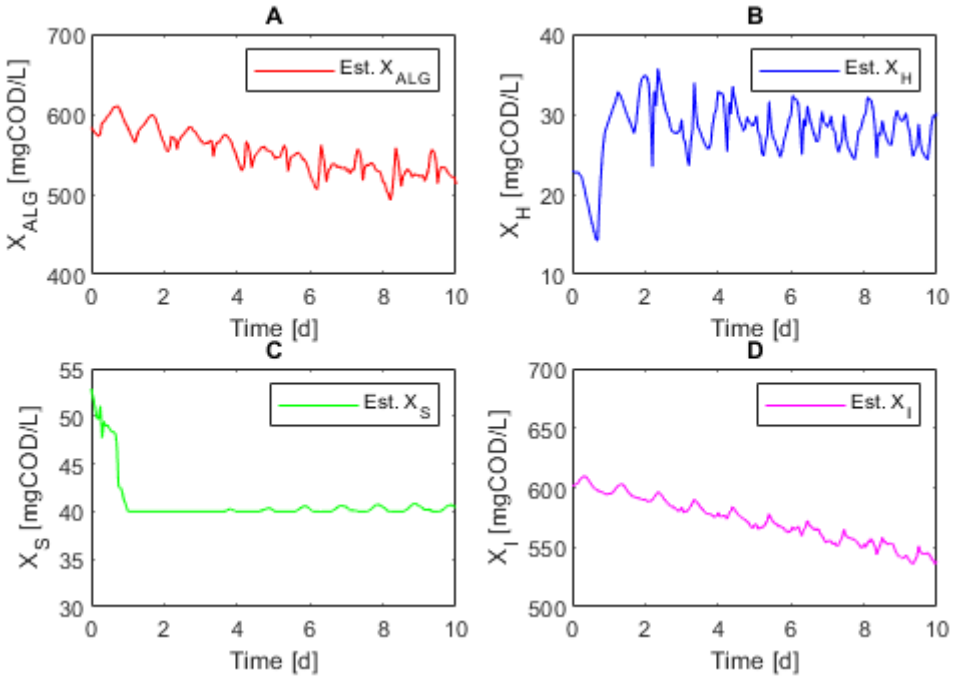

Fig. 5.13. Estimated values of the biomass components: microalgae biomass concentration (A), heterotrophic bacteria concentration (B), slowly biodegradable particulate organic matter (C), and inert particulate organic matter (D).

The measured and estimated values of the TOC in the effluent are presented in Fig. 5.14A. The online monitoring of the TOC concentration is imperative for the evaluation of effluent water quality. Fig. 5.14B and Fig. 5.14C illustrate the estimated values of readily biodegradable soluble organic matter and inert soluble organic matter, respectively, as components of the TOC.

The quality of effluent water is also contingent upon the concentrations of dissolved ammonium and dissolved phosphate. The measured and estimated values of dissolved ammonium and dissolved phosphate concentration are illustrated in Fig. 5.15A and Fig. 5.15B, respectively. As demonstrated in Fig. 5.15A, the estimate of the ammonium concentration in the effluent exhibits a slight overestimation relative to the actual value. This phenomenon can be attributed to the observation that the proliferation of microalgae and heterotrophic bacteria (the two predominant microorganisms groups in the HRAP) is exclusively associated with the utilization of ammonium. This association disregards the microalgae growth on S_{NO3}, as well as the heterotrophic bacteria aerobic growth on nitrate and the heterotrophic bacteria anoxic growth on nitrite and nitrate (as summarized in

Table 5.7). This finding suggests that the reduced model attributes the observed growth exclusively to nitrogen species in the form of S_{NH4}, which may lead to an overestimation of this component in the HRAP. In a similar fashion, the phosphate estimation (Fig. 5.15B) exhibits a slight increase compared to the actual value of S_{PO4} concentration. This discrepancy can be attributed to the reduced model incorporating a smaller number of nutrients utilized by microalgae and bacteria for its growth, resulting in an overestimation of these components within the reduced model. Nevertheless, these discrepancies between the actual and estimated values are acceptable given the variation range of these components, as well as the potential inaccuracies in the analytical procedures employed to obtain the actual values of these variables. The validity of this assertion is supported by the results presented in Fig. 5.14 and Fig. 5.15. These figures demonstrate that the estimated values fall within the uncertainty limits that have been established in the measurement of these variables.

The MHE approach assessed in this study effectively estimated the concentrations of particulate and soluble components in the WWTP, even when a limited number of samples are available. These results suggest that further enhancement of the application of control and optimization strategies in wastewater treatment plants is possible.

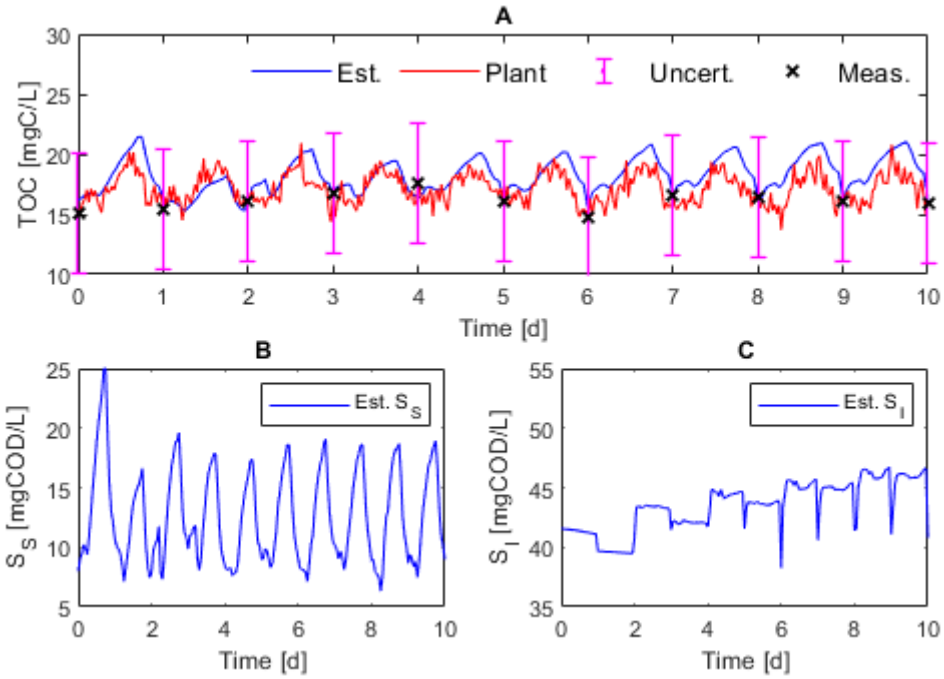

Fig. 5.14. Measured and estimated values of the TOC (A). Estimated values of the readily biodegradable soluble organic matter (B) and inert soluble organic matter (C).

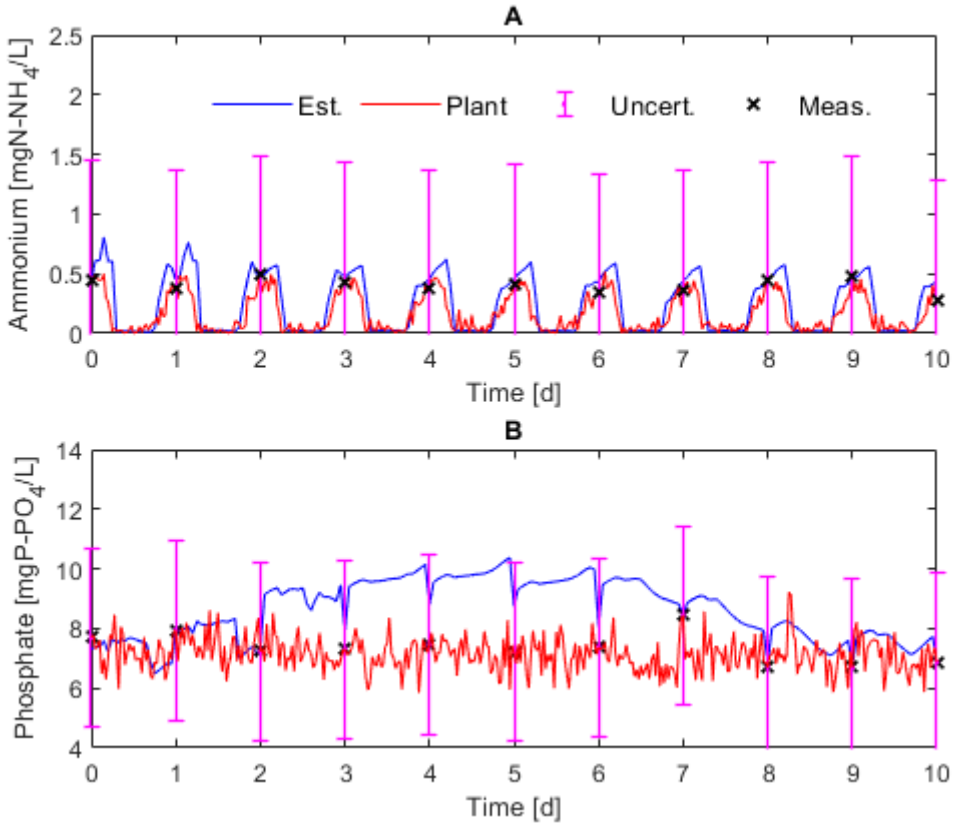

Fig. 5.15. Measured and estimated values of the dissolved ammonium concentration (A) and dissolved phosphate concentration (B).

Despite the existence of analytical measurements on a daily basis, the employment of a state estimator offers insights into the progression of wastewater components throughout the entirety of the experimental period, a situation that has been previously observed in simulation results. State estimators serve as instrumental tools for the analysis of water quality over the course of a day. Leveraging this analysis, control actions can be implemented in a targeted and informed manner. As illustrated in Fig. 5.15, which depicts the time course of dissolved ammonium concentration, there is a demonstrable variation in the dynamics of dissolved ammonium over the course of a day. Specifically, higher values of ammonium are observed during nocturnal hours, which can be attributed to the assimilation of dissolved ammonium by microalgae during daylight hours. Given that the samples were hypothesized to be drawn during the night, these values are representative of a particular moment in the process dynamics evolution, which underscores the importance of continuous state estimation.

Parameter estimation is paramount for characterizing the kinetics of the key processes and chemical reactions, as well as the operational conditions in the HRAP. The results of parameter estimation for the parameters described by Eq. (5.15) are provided in Fig. 5.16. Fig. 5.16 shows that the estimated parameters exhibited a high degree of proximity to the "real values" of the parameters assumed in the plant. As demonstrated in Fig. 5.11 - Fig. 5.15, the simulation results substantiate the validity of the selected parameter values for predicting the process's state evolution. In order to ensure the effective implementation of model-based control strategies within the WWTP, it is imperative to establish precise parameter estimations.

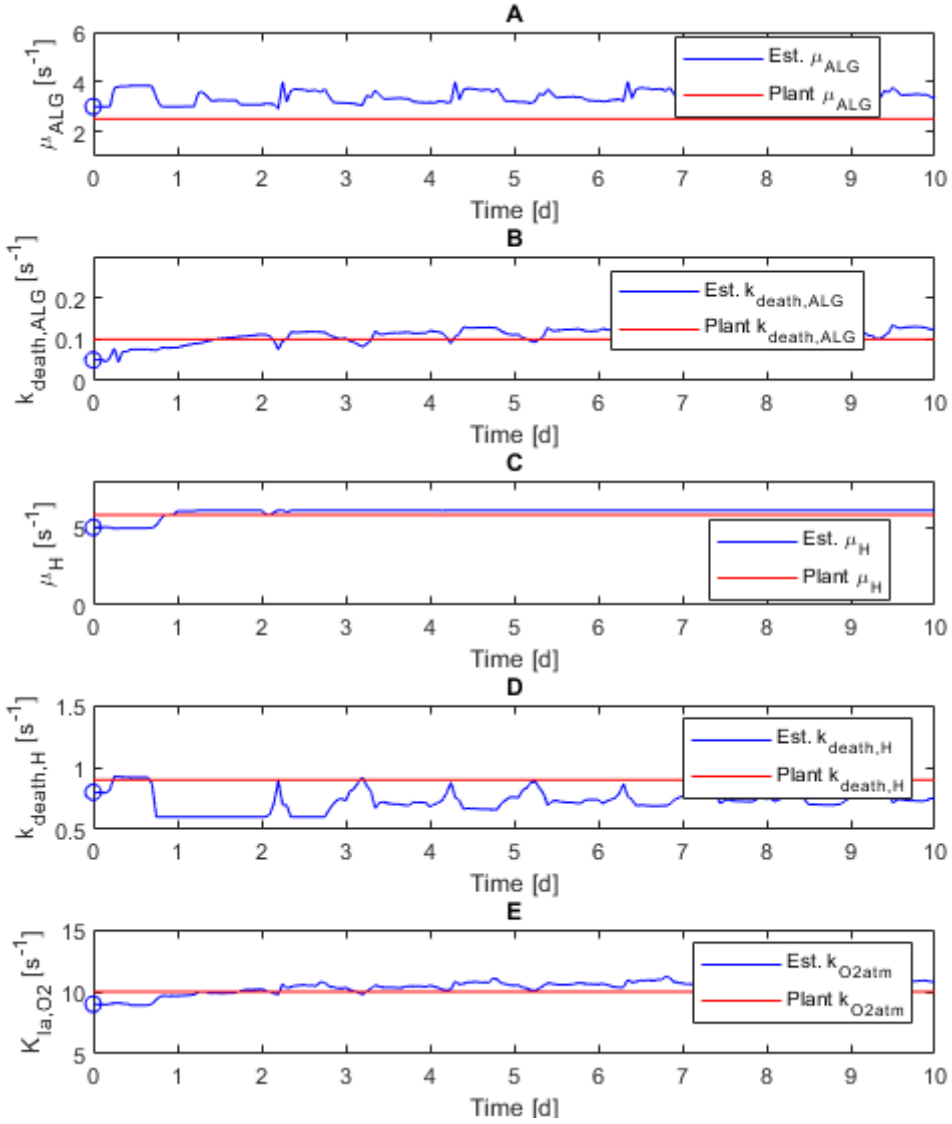

Fig. 5.16. Measured and estimated values of the parameters in the HRAP. The circles represent the initial guess for parameter values that were utilized in the optimization problem.

In order to evaluate the robustness of the estimator under different operational conditions, variations in the incident light were considered during the final three days of the estimation process. As illustrated in Fig. 5.17, the radiation profile under consideration comprises seven days with uniform radiation conditions, analogous to those previously illustrated in Fig. 5.4D, and three days characterized by substantial cloud cover. The estimation results for this condition are illustrated in Fig. 5.18 to Fig. 5.20. The dissolved oxygen concentration in the HRAP under fluctuating solar radiation is depicted in Fig. 5.18, where it is demonstrated that the available solar radiation during the last three days of operation affects the maximum values of dissolved oxygen concentration in the photobioreactor, owing to a decline in microalgae activity. The reliability of the estimator in reproducing the trend in the dissolved oxygen concentration is indicative of its effectiveness in a variety of environmental conditions and in the presence of noisy measurements. This reliability is indicative of the robustness of the estimator.

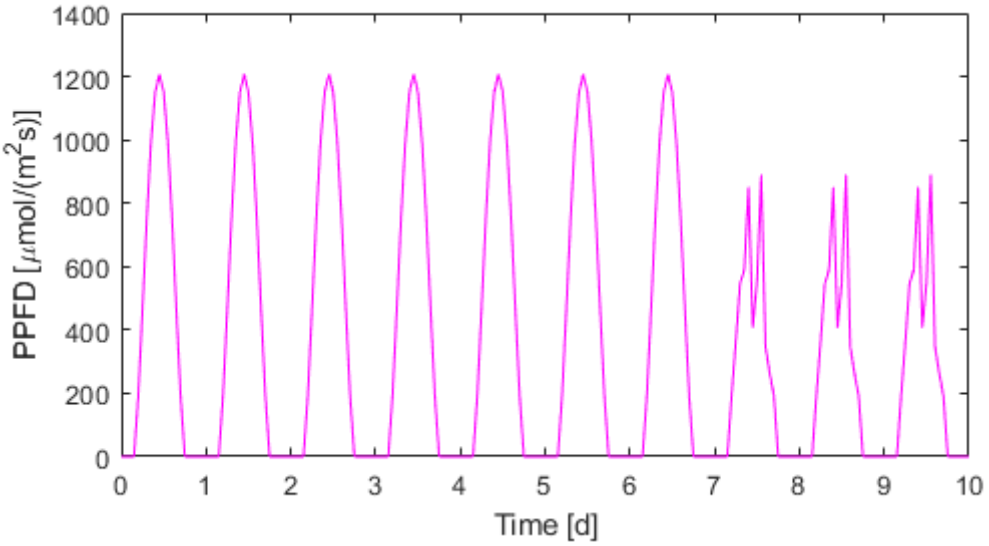

Fig. 5.17. Profile of the photosynthetic photon flux density considered over the course of ten days of operation.

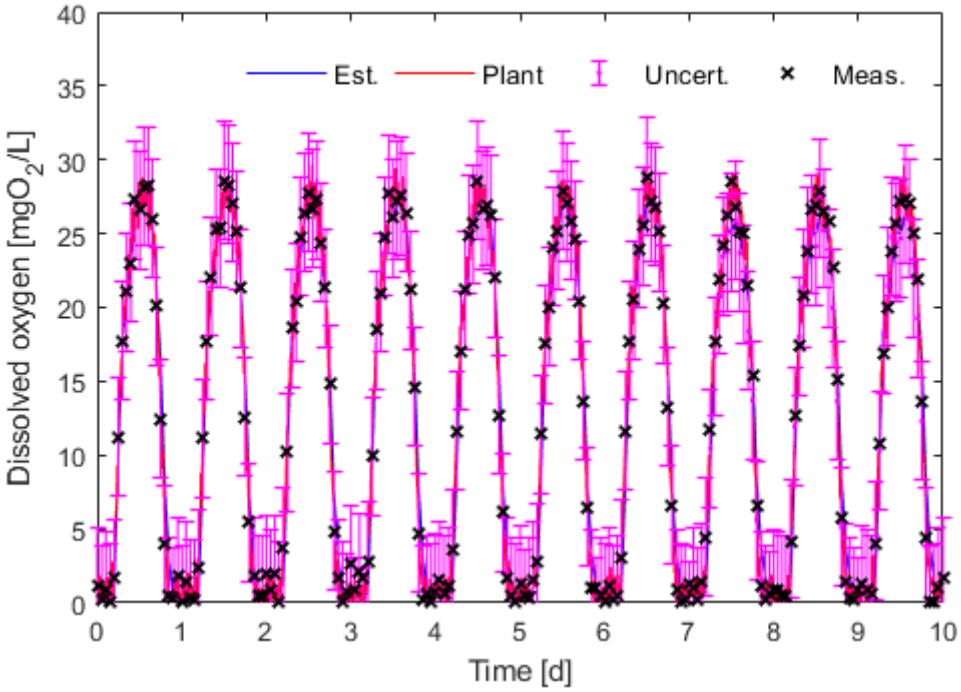

Fig. 5.18. Measured and estimated values of the dissolved oxygen in the HRAP under fluctuating solar radiation.

Fig. 5.19 illustrates the measured and estimated values of biomass concentration under fluctuating solar radiation and also demonstrates the robust behavior of the estimator, effectively replicating the measured values of biomass concentration in the HRAP (Fig. 5.19A), the effluent flow (Fig. 5.19B), and the wastage flow (Fig. 5.19C).

The performance of the estimator in predicting the concentration of dissolved components in the HRAP under fluctuating solar radiation is illustrated in Fig. 5.20. Predicted values of the dissolved total organic carbon concentration (Fig. 5.20A), ammonium concentration (Fig. 5.20B), and phosphate concentration (Fig. 5.20C) demonstrate slight overestimation, as previously evidenced in simulation results. Nevertheless, the discrepancies observed in these estimations fall within the permissible uncertainty range (as indicated by the error bars), even in the presence of significant environmental variations and unreliable measurements.

The simulation results demonstrate the efficacy of the MHE approach in online estimation of the most relevant variables of a wastewater treatment process, even in the presence of noisy measurements, model inaccuracies, varying environmental conditions, and multi-

rate measurements. The MHE has the capacity to provide online estimation for measured variables and for variables that cannot be measured directly. The findings, in conjunction with the reduced estimation times observed, underscore the promise of state estimation leveraging the MHE technique in conjunction with control and optimization strategies within wastewater treatment facilities, particularly in the context of low dynamics that characterize wastewater treatment processes.

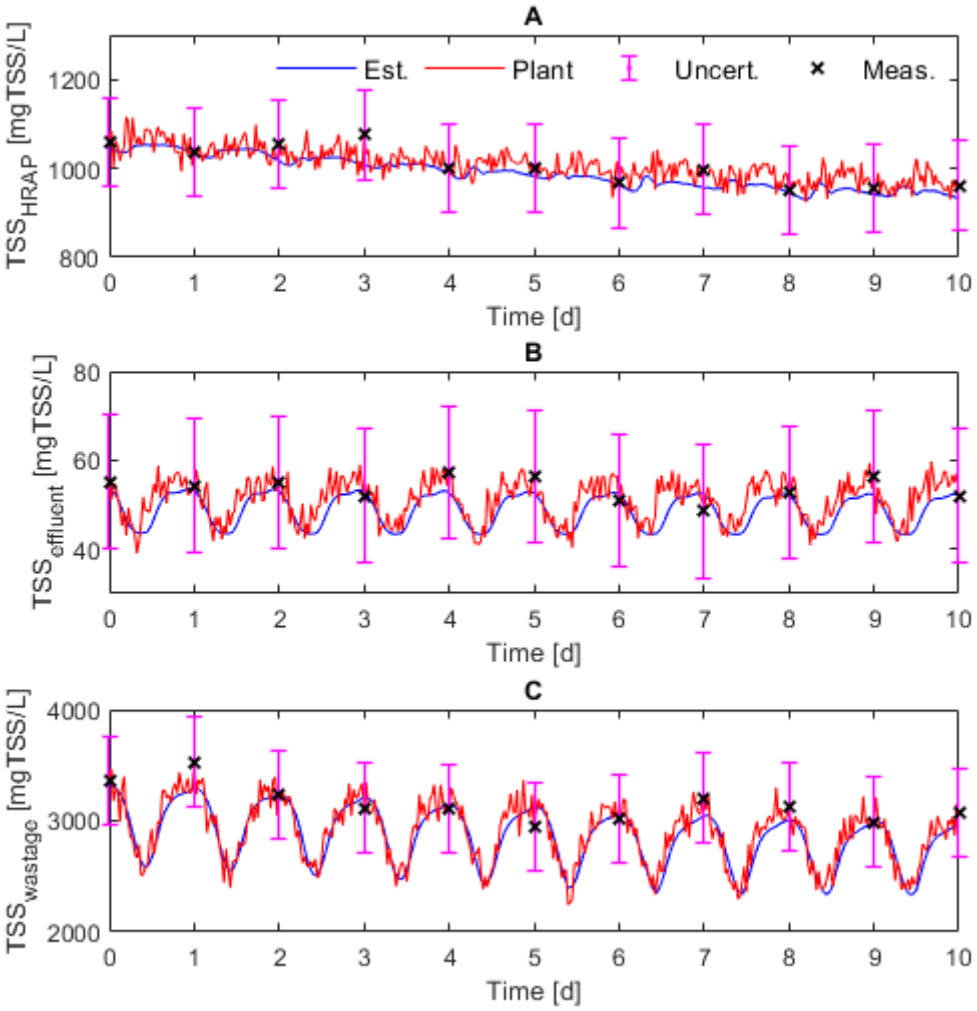

Fig. 5.19. Measured and estimated values of the biomass concentration in the HRAP (A), in the effluent (B), and in the wastage stream (C) under fluctuating solar radiation.

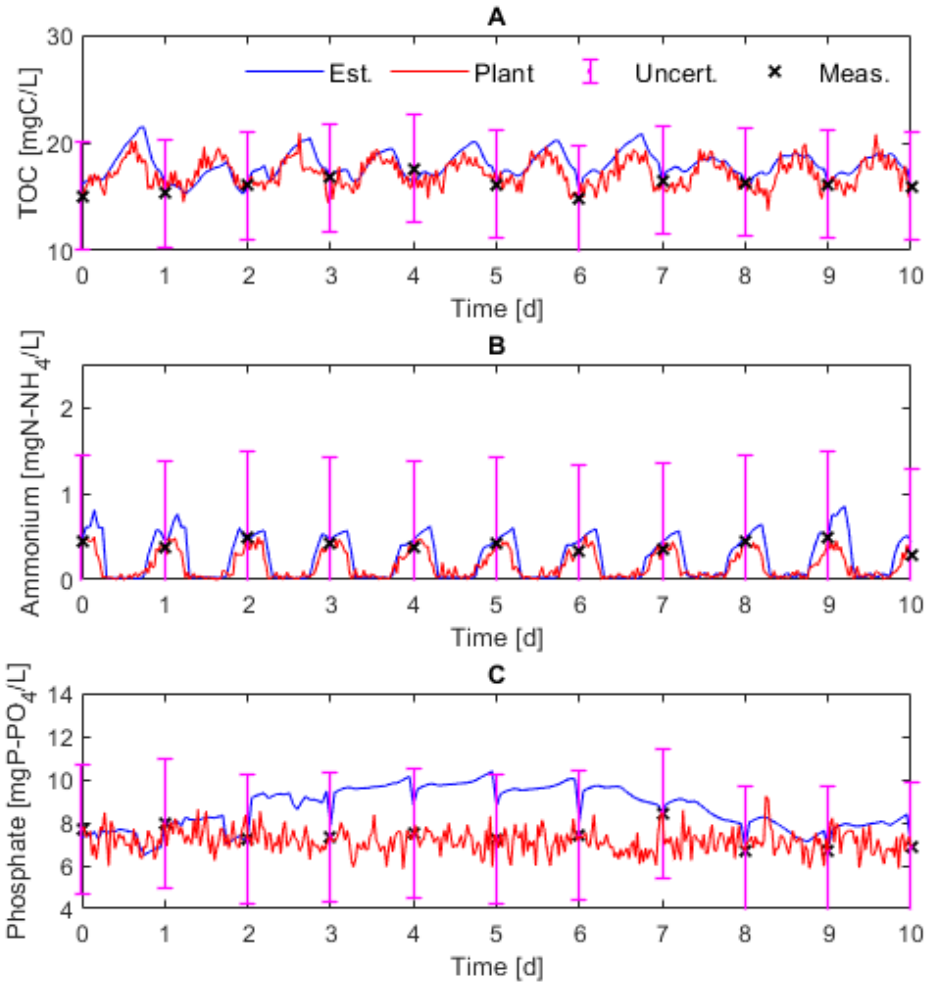

Fig. 5.20. Measured and estimated values of the dissolved TOC concentration (A), dissolved ammonium concentration (B), and dissolved phosphate concentration (C) under fluctuating solar radiation.

5.7. Conclusions

This chapter proposes the utilization of the MHE technique for a microalgae-based wastewater treatment process, with a focus on the estimation of multiple states and parameters concurrently to evaluate the effluent water quality. The utilization of an estimation model characterized by multiple states and parameters, exhibiting a substantial structural mismatch with respect to the plant model, was contemplated. Multi-rate measurements obtained from online measurements and analytical procedures were used to enhance the performance of the estimator. The simulation results confirmed the efficacy and robustness of MHE in the online estimation of the most pertinent variables

in the microalgae-based wastewater treatment process. Furthermore, the simulation results demonstrated MHE's potential for future application in the development of control and optimization strategies, which requires the knowledge of system states and parameters.

6. Economic MPC in microalgae-bacteria wastewater treatment

This Chapter expounds the development of an economic MPC for an industrial microalgae-bacteria based wastewater treatment plant with biomass harvesting. The eMPC has been developed with the objective of controlling the plant and optimizing biomass yield to ensure maximum profit from biomass sales as a bioestimulant. The predictive controller utilizes the estimated variables provided by the MHE algorithm in the model to predict the future evolution of the system and to calculate the future control actions. The sequence of future control actions is calculated using an optimization procedure that aims to minimize a cost function, while respecting the operational constraints.

6.1. Economic Model Predictive Control

The optimal operation and control of dynamic systems and processes has been a subject of significant research for many years. One methodology for enhancing process performance while achieving operational targets and constraints is the online implementation of optimal control problem (OCP) solutions. In essence, the control actions for the manipulated inputs of a process are determined by formulating and solving a dynamic optimization problem online. This problem takes advantage of a dynamic process model while accounting for process constraints. The online resolution of complex dynamic optimization problems is becoming an increasingly viable option as a control scheme to improve the steady-state and dynamic performance of process operations.

The process performance of a chemical or biological process typically refers to the process economics and encapsulates multiple objectives, including profitability, efficiency, variability, capacity, sustainability, and so forth. Conventionally, a hierarchical strategy for planning, scheduling, optimization, and control has been employed in the process industries. A block diagram illustrating the hierarchical strategy is presented in Fig. 6.1. While the block diagram offers a comprehensive overview of the primary components, it must be noted that it presents a simplified representation of the modern planning/scheduling, optimization, and control systems that are employed in the process industry. It is important to acknowledge that each layer of the block diagram may be comprised of numerous distributed and hierarchical computing units (Ellis, Durand and Christofides, 2014; Ellis, Liu and Christofides, 2021).

The upper layer, designated as real-time optimization (RTO), is responsible for process optimization. Within the RTO layer, a metric quantifying the operating profit or operating cost is optimized with respect to an up-to-date and rigorous steady-state process model to ascertain the optimal process steady-state. The resultant computed steady state is then transmitted to the feedback process control systems, which consist of the supervisory control and regulatory control layers. The process control system utilizes manipulated inputs to regulate the process, thereby ensuring its operation at a steady state. The process control system must function in order to reject disturbances and, ideally, guide the trajectory of the process dynamics along an optimal path to the steady-state.

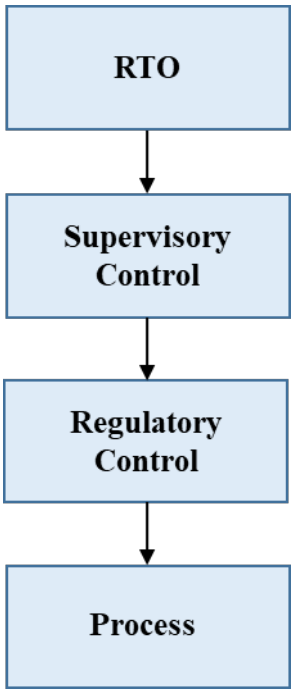

Fig. 6.1. Traditional paradigm in process industries for process optimization and control (Ellis, Durand and Christofides, 2014)

The advanced or supervisory process control layer of Fig. 6.1 comprises control algorithms that are utilized to account for process constraints, coupling of process variables and processing units, and operating performance. In advanced process control, model predictive control employs a dynamic model of the process in an optimization problem to predict the future evolution of the process over a finite-time horizon and to determine the optimal input trajectory with respect to a performance index (Camacho and Bordons, 2007). The performance index is typically the sum of squared errors between output predictions and its desired set points. Furthermore, MPC possesses the capacity to address process constraints and multi-variable interactions that are inherent to the optimization problem. Consequently, it possesses the capacity to regulate constrained multiple-input multiple-output systems in an optimal manner.

The regulatory control layer is composed of predominantly single-input, single-output control loops, such as PID control loops, which function to implement the control actions computed by the supervisory control layer. In essence, this layer ensures that the control actuators achieve the control action requested by the MPC layer.

Notice that RTO does not consider dynamics aspects in its formulation and it is executed typically every several hours when process reaches steady state, which limits its efficiency. In an effort to integrate economic process optimization and process control, as well as to realize the possible process performance improvement achieved by consistently dynamic, transient, or time-varying operation, economic MPC has been proposed. This approach, instead of minimizing the errors between output predictions and set points, incorporates a general cost function or economic performance index in its formulation. This cost function may be a direct or indirect reflection of the process economics and its optimization is computed at high frequency, every sampling time of the controller.

Broadly, economic model predictive control can be characterized by the following optimization problem (Ellis, Durand and Christofides, 2014):

$$\min_{u\in S(\Delta)} \int_{t_k}^{t_{pred}} \ell_e\big(\tilde{x}(t), u(t)\big)\mathrm{dt} \tag{6.1}$$

$$s.t. \qquad \dot{\tilde{x}}(t) = f(\tilde{x}(t), u(t), 0) \tag{6.2}$$

$$\tilde{x}(0) = x(t_k) \tag{6.3}$$

$$g\big(\tilde{x}(t), u(t)\big) \leq 0, \quad \forall t \in [0, t_{pred}] \tag{6.4}$$

where the decision variables of the optimization problem are the trajectories of the manipulated variables of the process ($u \in S(\Delta)$) over the prediction horizon, i.e., the time interval $[t_k, t_{pred})$, and $\tilde{x}$ denotes the predicted state trajectory over the prediction horizon. The objective function ℓ_e of Eq. (6.1) is the process economic cost function that the eMPC optimizes through dynamic operation of the process. $\ell_e(\tilde{x}, u)$ is a direct or indirect reflection of the (instantaneous) process economics. A dynamic model, typically the nominal process model, is used as a constraint (6.2) and is initialized through a state measurement obtained at every sampling instant (6.3). In addition to the model constraints of Equations (6.2) - (6.4), process operation or economics-based constraints are often added.

6.2. Economic MPC formulation for a microalgae-bacteria based WWTP

The present study considers a hypothetical microalgae-bacteria-based WWTP with the configuration illustrated in Fig. 5.3, operating under the conditions described in Section Fig. 5.2. In the preceding chapter, it was hypothesized that measurements obtained by analytical procedures are available on a daily basis, while online measurements are available at considerably higher sampling rates. In order to design a pertinent online eMPC strategy, it is imperative to combine model predictive control and state estimation using MHE. In each sample time, the MHE provides estimated values of the states, parameters and model uncertainties. These are used by the MPC model to calculate the sequence of future control actions. The aforementioned procedure is summarized in Fig. 6.2.

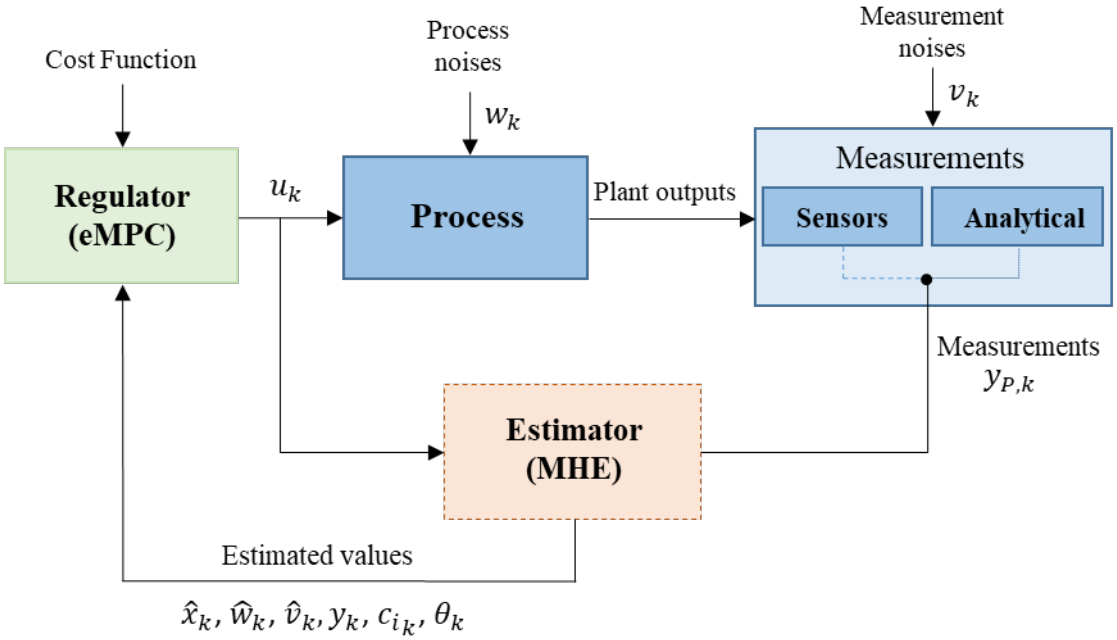

Fig. 6.2. Scheme combining state estimation and model predictive control

The eMPC searches for the control moves $\Delta \boldsymbol{u}_{k+i}$ $(i = 0,1,2,\ldots,n_u - 1)$ that minimize the cost function (6.5) subject to constraints (6.6) to (6.11) and the computations are repeating every sampling time, following a moving horizon policy. The process is represented by a continuous dynamic model (6.6) and (6.7), which is assumed to be continuously differentiable. In the formulation, $\mathbf{x} \in \mathbb{R}^{n_x}$ is used to represent the states, $\mathbf{u} \in \mathbb{R}^{n_u}$ is used to represent the control actions, and $\mathbf{y} \in \mathbb{R}^{n_y}$ is used to represent

measured outputs. The estimation of the actual states ($\hat{\mathbf{x}} \in \mathbb{R}^{n_x}$), disturbances ($\boldsymbol{v} \in \mathbb{R}^{n_y}$ and $\boldsymbol{w} \in \mathbb{R}^{n_x}$), and parameters ($\boldsymbol{\theta} \in \mathbb{R}^{n_p}$) is achieved by the MHE (Section 5.1). As the model is formulated in continuous time, $\boldsymbol{u}$, and $\boldsymbol{y}$ are functions of t. However, for the sake of simplicity, this dependence has been omitted in the present document. Utilizing a control vector parameterization approach, the control actions are permitted to change solely at regular time intervals $\Delta t = t_k - t_{k-1}$. For the purposes of this study, k denotes the current sampling time. The control actions $\mathbf{u_k} \in \mathbb{R}^{n_u}$, computed and applied at time t_k, are kept constant within each time interval $[t_k, t_{k+1})$, as in Eq. (6.10). The current and future control moves, denoted as $\Delta \boldsymbol{u}_{k+i}, i = 0, 1, 2, \dots, n_u - 1$, defined in (6.11), are the decision variables of problem (6.5) - (6.12). The selection of the control horizon n_u and other tuning parameters is governed by the usual rules of MPC.

The model allows to compute predictions of the cost function and constraints over a future horizon from t_k to the final prediction horizon t_{pred}. n_{pred} refers to the number of time instants from t_k to reach t_{pred}.

The control moves are computed every sampling time from the current time t_k to a control horizon t_{k+n_u}, after which, $\Delta \boldsymbol{u}_{k+i} = 0$, but only the first control move $\Delta \boldsymbol{u}_k$ is applied to the process.

$$\min_{\substack{\Delta u_{k+1} \\ i=0,\dots,n_u-1}} \int_{t=0}^{t=t_{pred}} \ell_e\big(\boldsymbol{x}(t), \boldsymbol{u}(t)\big) + \sum_{i=0}^{n_u-1} \Delta \boldsymbol{u}_{k+i}^T \boldsymbol{Q}_u \Delta \boldsymbol{u}_{k+i} \tag{6.5}$$

$$s.t. \qquad f(\dot{\boldsymbol{x}}, \boldsymbol{x}, \boldsymbol{u}, \boldsymbol{w}_k, \boldsymbol{v}_k, \boldsymbol{\theta}_k) = \mathbf{0}, \qquad \forall t \in \left[t_k, t_{pred}\right] \tag{6.6}$$

$$h(\boldsymbol{x}, \boldsymbol{u}, \boldsymbol{y}, \boldsymbol{w}_k, \boldsymbol{v}_k, \boldsymbol{\theta}_k) = \mathbf{0}, \qquad \forall t \in \left[t_k, t_{pred}\right] \tag{6.7}$$

$$\boldsymbol{u}^L \leq \boldsymbol{u}_{k+i} \leq \boldsymbol{u}^U, \qquad i = 0, 1, \dots, n_{pred} - 1 \tag{6.8}$$

$$\boldsymbol{u}_{k+i} = \boldsymbol{u}_{k+i-1} + \Delta \boldsymbol{u}_{k+i}, \qquad i = 0, 1, \dots, n_{pred} - 1 \tag{6.9}$$

$$\boldsymbol{u}(t) = \boldsymbol{u}_{k+i}, \quad t \in [t_{k+i}, t_{k+i+1}] \qquad i = 0, 1, \dots, n_{pred} - 1 \tag{6.10}$$

$$\Delta \boldsymbol{u}_{k+i} = 0, \qquad i = n_u, \dots, n_{pred} - 1 \tag{6.11}$$

$$\boldsymbol{x}(t_k) = \hat{\boldsymbol{x}}_k \tag{6.12}$$

The cost function (6.5) comprises two terms:

1. The first term $\int_{t=0}^{t=t_{pred}} \ell_e\big(\boldsymbol{x}(t), \boldsymbol{u}(t)\big)$, corresponds to an economic objective computed with the value of the model variables and control actions. It is hypothesized that the value of ℓ_e at any given time instant k can be calculated from process measurements and control actions.
2. The second term $\sum_{i=0}^{n_u-1} \Delta \boldsymbol{u}_{k+i}^T \boldsymbol{Q}_u \Delta \boldsymbol{u}_{k+i}$ penalizes changes in the manipulated variables. $\boldsymbol{Q}_u$ is a positive definite matrix, with weighting factors on the control moves ($\Delta \boldsymbol{u}$), which can be regarded as tuning factors for the purposes of normalization and stabilization, as in the current practice of MPC.

The cost function is constrained by the model (6.6) - (6.7), and the inequality constraints (6.8). To solve (6.5) - (6.12), at each sampling time k, it is necessary to initialize the model states $\boldsymbol{x}(t_k)$, disturbances, and parameters to the values of $\widehat{\boldsymbol{x}}_k$, $\boldsymbol{w}_k$, $\boldsymbol{v}_k$, and $\boldsymbol{\theta}_k$, respectively. The following section presents the algorithm for solving the eMPC problem with estimations provided by the MHE.

eMPC algorithm using MHE and multi-rate measurements

i. Initialization

1. Collect n_e previous data of variables $\boldsymbol{u}_{k-i}$, $\boldsymbol{y}_{P,k-i}$, where i $= 1, \dots, n_e$.

MHE algorithm: given $\boldsymbol{Q}_x, \boldsymbol{Q}_y$ and $\boldsymbol{Q}_w$

2. Initialize $\widehat{\boldsymbol{x}}_{k-n_e}$
   a. For measured states, consider $\widehat{\boldsymbol{x}}_{k-n_e}^M = \boldsymbol{y}_{P,k-n_e}^S$, being $\widehat{\boldsymbol{x}}_{k-n_e}^M$ the subset of states that are measured, and $\boldsymbol{y}_{P,k-n_e}^S$ the subset of $\boldsymbol{y}_{P,k-n_e}$ containing the measured states in $k - n_e$.
   b. For unmeasured states, use the values predicted by the model with $\boldsymbol{v}_{k-i} = 0, \boldsymbol{w}_{k-i} = 0$, and $\boldsymbol{\theta} = \boldsymbol{\theta}_0$, i $= 1, \dots, n_e$. Being $\boldsymbol{\theta}_0$ the initial guess for parameters.
3. Solve the MHE problem (5.1) - (5.7) to find the past values of the states $\boldsymbol{x}_{k-n_e}^*$, disturbances $\boldsymbol{v}_{k-i}^*, \boldsymbol{w}_{k-i}^*$, inlet concentration values $\boldsymbol{c_i}_{k-i}^*$, and parameters $\boldsymbol{\theta}_{k-i}^*$, i $= 1, \dots, n_e$.

4. Evaluate the estimated state $\widehat{\boldsymbol{x}}_k$ from t_{k-n_e} to t_k. Estimate the values of the disturbances and parameters using $\boldsymbol{v}_k = v^*_{k-i}$, $\boldsymbol{w}_k = w^*_{k-i}$, $\boldsymbol{c_{i}}_k = \boldsymbol{c_{i}}^*_{k-i}$, and $\boldsymbol{\theta}_k = \boldsymbol{\theta}^*_{k-i}$.
5. Update $\widehat{\boldsymbol{x}}_{k-n_e} = \boldsymbol{x}^*_{k-n_e}$.

<u>eMPC controller:</u>

6. Go to step 11.

ii. For next iterations

<u>MHE algorithm:</u>

7. Collect n_e previous data of variables $\boldsymbol{u}_{k-i}$, $\boldsymbol{y}_{P,k-i}$, where i $= 1, \dots, n_e$.
8. Solve the MHE problem (5.1) - (5.7) to find the past values of the states $\boldsymbol{x}^*_{k-n_e}$, disturbances $\boldsymbol{v}^*_{k-i}$, $\boldsymbol{w}^*_{k-i}$, and parameters $\boldsymbol{\theta}^*_{k-i}$, i $= 1, \dots, n_e$.
9. Evaluate the estimated state $\widehat{\boldsymbol{x}}_k$ from t_{k-n_e} to t_k. Estimate the values of the disturbances and parameters using $\boldsymbol{v}_k = \boldsymbol{v}^*_{k-i}$, $\boldsymbol{w}_k = \boldsymbol{w}^*_{k-i}$, and $\boldsymbol{\theta}_k = \boldsymbol{\theta}^*_{k-i}$.
10. Update $\widehat{\boldsymbol{x}}_{k-n_e} = \boldsymbol{x}^*_{k-n_e}$.

<u>eMPC controller:</u>

11. Solve problem (6.5) - (6.12) using $\widehat{\boldsymbol{x}}_k$, $\boldsymbol{v}_k$, $\boldsymbol{w}_k$, and $\boldsymbol{\theta}_k$ from MHE.
12. Apply $\Delta\boldsymbol{u}_k$ to the process.
13. Wait for the next sampling time and update $k = k + 1$.
14. Go to step 7.

6.2.1. Case study

The present study hypothesizes that the WWTP depicted in Fig. 5.3 treats wastewater from agricultural activities. Consequently, the harvested biomass could be utilized as a bioestimulant, representing a valuable product. In this facility, the wastage flow rate ($Q_{wast.}$) is regarded as the manipulated variable for this purpose. The same operating conditions, inlet flows, measured variables, and measurement noise of the plant described in Section 5.3 were considered. In a similar fashion, the reduced model contemplated in Section 5.4 was employed as a prediction model in the present case study.

The eMPC is intended to maximize the profit resulting from bioestimulant sales. Subsequently, the cost function is defined by Equation (6.13), in which p_B is the price of the biomass. The terms n_p and n_u refer to the prediction horizon and the control horizon, respectively. The change in the control action ($\Delta Q_{wast.}$), as well as a weight that penalizes the control effort (MS), are also included in the cost function. The cost function is subject to the model described in Table 5.4 and the constraints defined in Eq. (6.14) - (6.18). The aforementioned constraints are associated with the biomass concentration in the various streams of the process.

$$\min_{\substack{Q_{wast.} \\ i \to 1 \dots n_u}} \left(-p_B \int_{t=0}^{t=t_{n_p}} Q_{wast.} \cdot TSS_{wastage} \mathrm{dt} + \sum_{j=1}^{n_u - 1} MS \cdot \Delta Q_{wast.\,j} \right) \quad (6.13)$$

$$s.t. \qquad 0.8 \frac{kg}{m^3} \leq TSS_{HRAP} \leq 1.2\ kg/m^3 \quad (6.14)$$

$$TSS_{effluent} \leq 0.06\ kg/m^3 \quad (6.15)$$

$$TSS_{wastage} \geq 2\ kg/m^3 \quad (6.16)$$

$$0.5\ m^3/d\ \leq Q_{wast.} \leq 60\ m^3/d \quad (6.17)$$

$$0\ m^3/d\ \leq \Delta Q_{wast.} \leq 4\ m^3/d \quad (6.18)$$

The constraint (6.14) corresponding to the biomass concentration in the HRAP, it is intended to ensure sufficient microalgae biomass within the HRAP to facilitate effective wastewater treatment without affecting the light penetration into the HRAP. The objective of constraining the TSS concentration in the effluent (6.15) is to adhere to the limitations imposed by legislation concerning the permissible TSS concentration in the effluent flow. The biomass concentration in the wastage flow is also constrained (6.16) to achieve the concentration values necessary for the biomass to be sold as a bioestimulant. Additionally, constraints on the control action (6.17) and in the control effort are also considered (6.18). It is hypothesized that the biomass price is $p_B = 1€/kg$. The parameters of the eMPC are summarized in Table 6.1.

As was hypothesized in the preceding chapter, it was posited that the samples of biomass are available on a daily basis. In order to design a pertinent online eMPC strategy, it is

imperative to combine model predictive control and state estimation using MHE in order to estimate the biomass values at a higher frequency. The procedure used was illustrated in Fig. 6.2 and is described in the algorithm of Section 6.2.

The simulation of the WWTP was formulated in continuous-time domain in MATLAB®. The MHE problem and the dynamic optimization problem in the economic controller were formulated using MPCTools. The controller was solved using the sequential quadratic algorithm, which is available in the *fmincon* NLP solver. It is hypothesized that the stabilization of the microbial population occurs at day 50 after the inoculation of the photobioreactors, thus marking the initiation of the optimization process. It is hypothesized that during the initial 50-day period, the system operates at a constant wastage flow rate of $15\ m^3/d$. The calculus of the control action was performed at 1.2-hour intervals (the sampling time for dissolved oxygen measurements). The mean elapsed time for the entire problem (MHE + controller) to be resolved at each sampling time was 38.54 seconds on a PC with the following hardware specifications: an 13th Gen Intel® Core™ i9-13900K processor (3.0 GHz), 128 GB of RAM memory, and a 500 GB hard-disk drive.

Table 6.1. Parameters of the eMPC controller

Parameter	**Description**	**Value**
n_p	Prediction horizon	10 d (200 samples)
n_u	Control horizon	2 d (40 samples)
MS	Weight in the control effort	100

6.3. Simulation results

The simulation results for the eMPC operation during fifteen days under the previously described conditions are provided in Fig. 6.3 through Fig. 6.5. It is important to note that, due to the influence of the solar cycle, the process is never in a steady state but rather follows a cyclical operation, as illustrated in Fig. 6.5. The eMPC slowly pushes the process towards the optimal operating conditions. Fig. 6.3 shows the evolution of the cost function, which indicates that the calculated profit is higher during the day due to microalgae growth.

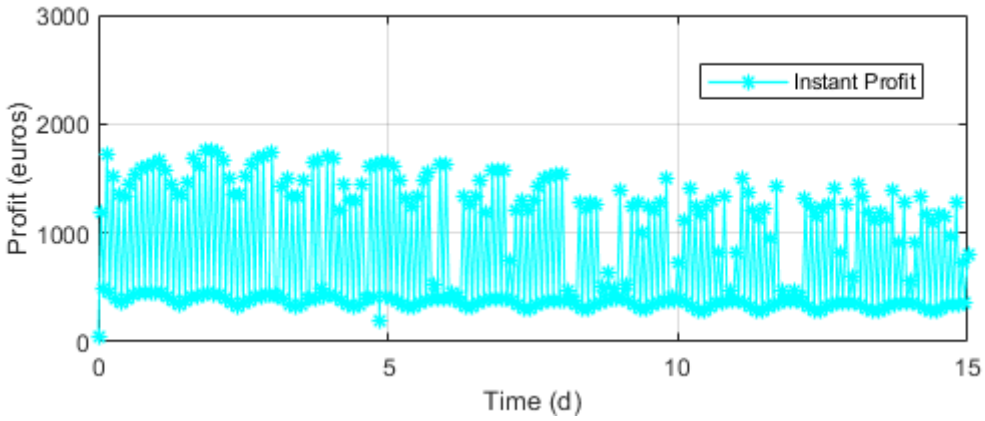

Fig. 6.3. Calculated profit from biomass sold as a bioestimulant (eMPC)

The control actions calculated for the eMPC are illustrated in Fig. 6.4. The biomass evolution in the HRAP, in the effluent flow, and in the wastage flow are represented in Fig. 6.5 (without considering the noise in the measurements). As demonstrated in Fig. 6.4 and Fig. 6.5, the eMPC is able to satisfy the constraints imposed on the manipulated variable and the states, respectively. Transitory violations of constraints illustrated in the biomass concentration in the wastage flow are attributable to discrepancies between the prediction model used and the actual plant values.

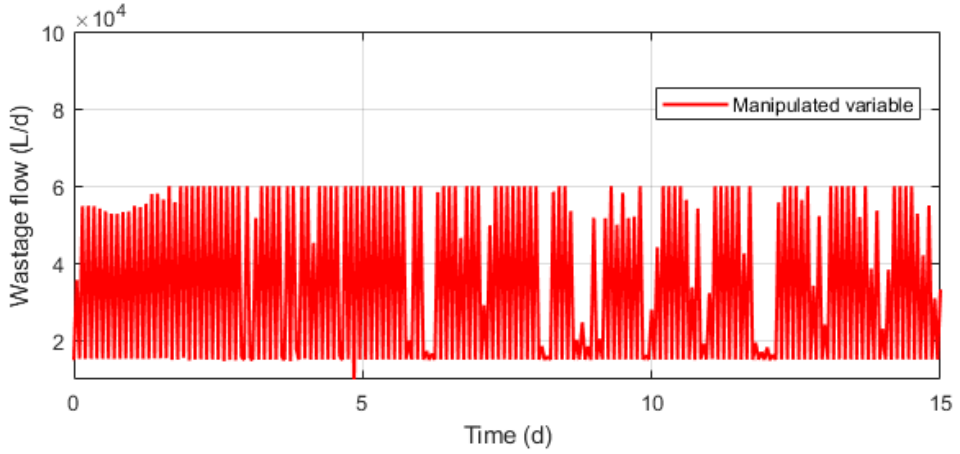

Fig. 6.4. Control actions applied to the WWTP

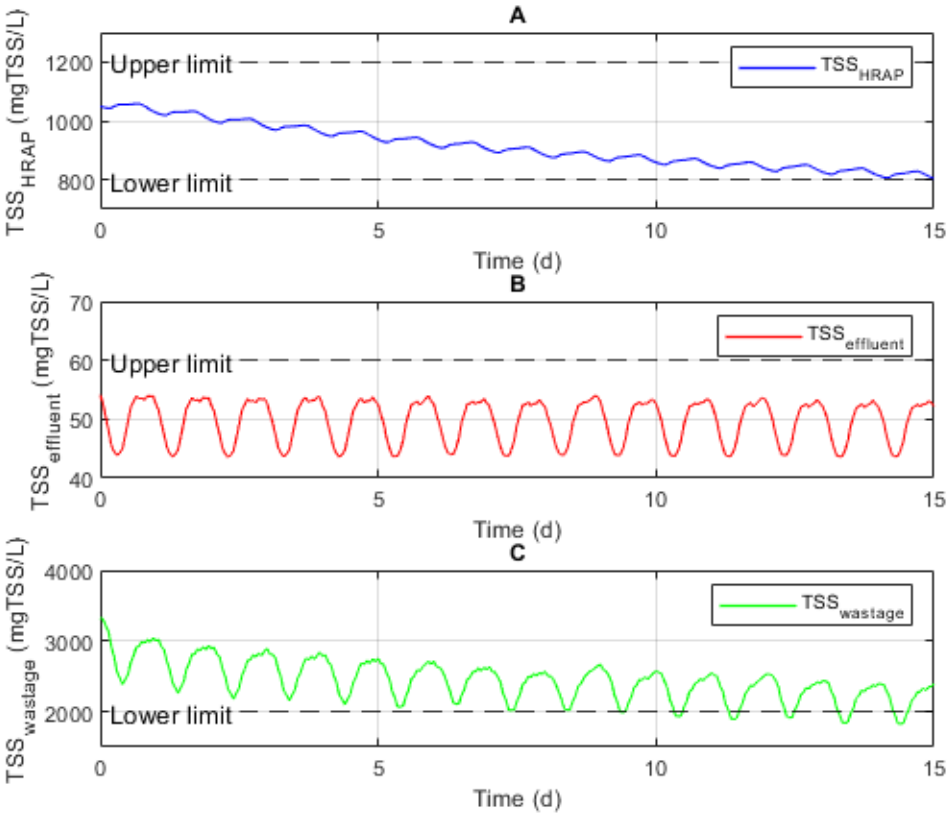

Fig. 6.5. Biomass evolution in the HRAP (A), the effluent flow (B), and in the wastage flow (C)

As illustrated in Fig. 6.6, the estimated, measured, and actual dissolved oxygen concentration values are presented. The estimation performed by the MHE is used to calculate the future values of the plant states. The actual plant values (considering noise in the measurements) of the biomass concentration in the HRAP, the effluent, and in the wastage stream are illustrated in Fig. 6.7. The plant (noisy) values of the dissolved TOC concentration, dissolved ammonium concentration, and dissolved phosphate concentration in the HRAP are represented in Fig. 6.8. The low values of dissolved components in the effluent, as well as the low values of the TSS concentration in the effluent flow, indicate that an adequate wastewater treatment is obtained in a concurrent manner with maximizing the biomass production in the WWTP.

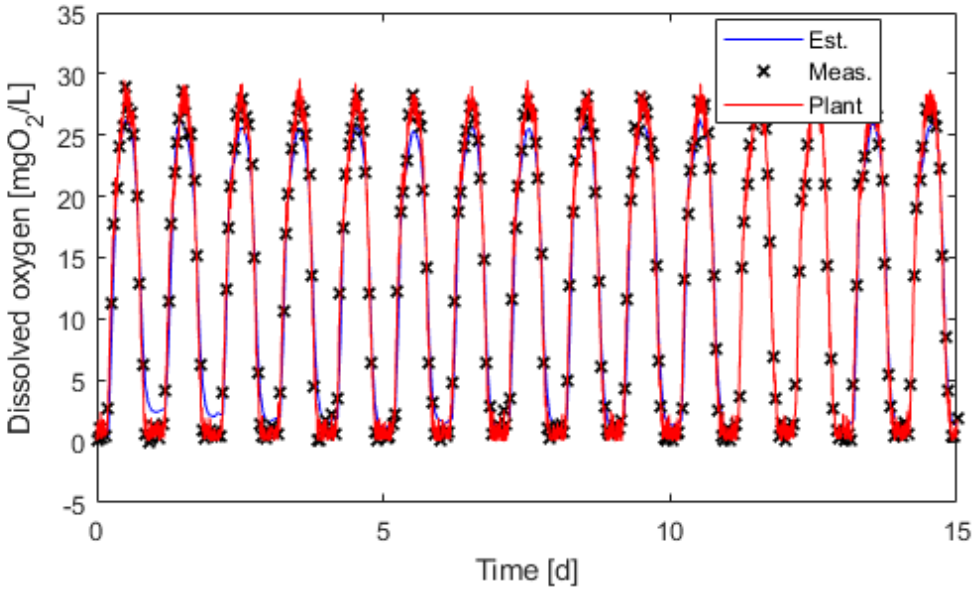

Fig. 6.6. Dissolved oxygen concentration in the HRAP

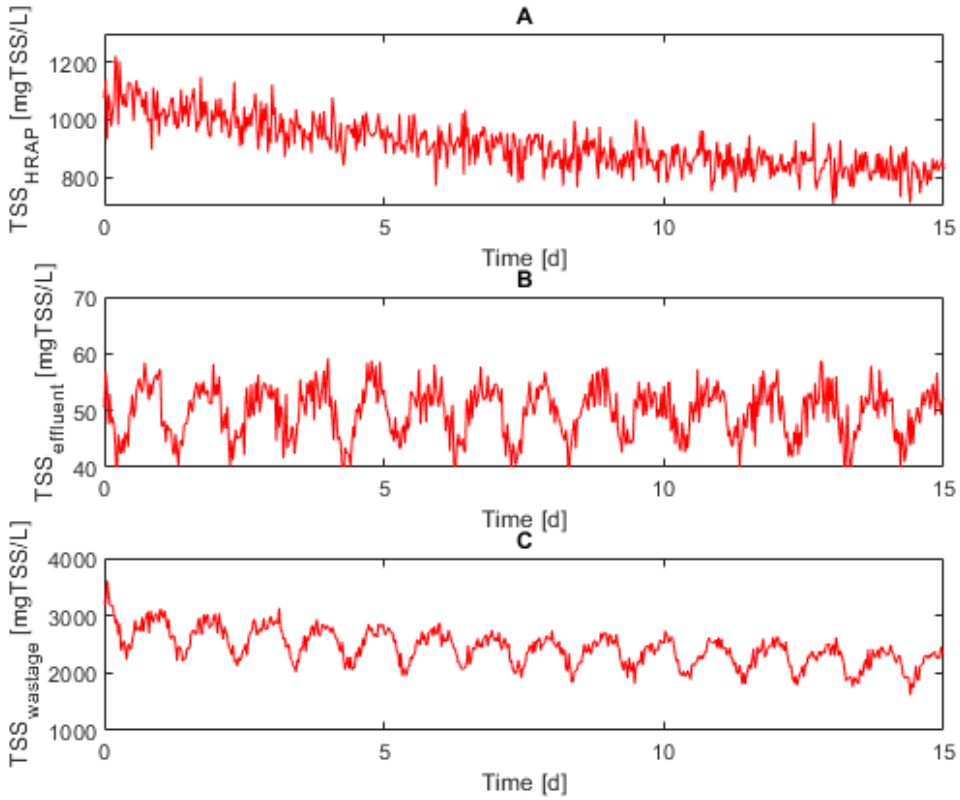

Fig. 6.7. Biomass concentration in the HRAP (A), the effluent flow (B), and the wastage flow (C)

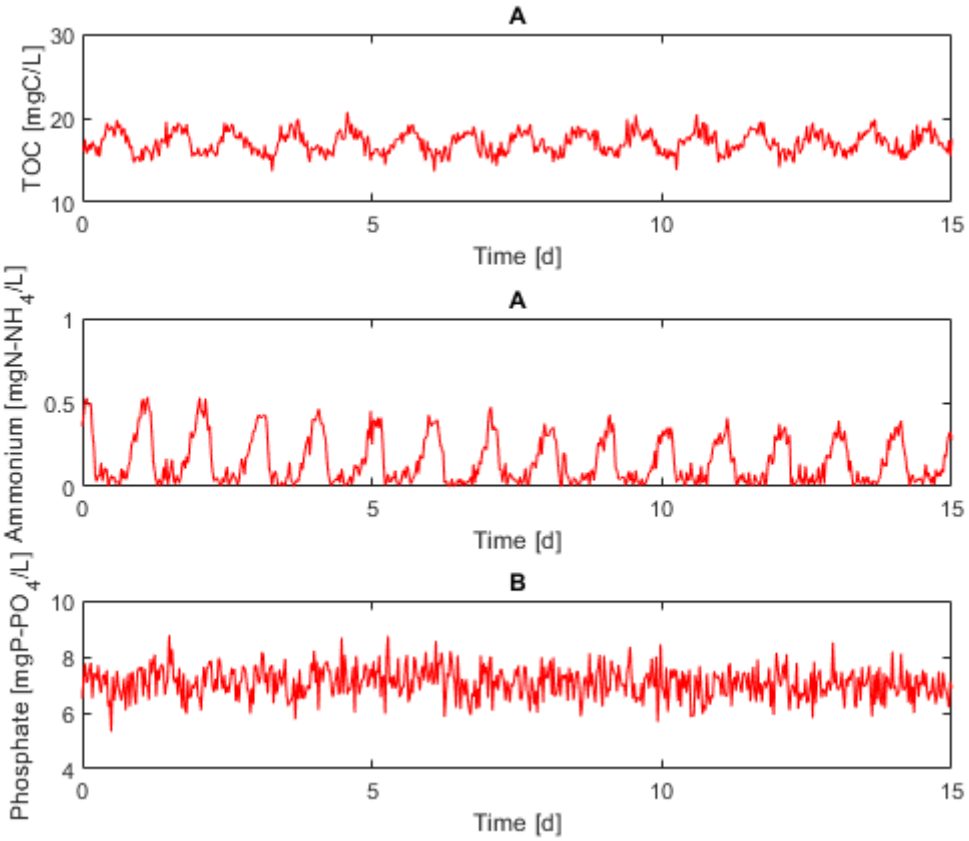

Fig. 6.8. Dissolved TOC concentration (A), dissolved ammonium concentration (B), and dissolved phosphate concentration (C) in the HRAP

In order to facilitate a comparison of the WWTP operation at a constant wastage flow rate of 15 m^3/d, the plant simulation was conducted over the course of 65 days of the system operation. The flow rate value under consideration enables the accomplishment of the constraints specified in (6.14) to (6.16), as illustrated in Fig. 6.9. The profit obtained during the period between days 50 and 65 is illustrated in Fig. 6.10. A comparison of Fig. 6.3 and Fig. 6.10 demonstrates the merits of operating the WWTP according to an eMPC control strategy.

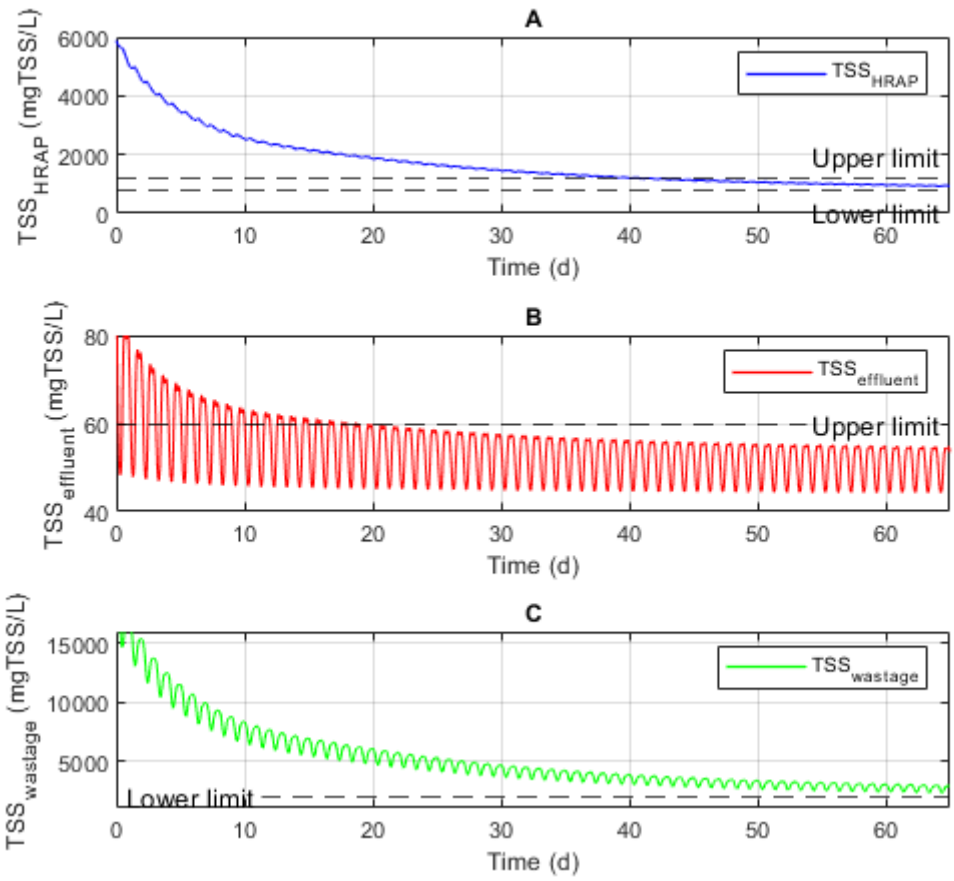

Fig. 6.9. Biomass evolution in the HRAP (A), the effluent flow (B), and in the wastage flow (C) under constant wastage flow rate

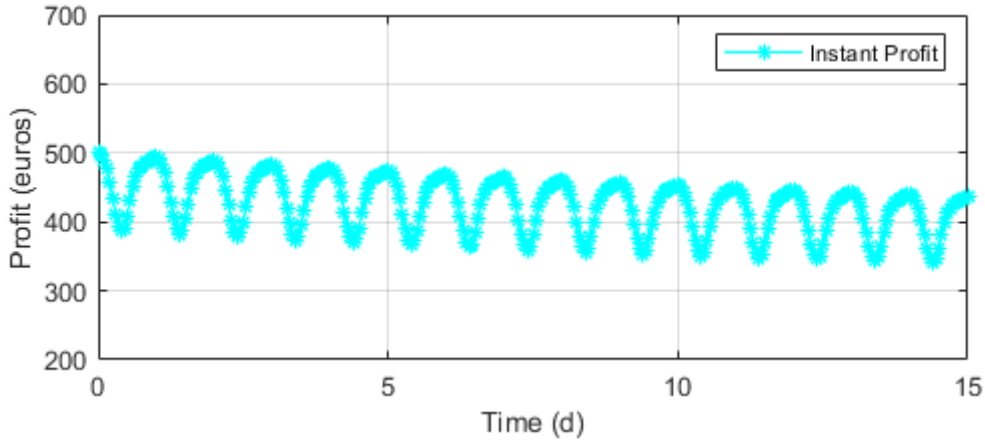

Fig. 6.10. Calculated profit from biomass sold as a bioestimulant (constant wastage flow rate)

6.4. Conclusions

This chapter proposes the utilization of an economic predictive controller for a microalgae-based wastewater treatment plant with biomass harvesting. The hypothetical wastewater treatment plant under consideration includes a sedimentation stage in order to concentrate the microalgae biomass. The eMPC was conceived with the objective of maximizing the financial gain derived from biomass sales, despite the inherent uncertainties associated with the process. The predictive controller leverages the estimated variables provided by the MHE algorithm in the model to predict the future evolution of the system and to calculate the future control actions. The findings revealed that the profits obtained under the eMPC operation strategy were superior to those obtained under constant operational values, thereby demonstrating the merits of employing optimization strategies in WWTPs.

7. Final conclusions and future work

7.1. Final conclusions

This thesis deals with the modeling of anoxic-aerobic photobioreactors configurations for microalgae-bacteria based wastewater treatment, as well as with the optimization of the operation of WWTPs by means of advanced control strategies. In order to address the challenge posed by the scarcity of online measurements in microalgae-based wastewater treatment plants, a moving horizon estimator has been proposed. The estimation provided by the MHE was utilized to implement an eMPC in a hypothetical industrial wastewater treatment plant with microalgae and bacteria. The following list enumerates the primary contributions:

- The modeling of anoxic-aerobic algal-bacterial photobioreactor configurations with biomass recycling. A model was developed to simulate the continuous operation of the integrated system, encompassing all components of the plant, including the open photobioreactor, the enclosed anoxic reactor, and the secondary settler. This model enabled the simulation of the entire system, thereby providing a comprehensive representation of the plant's functionality. A sensitivity analysis was conducted to ascertain the most pertinent parameters of the model for estimation. Parameter estimation was conducted using a robust estimator in order to address the uncertainties imposed by unreliable measurements. The simulation results closely match with the experimental data, thereby further validating the model's accuracy and its capacity to assess the performance of anoxic-aerobic configurations under diverse scenarios. The results of the modelling and parameter estimation in an anoxic aerobic configuration treating different dilutions of digestate were presented in the paper: *"Parameter estimation in anoxic aerobic algal-bacterial photobioreactor devoted to carbon and nutrient removal. Algal Research, Volume 86, March 2025, Ref. 103917. ISSN 2211-9264. https://doi.org/10.1016/j.algal.2025.103917."*
- The development of a methodology for parameter estimation in biological systems. The proposed methodology addresses a series of optimization problems of escalating complexity, enabling the estimation of model parameters in a gradual manner while circumventing convergence issues. The proposed methodology has been applied to the problem of parameter estimation in an anoxic-aerobic algal

bacterial photobioreactor configuration for domestic wastewater treatment. The methodology was presented in the contribution: *"Parameter estimation approach applied to microalgae-bacteria photobioreactor, in: COMPUTER-AIDED CHEMICAL ENGINEERING, 52 - PROCEEDINGS OF THE 33rd European Symposium on Computer Aided Process Engineering (ESCAPE33), vol. 1, https://doi.org/10.1016/B978-0-443-15274-0.50115-3."*

- The development of a library of components for the simulation of wastewater treatment plants based on microalgae-bacteria consortia. This library is composed of diverse components that can be interconnected, thereby enabling the simulation of various configurations of wastewater treatment plants with microalgae and bacteria. This contribution was presented in the congress communication: *"Librería para sistemas de tratamiento de aguas residuales con microalgas y bacterias. XLIII Jornadas de Automática: libro de actas. 7-9 de septiembre de 2022, Logroño, La Rioja, España, pp. 493-499. A Coruña: Universidade da Coruña, Servizo de Publicacións, 2022. XXI, 1075 p. ISBN: 978-84-9749-841-8. DOI: https://doi.org/10.17979/spudc.9788497498418."*
- The implementation of algorithms for real-time estimation of unknown and unmeasured variables. A state estimator based on the MHE algorithm was proposed to estimate unmeasured states, parameters, and model uncertainties in cases when the measurements are not available at uniform time periods. The present study proposes the utilization of MHE technique for an industrial microalgae-based wastewater treatment process, with a focus on the estimation of multiple states and parameters concurrently to evaluate the effluent water quality. The simulation results demonstrate the efficacy of the MHE approach in online estimation of the most relevant variables of a wastewater treatment process, even in the presence of noisy measurements, model inaccuracies, varying environmental conditions, and multi-rate measurements. The main results obtained during this stage of the research were incorporated into the paper: *"Moving horizon estimation in microalgae-bacteria based wastewater treatment using online and analytical multi-rate measurements. Algal Research, Volume 91, October 2025, Ref. 104338. ISSN 2211-9264. https://doi.org/10.1016/j.algal.2025.104338."*

- The design of an economic predictive controller for a microalgae-based wastewater treatment plant with biomass harvesting. The development of the eMPC was driven by the objective of optimizing biomass yield to ensure maximum profit from biomass sales as a bioestimulant. The predictive controller utilizes the estimated variables provided by the MHE algorithm in the model to predict the future evolution of the system and to calculate the future control actions. The sequence of future control actions is calculated using an optimization procedure that aims to minimize future errors with respect to the desired operating points of the plant, while respecting its operational constraints.
- The design of a laboratory-scale microalgae-bacteria wastewater treatment plant with an SCADA system that allows the online monitoring of the process, and the implementation of state estimators and control strategies.

These results substantiate the possibility of developing models capable of simulating a range of microalgae–bacteria-based WWTP configurations, as well as using these models to support decision-making in process operations. Likewise, the findings demonstrate that the application of appropriate modeling and optimization techniques enables the real-time estimation of unmeasurable variables, which is crucial for the effective operation and optimization of wastewater treatment plants.

7.2. Future Work

Future research on this topic will focus on:

- Testing alternative discretization techniques, such as orthogonal collocation, in order to enhance computational performance while preserving solution accuracy and stability.
- The application of the Modifier Adaptation algorithms to MPC control in wastewater treatment processes with microalgae and bacteria. Due to the daily and seasonal variability that occurs in systems based on microalgae and bacteria, in the future, we intend to incorporate Modifier Adaptation techniques into the eMPC that will allow the problem to be adapted to the changes caused by this variability, thereby ensuring that the optimal actions calculated are not affected by the use of an incorrect model.

- Testing proposed estimation algorithms and control strategies in a real wastewater treatment plant with microalgae and bacteria.

References

Abdollahi, J. and Dubljevic, S. (2012) ‘Lipid production optimization and optimal control of heterotrophic microalgae fed-batch bioreactor’, *Chemical Engineering Science*, 84, pp. 619–627. Available at: https://doi.org/10.1016/j.ces.2012.09.005.

Acién, F.G. *et al.* (2012) ‘Production cost of a real microalgae production plant and strategies to reduce it’, *Biotechnology Advances*, 30(6), pp. 1344–1353. Available at: https://doi.org/10.1016/j.biotechadv.2012.02.005.

Alcántara, C. *et al.* (2015) ‘Evaluation of wastewater treatment in a novel anoxic-aerobic algal-bacterial photobioreactor with biomass recycling through carbon and nitrogen mass balances’, *Bioresource Technology*, 191, pp. 173–186. Available at: https://doi.org/10.1016/j.biortech.2015.04.125.

Alcántara, C., García-Encina, P.A. and Muñoz, R. (2013) ‘Evaluation of mass and energy balances in the integrated microalgae growth-anaerobic digestion process’, *Chemical Engineering Journal*, 221, pp. 238–246. Available at: https://doi.org/10.1016/j.cej.2013.01.100.

Alessandri, A. and Battistelli, G. (2020) ‘Moving horizon estimation: Open problems, theoretical progress, and new application perspectives’, *International Journal of Adaptive Control and Signal Processing*, 34(6), pp. 703–705. Available at: https://doi.org/10.1002/acs.3127.

de Andrade, G.A. *et al.* (2016) ‘Distributed Sliding Mode Control of pH in Tubular Photobioreactors’, *IEEE Transactions on Control Systems Technology*, 24(4), pp. 1160–1173. Available at: https://doi.org/10.1109/TCST.2015.2480840.

de Andrade, Gustavo.A. *et al.* (2016) ‘Optimization of biomass production in outdoor tubular photobioreactors’, *Journal of Process Control*, 37, pp. 58–69. Available at: https://doi.org/10.1016/j.jprocont.2015.10.001.

Araujo Pimentel, G. *et al.* (2015) ‘An Observer-based Robust Control Strategy for Overflow Metabolism Cultures in Fed-Batch Bioreactors’, *IFAC-PapersOnLine*, 48(8), pp. 1081–1086.

Arnold, E. and Dietze, S. (2001) ‘Nonlinear Moving Horizon State Estimation of an Activated Sludge Model’, *IFAC Proceedings Volumes*, 34(8), pp. 545–550.

Aslan, S. and Kapdan, I.K. (2006) ‘Batch kinetics of nitrogen and phosphorus removal from synthetic wastewater by algae’, *Ecological Engineering*, 28(1), pp. 64–70. Available at: https://doi.org/10.1016/j.ecoleng.2006.04.003.

Awuah, Esi. (2007) *Pathogen Removal Mechanisms in Macrophyte and Algal Waste Stabilization Ponds*.

De Baar, H. (1994) ‘von Liebig ’ s Law of the Minimum and Plankton Ecology’, *Progress in Oceanography*, 33, pp. 347–386.

Barceló-Villalobos, M. *et al.* (2022) ‘A new control strategy to improve the mass transfer capacity and reduce air injection costs in raceway reactors’, *New Biotechnology*, 70(April), pp. 49–56. Available at: https://doi.org/10.1016/j.nbt.2022.04.005.

Bausa, I. *et al.* (2022) ‘Modeling and simulation of anoxic-aerobic algalbacterial photobioreactor for nutrients removal’, in L. Montastruc and S. Negny (eds.) *COMPUTER-AIDED CHEMICAL ENGINEERING, 51 - PROCEEDINGS OF THE 32nd European Symposium on Computer Aided Process Engineering (ESCAPE32), June 12-15, 2022, Toulouse, France*. © 2022 Elsevier B.V. All rights reserved., pp. 151–156. Available at: https://doi.org/http://dx.doi.org/10.1016/B978-0-323-95879-0.50026-6.

Berenguel, M. *et al.* (2004) ‘Model predictive control of pH in tubular photobioreactors’, *Journal of Process Control*, 14(4), pp. 377–387. Available at: https://doi.org/10.1016/j.jprocont.2003.07.001.

Bernard, O. and Rémond, B. (2012) ‘Validation of a simple model accounting for light and temperature effect on microalgal growth’, *Bioresource Technology*, 123, pp. 520–527. Available at: https://doi.org/10.1016/j.biortech.2012.07.022.

Bogaerts, P. and Coutinho, D. (2014) ‘Robust nonlinear state estimation of bioreactors based on H∞ hybrid observers’, *Computers and Chemical Engineering*, 60, pp. 315–328. Available at: https://doi.org/10.1016/j.compchemeng.2013.09.013.

Borchardt, D. and Reichert, P. (2001) ‘River Water Quality Model no. 1 (RWQM1): Case study I. Compartmentalisation approach applied to oxygen balances in the River Lahn (Germany)’, *Water Science and Technology*, 43(5), pp. 41–49. Available at: https://doi.org/10.2166/wst.2001.0247.

Broekhuizen, N. *et al.* (2012) ‘Modification, calibration and verification of the IWA River Water Quality Model to simulate a pilot-scale high rate algal pond’, *Water Research*, 46(9), pp. 2911–2926. Available at: https://doi.org/10.1016/j.watres.2012.03.011.

Buehner, M.R. *et al.* (2009) ‘Microalgae growth modeling and control for a vertical flat panel photobioreactor’, *Proceedings of the American Control Conference*, pp. 2301–2306. Available at: https://doi.org/10.1109/ACC.2009.5160260.

Busch, J. *et al.* (2013) ‘State estimation for large-scale wastewater treatment plants’, *Water Research*, 47(13), pp. 4774–4787. Available at: https://doi.org/10.1016/j.watres.2013.04.007.

Camacho, E.F. and Bordons, C. (2007) *Model Predictive control*, *Advanced Textbooks in Control and Signal Processing*. London: Springer London (Advanced Textbooks in Control and Signal Processing). Available at: https://doi.org/10.1007/978-0-85729-398-5.

Camacho Rubio, F. *et al.* (1999) ‘Prediction of dissolved oxygen and carbon dioxide concentration profiles in tubular photobioreactors for microalgal culture’, *Biotechnology and Bioengineering*, 62(1), pp. 71–86. Available at: https://doi.org/10.1002/(SICI)1097-0290(19990105)62:1<71::AID-BIT9>3.0.CO;2-T.

Caparroz, M. *et al.* (2023) ‘Modelado y control del pH en la producción de microalgas en reactores raceway usando técnicas de adaptación de parámetros’, *Revista Iberoamericana de Automática e Informática industrial*, 20(4), pp. 379–388. Available at: https://doi.org/10.4995/riai.2023.19103.

Carreño-Zagarra, J.J. *et al.* (2019) ‘Linear active disturbance rejection control for a raceway photobioreactor’, *Control Engineering Practice*, 85(June 2018), pp. 271–279. Available at: https://doi.org/10.1016/j.conengprac.2019.02.007.

Casagli, F. *et al.* (2021) ‘ALBA: A comprehensive growth model to optimize algae-bacteria wastewater treatment in raceway ponds’, *Water Research*, 190. Available at: https://doi.org/10.1016/j.watres.2020.116734.

Chae, K.J. and Kang, J. (2013) ‘Estimating the energy independence of a municipal wastewater treatment plant incorporating green energy resources’, *Energy Conversion and Management*, 75, pp. 664–672. Available at: https://doi.org/10.1016/j.enconman.2013.08.028.

Costache, T.A. *et al.* (2013) 'Comprehensive model of microalgae photosynthesis rate as a function of culture conditions in photobioreactors', *Applied Microbiology and Biotechnology*, 97(17), pp. 7627–7637. Available at: https://doi.org/10.1007/s00253-013-5035-2.

Dewasme, L. *et al.* (2015) 'State estimation and predictive control of fed-batch cultures of hybridoma cells', *Journal of Process Control*, 30, pp. 50–57. Available at: https://doi.org/10.1016/j.jprocont.2014.12.006.

Dhaouefi, Z. *et al.* (2018) 'Assessing textile wastewater treatment in an anoxic-aerobic photobioreactor and the potential of the treated water for irrigation', *Algal Research*, 29(August 2017), pp. 170–178. Available at: https://doi.org/10.1016/j.algal.2017.11.032.

EA Internacional (2024) 'Proosis'.

EA International (2022) *EcosimPro | PROOSIS - Modelling and Simulation Toolkits and Services*. Available at: https://www.ecosimpro.com/ (Accessed: 18 July 2022).

Eilers, P.H.C. and Peeters, J.C.H. (1988) 'A model for the relationship between light intensity and the rate of photosynthesis in phytoplankton', *Ecological Modelling*, 42, pp. 199–215.

Ellis, M., Durand, H. and Christofides, P.D. (2014) 'A tutorial review of economic model predictive control methods', *Journal of Process Control*, 24(8), pp. 1156–1178. Available at: https://doi.org/10.1016/j.jprocont.2014.03.010.

Ellis, M., Liu, J. and Christofides, P.D. (2021) *Economic Model Predictive Control*, *Encyclopedia of Systems and Control*. Springer Cham. Available at: https://doi.org/10.1007/978-3-030-44184-5_6.

Elsheikh, M. *et al.* (2021) 'A comparative review of multi-rate moving horizon estimation schemes for bioprocess applications', *Computers and Chemical Engineering*, 146. Available at: https://doi.org/10.1016/j.compchemeng.2020.107219.

Farza, M. *et al.* (2019) 'A new filtered high gain observer design for the estimation of the components concentrations in a photobioreactor in microalgae culture', *IFAC-PapersOnLine*, 52(1), pp. 904–909. Available at: https://doi.org/10.1016/j.ifacol.2019.06.177.

Fernández, I. *et al.* (2010) 'Modelling and control issues of pH in tubular photobioreactors', *IFAC Proceedings Volumes (IFAC-PapersOnline)*, 43(6), pp. 186–191. Available at: https://doi.org/10.3182/20100707-3-BE-2012.0046.

Fernández, I. *et al.* (2012) 'Dynamic model of microalgal production in tubular photobioreactors', *Bioresource Technology*, 126, pp. 172–181. Available at: https://doi.org/10.1016/j.biortech.2012.08.087.

Fernández, I., Acién, F.G., Berenguel, M., Guzmán, J.L., *et al.* (2014) 'A Lumped parameter chemical-physical model for tubular photobioreactors', *Chemical Engineering Science*, (112), pp. 116–129.

Fernández, I., Acién, F.G., Berenguel, M. and Guzmán, J.L. (2014) 'First principles model of a tubular photobioreactor for microalgal production', *Industrial and Engineering Chemistry Research*, 53(27), pp. 11121–11136. Available at: https://doi.org/10.1021/ie501438r.

Fernández, I., Acién, F.G., *et al.* (2016) 'Dynamic model of an industrial raceway reactor for microalgae production', *Algal Research*, 17, pp. 67–78. Available at: https://doi.org/10.1016/j.algal.2016.04.021.

Fernández, I., Berenguel, M., *et al.* (2016) 'Hierarchical control for microalgae biomass production in photobiorreactors', *Control Engineering Practice*, 54, pp. 246–255. Available at: https://doi.org/10.1016/j.conengprac.2016.06.007.

García, D. *et al.* (2017) 'Enhanced carbon, nitrogen and phosphorus removal from domestic wastewater in a novel anoxic-aerobic photobioreactor coupled with biogas upgrading', *Chemical Engineering Journal*, 313, pp. 424–434. Available at: https://doi.org/10.1016/j.cej.2016.12.054.

García, J. *et al.* (2006) 'Long term diurnal variations in contaminant removal in high rate ponds treating urban wastewater', *Bioresource Technology*, 97(14), pp. 1709–1715. Available at: https://doi.org/10.1016/j.biortech.2005.07.019.

García-Mañas, F. *et al.* (2019) 'Biomass estimation of an industrial raceway photobioreactor using an extended Kalman filter and a dynamic model for microalgae production', *Algal Research*, 37(November 2018), pp. 103–114. Available at: https://doi.org/10.1016/j.algal.2018.11.009.

Gill, P.E., Murray, W. and Saunders, M.A. (2005) ‘SNOPT: An SQP algorithm for large-scale constrained optimization’, *SIAM Review*, 47(1), pp. 99–131. Available at: https://doi.org/10.1137/S0036144504446096.

de Godos, I., Vargas, V.A., *et al.* (2014) ‘Assessing carbon and nitrogen removal in a novel anoxic-aerobic cyanobacterial-bacterial photobioreactor configuration with enhanced biomass sedimentation’, *Water Research*, 61, pp. 77–85. Available at: https://doi.org/10.1016/j.watres.2014.04.050.

de Godos, I., Mendoza, J.L., *et al.* (2014) ‘Evaluation of carbon dioxide mass transfer in raceway reactors for microalgae culture using flue gases’, *Bioresource Technology*, 153, pp. 307–314. Available at: https://doi.org/10.1016/j.biortech.2013.11.087.

Gujer, W. *et al.* (1995) ‘The Activated Sludge Model No. 2: Biological phosphorus removal’, *Water Science and Technology*, 31(2), pp. 1–11. Available at: https://doi.org/10.1016/0273-1223(95)00175-M.

Gujer, W. *et al.* (1999) ‘Activated Sludge Model No.3’, *Water Science and Technology*, 39(1), pp. 183–193.

Guzmán, J.L., Acién, F.G. and Berenguel, M. (2021) ‘Modelling and control of microalgae production in industrial photobioreactors’, *Revista Iberoamericana de Automática e Informática industrial*, 18(1), pp. 1–18. Available at: https://doi.org/10.4995/riai.2020.13604.

Haverbeke, N. *et al.* (2008) ‘Nonlinear model predictive control with moving horizon state and disturbance estimation - Application’, *IFAC Proceedings Volumes (IFAC-PapersOnline)*, 17(1 PART 1). Available at: https://doi.org/10.3182/20080706-5-KR-1001.3211.

Havlik, I. *et al.* (2022) ‘On-Line Monitoring of Biological Parameters in Microalgal Bioprocesses Using Optical Methods’, *Energies*, 15(3), pp. 1–27. Available at: https://doi.org/10.3390/en15030875.

Henze, M. *et al.* (2000) *Activated sludge models ASM1, ASM2, ASM2d and ASM3*. Edited by IWA TASK GROUP ON MATHEMATICAL MODELLING FOR DESIGN AND OPERATION OF BIOLOGICAL WASTEWATER TREATMENT. London: IWA Publishing.

Hindmarsh, A.C. *et al.* (2005) 'SUNDIALS: Suite of nonlinear and differential/algebraic equation solvers', *ACM Transactions on Mathematical Software*, 31(3), pp. 363–396. Available at: https://doi.org/10.1145/1089014.1089020.

Hoyo, Á. *et al.* (2019) 'Control predictivo lineal del PH en un fotobiorreactor Raceway', pp. 414–420. Available at: https://doi.org/10.17979/spudc.9788497497169.414.

Hoyo, Á. *et al.* (2022) 'Robust control of pH in a raceway photo- biorreactor', *Revista Iberoamericana de Automática e Informática industrial*, 19(3), pp. 274–283. Available at: https://doi.org/10.4995/riai.2022.16731.

Huber, P.J. (2011) 'Robust Statistics', in M. Lovric (ed.) *International Encyclopedia of Statistical Science*. Springer, Berlin, Heidelberg. Available at: https://doi.org/https://doi.org/10.1007/978-3-642-04898-2_594.

Huber, P.J. and Ronchetti, E.M. (2009) *Robust Statistics*. Second Edi. New Jersey: John Wiley and Sons, Inc.

Iacopozzi, I. *et al.* (2007) 'A modified Activated Sludge Model No. 3 (ASM3) with two-step nitrification-denitrification', *Environmental Modelling and Software*, 22(6), pp. 847–861. Available at: https://doi.org/10.1016/j.envsoft.2006.05.009.

Ifrim, G.A. *et al.* (2013) 'Multivariable feedback linearizing control of Chlamydomonas reinhardtii photoautotrophic growth process in a torus photobioreactor', *Chemical Engineering Journal*, 218, pp. 191–203. Available at: https://doi.org/10.1016/j.cej.2012.11.133.

Jerono, P., Schaum, A. and Meurer, T. (2018) 'Observer Design for the Droop Model with Biased Measurement: Application to Haematococcus Pluvialis', *Proceedings of the IEEE Conference on Decision and Control*, 2018-Decem(Cdc), pp. 6295–6300. Available at: https://doi.org/10.1109/CDC.2018.8619063.

Kalman, R.E. (1960) 'A New Approach to Linear Filtering and Prediction Problems', *Journal of Basic Engineering*, 82(1), pp. 35–45. Available at: https://doi.org/10.1115/1.3662552.

Kalman, R.E. and Bucy, R.S. (1961) 'New Results in Linear Filtering and Prediction Theory', *Journal of Basic Engineering*, 83(1), pp. 95–108. Available at: https://doi.org/10.1115/1.3658902.

Langergraber, G. *et al.* (2009) ‘CWM1: A general model to describe biokinetic processes in subsurface flow constructed wetlands’, *Water Science and Technology*, 59(9), pp. 1687–1697. Available at: https://doi.org/10.2166/wst.2009.131.

Li, J., Xu, N.S. and Su, W.W. (2003) ‘Online estimation of stirred-tank microalgal photobioreactor cultures based on dissolved oxygen measurement’, *Biochemical Engineering Journal*, 14(1), pp. 51–65. Available at: https://doi.org/10.1016/S1369-703X(02)00135-3.

Luenberger, D.G. (1964) ‘Observing the State of a Linear System’, *IEEE Transactions on Military Electronics*, 8(2), pp. 74–80. Available at: https://doi.org/10.1109/TME.1964.4323124.

Luenberger, D.G. (1966) ‘Observers for Multivariable Systems’, *IEEE Transactions on Automatic Control*, 11(2), pp. 190–197. Available at: https://doi.org/10.1109/TAC.1966.1098323.

Luenberger, D.G. (1967) ‘Canonical Forms for Linear Multivariable Systems’, *IEEE Transactions on Automatic Control*, AC-12(3), pp. 290–293.

Luenberger, D.G. (1971) ‘An Introduction to Observers’, *IEEE Transactions on Automatic Control*, 16(6), pp. 596–602. Available at: https://doi.org/10.1109/TAC.1971.1099826.

Mailleret, L., Gouzé, J.L. and Bernard, O. (2005) ‘Nonlinear control for algae growth models in the chemostat’, *Bioprocess and Biosystems Engineering*, 27(5), pp. 319–327. Available at: https://doi.org/10.1007/s00449-005-0410-8.

Marsollier, L. *et al.* (2004) ‘Aquatic Plants Stimulate the Growth of and Biofilm Formation by Mycobacterium ulcerans in Axenic Culture and Harbor These Bacteria in the Environment’, *Applied and Environmental Microbiology*, 70(2), pp. 1097–1103. Available at: https://doi.org/10.1128/AEM.70.2.1097-1103.2004.

Martinez, M.E. *et al.* (1997) ‘Influence of light intensity on the kinetic and yield parameters of Chlorella pyrenoidosa mixotrophic growth’, *Process Biochemistry*, 32(2), pp. 93–98.

MathWorks Inc. (2024) ‘MATLAB’.

Mazaeda, R. *et al.* (2011) ‘Librería de Modelos Orientada a Objetos para la Simulación del Cuarto de Azúcar: Cristalizador Continuo por Evaporación al Vacío’, *RIAI - Revista*

Iberoamericana de Automatica e Informatica Industrial, 8(1), pp. 100–111. Available at: https://doi.org/10.4995/RIAI.2011.01.12.

McGinn, P.J. *et al.* (2017) 'Maximizing the productivity of the microalgae Scenedesmus AMDD cultivated in a continuous photobioreactor using an online flow rate control', *Bioprocess and Biosystems Engineering*, 40(1), pp. 63–71. Available at: https://doi.org/10.1007/s00449-016-1675-9.

Mendoza, J.L., Granados, M.R., de Godos, I., Acién, F.G., Molina, E., Banks, C., *et al.* (2013) 'Fluid-dynamic characterization of real-scale raceway reactors for microalgae production', *Biomass and Bioenergy*, 54, pp. 267–275. Available at: https://doi.org/10.1016/j.biombioe.2013.03.017.

Mendoza, J.L., Granados, M.R., de Godos, I., Acién, F.G., Molina, E., Heaven, S., *et al.* (2013) 'Oxygen transfer and evolution in microalgal culture in open raceways', *Bioresource Technology*, 137, pp. 188–195. Available at: https://doi.org/10.1016/j.biortech.2013.03.127.

de Menezes, D.Q.F. *et al.* (2021) 'A review on robust M-estimators for regression analysis', *Computers and Chemical Engineering*, 147. Available at: https://doi.org/10.1016/j.compchemeng.2021.107254.

Metcalf & Eddy Inc. (2003) *Wastewater Engineering : Treatment and Reuse*. Fouth Edit. Boston: McGraw-Hill.

Mohd Ali, J. *et al.* (2015) 'Review and classification of recent observers applied in chemical process systems', *Computers and Chemical Engineering*, 76, pp. 27–41. Available at: https://doi.org/10.1016/j.compchemeng.2015.01.019.

Molina Grima, E. *et al.* (1994) 'A mathematical model of microalgae growth in light limited chemostat cultures', *J. Chem. Technol. Biotechnol.*, (61), pp. 167–173.

Moreno, J.A. and Alvarez, J. (2015) 'On the estimation problem of a class of continuous bioreactors with unknown input', *Journal of Process Control*, 30, pp. 34–49. Available at: https://doi.org/10.1016/j.jprocont.2014.12.005.

Muñoz, R. and Guieysse, B. (2006) 'Algal-bacterial processes for the treatment of hazardous contaminants: A review', *Water Research*, 40(15), pp. 2799–2815. Available at: https://doi.org/10.1016/j.watres.2006.06.011.

Nordio, R. *et al.* (2023) ‘Influence of pH and dissolved oxygen control strategies on the performance of pilot-scale microalgae raceways using fertilizer or wastewater as the nutrient source’, *Journal of Environmental Management*, 345(August). Available at: https://doi.org/10.1016/j.jenvman.2023.118899.

Novak, T. and Brune, D.E. (1985) ‘Inorganic carbon limited growth kinetics of some freshwater algae’, *Water Res*, 19(2), pp. 215–225.

Oswald, W.J. and Gotaas, H.B. (1957) ‘Photosynthesis in Sewage Treatment’, *Transactions of the American Society of Civil Engineers*, 122(1), pp. 73–97. Available at: https://doi.org/10.1061/TACEAT.0007483.

Palacin, L.G. *et al.* (2011) ‘New dynamic library of reverse osmosis plants with fault simulation’, *Desalination and Water Treatment*, 25(1–3), pp. 127–132. Available at: https://doi.org/10.5004/dwt.2011.1434.

Parakh, S.K. *et al.* (2020) ‘Integrating gravity settler with an algal membrane photobioreactor for in situ biomass concentration and harvesting’, *Bioresource Technology*, 315(July). Available at: https://doi.org/10.1016/j.biortech.2020.123822.

Passos, F. *et al.* (2017) ‘Towards energy neutral microalgae-based wastewater treatment plants’, *Algal Research*, 28(May), pp. 235–243. Available at: https://doi.org/10.1016/j.algal.2017.11.006.

Pataro, I.M.L. *et al.* (2023) ‘A learning-based model predictive strategy for pH control in raceway photobioreactors with freshwater and wastewater cultivation media’, *Control Engineering Practice*, 138(March), p. 105619. Available at: https://doi.org/10.1016/j.conengprac.2023.105619.

Pawlowski, A., Mendoza, J.L., *et al.* (2014) ‘Effective utilization of flue gases in raceway reactor with event-based pH control for microalgae culture’, *Bioresource Technology*, 170, pp. 1–9. Available at: https://doi.org/10.1016/j.biortech.2014.07.088.

Pawlowski, A., Fernández, I., *et al.* (2014) ‘Event-based predictive control of pH in tubular photobioreactors’, *Computers and Chemical Engineering*, 65, pp. 28–39. Available at: https://doi.org/10.1016/j.compchemeng.2014.03.001.

Pawlowski, A. *et al.* (2015) ‘Selective pH and dissolved oxygen control strategy for a raceway reactor within an event-based approach’, *Control Engineering Practice*, 44, pp. 209–218. Available at: https://doi.org/10.1016/j.conengprac.2015.08.004.

Pawlowski, A. *et al.* (2017) ‘Event-Based Control Systems for Microalgae Culture in Industrial Reactors’, in B.N. Tripathi and D. Kumar (eds.) *Prospects and Challenges in Algal Biotechnology*. Singapore: Springer Singapore, pp. 1–48. Available at: https://doi.org/10.1007/978-981-10-1950-0_1.

Pawlowski, A. *et al.* (2019) ‘Control system for pH in raceway photobioreactors based on wiener models’, *IFAC-PapersOnLine*, 52(1), pp. 928–933. Available at: https://doi.org/10.1016/j.ifacol.2019.06.181.

Porras Reyes, L., Havlik, I. and Beutel, S. (2024) ‘Software sensors in the monitoring of microalgae cultivations’, *Reviews in Environmental Science and Biotechnology*, 23(1), pp. 67–92. Available at: https://doi.org/10.1007/s11157-023-09679-8.

Raïssi, T., Ramdani, N. and Candau, Y. (2005) ‘Bounded error moving horizon state estimator for non-linear continuous-time systems: Application to a bioprocess system’, *Journal of Process Control*, 15(5), pp. 537–545. Available at: https://doi.org/10.1016/j.jprocont.2004.10.002.

Rawlings, J.B. (2014) ‘Encyclopedia of Systems and Control’, in *Encyclopedia of Systems and Control*. Springer-Verlag London, pp. 1–7. Available at: https://doi.org/10.1007/978-1-4471-5102-9.

Rawlings, J.B. and Bakshi, B.R. (2006) ‘Particle filtering and moving horizon estimation’, *Computers and Chemical Engineering*, 30(10–12), pp. 1529–1541. Available at: https://doi.org/10.1016/j.compchemeng.2006.05.031.

Real Decreto 509/1996, de 15 de marzo (1996). Ministerio De Obras Públicas, Ministerio de Medio Ambiente.

Reichert, P. (1994) ‘AQUASIM – A TOOL FOR SIMULATION AND DATA ANALYSIS OF AQUATIC SYSTEMS’, *Water Science and Technology*, 30(2), pp. 21–30. Available at: https://doi.org/10.2166/wst.1994.0025.

Reichert, P. (2001) ‘River Water Quality Model no. 1 (RWQM1): Case study II. Oxygen and nitrogen conversion processes in the River Glatt (Switzerland)’, *Water Science and Technology*, 43(5), pp. 51–60. Available at: https://doi.org/10.2166/wst.2001.0249.

Reichert, P. *et al.* (2001) ‘River water quality model no. 1 (RWQM1): II. Biochemical process equations’, *Water Science and Technology*, 43(5), pp. 11–30.

Rey, W.J.J. (1983) *Introduction to Robust and Quasi-Robust Statistical Methods*. Springer-Verlag. Available at: https://doi.org/10.1007/978-3-642-69389-2.

Risbeck, M.J. and Rawlings, J.B. (2016) 'MPCTools: Nonlinear model predictive control tools for CasADi'.

Rodríguez-Mata, A. *et al.* (2011) 'Nonlinear high-gain observers with integral action: Application to bioreactors', in *8th International Conference on Electrical Engineering, Computing Science and Automatic Control (CCE)*. Merida City, Mexico: IEEE, pp. 1–6. Available at: https://doi.org/10.1109/ICEEE.2011.6106611.

Rodríguez-Miranda, E. *et al.* (2019) 'Daytime/nighttime event-based pi control for the PH of a microalgae raceway reactor', *Processes*, 7(5), pp. 1–16. Available at: https://doi.org/10.3390/pr7050247.

Rodríguez-Miranda, E. *et al.* (2020) 'Diurnal and nocturnal pH control in microalgae raceway reactors by combining classical and event-based control approaches', *Water Science and Technology*, 82(6), pp. 1155–1165. Available at: https://doi.org/10.2166/wst.2020.260.

Rodríguez-Torres, M.J. *et al.* (2021) 'Modelling and ph control in raceway and thin-layer photobioreactors for wastewater treatment', *Energies*, 14(4), pp. 1–14. Available at: https://doi.org/10.3390/en14041099.

Romero-García, J.M. *et al.* (2012) 'Filtered Smith Predictor to control pH during enzymatic hydrolysis of microalgae to produce l-aminoacids concentrates', *Chemical Engineering Science*, 82, pp. 121–131. Available at: https://doi.org/10.1016/j.ces.2012.07.024.

Ruíz Guirola, M. (2023) *EVALUACIÓN DEL RENDIMIENTO DE FOTOBIORREACTORES PARA EL TRATAMIENTO DE AGUAS RESIDUALES DOMÉSTICAS*. TRABAJO FIN DE MÁSTER. UNIVERSIDAD DE VALLADOLID.

Ruiz-Marin, A., Mendoza-Espinosa, L.G. and Stephenson, T. (2010) 'Growth and nutrient removal in free and immobilized green algae in batch and semi-continuous cultures treating real wastewater', *Bioresource Technology*, 101(1), pp. 58–64. Available at: https://doi.org/10.1016/j.biortech.2009.02.076.

Sah, L. *et al.* (2011) '3D model for a secondary facultative pond', *Ecological Modelling*, 222(9), pp. 1592–1603. Available at: https://doi.org/10.1016/j.ecolmodel.2011.02.021.

Sánchez-Zurano, A. *et al.* (2021) 'ABACO: A new model of microalgae-bacteria consortia for biological treatment of wastewaters', *Applied Sciences*, 11(3), pp. 1–24. Available at: https://doi.org/10.3390/app11030998.

Silva, H.J. and Pirt, J. (1984) 'Carbon dioxide inhibition of photosynthetic growth of chlorella', *Journal of general Microbiology*, (130), pp. 2833–2838.

Smith, B.T. and Davis, R.H. (2013) 'Particle concentration using inclined sedimentation via sludge accumulation and removal for algae harvesting', *Chemical Engineering Science*, 91, pp. 79–85. Available at: https://doi.org/10.1016/j.ces.2013.01.007.

Solimeno, A. *et al.* (2015) 'New mechanistic model to simulate microalgae growth', *Algal Research*, 12, pp. 350–358. Available at: https://doi.org/10.1016/j.algal.2015.09.008.

Solimeno, A. *et al.* (2017a) 'Integral microalgae-bacteria model (BIO_ALGAE): Application to wastewater high rate algal ponds', *Science of the Total Environment*, 601–602, pp. 646–657. Available at: https://doi.org/10.1016/j.scitotenv.2017.05.215.

Solimeno, A. *et al.* (2017b) 'Integral microalgae-bacteria model (BIO_ALGAE): Application to wastewater high rate algal ponds', *Science of the Total Environment*, 601–602, pp. 646–657. Available at: https://doi.org/10.1016/j.scitotenv.2017.05.215.

Solimeno, A., Acien, F.G. and García, J. (2017) 'Mechanistic model for design, analysis, operation and control of microalgae cultures: Calibration and application to tubular photobioreactors', *Algal Research*, 21, pp. 236–246. Available at: https://doi.org/10.1016/j.algal.2016.11.023.

Solimeno, A. and García, J. (2017) 'Microalgae-bacteria models evolution: From microalgae steady-state to integrated microalgae-bacteria wastewater treatment models – A comparative review', *Science of the Total Environment*, 607–608, pp. 1136–1150. Available at: https://doi.org/10.1016/j.scitotenv.2017.07.114.

Solimeno, A. and García, J. (2019) 'Microalgae and bacteria dynamics in high rate algal ponds based on modelling results: Long-term application of BIO_ALGAE model', *Science of the Total Environment*, 650, pp. 1818–1831. Available at: https://doi.org/10.1016/j.scitotenv.2018.09.345.

Solimeno, A., Gómez-Serrano, C. and Acién, F.G. (2019a) 'BIO_ALGAE 2: improved model of microalgae and bacteria consortia for wastewater treatment', *Environmental*

Science and Pollution Research, 26(25), pp. 25855–25868. Available at: https://doi.org/10.1007/s11356-019-05824-5.

Solimeno, A., Gómez-Serrano, C. and Acién, F.G. (2019b) 'BIO_ALGAE 2: improved model of microalgae and bacteria consortia for wastewater treatment', *Environmental Science and Pollution Research*, 26(25), pp. 25855–25868. Available at: https://doi.org/10.1007/s11356-019-05824-5.

Solimeno, A., Samsó, R. and García, J. (2016) 'Parameter sensitivity analysis of a mechanistic model to simulate microalgae growth', *Algal Research*, 15, pp. 217–223. Available at: https://doi.org/10.1016/j.algal.2016.02.027.

Von Sperling, M. (2007) *Waste stabilization ponds*. London: IWA Publishing.

Stiles, W.A.V. *et al.* (2018) 'Using microalgae in the circular economy to valorise anaerobic digestate: challenges and opportunities', *Bioresource Technology*, 267(July), pp. 732–742. Available at: https://doi.org/10.1016/j.biortech.2018.07.100.

Su, W.W., Li, J. and Xu, N.S. (2003) 'State and parameter estimation of microalgal photobioreactor cultures based on local irradiance measurement', *Journal of Biotechnology*, 105(1–2), pp. 165–178. Available at: https://doi.org/10.1016/S0168-1656(03)00188-3.

Takács, I., Patryioand, G.G. and Nolasco, D. (1991) 'A Dynamic Model of the Clarification-Thickening Process', *Wat. Res.*, 25(10), pp. 1263–1271.

Tebbani, S., Titica, M., *et al.* (2013) *Estimation of chlamydomonas reinhardtii growth in a torus photobioreactor*, *IFAC Proceedings Volumes (IFAC-PapersOnline)*. IFAC. Available at: https://doi.org/10.3182/20131216-3-IN-2044.00053.

Tebbani, S., Le Brusquet, L., *et al.* (2013) 'Robust moving horizon state estimation: Application to bioprocesses', *2013 17th International Conference on System Theory, Control and Computing, ICSTCC 2013; Joint Conference of SINTES 2013, SACCS 2013, SIMSIS 2013 - Proceedings*, pp. 539–544. Available at: https://doi.org/10.1109/ICSTCC.2013.6689014.

Tebbani, S. *et al.* (2014) 'Nonlinear predictive control for maximization of CO2 bio-fixation by microalgae in a photobioreactor', *Bioprocess and Biosystems Engineering*, 37(1), pp. 83–97. Available at: https://doi.org/10.1007/s00449-013-0928-0.

Tebbani, S., Lopes, F. and Becerra Celis, G. (2015) ‘Nonlinear control of continuous cultures of Porphyridium purpureum in a photobioreactor’, *Chemical Engineering Science*, 123, pp. 207–219. Available at: https://doi.org/10.1016/j.ces.2014.11.016.

Tejido-Núñez, Y. (2020) *Microalgae-based wastewater treatment processes: Implementation in acuaculture sector and WWTP*. Universidad de Navarra.

Torres-Franco, A.F. *et al.* (2021) ‘Assessment of the performance of an anoxic-aerobic microalgal-bacterial system treating digestate’, *Chemosphere*, 270. Available at: https://doi.org/10.1016/j.chemosphere.2020.129437.

Tuveri, A. *et al.* (2023) ‘A regularized Moving Horizon Estimator for combined state and parameter estimation in a bioprocess experimental application’, *Computers and Chemical Engineering*, 172(July 2022). Available at: https://doi.org/10.1016/j.compchemeng.2023.108183.

Unión Europea (1991) *Directiva 91/271/CEE sobre el tratamiento de las aguas residuales urbanas. Manual de interpretación y elaboración de informes*. Available at: https://www.miteco.gob.es/es/agua/publicaciones/03_Manual_Directiva_91_271_CEE_tcm30-214069.pdf.

Vilas, C. *et al.* (2008) ‘Desarrollo de una librería de componentes en Ecosimpro para la operación de...’, *RIAI- Revista Iberoamericana de Automática e Informática Industrial*, 5(1), pp. 51–65.

Water Service Corporation (2024) *Wastewater treatment, Carolina Water Service of North Carolina*. Available at: https://www.myutility.us/carolinawater/water-smart/utility-systems (Accessed: 5 March 2025).

Wu, X. and Merchuk, J. (2001) ‘A model integrating fluid dynamics in photosynthesis and photoinhibition processes’, *Chemical Engineering Science*, (56), pp. 3527–3538.

Yin, X., Decardi-Nelson, B. and Liu, J. (2018) ‘Subsystem decomposition and distributed moving horizon estimation of wastewater treatment plants’, *Chemical Engineering Research and Design*, 134(2013), pp. 405–419. Available at: https://doi.org/10.1016/j.cherd.2018.04.032.

Yoo, S.J. *et al.* (2015) ‘A comparative study of soft sensor design for lipid estimation of microalgal photobioreactor system with experimental validation’, *Bioresource*

Technology, 179, pp. 275–283. Available at: https://doi.org/10.1016/j.biortech.2014.12.029.

Yoo, S.J. *et al.* (2016) 'Optimization of microalgal photobioreactor system using model predictive control with experimental validation', *Bioprocess and Biosystems Engineering*, 39(8), pp. 1235–1246. Available at: https://doi.org/10.1007/s00449-016-1602-0.

Appendices

Appendix 1. Parameters used in the photobioreactor and anoxic reactor model

Table A1.1. Matrix of stoichiometric parameters

	S_{NH4}	S_{NH3}	S_{NO3}	S_{NO2}	S_{CO2}	S_{HCO3}	S_{CO3}	S_{PO4}	S_{O2}	S_H	S_{OH}	S_S	S_I	X_{ALG}	X_S	X_I	X_H	X_{AOB}	X_{NOB}
ρ_1	$v_{1,1}$				$v_{5,1}$			$v_{8,1}$	$v_{9,1}$	$v_{10,1}$				$v_{14,1}$					
ρ_2			$v_{3,2}$		$v_{5,2}$			$v_{8,2}$	$v_{9,2}$	$v_{10,2}$				$v_{14,2}$					
ρ_3	$v_{1,3}$				$v_{5,3}$			$v_{8,3}$	$v_{9,3}$	$v_{10,3}$				$v_{14,3}$					
ρ_4	$v_{1,4}$				$v_{5,4}$			$v_{8,4}$	$v_{9,4}$	$v_{10,4}$				$v_{14,4}$	$v_{15,4}$	$v_{16,4}$			
ρ_5	$v_{1,5}$				$v_{5,5}$			$v_{8,5}$	$v_{9,5}$	$v_{10,5}$		$v_{12,5}$					$v_{17,5}$		
ρ_6			$v_{3,6}$		$v_{5,6}$			$v_{8,6}$	$v_{9,6}$	$v_{10,6}$		$v_{12,6}$					$v_{17,6}$		
ρ_7				$v_{4,7}$	$v_{5,7}$			$v_{8,7}$		$v_{10,7}$		$v_{12,7}$					$v_{17,7}$		
ρ_8			$v_{3,8}$		$v_{5,8}$			$v_{8,8}$		$v_{10,8}$		$v_{12,8}$					$v_{17,8}$		
ρ_9	$v_{1,9}$				$v_{5,9}$			$v_{8,9}$	$v_{9,9}$	$v_{10,9}$							$v_{17,9}$		
ρ_{10}	$v_{1,10}$		$v_{3,10}$	$v_{4,10}$	$v_{5,10}$			$v_{8,10}$		$v_{10,10}$							$v_{17,10}$		
ρ_{11}															$v_{15,11}$	$v_{16,11}$	$v_{17,11}$		
ρ_{12}	$v_{1,12}$			$v_{4,12}$	$v_{5,12}$			$v_{8,12}$	$v_{9,12}$	$v_{10,12}$								$v_{18,12}$	
ρ_{13}			$v_{3,13}$	$v_{4,13}$	$v_{5,13}$			$v_{8,13}$	$v_{9,13}$	$v_{10,13}$									$v_{19,13}$
ρ_{14}	$v_{1,14}$				$v_{5,14}$			$v_{8,14}$	$v_{9,14}$	$v_{10,14}$								$v_{18,14}$	
ρ_{15}	$v_{1,15}$				$v_{5,15}$			$v_{8,15}$	$v_{9,15}$	$v_{10,15}$									$v_{19,15}$
ρ_{16}															$v_{15,16}$	$v_{16,16}$		$v_{18,16}$	
ρ_{17}															$v_{15,17}$	$v_{16,17}$			$v_{19,17}$

ρ_{18}	$v_{1,18}$				$v_{5,18}$			$v_{8,18}$		$v_{10,18}$		$v_{12,18}$	$v_{13,18}$		$v_{15,18}$				
ρ_{19}					$v_{5,19}$	$v_{6,19}$				$v_{10,19}$									
ρ_{20}						$v_{6,20}$	$v_{7,20}$			$v_{10,20}$									
ρ_{21}	$v_{1,21}$	$v_{2,21}$								$v_{10,21}$									
ρ_{22}										$v_{10,22}$	$v_{11,22}$								
ρ_{23}									$v_{9,23}$										
ρ_{24}					$v_{5,24}$														
ρ_{25}		$v_{2,25}$																	

Table A1.2. Values of biokinetic, chemical and physic parameters

Parameters	Description	Value	Unit	Source
Microalgae (X_{ALG})				
μ_{ALG}	Maximum growth rate of X_{ALG}	0.7	d^{-1}	Estimated
$k_{resp,ALG}$	Endogenous respiration constant	0.1	d^{-1}	(Reichert *et al.*, 2001)
$k_{death,ALG}$	Decay constant	0.05	d^{-1}	Estimated
$K_{C,ALG}$	Saturation constant of X_{ALG} on S_{CO2}	4E-3	$gC\ m^{-3}$	(Novak and Brune, 1985)
$I_{CO2,ALG}$	Inhibition constant of X_{ALG} on S_{CO2}	120	$gC\ m^{-3}$	(Silva and Pirt, 1984)
$K_{N,ALG}$	Saturation constant of X_{ALG} on nitrogen	0.1	$gN\ m^{-3}$	(Reichert *et al.*, 2001)
$K_{O2,ALG}$	Saturation constant of X_{ALG} on S_{O2}	0.2	$gO_2\ m^{-3}$	(Reichert *et al.*, 2001)
$K_{P,ALG}$	Saturation constant of X_{ALG} for S_{HPO4}	0.02	$gP\ m^{-3}$	(Reichert *et al.*, 2001)
Heterotrophic bacteria (X_H)				
μ_H	Maximum growth rate of X_H	2.5	d^{-1}	Estimated
η_H	Anoxic reduction factor for X_H	0.6	–	(Gujer *et al.*, 1999)
$k_{resp,H}$	Endogenous respiration rate of X_H	0.3	d^{-1}	(Reichert *et al.*, 2001)
$K_{O2,H}$	Saturation constant of X_H for S_{O2}	0.2	$gO_2\ m^{-3}$	(Reichert *et al.*, 2001)
$K_{N,H}$	Saturation constant of X_H for S_N	0.2	$gN\ m^{-3}$	(Reichert *et al.*, 2001)
$K_{S,H}$	Saturation constant of X_H for S_S	20	$gCOD\ m^{-3}$	(Henze *et al.*, 2000)
$K_{NO3,H,anox}$	Saturation constant of X_H for S_{NO3}	0.5	$gN\ m^{-3}$	(Reichert *et al.*, 2001)
$K_{NO2,H,anox}$	Saturation constant of X_H for S_{NO2}	0.2	$gN\ m^{-3}$	(Reichert *et al.*, 2001)
$K_{P,H}$	Saturation constant of X_H for S_{HPO4}	0.02	$gP\ m^{-3}$	(Reichert *et al.*, 2001)
$k_{death,H}$	Decay constant of X_H	0.8	d^{-1}	Estimated
Autotrophic bacteria: ammonia oxidizing bacteria (X_{AOB}) and nitrite oxidizing bacteria (X_{NOB})				
μ_{AOB}	Maximum growth rate of X_{AOB}	0.63	d^{-1}	(Casagli *et al.*, 2021)
μ_{NOB}	Maximum growth rate of X_{NOB}	1.1	d^{-1}	(Casagli *et al.*, 2021)
$K_{O2,AOB}/K_{O2,NOB}$	Saturation constant of X_{AOB} / X_{NOB} for S_{O2}	0.5	$gO_2\ m^{-3}$	(Reichert *et al.*, 2001)
$K_{NH4,AOB}$	Saturation constant of X_{AOB} on S_{NH4}	0.5	$gN\ m^{-3}$	(Reichert *et al.*, 2001)
$K_{I,NH4}$	Ammonia inhibition constant of X_{NOB}	5.0	$gN\ m^{-3}$	(Henze *et al.*, 2000)

$K_{NO2,NOB}$	Saturation constant of X_{NOB} for S_{NO2}	0.5	gN m^{-3}	(Henze *et al.*, 2000)
$K_{C,AOB}/K_{C,NOB}$	Saturation constant of X_{AOB} / X_{NOB} for S_{HCO3}	0.5	gC m^{-3}	(Henze *et al.*, 2000)
$K_{P,AOB}/K_{P,NOB}$	Saturation constant of X_{AOB} / X_{NOB} for S_{HPO4}	0.02	gP m^{-3}	(Reichert *et al.*, 2001)
$k_{resp,AOB}/k_{resp,NOB}$	Endogenous respiration rate of X_{AOB} /X_{NOB}	0.05	d^{-1}	(Reichert *et al.*, 2001)
$k_{death,AOB}$	Decay constant of X_{AOB}	0.1	d^{-1}	(Casagli *et al.*, 2021)
$k_{death,NOB}$	Decay constant of X_{NOB}	0.08	d^{-1}	(Casagli *et al.*, 2021)
Hydrolysis				
k_{HYD}	Hydrolysis rate constant	3.0	d^{-1}	(Reichert *et al.*, 2001)
Photorespiration factor of microalgae				
K_{PR}	Inhibition constant of photorespiration	0.03	–	(Solimeno, Samsó and García, 2016)
τ	Excess of S_{O2} coefficient	3.5	–	(Fernández, Acién, Berenguel, Guzmán, *et al.*, 2014)
S_{O2}^{SAT}	S_{O2} air saturation	9.07	gO_2 m^{-3}	(Fernández, Acién, Berenguel, Guzmán, *et al.*, 2014)
Light factor of microalgae				
α	Activation rate	1.9E-3	$(\mu E\ m^{-2})^{-1}$	(Wu and Merchuk, 2001)
β	Inhibition rate	5.7E-7	$(\mu E\ m^{-2})^{-1}$	(Wu and Merchuk, 2001)
γ	Production rate	0.14	s^{-1}	(Wu and Merchuk, 2001)
δ	Recovery rate	4.7E-4	s^{-1}	(Wu and Merchuk, 2001)
K_I	Biomass extinction coefficient	0.07	$m^2\ g^{-1}$	(Molina Grima *et al.*, 1994)
pH cardinal factor				
$pH_{ALG,max}$	Maximum pH value for X_{ALG}	12.3	–	(Solimeno, Gómez-Serrano and Acién, 2019b)
$pH_{ALG,min}$	Minimum pH value for X_{ALG}	4	–	(Solimeno, Gómez-Serrano and Acién, 2019b)
$pH_{ALG,opt}$	Optimum pH value for X_{ALG}	8.8	–	(Solimeno, Gómez-Serrano and Acién, 2019b)
$pH_{H,max}$	Maximum pH value for X_H	11.2	–	(Solimeno, Gómez-Serrano and Acién, 2019b)
$pH_{H,min}$	Minimum pH value for X_H	2	–	(Solimeno, Gómez-Serrano and Acién, 2019b)
$pH_{H,opt}$	Optimum pH value for X_H	8.2	–	(Solimeno, Gómez-Serrano and Acién, 2019b)
$pH_{N,max}$	Maximum pH value for X_{AOB} and X_{NOB}	11	–	(Solimeno, Gómez-Serrano and Acién, 2019b)
$pH_{N,min}$	Minimum pH value for X_{AOB} and X_{NOB}	2	–	(Solimeno, Gómez-Serrano and Acién, 2019b)
$pH_{N,opt}$	Optimum pH value for X_{AOB} and X_{NOB}	7	–	Experimental

Temperature cardinal factor				
$T_{ALG,max}$	Maximum temperature value for X_{ALG}	46	°C	(Solimeno, Gómez-Serrano and Acién, 2019b)
$T_{ALG,min}$	Minimum temperature value for X_{ALG}	7	°C	(Solimeno, Gómez-Serrano and Acién, 2019b)
$T_{ALG,opt}$	Optimum temperature value for X_{ALG}	26	°C	(Solimeno, Gómez-Serrano and Acién, 2019b)
$T_{N,max}$	Maximum temperature value for X_{AOB} and X_{NOB}	40	°C	(Solimeno, Gómez-Serrano and Acién, 2019b)
$T_{N,min}$	Minimum temperature value for X_{AOB} and X_{NOB}	13	°C	(Solimeno, Gómez-Serrano and Acién, 2019b)
$T_{N,opt}$	Optimum temperature value for X_{AOB} and X_{NOB}	31	°C	Experimental
Heterotrophic bacteria thermal factor				
$T_{H,opt}$	Optimum temperature value for X_H	20	°C	(Reichert *et al.*, 2001)
θ	Temperature coefficient for X_H	1.07		(Von Sperling, 2007)

Parameters	**Equations**
Chemical equilibrium $CO_2 \leftrightarrow HCO_3^-$	$K_{eq,1} = 10^{17.843-\frac{3404.71}{273.15+T}-0.032786(273.15+T)}$
Chemical equilibrium $HCO_3^- \leftrightarrow CO_3^{2-}$	$K_{eq,2} = 10^{9.494-\frac{2902.39}{273.15+T}-0.02379(273.15+T)}$
Chemical equilibrium $NH_4^+ \leftrightarrow NH_3$	$K_{eq,3} = 10^{2.891-\frac{2727}{(273.15+T)}}$
Chemical equilibrium $H^+ \leftrightarrow OH^-$	$K_{eq,w} = 10^{-\frac{4470.99}{273.15+T}+12.0875-0.01706(273.15+T)}$

Kinetics parameters				
$k_{eq,1}$	Dissociation constant of $CO_2 \leftrightarrow HCO_3^-$.	100000	d^{-1}	(Reichert *et al.*, 2001)
$k_{eq,2}$	Dissociation constant of $HCO_3^- \leftrightarrow CO_3^{2-}$	10000	d^{-1}	(Reichert *et al.*, 2001)
$k_{eq,3}$	Dissociation constant of $NH_4^+ \leftrightarrow NH_3$	10000	d^{-1}	(Reichert *et al.*, 2001)
$k_{eq,w}$	Dissociation constant of $H^+ \leftrightarrow OH^-$	10000	g m^{-3} d^{-1}	(Reichert *et al.*, 2001)
Transfer of gases to the atmosphere				
$K_{la,O2}$	Mass transfer coefficient for S_{O2}	0.62	d^{-1}	Estimated
$K_{la,CO2}$	Mass transfer coefficient for S_{CO2}	4.94	d^{-1}	Estimated
$K_{la,NH3}$	Mass transfer coefficient for S_{NH3}	1	d^{-1}	Estimated

Table A1.3. Values of fractions of carbon, hydrogen, oxygen, and nitrogen in microalgae and bacteria biomass

Parameters	Description	Value	Unit	Source
Fractions of microalgal biomass (X_{ALG})				
$i_{C,ALG}$	Fraction of carbon in microalgae	0.387	gC $gCOD^{-1}$	(Reichert *et al.*, 2001)
$i_{H,ALG}$	Fraction of hydrogen in microalgae	0.075	gH $gCOD^{-1}$	(Reichert *et al.*, 2001)
$i_{O,ALG}$	Fraction of oxygen in microalgae	0.269	gO_2 $gCOD^{-1}$	(Reichert *et al.*, 2001)
$i_{N,ALG}$	Fraction of nitrogen in microalgae	0.065	gN $gCOD^{-1}$	(Reichert *et al.*, 2001)
$i_{P,ALG}$	Fraction of phosphorus in microalgae	0.01	gP $gCOD^{-1}$	(Reichert *et al.*, 2001)
Fractions of bacteria biomass (X_H, X_{AOB}, X_{NOB})				
$i_{C,BM}$	Fraction of carbon in bacteria	0.323	gC $gCOD^{-1}$	(Reichert *et al.*, 2001)
$i_{H,BM}$	Fraction of hydrogen in bacteria	0.060	gH $gCOD^{-1}$	(Reichert *et al.*, 2001)
$i_{O,BM}$	Fraction of oxygen in bacteria	0.077	gO_2 $gCOD^{-1}$	(Reichert *et al.*, 2001)
$i_{N,BM}$	Fraction of nitrogen in bacteria	0.075	gN $gCOD^{-1}$	(Reichert *et al.*, 2001)
$i_{P,BM}$	Fraction of phosphorus in bacteria	0.018	gP $gCOD^{-1}$	(Reichert *et al.*, 2001)
Fractions of slowly biodegradable substrates (X_S)				
$i_{C,XS}$	Fraction of carbon in X_S	0.318	gC $gCOD^{-1}$	(Reichert *et al.*, 2001)
$i_{H,XS}$	Fraction of hydrogen in X_S	0.045	gH $gCOD^{-1}$	(Reichert *et al.*, 2001)
$i_{O,XS}$	Fraction of oxygen in X_S	0.077	gO_2 $gCOD^{-1}$	(Reichert *et al.*, 2001)
$i_{N,XS}$	Fraction of nitrogen in X_S	0.034	gN $gCOD^{-1}$	(Reichert *et al.*, 2001)
$i_{P,XS}$	Fraction of phosphorus in X_S	0.005	gP $gCOD^{-1}$	(Reichert *et al.*, 2001)
Fractions of inert particulate organics (X_I)				
$i_{C,XI}$	Fraction of carbon in X_I	0.327	gC $gCOD^{-1}$	(Reichert *et al.*, 2001)
$i_{H,XI}$	Fraction of hydrogen in X_I	0.037	gH $gCOD^{-1}$	(Reichert *et al.*, 2001)
$i_{O,XI}$	Fraction of oxygen in X_I	0.075	gO_2 $gCOD^{-1}$	(Reichert *et al.*, 2001)
$i_{N,XI}$	Fraction of nitrogen in X_I	0.016	gN $gCOD^{-1}$	(Reichert *et al.*, 2001)
$i_{P,XI}$	Fraction of phosphorus in X_I	0.005	gP $gCOD^{-1}$	(Reichert *et al.*, 2001)
Fractions of readily biodegradable substrates (S_S)				
$i_{C,SS}$	Fraction of carbon in S_S	0.318	gC $gCOD^{-1}$	(Reichert *et al.*, 2001)
$i_{H,SS}$	Fraction of hydrogen in S_S	0.045	gH $gCOD^{-1}$	(Reichert *et al.*, 2001)
$i_{O,SS}$	Fraction of oxygen in S_S	0.078	gO_2 $gCOD^{-1}$	(Reichert *et al.*, 2001)
$i_{N,SS}$	Fraction of nitrogen in S_S	0.034	gN $gCOD^{-1}$	(Reichert *et al.*, 2001)
$i_{P,SS}$	Fraction of phosphorus in S_S	0.005	gP $gCOD^{-1}$	(Reichert *et al.*, 2001)
Fractions of soluble inert organics (S_I)				
$i_{C,SI}$	Fraction of carbon in S_I	0.327	gC $gCOD^{-1}$	(Reichert *et al.*, 2001)
$i_{H,SI}$	Fraction of hydrogen in S_I	0.037	gH $gCOD^{-1}$	(Reichert *et al.*, 2001)
$i_{O,SI}$	Fraction of oxygen in S_I	0.075	gO_2 $gCOD^{-1}$	(Reichert *et al.*, 2001)
$i_{N,SI}$	Fraction of nitrogen in S_I	0.016	gN $gCOD^{-1}$	(Reichert *et al.*, 2001)

$i_{P,SI}$	Fraction of phosphorus in S_I	0.005	gP $gCOD^{-1}$	(Reichert *et al.*, 2001)
Fractions of inert produced by biomass degradation				
f_{ALG}	Production of X_I in endogenous respiration of X_{ALG}	0.1	gCOD $gCOD^{-1}$	(Sah *et al.*, 2011)
f_{XI}	Production of X_I in endogenous respiration of X_H	0.1	gCOD $gCOD^{-1}$	(Sah *et al.*, 2011)
f_{SI}	Production of S_I in hydrolysis of X_S	0	gCOD $gCOD^{-1}$	(Henze *et al.*, 2000)
Yield of biomass				
Y_{ALG}	Yield of X_{ALG}	0.62	gCOD $gCOD^{-1}$	(Reichert *et al.*, 2001)
Y_H	Yield of X_H on S_{O2}	0.6	gCOD $gCOD^{-1}$	(Reichert *et al.*, 2001)
$Y_{H,NO3}$	Yield of X_H on S_{NO3}	0.5	gCOD $gCOD^{-1}$	(Reichert *et al.*, 2001)
$Y_{H,NO2}$	Yield of X_H on S_{NO2}	0.3	gCOD $gCOD^{-1}$	(Reichert *et al.*, 2001)
Y_{AOB}	Yield of X_{AOB}	0.13	gCOD $gCOD^{-1}$	(Reichert *et al.*, 2001)
Y_{NOB}	Yield of X_{NOB}	0.03	gCOD $gCOD^{-1}$	(Reichert *et al.*, 2001)
K_{HYD}	Hydrolysis saturation constant	1	gCOD $gCOD^{-1}$	(Reichert *et al.*, 2001)

Table A1.4. Mathematical expressions of the stoichiometric coefficients

Stoichiometric coefficients	**Unit**
Growth of X_{ALG} on S_{NH4}	
$v_{1,1} = -i_{N,ALG}$	gN $gCOD^{-1}$
$v_{5,1} = -i_{C,ALG}$	gC $gCOD^{-1}$
$v_{8,1} = -i_{P,ALG}$	gP $gCOD^{-1}$
$v_{9,1} = 8i_{C,ALG}/3 + 8i_{H,ALG} - i_{O,ALG} - 12i_{N,ALG}/7 + 40i_{P,ALG}/31$	gO_2 $gCOD^{-1}$
$v_{10,1} = i_{N,ALG}/14 - 2i_{P,ALG}/31$	gH $gCOD^{-1}$
$v_{14,1} = 1$	gCOD $gCOD^{-1}$
Growth of X_{ALG} on S_{NO3}	
$v_{3,2} = -i_{N,ALG}$	gN $gCOD^{-1}$
$v_{5,2} = -i_{C,ALG}$	gC $gCOD^{-1}$
$v_{8,2} = -i_{P,ALG}$	gP $gCOD^{-1}$
$v_{9,2} = 8i_{C,ALG}/3 + 8i_{H,ALG} - i_{O,ALG} + 20i_{N,ALG}/7 + 40i_{P,ALG}/31$	gO_2 $gCOD^{-1}$
$v_{10,2} = -i_{N,ALG}/14 - 2i_{P,ALG}/31$	gH $gCOD^{-1}$
$v_{14,2} = 1$	gCOD $gCOD^{-1}$
Endogenous respiration of X_{ALG}	
$v_{1,3} = i_{N,ALG} - f_{ALG}\, i_{N,XI}$	gN $gCOD^{-1}$
$v_{5,3} = i_{C,ALG} - f_{ALG}\, i_{C,XI}$	gC $gCOD^{-1}$
$v_{8,3} = i_{P,ALG} - f_{ALG}\, i_{P,XI}$	gP $gCOD^{-1}$
$v_{9,3} = (i_{O,ALG} - f_{ALG}\, i_{O,XI}) - 8(i_{H,ALG} - f_{ALG}\, i_{H,XI}) - 8/3\,(i_{C,ALG} - f_{ALG}\, i_{C,XI}) + 12/7\,(i_{N,ALG} - f_{ALG}\, i_{N,XI}) - 40/31\,(i_{P,ALG} - f_{ALG}\, i_{P,XI})$	gO_2 $gCOD^{-1}$
$v_{10,3} = -1/14\,(i_{N,ALG} - f_{ALG}\, i_{N,XI}) + 2/31\,(i_{P,ALG} - f_{ALG}\, i_{P,XI})$	gH $gCOD^{-1}$
$v_{14,3} = -1$	gCOD $gCOD^{-1}$
Decay of X_{ALG}	
$v_{1,4} = i_{N,ALG} - (1 - f_{ALG})Y_{ALG}\, i_{N,XS} - f_{ALG}Y_{ALG}\, i_{N,ALG}$	gN $gCOD^{-1}$
$v_{5,4} = i_{C,ALG} - (1 - f_{ALG})Y_{ALG}\, i_{C,XS} - f_{ALG}Y_{ALG}\, i_{C,ALG}$	gC $gCOD^{-1}$
$v_{8,4} = i_{P,ALG} - (1 - f_{ALG})Y_{ALG}\, i_{P,XS} - f_{ALG}Y_{ALG}\, i_{P,ALG}$	gP $gCOD^{-1}$
$v_{9,4} = (i_{O,ALG} - f_{ALG}\, i_{O,XI}) - 8(i_{H,ALG} - f_{ALG}\, i_{H,XI}) - 8/3\,(i_{C,ALG} - f_{ALG}\, i_{C,XI}) + 12/7\,(i_{N,ALG} - f_{ALG}\, i_{N,XI}) - 40/31\,(i_{P,ALG} - f_{ALG}\, i_{P,XI})$	gO_2 $gCOD^{-1}$
$v_{10,4} = -1/14\,(i_{N,ALG}\,(1 - f_{ALG})Y_{ALG}\, i_{N,XS} - f_{ALG}Y_{ALG}\, i_{N,XI}) + 2/31\,(i_{P,ALG}\,(1 - f_{ALG})Y_{ALG}\, i_{P,XS} - f_{ALG}Y_{ALG}\, i_{P,XI})$	gH $gCOD^{-1}$
$v_{14,4} = -1$	gCOD $gCOD^{-1}$
$v_{15,4} = (1 - f_{ALG})Y_{ALG}$	gCOD $gCOD^{-1}$
$v_{16,4} = f_{ALG}Y_{ALG}$	gCOD $gCOD^{-1}$
Aerobic growth of X_H on S_{NH4}	

$v_{1,5} = i_{N,SS}/Y_H - i_{N,BM}$	gN gCOD^{-1}
$v_{5,5} = i_{C,SS}/Y_H - i_{C,BM}$	gC gCOD^{-1}
$v_{8,5} = i_{P,SS}/Y_H - i_{P,BM}$	gP gCOD^{-1}
$v_{9,5} = -(1 - Y_H)/ Y_H$	gO_2 gCOD^{-1}
$v_{10,5} = -1/14\left(i_{N,SS}/Y_H - i_{N,BM}\right) + 2/31\left(i_{P,SS}/Y_H - i_{P,BM}\right)$	gH gCOD^{-1}
$v_{12,5} = -1/Y_H$	gCOD gCOD^{-1}
$v_{17,5} = 1$	gCOD gCOD^{-1}
Aerobic growth of X_H on S_{NO3}	
$v_{3,6} = i_{N,SS}/Y_H - i_{N,BM}$	gN gCOD^{-1}
$v_{5,6} = i_{C,SS}/Y_H - i_{C,BM}$	gC gCOD^{-1}
$v_{8,6} = \left(i_{P,SS}/Y_H - i_{P,BM}\right)$	gP gCOD^{-1}
$v_{9,6} = -(1 - Y_H)/ Y_H$	gO_2 gCOD^{-1}
$v_{10,6} = -1/14\left(i_{N,SS}/Y_H - i_{N,BM}\right) + 2/31\left(i_{P,SS}/Y_H - i_{P,BM}\right)$	gH gCOD^{-1}
$v_{12,6} = -1/Y_H$	gCOD gCOD^{-1}
$v_{17,6} = 1$	gCOD gCOD^{-1}
Anoxic growth of X_H on S_{NO2}	
$v_{4,7} = -(1 - Y_{H,NO2})/(1.71Y_{H,NO2})$	gN gCOD^{-1}
$v_{5,7} = \left(i_{C,SS}/Y_{H,NO2} - i_{C,BM}\right)$	gC gCOD^{-1}
$v_{8,7} = \left(i_{P,SS}/Y_{H,NO2} - i_{P,BM}\right)$	gP gCOD^{-1}
$v_{10,7} = 1/24\left(i_{O,SS}/Y_{H,NO2} - i_{O,BM}\right) - 1/3\left(i_{H,SS}/Y_{H,NO2} - i_{H,BM}\right)$ $- 1/9\left(i_{C,SS}/Y_{H,NO2} - i_{C,BM}\right) + 1/93\left(i_{P,SS}/Y_{H,NO2} - i_{P,BM}\right)$	gH gCOD^{-1}
$v_{12,7} = -1/Y_{H,NO2}$	gCOD gCOD^{-1}
$v_{17,7} = 1$	gCOD gCOD^{-1}
Anoxic growth of X_H on S_{NO3}	
$v_{3,8} = -(1 - Y_{H,NO3})/(1.14Y_{H,NO3})$	gN gCOD^{-1}
$v_{5,8} = \left(i_{C,SS}/Y_{H,,NO3} - i_{C,BM}\right)$	gC gCOD^{-1}
$v_{8,8} = \left(i_{P,SS}/Y_{H,NO3} - i_{P,BM}\right)$	gP gCOD^{-1}
$v_{10,8} = 1/14\left(i_{N,SS}/Y_{H,NO3} - i_{N,BM}\right) + 2/31\left(i_{P,SS}/Y_{H,NO3} - i_{P,BM}\right)$	gH gCOD^{-1}
$v_{12,8} = -1/Y_{H,NO3}$	gCOD gCOD^{-1}
$v_{17,8} = 1$	gCOD gCOD^{-1}
Aerobic endogenous respiration of X_H	
$v_{1,9} = i_{N,BM} - f_{XI}\, i_{N,XI}$	gN gCOD^{-1}
$v_{5,9} = i_{C,BM} - f_{X1}\, i_{C,XI}$	gC gCOD^{-1}
$v_{8,9} = i_{P,BM} - f_{X1}\, i_{P,XI}$	gP gCOD^{-1}
$v_{9,9} = -(1 - f_{X1})/2$	gO_2 gCOD^{-1}
$v_{10,9} = -1/14\left(i_{N,BM} - f_{XI}\, i_{N,XI}\right) + 2/31\left(i_{P,BM} - f_{XI}\, i_{P,XI}\right)$	gH gCOD^{-1}

$v_{17,9} = -1$	gCOD gCOD^{-1}
Anoxic endogenous respiration of X_H	
$v_{1,10} = i_{N,BM} - f_{XI}\, i_{N,XI}$	gN gCOD^{-1}
$v_{3,10} = (f_{XI} - 1)/1.14$	gN gCOD^{-1}
$v_{4,10} = (1 - f_{XI})/1.14$	gN gCOD^{-1}
$v_{5,10} = i_{C,BM} - f_{XI} i_{C,XI}$	gC gCOD^{-1}
$v_{8,10} = i_{P,BM} - f_{XI} i_{P,XI}$	gP gCOD^{-1}
$v_{10,10} = 1/40\,(i_{O,BM} - f_{XI} i_{O,XI}) - 1/5\,(i_{H,BM} - f_{XI} i_{H,XI}) - 1/15\,(i_{C,BM} - f_{XI} i_{C,XI}) + 1/35\,(i_{N,BM} - f_{XI} i_{N,XI}) - 1/31\,(i_{P,BM} - f_{XI} i_{P,XI})$	gH gCOD^{-1}
$v_{17,10} = -1$	gCOD gCOD^{-1}
Decay of X_H	
$v_{15,11} = (1 - f_{XI}) Y_H$	gCOD gCOD^{-1}
$v_{16,11} = f_{XI} Y_H$	gCOD gCOD^{-1}
$v_{17,11} = -1$	gCOD gCOD^{-1}
Growth of ammonia oxidizing bacteria (X_{AOB})	
$v_{1,12} = -1/Y_{AOB} - i_{N,BM}$	gN gCOD^{-1}
$v_{4,12} = 1/Y_{AOB} - i_{N,BM}$	gN gCOD^{-1}
$v_{5,12} = -i_{C,BM}$	gC gCOD^{-1}
$v_{8,12} = -i_{P,BM}$	gP gCOD^{-1}
$v_{9,12} = (1 - 3.43/Y_{AOB})$	gO_2 gCOD^{-1}
$v_{10,12} = 2/14 Y_{AOB} - 1/14\,(i_{N,BM}) - 2/31\,(i_{P,BM})$	gH gCOD^{-1}
$v_{18,12} = 1$	gCOD gCOD^{-1}
Growth of nitrite oxidizing bacteria (X_{NOB})	
$v_{3,13} = 1/Y_{NOB} - i_{N,BM}$	gN gCOD^{-1}
$v_{4,13} = -1/Y_{NOB}$	gN gCOD-1
$v_{5,13} = -i_{C,BM}$	gC gCOD^{-1}
$v_{8,13} = -i_{P,BM}$	gP gCOD^{-1}
$v_{9,13} = (1 - 1.14/Y_{NOB})$	gO_2 gCOD^{-1}
$v_{10,13} = -1/14\,(i_{N,BM}) - 2/31\,(i_{P,BM})$	gH gCOD^{-1}
$v_{19,13} = 1$	gCOD gCOD^{-1}
Endogenous respiration of X_{AOB}	
$v_{1,14} = i_{N,BM} - f_{XI}\, i_{N,XI}$	gN gCOD^{-1}
$v_{5,14} = i_{C,BM} - f_{XI} i_{C,XI}$	gC gCOD^{-1}
$v_{8,14} = i_{P,BM} - f_{XI} i_{P,XI}$	gP gCOD^{-1}
$v_{9,14} = -(1 - f_{XI})$	gO_2 gCOD^{-1}

$v_{10,14} = -1/14\,(i_{N,BM} - f_{XI}\,i_{N,XI}) + 2/31\,(i_{P,BM} - f_{XI}\,i_{P,XI})$	gH gCOD^{-1}
$v_{18,14} = -1$	gCOD gCOD^{-1}
Endogenous respiration of X_{NOB}	
$v_{1,15} = i_{N,BM} - f_{XI}\,i_{N,XI}$	gN gCOD^{-1}
$v_{5,15} = i_{C,BM} - f_{XI} i_{C,XI}$	gC gCOD^{-1}
$v_{8,15} = i_{P,BM} - f_{XI} i_{P,XI}$	gP gCOD^{-1}
$v_{9,15} = -(1 - f_{XI})$	gO_2 gCOD^{-1}
$v_{10,15} = -1/14\,(i_{N,BM} - f_{XI}\,i_{N,XI}) + 2/31\,(i_{P,BM} - f_{XI}\,i_{P,XI})$	gH gCOD^{-1}
$v_{19,15} = -1$	gCOD gCOD^{-1}
Decay of X_{AOB} and X_{NOB}	
$v_{15,16} = (1 - f_{XI})Y_{AOB}$	gCOD gCOD^{-1}
$v_{16,16} = f_{XI} Y_{AOB}$	gCOD gCOD^{-1}
$v_{18,16} = -1$	gCOD gCOD^{-1}
$v_{15,17} = (1 - f_{XI})Y_{NOB}$	gCOD gCOD^{-1}
$v_{16,17} = f_{XI} Y_{NOB}$	gCOD gCOD^{-1}
$v_{19,17} = -1$	gCOD gCOD^{-1}
Hydrolysis	
$v_{1,18} = -(1 - f_{SI}) i_{N,SS} - f_{SI} i_{N,SI} + i_{N,XS}$	gN gCOD^{-1}
$v_{5,18} = i_{C,XS} - (1 - f_{SI}) Y_{HYD} i_{C,SS} - f_{SI} Y_{HYD} i_{C,SI}$	gC gCOD^{-1}
$v_{8,18} = i_{P,XS} - (1 - f_{SI}) Y_{HYD} i_{P,SS} - f_{I,XS} Y_{HYD} i_{P,SI}$	gP gCOD^{-1}
$v_{10,18} = -1/14\,(i_{N,XS} - (1 - f_{SI}) Y_{HYD} i_{N,SS} - f_{SI} Y_{HYD} i_{N,SI}) + 2/31\,(i_{P,XS} - (1 - f_{SI}) Y_{HYD} i_{P,SS} - f_{SI} Y_{HYD} i_{P,SI})$	gH gCOD^{-1}
$v_{12,18} = (1 - f_{SI}) Y_{HYD}$	gCOD gCOD^{-1}
$v_{13,18} = (f_{SI}) Y_{HYD}$	gCOD gCOD^{-1}
$v_{15,18} = -1$	gCOD gCOD^{-1}
Chemical equilibria $CO_2 \leftrightarrow HCO_3^-$	
$v_{5,19} = -1$	gC gC^{-1}
$v_{6,19} = 1$	gC gC^{-1}
$v_{10,19} = 1/12$	gH gC^{-1}
Chemical equilibria $HCO_3^- \leftrightarrow CO_3^{2-}$	
$v_{6,20} = -1$	gC gC^{-1}
$v_{7,20} = 1$	gC gC^{-1}
$v_{10,20} = 1/12$	gH gC^{-1}
Chemical equilibria $NH_4^+ \leftrightarrow NH_3$	
$v_{1,21} = -1$	gN gN^{-1}
$v_{2,21} = 1$	gN gN^{-1}

$v_{10,21} = 1/14$	gH gN^{-1}
Chemical equilibria $H^+ \leftrightarrow OH^-$	
$v_{10,22} = 1$	gH gH^{-1}
$v_{11,22} = 1$	gH gH^{-1}
Oxygen transfer to the atmosphere	
$v_{9,23} = 1$	–
Carbon dioxide transfer to the atmosphere	
$v_{5,24} = 1$	–
Ammonia transfer to the atmosphere	
$v_{2,25} = 1$	–

Appendix 2. Initial values for simulation (Section 4.1.2)

Table A2.1. Initial concentrations of components in the anoxic reactor and photobioreactor

Component	Description	Value		Units
		Photobioreactor	Anoxic Reactor	
X_{ALG}	Microalgae biomass	201.3 (1)	422.4 (1)	mgTSS L^{-1}
X_H	Heterotrophic bacteria	68.25 (2)	143.22 (2)	mgTSS L^{-1}
X_{AOB}	Ammonium oxidizing bacteria	0.2 (3)	0.43 (3)	mgTSS L^{-1}
X_{NOB}	Nitrite oxidizing bacteria	2.04 (3)	4.29 (3)	mgTSS L^{-1}
X_S	Slowly biodegradable particulate organic matter	283.64 (2)	595.17 (2)	mgTSS L^{-1}
X_I	Inert soluble organic matter	56.81 (2)	119.21 (2)	mgTSS L^{-1}
S_{NH4}	Ammonium nitrogen	2.09	18.1	mgN-NH_4 L^{-1}
S_{NH3}	Ammonia nitrogen	1	1	mgN-NH_3 L^{-1}
S_{NO3}	Nitrate nitrogen	0	0	mgN-NO_3 L^{-1}
S_{NO2}	Nitrite nitrogen	0.7	2.6	mgN-NO_2 L^{-1}
S_{CO2}	Dissolved carbon dioxide	1	2	mgC-CO_2 L^{-1}
S_{HCO3}	Bicarbonate	163.1	164	mgC-HCO_3 L^{-1}
S_{CO3}	Carbonate	9	1.4	mgC-CO_3 L^{-1}
S_{PO4}	Phosphate phosphorus	0	5.4	mgP-PO_4 L^{-1}
S_{O2}	Dissolved oxygen	1.48	0.09	mgO_2 L^{-1}
S_H	Hydrogen ions	6.07e-07	2.47e-06	mgH L^{-1}
S_{OH}	Hydroxide ions	0.28	0.7e-01	mgH-OH L^{-1}
S_S	Readily biodegradable soluble organic matter	8.74 (4)	39.07 (4)	mgCOD L^{-1}
S_I	Inert soluble organic matter	50 (4)	70 (4)	mgCOD L^{-1}

Photosynthetic model

State	Description	Value	Units
x_1	Microalgae in open state	1	-
x_2	Microalgae in activated state	0	-
x_3	Microalgae in inhibited state	0	-

(1) Both anoxic and aerobic reactor were inoculated with a microalgae- bacteria consortia in which the third part of the total biomass corresponding to microalgae biomass.

(2) The composition of the activated sludge biomass (corresponding with 2/3 of the total biomass) was assumed composed of: 16.7% of X_H, 13.7% of X_I, and 69.05% of X_S (considering the composition similar to the adopted by the ASM2).

(3) Since the facility was a short set-up period (previous to data recorded), was assumed a nitrifying bacteria composition of 0.05% of X_{AOB} and 0.5% of $X_{NOB.}$

(4) Values of S_I and S_S were estimated according to COD tests.

Table A2.2. Initial values of biomass concentration in the settler

Component	Description	Value	Units
$TSS_{effluent}$	Total suspended solids concentration in the top layer	70	mgTSS L^{-1}
TSS_2	Total suspended solids concentration in layer 2	80	mgTSS L^{-1}
TSS_3	Total suspended solids concentration in layer 3	100	mgTSS L^{-1}
TSS_4	Total suspended solids concentration in layer 4	130	mgTSS L^{-1}
TSS_5	Total suspended solids concentration in layer 5	200	mgTSS L^{-1}
TSS_6	Total suspended solids concentration in layer 6	600	mgTSS L^{-1}
TSS_7	Total suspended solids concentration in layer 7 (feeding layer)	700	mgTSS L^{-1}
TSS_8	Total suspended solids concentration in layer 8	1200	mgTSS L^{-1}
TSS_9	Total suspended solids concentration in layer 9	1700	mgTSS L^{-1}
$TSS_{wastage}$	Total suspended solids concentration in the bottom layer	2250	mgTSS L^{-1}

Appendix 3. Initial values for simulation (Section 5.4)

Table A3.1. Initial concentrations of components in the HRAP

Component	Description	Value	Units
X_{ALG}	Microalgae biomass	3550 (1)	mgTSS L^{-1}
X_H	Heterotrophic bacteria	592.85 (2)	mgTSS L^{-1}
X_{AOB}	Ammonium oxidizing bacteria	3.55 (3)	mgTSS L^{-1}
X_{NOB}	Nitrite oxidizing bacteria	1.775 (3)	mgTSS L^{-1}
X_S	Slowly biodegradable particulate organic matter	2458.375 (2)	mgTSS L^{-1}
X_I	Inert soluble organic matter	493.45 (2)	mgTSS L^{-1}
S_{NH4}	Ammonium nitrogen	8	mgN-NH_4 L^{-1}
S_{NH3}	Ammonia nitrogen	0.049	mgN-NH_3 L^{-1}
S_{NO3}	Nitrate nitrogen	0	mgN-NO_3 L^{-1}
S_{NO2}	Nitrite nitrogen	0	mgN-NO_2 L^{-1}
S_{CO2}	Dissolved carbon dioxide	7.1	mgC-CO_2 L^{-1}
S_{HCO3}	Bicarbonate	42	mgC-HCO_3 L^{-1}
S_{CO3}	Carbonate	0.9	mgC-CO_3 L^{-1}
S_{PO4}	Phosphate phosphorus	7	mgP-PO_4 L^{-1}
S_{O2}	Dissolved oxygen	10	mgO_2 L^{-1}
S_H	Hydrogen ions	9.7375e-05	mgH L^{-1}
S_{OH}	Hydroxide ions	0.0018	mgH-OH L^{-1}
S_S	Readily biodegradable soluble organic matter	8 (4)	mgCOD L^{-1}
S_I	Inert soluble organic matter	40 (4)	mgCOD L^{-1}
Photosynthetic model			
x_1	Microalgae in open state	1	-
x_2	Microalgae in activated state	0	-
x_3	Microalgae in inhibited state	0	-

(1) The HRAP was considered inoculated with 2.5 gVSS/L of microalgae consortia.

(2) The composition of the activated sludge biomass (corresponding with 2.5 gVSS/L of activated sludge.) was assumed composed of: 16.7% of X_H, 13.9% of X_I, and 69.25% of X_S (considering the composition similar to the adopted by the ASM2 (Henze *et al.*, 2000)).

(3) A nitrifier bacteria composition of 0.1% of X_{AOB} and 0.05% of X_{NOB} was assumed.

(4) Values of S_I and S_S were estimated according to COD tests for similar wastewater composition.

Table A3.2. Initial values of biomass concentration in the settler

Component	Description	Value	Units
$TSS_{effluent}$	Total suspended solids concentration in the top layer	100	mgTSS L^{-1}
TSS_2	Total suspended solids concentration in layer 2	200	mgTSS L^{-1}
TSS_3	Total suspended solids concentration in layer 3	300	mgTSS L^{-1}
TSS_4	Total suspended solids concentration in layer 4	400	mgTSS L^{-1}
TSS_5	Total suspended solids concentration in layer 5	500	mgTSS L^{-1}
TSS_6	Total suspended solids concentration in layer 6	1000	mgTSS L^{-1}
TSS_7	Total suspended solids concentration in layer 7 (feeding layer)	2000	mgTSS L^{-1}
TSS_8	Total suspended solids concentration in layer 8	4000	mgTSS L^{-1}
TSS_9	Total suspended solids concentration in layer 9	6000	mgTSS L^{-1}
$TSS_{wastage}$	Total suspended solids concentration in the bottom layer	20000	mgTSS L^{-1}

Appendix 4. SCADA for microalgae- bacteria WWTP

The main window of the SCADA (Fig. A4.1) is comprised of two distinct segments. The left side of the interface contains the “Navigation pane” buttons (labeled “A”), which facilitate the navigation between the various windows of the SCADA system. Indicators labeled as “B” allow for the visualization of the control mode in which the system is operating, while the button labeled “C” is used to terminate the execution of the SCADA program. The right side of the main window (section labeled “D”) displays the real-time values of the measured variables, including pH, dissolved oxygen concentration, and temperature, as well as the input flow to each reactor. The section labeled "E" is intended to provide a visual indication of the pump's operational status, thereby communicating its current status as either active or deactivated. Furthermore, it enables the selection of the channel on which each pump is connected. In the section designated “F”, the selectors f_{s1} and f_{s2} permit the cessation of data recording or the DAQ connection, respectively, for each reactor. Consequently, the status of data recording (indicators f_{i1}) and the status of the connection of the LabQuest Mini devices for each reactor (indicators f_{i2}) are indicated on the right side of the main window. Indicators f_{i2} facilitate the identification of connection failures in LabQuest Mini devices. The objective of the selectors f_{s1} is to enable uninterrupted system functionality and data visualization during probes calibration or cleaning tasks. In the event that the "calibration mode" (selectors f_{s1}) is activated, all SCADA functions remain operational; only the data recording of variables in the Excel file is suspended until the "calibration mode" is deactivated.

The window for each reactor (Fig. A4.2) also facilitates navigation between the various windows of the SCADA system, as well as the selection of "calibration mode" and "automatic control mode." The window also displays the operational values of the variables (pH, dissolved oxygen, temperature, and input flow). In the event that the "automatic control mode" is selected, it is imperative that the set point for the dissolved oxygen concentration be provided, in conjunction with the parameters for the PID controller.

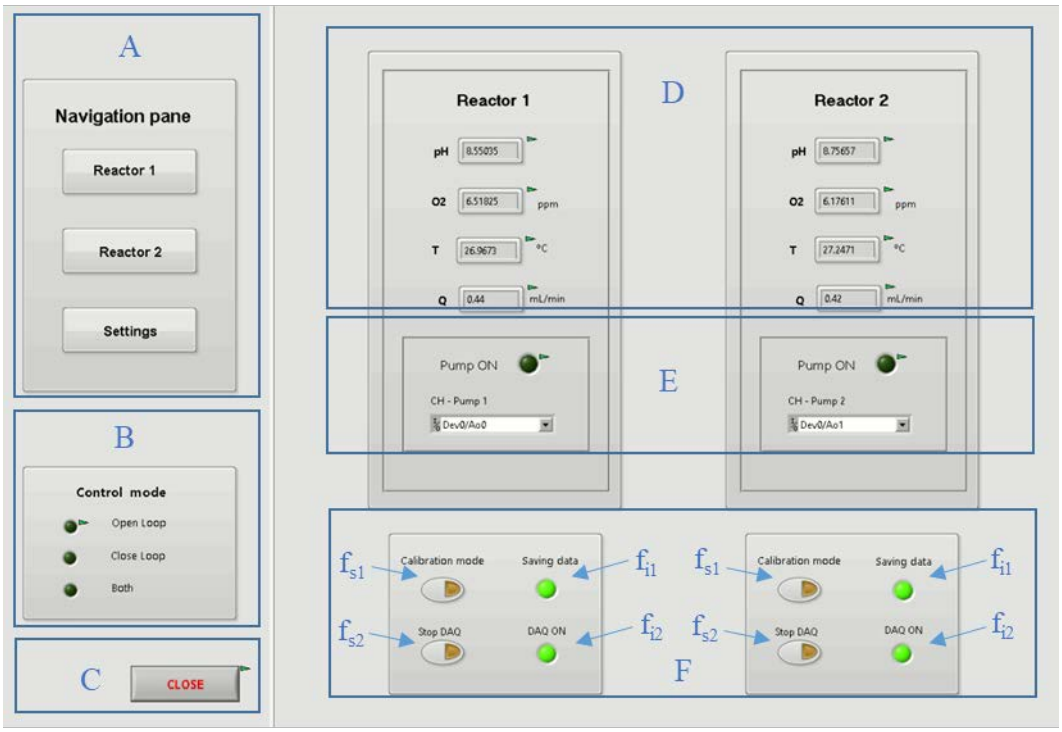

Fig. A4.1. Main window of the SCADA

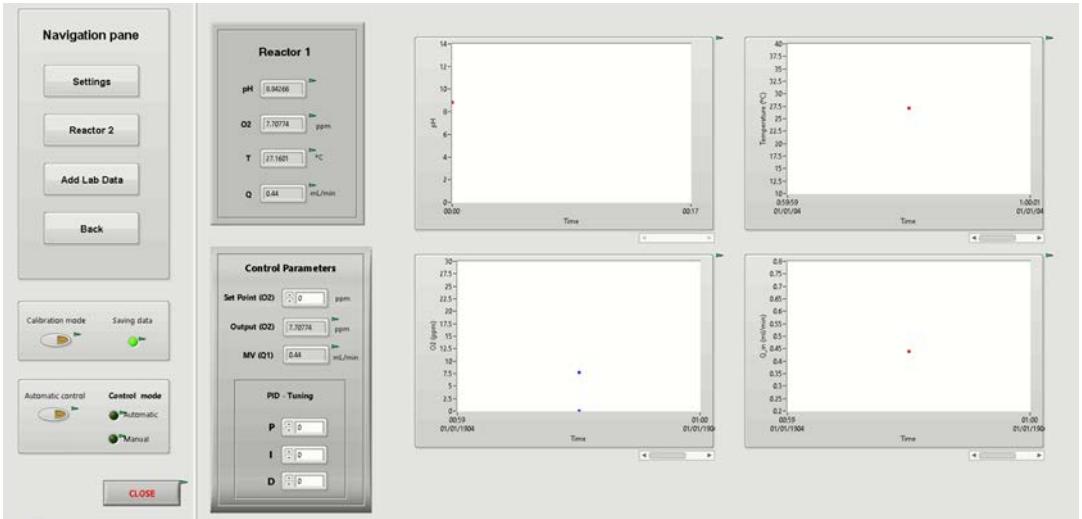

Fig. A4.2. Reactor 1 window

The "Settings" window of the SCADA (Fig. A4.3) facilitates the configuration of operational parameters associated with the input flow to each photobioreactor. The values

of the slope of the calibration curve, which must be obtained through experimental means, as well as the desired input flow rate, are to be provided. Due to the limited dimensions of the laboratory-scale plant, fixed input flows (and, consequently, the associated voltage values) were selected. To achieve the desired input flow values, a mathematical relationship was formulated, with the variable to be modified being the time of pump activation.

Fig. A4.3. Settings window of the SCADA